SYNTHESIS AND CHARACTERISATION

OF NOVEL, REDOX-ACTIVE COMPLEXES

OF RUTHENIUM AND OSMIUM

Lockhart E. Horsburgh

Ph.D. Thesis

University of Edinburgh

1994

DECLARATION

Except where specific reference is made to other sources, the work presented in this thesis is the original work of the author. It has not been submitted, in whole or in part, for any other degree.

Lockhart E. Horsburgh

\

I remember the lost confusion of innocence.

- K. Nardi

ACKNOWLEDGEMENTS

Abstract

This thesis reports the synthesis and characterisation of a number of novel complexes of Ru and Os. The complexes studied all have more than one redox centre. A major objective of this research was investigation of the redox behaviour of the complexes formed, primarily by electrochemical and *in situ* spectroelectrochemical studies.

In chapter 1 the electrochemical and *in situ* spectroelectrochemical techniques employed during this work are discussed.

Chapters 2 and 3 report reactions of tetracyanoethylene (tcne) and tetracyanoquinodimethane (tcnq) with various complexes of Ru and Os. In the vast majority of cases tcnx (x = e or q) was found to coordinate to the metal centre via nitrogen. Electrochemical and spectroelectrochemical studies were employed to elucidate the nature of the frontier orbitals. In general the complexes exhibited facile ligand-based reductions while oxidative processes were metal-based.

In chapter 2 reactions of tcnx with *cis*-Ru(bpy)$_2$Cl$_2$ (bpy = 2,2'-bipyridyl), and electrochemically induced reactions of tcne with [OsCl$_6$]$^{2-}$, [OsBr$_6$]$^{2-}$ and [OsCl$_5$(py)]$^-$ (py = pyridine) are reported.

Chapter 3 discusses reactions of tcnx with phosphine complexes of Ru and Os. Of particular interest was the formation of *trans*-[OsCl$_2$(PEt$_2$Ph)$_3${(NC)$_2$C=C(OH)(CN)}], the first reported example of metal-bound tricyanovinyl alcohol. In addition to studies of the redox processes, the mechanism of formation of the above complex was investigated.

Chapter 4 discusses trinuclear mixed valence complexes of general formula XL$_2$Ru(μ-X)$_3$Ru(μ-X)$_3$RuL$_2$X, where X = Cl or Br and L is a tertiary phosphine or arsine. In particular the nature of the metal-metal interactions was investigated, primarily by single crystal X-ray diffraction, electrochemistry and spectroelectrochemistry. The results obtained are generally consistent with Ru-Ru bonding and extensive delocalisation of the metal-based valence electrons.

List of Abbreviations

A	absorbance
Å	Angstrom (10^{-10}m)
a.c.	alternating current
bpy	2,2'-bipyridyl
br	broad
Bu	butyl
c.e.	counter electrode
CF	centre field
chp	deprotonated anion of 2-chloro-6-hydroxypyridine
Cp	cyclopentadienyl
Cp*	pentamethylcyclopentadienyl
CV	cyclic voltammogram
D_c	calculated density
DMF	dimethylformamide
DMSO	dimethylsulphoxide
DN	solvent donor number
dppe	(1,2-diphenylphosphino)ethane
E_{app}	applied potential
EAS	electronic absorption spectroscopy
EPR	electron paramagnetic resonance
EPRESISE	electron paramagnetic resonance *in situ* electrochemical [cell]
ESR	electron spin resonance
Et	ethyl
FAB	fast atom bombardment
fmn	fumaronitrile
HOMO	highest occupied molecular orbital
I	irreversible
IR	infra red
IVCT	inter valence charge transfer

K	degrees Kelvin
L	ligand
LMCT	ligand to metal charge transfer
LUMO	lowest unoccupied molecular orbital
M	mol/dm^3
m	medium
$[M]^+$	molecular ion (in mass spectra)
Me	methyl
MLCT	metal to ligand charge transfer
MO	molecular orbital
MS	mass spectrum
m/z	mass to charge ratio
NIR	near infra red
nmr	nuclear magnetic resonance
OTE	optically transparent electrode
Ph	phenyl
Pr	propyl
PTFE	polytetrafluoroethylene
py	pyridine
pyz	pyrazine
q	quasi-reversible
r	reversible
r.e.	reference electrode
s	strong
SCF	self consistent field
sh	shoulder
SHE	standard hydrogen electrode
SOMO	semi occupied molecular orbital
SW	sweep width
tcne	tetracyanoethylene
tcnq	7,7,8,8-tetracyanoqinodimethane

tcva	tricyanovinylalcohol
THF	tetrahydrofuran
TIRTLE	transparent to infra red thin layer electrode
tpt	tris(2-pyridyl)-1,3,5-triazine
trpy	2,2',6',2"-terpyridine
ttf	tetrathiafulvalene
UV	ultra violet
V	volts, or volume of unit cell
w	weak
w.e.	working electrode
α	degree of electron delocalisation in mixed-valence complexes
$\Delta_{1/2}$	half-height peak width
ε	extinction coefficient ($cm^{-1}mol^{-1}dm^3$)
μ	indicates a bridging ligand
μ_{eff}	effective magnetic moment
ν	scan rate in voltammetry, energy (in cm^{-1}) in spectroscopy
ν_{max}	energy (in cm^{-1}) of maximum absorption
ω	frequency of alternating potential in a.c. voltammetry

Notes

In Chapters 2 and 3, several of the complexes prepared are often referred to by codes. These codes consist of a letter (P, or N, depending on whether the starting complex contained P-donor or N-donor ligands) and a single digit number. The species are given below.

[N1]	$[Ru(bpy)_2Cl(tcne)]^+$
[N2]	$[Ru(bpy)_2Cl(tcnq)]^+$
[N3]	Not fully characterised. Possible alkene π-complex, formed by reaction of tcne and $AgBF_4$ with cis-$[Ru(bpy)_2Cl_2]$.

Chapter 1 Electrochemical and Spectroelectrochemical Techniques

Chapter 2 Tetracyanoethylene and Tetracyanoquinodimethane Complexes of Ruthenium and Osmium

Chapter 3 Reactions of tcnx with Phosphine Complexes of Ru and Os

Chapter 4 Trinuclear Mixed-Valence Complexes of Ruthenium

CH$_2$Cl$_2$.

1 Electrochemical and Spectroelectrochemical Techniques

1.1 Introduction

This thesis is concerned with the synthesis and characterisation of a number of novel, redox-active complexes of ruthenium and osmium. All the species studied contain more than one redox-active site, therefore an important feature of this work was the characterisation of the redox and charge transfer processes associated with the complexes.

Electron transfer processes are of considerable importance in chemistry. A great many reactions rely on the redox and charge-transfer properties of the species involved. Areas as diverse as corrosion (and its prevention), utilisation of solar energy and the chemistry of life itself, to name but a few, all involve charge transfer processes. The study of the redox properties of the species involved is therefore of prime importance.

Corrosion, the oxidation of metals (especially iron) by the actions of environmental agents, usually oxygen or water, results in weakening of structures, reduced electrical conductivity of high tension cables and many other problems. It arises from the facile oxidation of the metals concerned and may be inhibited by a number of methods, some of which rely on the redox properties of the metals.

One obvious option is coating the metal in a less readily oxidised species. This is best exemplified by tin ($Sn^{2+} + 2e^- \longrightarrow Sn$, $E^0 = -0.14$ V vs SHE)[1] and nickel ($Ni^{2+} + 2e^- \longrightarrow Ni$, $E^0 = -0.23$ V)[1] plating of iron and steel ($Fe^{2+} + 2e^- \longrightarrow Fe$, $E^0 = -0.41$ V)[1]. Provided the coating remains intact, oxidation of the iron by oxygen or moisture is prevented. If the coating is broken, however, electrons flow from iron to the less readily oxidised plating metal and the iron is oxidised more rapidly than if it were "unprotected".[2]

An alternative approach is to use a more readily oxidised metal for plating. In this case, when the coating is damaged the flow of electrons is from the coating to the protected metal, therefore corrosion is still inhibited. This is known as sacrificial corrosion of the more reactive metal. The best example of this is galvanised steel, in which zinc ($Zn^{2+} + 2e^- \longrightarrow Zn$, $E^0 = -0.76$ V)[1] is used as the plating metal.[2]

A third approach is employed in the case of aluminium, which is very readily oxidised ($Al^{3+} + 3e^- \longrightarrow Al$, $E^0 = -1.71$ V)[1]. Aluminium oxide, Al_2O_3 is extremely stable under atmospheric conditions, water impermeable and is sufficiently strong that it is not easily removed. Thus, in order to protect aluminium, a thick oxide layer is built up by making Al the anode in an electrolytic cell. This process, known as anodising, has also been used successfully with magnesium.[3]

In recent years, renewable, non-polluting energy sources have been the subject of considerable attention. Of particular interest has been efficient utilisation of solar energy for electricity generation or storage as "chemical energy". To this end, there

has been extensive research into "solar dyes", species which are able to absorb solar energy then release it such that it can be used in chemical reactions.

The criteria for an efficient solar dye are two-fold. It must be readily excited by solar energy, preferably visible light (ie. it must be strongly coloured). Also, the excited state must be sufficiently long lived to allow transfer of electrons or energy to other species.

Possibly the best known solar dye is the $[Ru(bpy)_3]^{2+}$ (bpy = 2,2'-bipyridyl) chromophore. This readily absorbs light in the blue-green region of the visible spectrum (ν_{max} = 22100 cm^{-1}, ε= 13700 mol^{-1}dm^{3}cm^{-1})[4]. Upon excitation an electron is transferred from Ru to one of the bipyridyl ligands, thus the excited state is best described as $[Ru^{III}(bpy)^0_2(bpy)^-]*^{2+}$.[4,5] The transferred electron is localised upon a single bipyridyl ligand, therefore excitation results in reduced symmetry and an excited state which is sufficiently long-lived to undergo chemical reaction.

The excited state, having unpaired electrons in a bpy-based π^*-LUMO and a metal-based dπ-orbital readily undergoes both oxidative and reductive "quenching" reactions, which include disproportionation to $[Ru(bpy)_3]^{3+}$ and $[Ru(bpy)_3]^{+}$.[6-8] Much of the interest stems from the discovery that $[Ru(bpy)_3]^{*2+}$ is thermodynamically capable of reacting with water to give H$_2$ and O$_2$.[9]

In $[Ru(bpy)_3]^{2+}$ and many other solar dyes, both the energy and the nature of the light-induced charge transfer process are vital to the effectiveness of the dye. The study of $[Ru(bpy)_3]^{2+}$ and related species is discussed in more detail in Chapter 2 (Section 2.2.2).

In biological systems redox chemistry is of considerable importance. Metalloenzymes are involved in such vital processes as photosynthesis, O_2 transport, and metabolism of food and toxins such as alcohol or peroxides.[10]

The correct function of many enzymes is dependent upon the redox properties of metal centres bound to the protein. The redox potential of the enzyme is dictated by the environment of the metal ion (ie. the nature of the ligands and their positions). The geometry of the ligands about the metal may, however be considerably distorted from the idealised geometries favoured by the metal centre (usually octahedral, tetrahedral or square planar) by the folding and other structural properties of the surrounding protein.[10]

The influence of the surrounding proteins is perhaps best exemplified by the case of the Cytochrome C enzymes, which generally act as electron transfer enzymes, primarily in the reduction or oxidation of other metalloenzymes.[11] All Cytochrome C enzymes contain iron in a "heme c" environment (See Figure 1.1), in which Fe is bound to five N atoms (the tetradentate porphyrin plus a histidine residue) and one S-donor (a methionine residue).[11]

Given the similarity of its immediate environment, the diversity of the $Fe^{II/III}$ redox potentials for Cytochrome C enzymes is astonishing. In Cytochrome C_2, the electron donor for photosynthetic and respiration centres in certain bacteria (notably of the *Rhodopseudomonas* family), E_m at pH = 7 varies between +0.288 V and +0.370 V (versus the standard hydrogen electrode).[11,12,13] In contrast, the Cytochrome C_3 enzymes, in which there are four heme c units per molecule, exhibit

E_m values of -0.29 to -0.205 V.[11,14] Cytochrome C_3 has been shown to act, for example, as an electron donor for the hydrogenase enzyme in sulphate reducing bacteria.[11,14]

Figure 1.1 Heme c

R = CH$_2$CH$_2$COOH

X = Y = CH(CH$_3$)CH$_2$SCH$_2$CH(NH$_2$)COOH
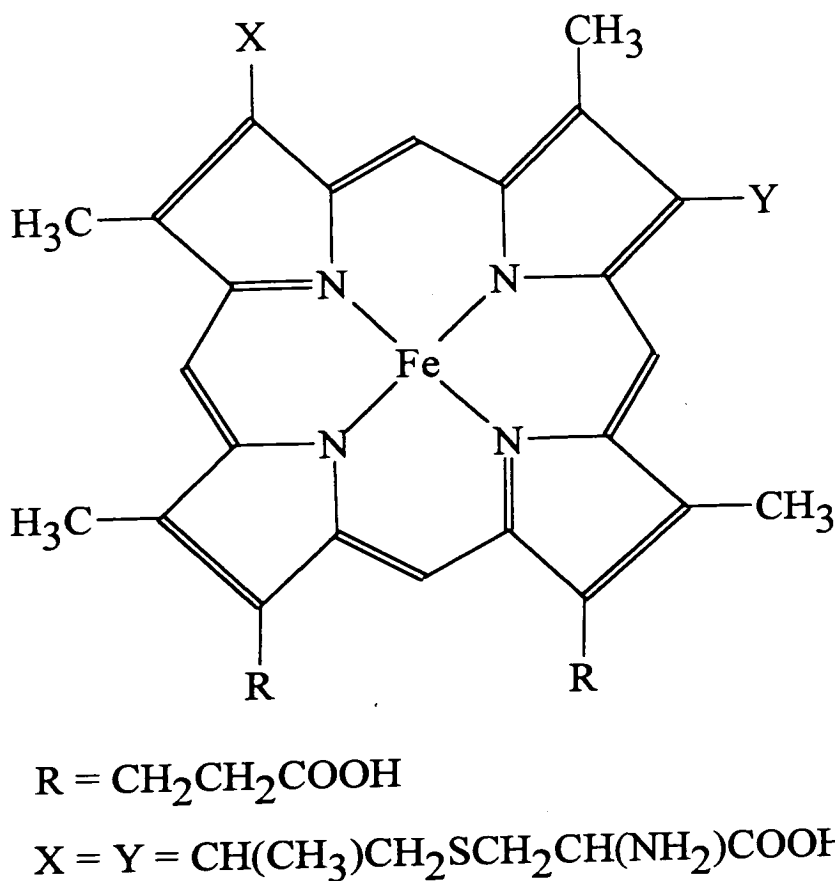
Knowledge of the redox and charge transfer properties of a given species are clearly important if we are to make efficient use of that species, or if we are to modify it in order to obtain a predictable change in its properties. Electrochemical and spectroelectrochemical techniques are methods of studying redox behaviour.

As a result of their rich redox chemistry, electrochemical techniques are frequently employed in the study of transition metal complexes. A brief introduction to the electrochemical techniques employed during the course of this research is given below, detailing electrode design, cell design, solvents and supporting electrolytes. A short discussion of spectroelectrochemical techniques is also provided.

1.2 Electrodes

A primary consideration in electrode and cell design is solution resistance. In the case of a "classical" two electrode cell (consisting of a working electrode and a nonpolarisable reference electrode), a voltage drop equal to iR_s, where R_s is the solution resistance, is included in the measured potential, ie. the applied potential, E_{appl}, and the potential at the working electrode, E, are related by the equation

$$E_{appl} = E + iR_s$$

Clearly, the larger the current passed, the greater the difference between the apparent and actual potentials at the working electrode. The iR_s term also becomes important when there is a high solution impedance, as is the case when electrochemical experiments are conducted in organic solvents.

Now consider a three electrode configuration, consisting of a working electrode (w.e.), a reference electrode (r.e.) and a counter (auxiliary) electrode (c.e.). A potential difference is generated and measured between the r.e. and w.e., and the resultant current between c.e. and w.e. is measured. The device used to measure the potential difference between w.e. and r.e. has a very high impedance, therefore the current passing between w.e. and r.e. is negligible and the significance of the iR_s term is greatly reduced. The minimal currents passing through the r.e. also mean that its potential remains equal to its open circuit value. As a result, three electrode systems are used in the majority of electrochemical experiments - all of the electrochemical studies reported in this thesis utilise such systems.

It should be noted, however, that not all of the iR_s term is removed by use of a three electrode system. There is a significant potential drop between w.e. and c.e. thus the solution may be thought of as a potentiometer. Except when the r.e. is placed exactly at the surface of the w.e. (for practical reasons this is impossible - if the r.e. is very close to the w.e. significant blocking of the solution current path at the w.e. surface occurs; furthermore, in many cases there is a need to protect the reference electrode from the species under study or being generated at the w.e. surface) some fraction of iR_s (called iR_u, where R_u is the uncompensated solution resistance) will apppear in the measured potential. In addition to this, any resistance in the w.e. itself will also appear in R_u. The equation relating the applied potential to the potential at the w.e. becomes

$$E_{appl} = E + iR_u$$

7

It is possible to compensate for or suppress R_u, by convolutive (semi integral) methods or inclusion of positive feedback circuitry within the potentiostat, to give but two examples.

As stated above, in the three electrode system current flow through the r.e. should be negligible thus leaving it unpolarised and stable. For these conditions to be successfully applied, the reference electrode must meet certain requirements:

1   The redox process taking place within the r.e. must be reversible and obey the Nernst equation.

2   The potential must not change with time or temperature and the resistance of this component must be fairly high.

3   It must not cause contamination of or be contaminated by the test solution (in practice a salt bridge between the r.e. solution and the w.e. solution compartment is usually employed).

During this research the reference electrode of choice was Ag/AgCl. The Ag/AgCl reference is kept in a separate compartment in a CH_2Cl_2 solution of $[Bu_4N][BF_4]$ (0.45 moldm^{-3}) and $[Bu_4N][Cl]$ (0.05 moldm^{-3}). In a small number of cases a Pt or Ag "pseudo reference" electrode was employed when other experimental requirements rendered use of a normal reference electrode unfeasible. In every case the reference electrode was standardised against ferrocene (at +0.55 V for Ag/AgCl). Potentials measured using pseudo reference electrodes were

subsequently corrected to correspond to the potential versus the Ag/AgCl reference electrode.

In all experiments Pt was used for the w.e. (due to its stability over a wide potential range) and c.e. (for which an inert material, ideally of low impedance, is required). In voltammetric studies the surface area of the c.e. was far greater than that of the w.e., the working electrode being a microelectrode disc, typically of diameter 1 mm, set into soft glass.

1.3 Solvent

There are a number of factors to consider when selecting a solvent suitable for electrochemical experiments. These are: sample solubility and stability, usable potential range, dielectric constant, accessible temperature range, vapour pressure, toxicity, donor or coordinating properties and ease of purification. In this work the most commonly used solvent was dichloromethane, although tetrahydrofuran, acetonitrile, acetone and dimethylformamide were occasionally employed.

1.4 Supporting Electrolyte

The supporting electrolyte is used primarily to raise the conductivity of the solution. It is employed in concentrations between 0.1 and 0.5 M to reduce the resistance between w.e. and c.e. and hence minimize errors in potential measurement

due to uncompensated solution resistance, R_u. The electrolyte also governs the structure of the double layer at the electrode solution interface, and the vast excess of electrolyte over the test species ensures that mass transport of the test species will be diffusion controlled.

A good electrolyte should be electrochemically stable over a wide potential range, readily soluble in the chosen solvents and fairly easy to prepare and purify. Additionally, the electrolyte should not react with the species under study. In the course of this research the only supporting electrolyte used was $[nBu_4N]^+[BF_4]^-$, with concentrations varied according to solvent (0.5 M for dichloromethane, 0.2 M for tetrahydrofuran or acetone, 0.1 M for acetonitrile or dimethylformamide).

1.5 Cell Design

There are a number of requirements for a good electrochemical cell:

1   It should have as low a resistance as possible, particularly when using organic solvents or high currents. In order to achieve this, the electrodes should be reasonably close to each other with (for voltammetric studies) the working electrode kept small so that all points on the w.e. surface are effectively the same distance from the much larger counter c.e.

2.   A symmetric electrical field should be established at the w.e by optimisation of the electrode geometry.

3. It must be possible to control the cell temperature.

4. The cell must be well protected from the surrounding environment (atmospheric oxygen, moisture etc.)

5. It should be designed for easy assembly and dismantling.

6. It should be possible to separate w.e. and c.e. for electrosynthetic and coulometric studies (in this work a different cell design is employed).

Typical cells for conventional (voltammetric, polarographic) electrochemistry and bulk electrogeneration are shown in Figures 1.2 and 1.3 respectively. The main difference between the cells is that the cell for bulk electrogeneration has the w.e. and c.e. compartments separated by a glass frit. The frit permits good electrical contact but prevents easy migration of chemical species between the compartments. Thus species generated at w.e and c.e during electrosynthesis are isolated.

1.6 Electrochemical Techniques

Prior to discussing the practical techniques it is necessary to define the terms commonly used to describe charge transfer processes. The definitions assume that the redox process concerned is chemically reversible (ie. the species under study does not undergo a chemical reaction as a result of the electrically induced charge transfer).

1. Reversible: The electron transfer process to or from the electrode occurs more rapidly than the rate of diffusion of the redox active species to the w.e.

Figure 1.2 Typical cell design for conventional electrochemistry

Key

C: Counter electrode
W: Working electrode
R: Reference electrode
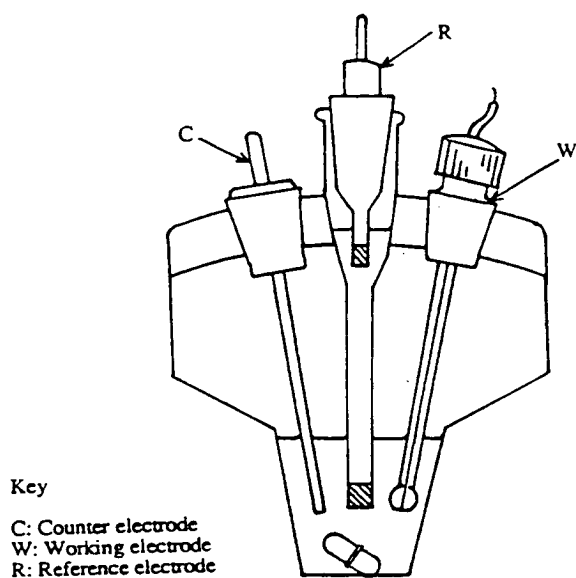
Figure 1.3 Three compartment cell for electrosynthesis

12
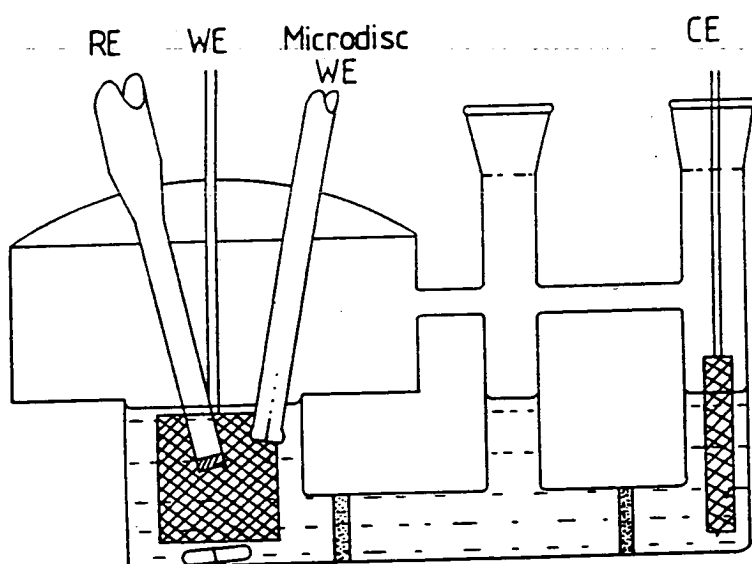
surface. This is also known as a Nernstian process because it is under these conditions that the Nernst equation applies:

$$E - E^{0'} = (RT/nF) \ln(C_O / C_R)$$

F is Faraday's constant; R is the universal gas constant; T is the temperature in Kelvin; C_O and C_R are the concentrations of the oxidised and reduced species respectively; E is the potential at the w.e.; $E^{0'}$ is the "standard potential" of the redox reaction, and n is the number of electrons passed in the charge transfer process.

2. Quasi-Reversible: The charge transfer process occurs at a rate comparable to the rate of diffusion, thus electron transfer is influenced by both charge transfer and diffusion kinetics.

3 Irreversible: The charge transfer process is considerably slower than the diffusion rate.

Another interesting case occurs when the charge transfer process is rapid but the product species undergoes further reaction at a rate comparable to or faster than the timescale of the electrochemical experiment. In this case, "partially reversible" behaviour will be observed.

It is also necessary to define the standard terms used to describe mass transfer in solutions.

1. Migration: Movement of a charged body under the influence of an electric field.

2. Diffusion: Movement of a species under the influence of a gradient of chemical potential (i.e. a concentration gradient).

13

3. <u>Convection</u>: Stirring (forced convection) or hydrodynamic transport (natural convection, generally caused by density gradients).

1.6.1 <u>Cyclic Voltammetry</u>

In cyclic voltammetry stationary electrodes are employed in "quiet" (unstirred) solutions. The large excess of supporting electrolyte in solution, the carefully selected scan rate and the thermostatically controlled cell ensure that convection and migration effects are effectively eliminated for the species under study, leaving diffusion as the means of mass transport between the bulk solution and the solution/electrode interface.

With respect to time, the potential is varied in a linear fashion, the scan rate, v, usually lying in the range 20 - 500 mVs^{-1}. The current, i, is recorded as a function of the potential, E.

A typical cyclic voltammogram for a reversible process is shown in Figure 1.4. The current response is of an asymmetric peaked form. In the forward potential sweep, as E approaches $E^{0'}$, reactant close to the electrode starts to be consumed and a current starts to flow. As the potential continues to sweep towards $E^{0'}$ depletion of reactant at the w.e. induces diffusion of more reactant to the surface. The concentration of reactant at the electrode surface falls to almost zero as E passes $E^{0'}$ therefore reactant flux reaches a maximum, then falls off as depletion becomes more widespread. As a result, the observed current rises sharply as the

potential approaches $E^{0'}$, reaches a maximum shortly after $E^{0'}$ then falls as reactant depletion becomes more widespread with a consequent reduction in diffusion toward the electrode surface. Beyond the peak the latter of these effects dominates.

Upon reaching a pre-set value, the "switching potential", the voltage sweep commences its return to the starting value using the same scan rate, v, as in the forward scan. The reversal current has a shape much like that of the forward peak but in the opposite direction. The position of the peak of the reverse wave is not at the same potential as the forward peak, being shifted in the direction of the starting potential.

The most interesting parameters obtained from the cyclic voltammogram are the peak current and the potential at the maximum of the forward curve, i_p^F and E_p^F respectively, and the corresponding parameters for the return curve (i_p^R and E_p^R). By measuring these parameters for a number of scan rates we can determine the nature of the charge transfer process as shown in Table 1.1.

Consider the forward scan of a Nernstian reductive process. Equations for the determination of E_p^F and i_p^F may be written as follows:

$$E_{1/2} = E^{0'} + (RT/nF)\ln[(D_O/D_R)^{1/2}]$$

Usually D_O/D_R is close to unity, therefore $E_{1/2} \approx E^{0'}$.

$$E_p^F - E_{1/2} = E_p^F - E^{0'} + (RT/nF)\ln[(D_O/D_R)^{1/2}]$$

$$= -1.109(RT/nF)$$

At 298 K,

$$i_p^F = (2.69 \times 10^5)n^{3/2}AD_O^{1/2}v^{1/2}C_O*$$

where i_P^F is in amperes, n is the number of electrons involved in the charge transfer process, A is the surface area of the w.e. (in cm^2), D_O and D_R are the diffusion coefficients of the oxidised and reduced species respectively (cm^{2}sec^{-1}), v is the scan rate (Vsec^{-1}) and C_O^* is the initial concentration of the oxidised species. At 298 K the peak potential is 28.5/n mV beyond $E_{1/2}$ and is independent of scan rate.

Figure 1.4   Typical cyclic voltammogram for a reversible process
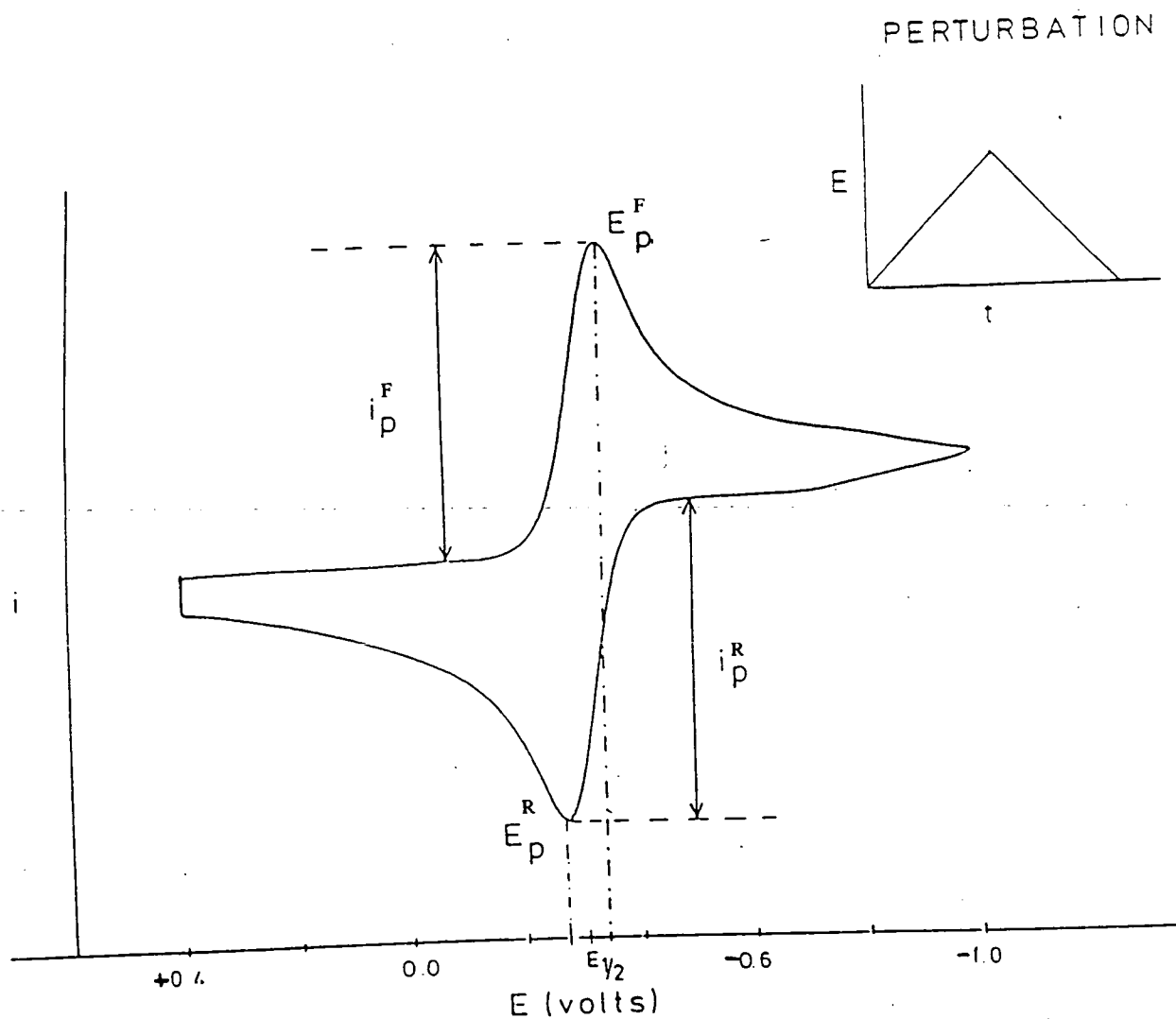
Table 1.1: Cyclic voltammetric criteria for reversible, quasi-reversible, partially reversible and irreversible charge transfer processes at 298K

Reversible

E_P independent of v

$E_P^F - E_P^R = 59/n$ mV, independent of v

$1/2[E_P^F + E_P^R] = E_{1/2}$, independent of concentration

$i_P /v^{1/2}$ is independent of v

$i_P^R /i_P^F = 1$ and is independent of v

Quasi-reversible

E_P shifts with v

$E_P^F - E_P^R$ increases as v increases

$i_P/v^{1/2}$ is not independent of v

i_P^R /i_P^F generally $= 1$

Partially reversible

E_P increases by $30/n$ mV for a ten fold increase in v, at low v

$i_P /v^{1/2}$ is not independent of v

$i_P^R/i_P^F < 1$, increases as v increases

Irreversible

E_P shifts with v

$i_P /v^{1/2}$ is not independent of v

There is no current on the reverse scan

v = scan rate in mVs^{-1}

n = number of electrons involved in the redox process

1.6.2   Voltammetry in a stirred solution

In order to determine if a redox process involves oxidation or reduction of the test species stirred linear voltammetry is often used. Figure 1.5 shows typical stirred and unstirred voltammograms for a reversible charge transfer process. By convention, processes with current traces above the $i = 0$ line are reductions and those below are oxidations. In this type of voltammetry the mass transport occurs by diffusion and convection. Typically a scan rate of 20 mVs^{-1} is used in stirred voltammetry. The diffusion limited current, i_d, is proportional to n, the number of electrons involved in the charge transfer process. A rotating disc electrode, although not employed in the work described in this thesis, is the most efficient method of applying this technique.

1.6.3   Alternating Current Voltammetry

Alternating current (a.c.) voltammetry involves the superposition of a small sinusoidally alternating potential upon a linear d.c. scan. The frequency of the alternating potential, ω, is typically in the range 10 - 100 Hz. Since the superimposed voltage is usually sinusoidal in nature an alternating current flows in addition to the d.c. response. The net alternating current component is recorded as a function of the linear d.c. potential. For a reversible redox process the output current signal recorded is a symmetric peak centred upon $E_{1/2}$ of the corresponding

d.c. polarogram, as shown in Figure 1.6. In the case of a.c. voltammetry the maximum current observed when studying a reversible process is proportional to the square of the number of electrons involved in the charge transfer process:

$$i_P = (n^2 F^2 A \omega^{1/2} D_O^{1/2} C_O * \ddot{A}E)/(4RT)$$

The above equation assumes that the amplitude, ΔE, of the a.c. component is less than $10/n$ mV.

Figure 1.5 Typical stirred and unstirred voltammograms
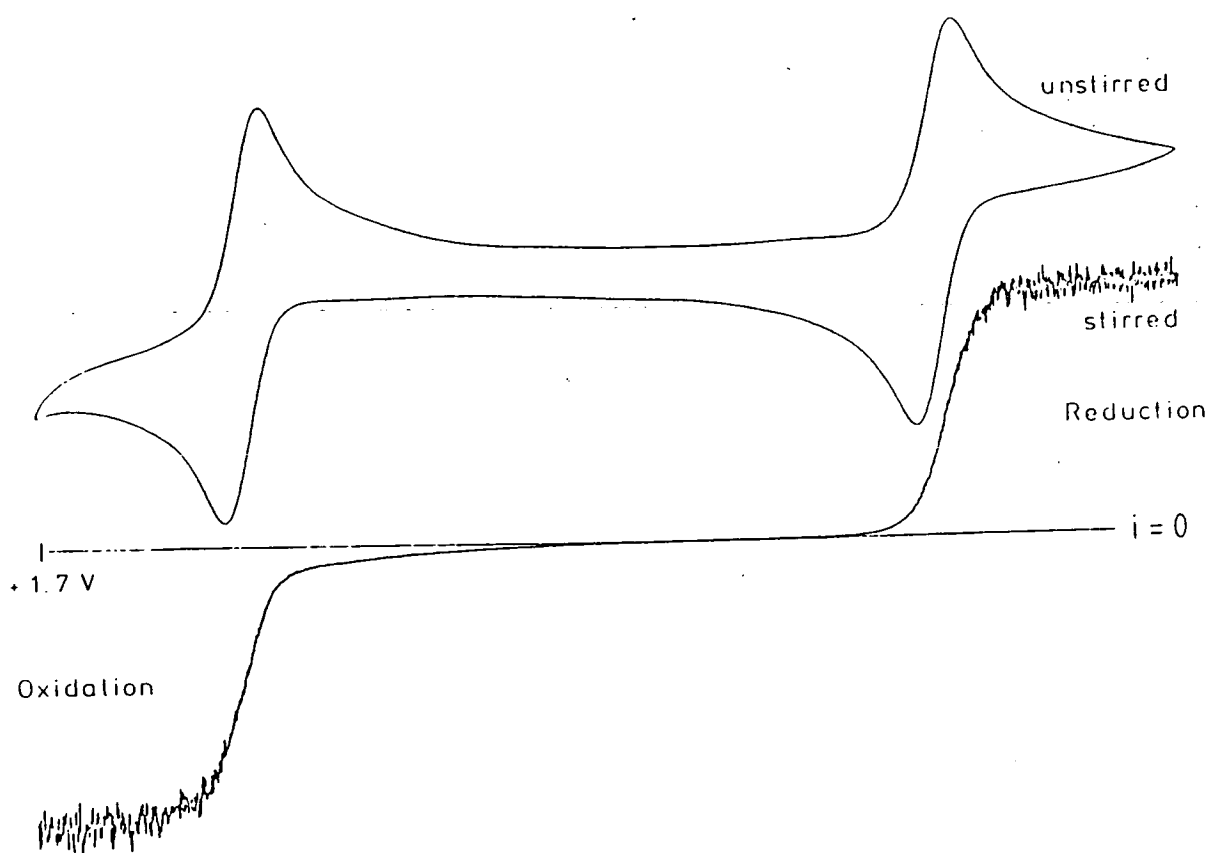
In a simple model, if the cell is considered as a capacitor-resistor network to which the sinusoidal voltage superimposed on a linear potential ramp is applied, the shape of the a.c. wave follows by considering it as the "first derivative" of the d.c. wave. However, it would be misleading to regard the a.c. voltammogram as merely a first derivative representation (although the first derivative analogy is useful for describing the shape of the wave). The a.c. experiment provides additional information via the new variable, ω, which effectively controls the "timescale" of the experiment thus making the experiment a more sensitive test of reversibility than the d.c. mode. Also, the "first derivative" model fails to explain the dependence of peak height on the frequency of the a.c. voltage.

Figure 1.6 Typical a.c. voltammogram for a reversible process
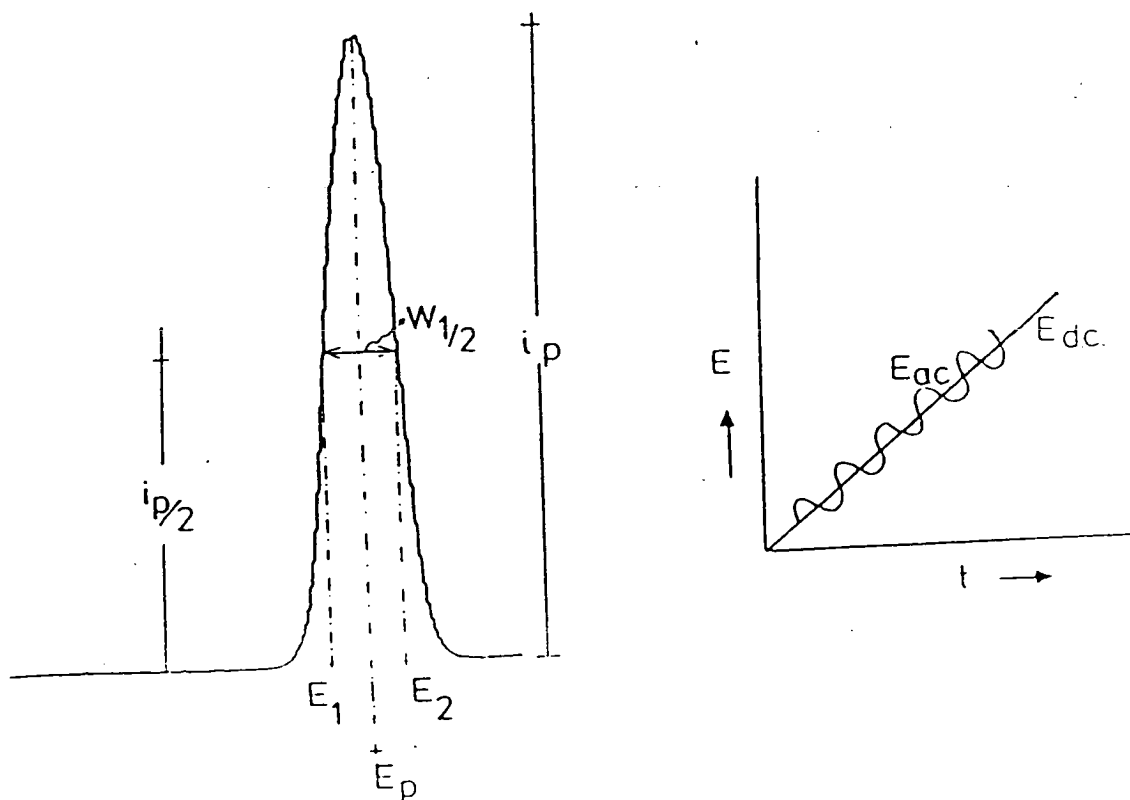
Under normal operating conditions a.c voltammetry will discriminate against "residual" background or capacitative current. This occurs because of the differing phase relationships which the two current components, faradaic and capacitative currents, have with respect to the applied voltage. Thus by phase sensitive detection, the faradaic current can be measured exclusively, with a consequent increase in sensitivity (making concentrations of 10^{-6} - 10^{-7} M detectable, while the d.c. techniques operate with concentrations of 10^{-4} - 10^{-6} M).

A further advantage of a.c. voltammetry is that it is possible to resolve waves which are separated by as little as 40 mV (150 mV separation is required for d.c. voltammetry).

Reversibility criteria for a.c. voltammetry:

(i) E_P is independent of ω; $W_{1/2}$ = 90/n mV at 298 K and is independent of ω.

(ii) A plot of i_P versus $\omega^{1/2}$ gives a straight line through the origin.

1.6.4   Electrosynthesis - Coulometry

Preparative scale electrosyntheses fall into two classes:

(i) Controlled current (galvanostatic)

(ii) Controlled potential (potentiostatic)

The latter method was the only one employed during the course of this research. In potentiostatic electrosynthesis a constant potential, selected to induce electrochemical reaction of the species under study, is maintained at the w.e.

throughout each electrogeneration. Effectively, for a reaction to go to completion, the fixed potential must be more than 60 mV beyond $E_{1/2}$.

The currents passing through the solution are relatively large as the surface area of the w.e. is considerably greater than for voltammetric studies (in order to minimise the timescale of the experiment). The w.e. and c.e. must be separated otherwise any products formed at the c.e. might cause interfering reactions at the working electrode.

The current is measured as a function of time, with the solution stirred throughout the experiment. A typical example of the resultant i versus t graph is shown in Figure 1.7. The area under the curve gives the total amount of electrical charge, Q, passed during the experiment. Thus, from an electrosynthetic experiment, assuming 100% efficiency, we can determine n, the number of electrons involved in the redox process, by using the equations below:

$$Q = \int_0^t i\, dt$$

and $Q = nFM.$

where n = number of electrons, M = number of moles of product and F = Faradays constant.

Figure 1.7 Typical current-time response for controlled potential electrolysis

Time

current
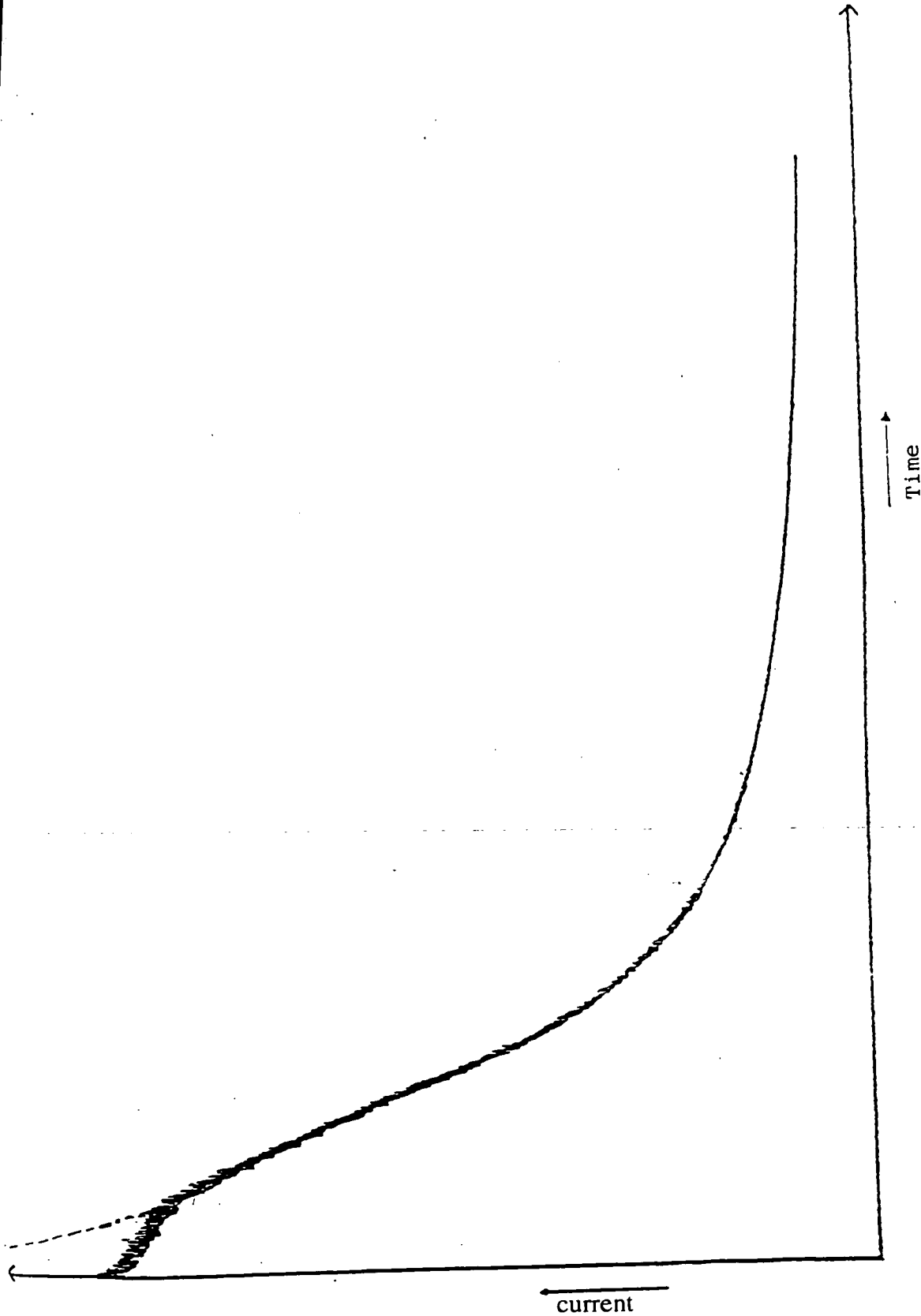
1.6.5   Spectroelectrochemistry

While many electrosyntheses are carried out primarily to investigate the number of electrons involved in the redox process, it is often desirable to study the products of the electrogeneration. This is usually achieved using spectroscopic means. The need to study the electrogenerated species is especially acute in cases where the species under study has more than one redox active centre, or in cases where electrosynthesis has been used to induce a chemical reaction.

Often, however, the species generated are highly sensitive to air, moisture, heat or other agencies of decomposition, hence transferring the electrogenerated species from electrochemical cells to spectroscopic cells and subsequent transfer to the spectrometer can often result in decomposition of the species one wishes to study. In order to eliminate such problems various spectroelectrochemical techniques have been developed. Spectroelectrochemistry is essentially electrosynthesis carried out within the cavity of a spectrometer.

A spectroelectrochemical cell is thus a coulometric three electrode cell which has been designed to meet the requirements (geometric etc.) of a particular form of spectroscopy. In the following sections a number of spectroelectrochemical cells are breifly discussed.

1.6.5.1   Electronic Absorption Spectroelectrochemistry

A suitable cell for UV/visible/NIR spectroelectrochemistry has two dominant requirements:

1   It should be possible to perform rapid electrogeneration within the light-beam path of the spectrophotometer (ie. the working electrode must lie in the beam path and have a large surface area).

2   The working electrode must not significantly affect the spectra recorded (ie. the w.e. must be transparent).

It was with these requirements in mind that the Optically Transparent Electrode (OTE) cell was designed and built within the department[15] (Figure 1.8), adhering to the principles reported by Murray *et al*[16].

The working electrode is made of fine platinum gauze (reinforced with 10% rhodium), which allows incident light to pass through (the small reduction in transmittance is dealt with by background correction) while providing sufficient surface area to handle large currents. The short path length of the quartz cuvette (typically 0.5 mm) also facilitates rapid electrogeneration. The c.e. and r.e. are separated from the bulk solution by glass frits, their compartments being held in the upper reservoir of the cell.

The cell assembly locates within a gas tight, double glazed PTFE cell block. A constant flow of nitrogen is passed between the inner windows, ensuring exclusion

Figure 1.8 Schematic of OTE cell
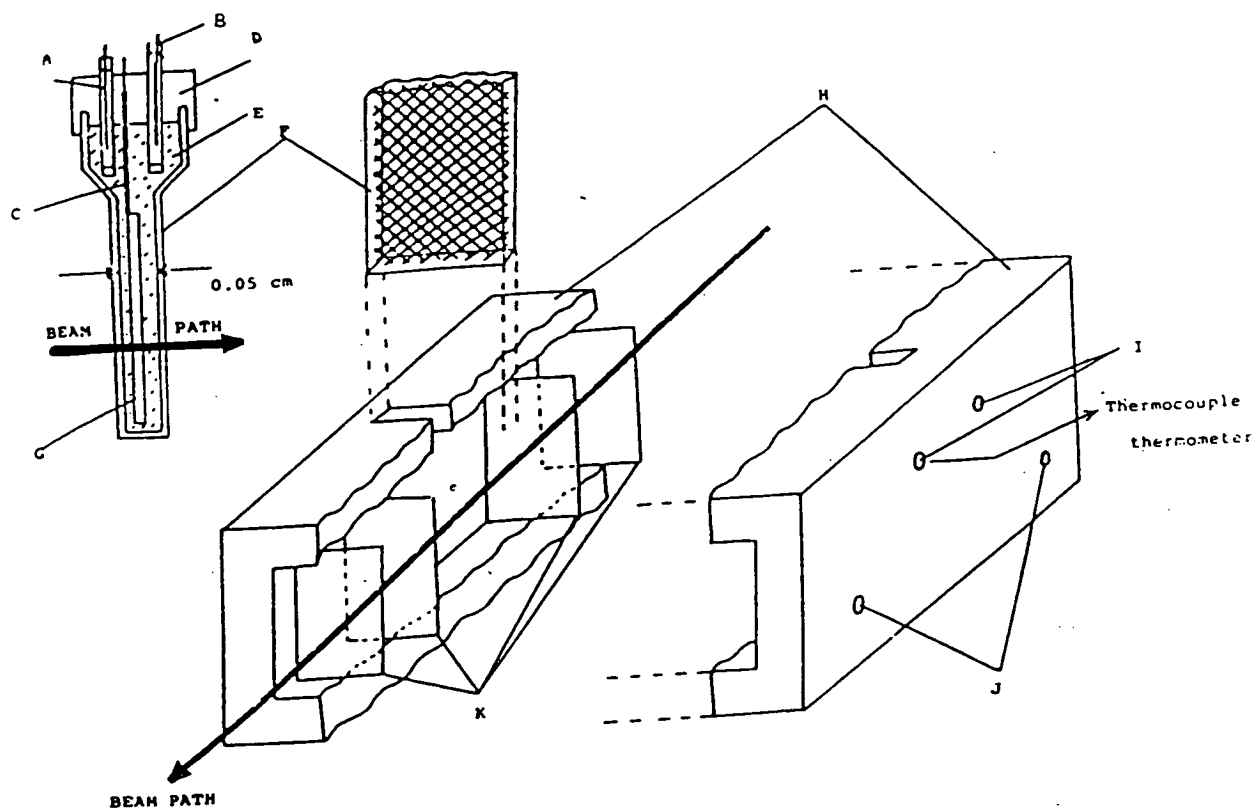
A Counter Electrode

B Reference Electrode

C Working Electrode connection protected from bulk
   solution by PTFE sleeve

D PTFE cell cap

E Test solution, deoxygenated with Ar or N_2

F 0.05 cm Infrasil Quartz cell containing platinum
   grid working electrode

G Platinum grid working electrode

H PTFE cell block

I Variable Temperature nitrogen inlet ports

J Dry nitrogen inlet ports (to prevent fogging of
   inner quartz windows)

K Infrasil Quartz cell block windows

of oxygen and moisture from the spectrophotometer cavity while also providing an efficient means of controlling the temperature (by the simple expedient of precooling the incoming nitrogen). At low temperatures, fogging of the quartz windows is prevented by passing dry nitrogen gas (at room temperature) between the inner and outer windows. The facile temperature control permitted by the cell block is a unique feature of the Edinburgh design.

There are two common types of spectroelectrochemical experiment conducted using the OTE cell:

1   Select one potential and record a series of spectra as a function of time until the electrosynthetic reaction achieves equilibrium.

2   Select a series of potentials (progressing from one side of $E_{1/2}$ to the other) and allow the system to equilibrate at each potential before recording the spectrum. From this type of experiment it is possible to determine the $E_{1/2}$ value by application of the Nernst equation:

$$E = E^{0\text{'}} + (RT/nF)\ln(C_O/C_R)$$

Experimentally, C_O/C_R is equal to the absorbance ratio, $r(\varepsilon)$:

$$r(\varepsilon) = [A(E) - A_R]/[A_O - A(E)]$$

Where $A(E)$ is the absorbance at a chosen wavelength at the applied potential E, A_R is the absorbance at that wavelength of the fully reduced species and A_O the corresponding absorbance of the fully oxidised species.

From the above it can be seen that a plot of E versus ln r(ε) will, for a Nernstian system, give a straight line of gradient RT/nF, and an intercept, when r(ε) = 0, corresponding to $E_{1/2}$.

In the case of Electronic Absorption Spectroscopy, finding a suitable supporting electrolyte is not usually problematic as there are a considerable number of supporting electrolytes (including Bu_4NBF_4, the electrolyte used throughout this work) which do not absorb significantly at energies lower than 50000 cm^{-1}.

When carrying out spectroelectrochemical experiments, it is important (unless the electrogeneration is employed as a deliberate means of inducing chemical reaction) to reverse the electrogeneration to reproduce the starting species as a test of reversibility; succesful regeneration of the starting spectrum being good evidence that a simple, one step, electrogeneration is involved.

An example of the results obtained with the OTE cell is shown in Figure 1.9. This shows the reduction of tetracyanoethylene (tcne), in dichloromethane, at a constant potential of +0.2 V relative to the Ag/AgCl reference. In this example, reduction induces collapse of the π-π* bands at 37000 and 39000 cm^{-1}, with corresponding growth of bands at 25000 cm^{-1} and above 45000 cm^{-1}. The isosbestic points at 35000 and 43000 cm^{-1} indicate that there were no intermediates formed which absorbed at these energies and suggest that reduction of tcne is a simple one step process, with no subsequent reaction of the reduction product.

Figure 1.9 Absorption spectral monitoring of reduction of tcne to tcne⁻ in CH_2Cl_2 at 240 K, E_{app} = +0.2 V vs Ag/AgCl.
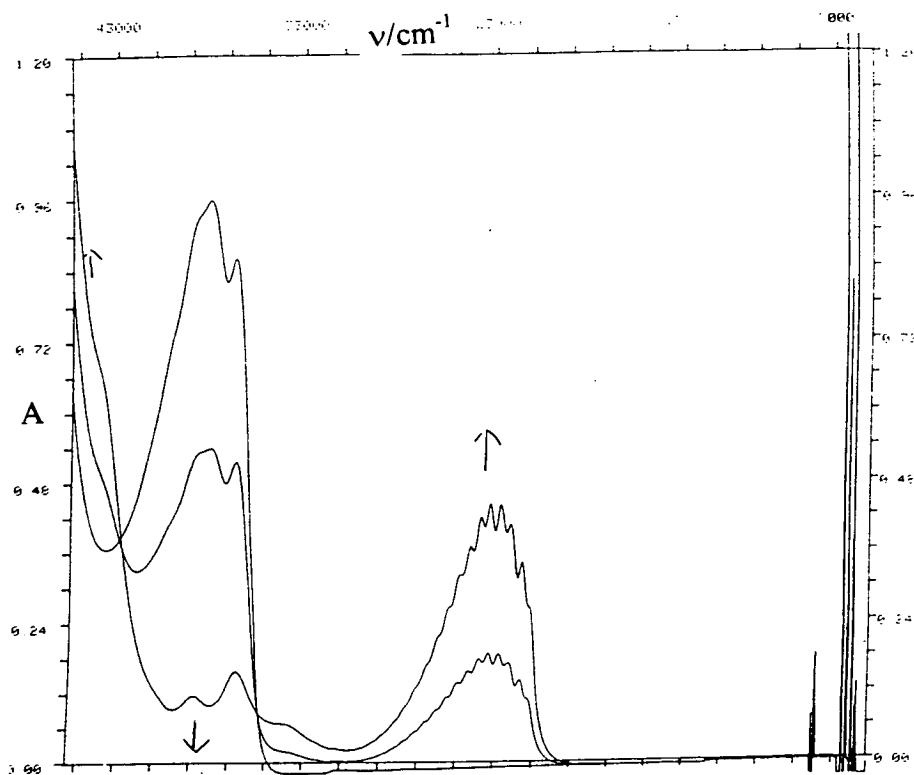
1.6.5.2 Vibrational Spectroelectrochemistry

Many of the requirements for an *in situ* electrosynthetic cell suitable for IR spectroscopy are similar to those which led to the design of the OTE cell. This is reflected in the design of the Transparent Infra Red Thin Layer Electrode (TIRTLE) cell (Figure 1.10), developed within the Department of Chemistry at Edinburgh University[17]. In addition to the requirements listed in 1.6.5.1, another important consideration is that the effectiveness of IR spectroelectrochemistry is greatly enhanced by use of a Fourier Transform Pulse IR spectrometer.

The TIRTLE cell is a "sandwich" design, with the significant differences from the OTE cell design arising from the differing geometrical restrictions of the IR spectrometer cavity and the difficulties working with common IR cell materials such as NaCl. The physical restrictions result in a much smaller reference electrode (a silver wire "pseudo reference" is often used but this can be given a chloride coating to make a miniaturised Ag/AgCl reference).

In the case of IR spectroelectrochemistry choice of supporting electrolyte is an important factor to consider as all common electrolytes will absorb somewhere in the IR spectral region. As the electrolyte is present in a far higher concentration than the species under study this naturally means that there will be areas of the spectrum from which it will be impossible to obtain any information. In practice, this limits the range of species suited to study to species with strong bands in relatively clear regions of the spectrum, such as carbonyl or cyano compounds.

1.6.5.3   EPR Spectroelectrochemistry

Many oxidations and reductions are one electron processes, therefore either the starting material or the product will have an unpaired electron. As a result, epr spectroelectrochemistry is a particularly important technique for study of the frontier orbitals of redox active materials.

The design requirements for an electrochemical cell for use in an epr spectrometer are very different to those for UV/visible/NIR and vibrational spectroscopy. In addition to the obvious geometric restrictions of an epr tube, the

Figure 1.10 Schematic of the TIRTLE cell

WE ——————
RE ——————
CE ——————

NaCl Block ——————

Path length of cell ≈ 0.1 mm

1 cm

CLAMPING AND SPRING MECHANISM

TEFLON ——————
RUBBER ——————
STEEL ——————
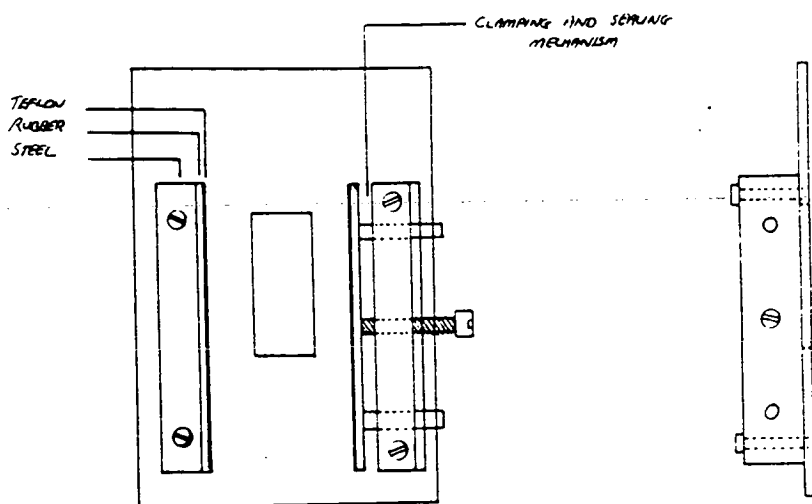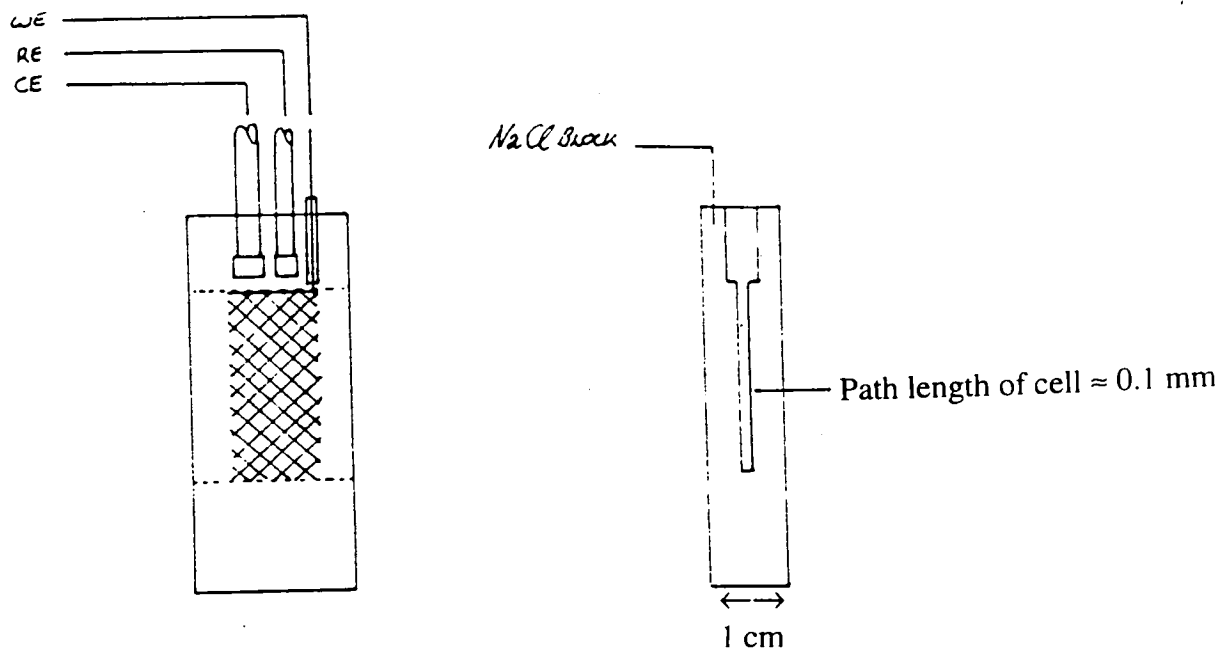
electrodes must not significantly interfere with the signal obtained from any epr active species formed or decomposed during the electrosynthesis.

These restrictions resulted in the design shown in Figure 1.11 for the Electron Paramagnetic Resonance *in situ* Electrochemical (EPRESISE) cell[18], initially designed within the Department of Chemistry, University of Edinburgh[19].

In this case the most effective design for the w.e was found to be a hollow Pt cylinder. The Pt counter electrode is kept in a separate compartment as before. The r.e. was a silver wire (with chloride coating if desired) running down the centre of the w.e. and insulated from the w.e. by a PTFE sleeve. A cooled supply of N_2 gas is employed to protect the generated species and enable variable temperature studies to be carried out in the range from 100 K to room temperature. In order to accommodate the cell, a wide bore EPR cavity is employed.

The cell design has important consequences in terms of tuning the epr cavity. In particular, it is appreciated that recording spectra with the EPRESISE cell is unlikely to allow the spectrometer to be tuned to the first standing wave, as a result of the increased cell diameter. This does not, however, cause any significant changes in the recorded spectra, therefore results obtained with the EPRESISE cell may be treated similarly to spectra recorded using conventional cells.

As a result of its large diameter, the cylindrical tube used was (with our spectrometer) only suited to the recording of anisotropic spectra, therefore the typical procedure was to carry out the electrosynthesis at temperatures of 230 - 250 K then freeze the solution in order to record the spectrum.

Figure 1.11 Schematic of the EPRESISE cell

Ag reference electrode

Insulation

Cylindrical Pt working electrode
diameter = 3 mm

Quartz EPR tube, outer diameter = 6 mm, inner = 4 mm

Glass frit

Quick-Fit B10 joint

Ag counter electrode
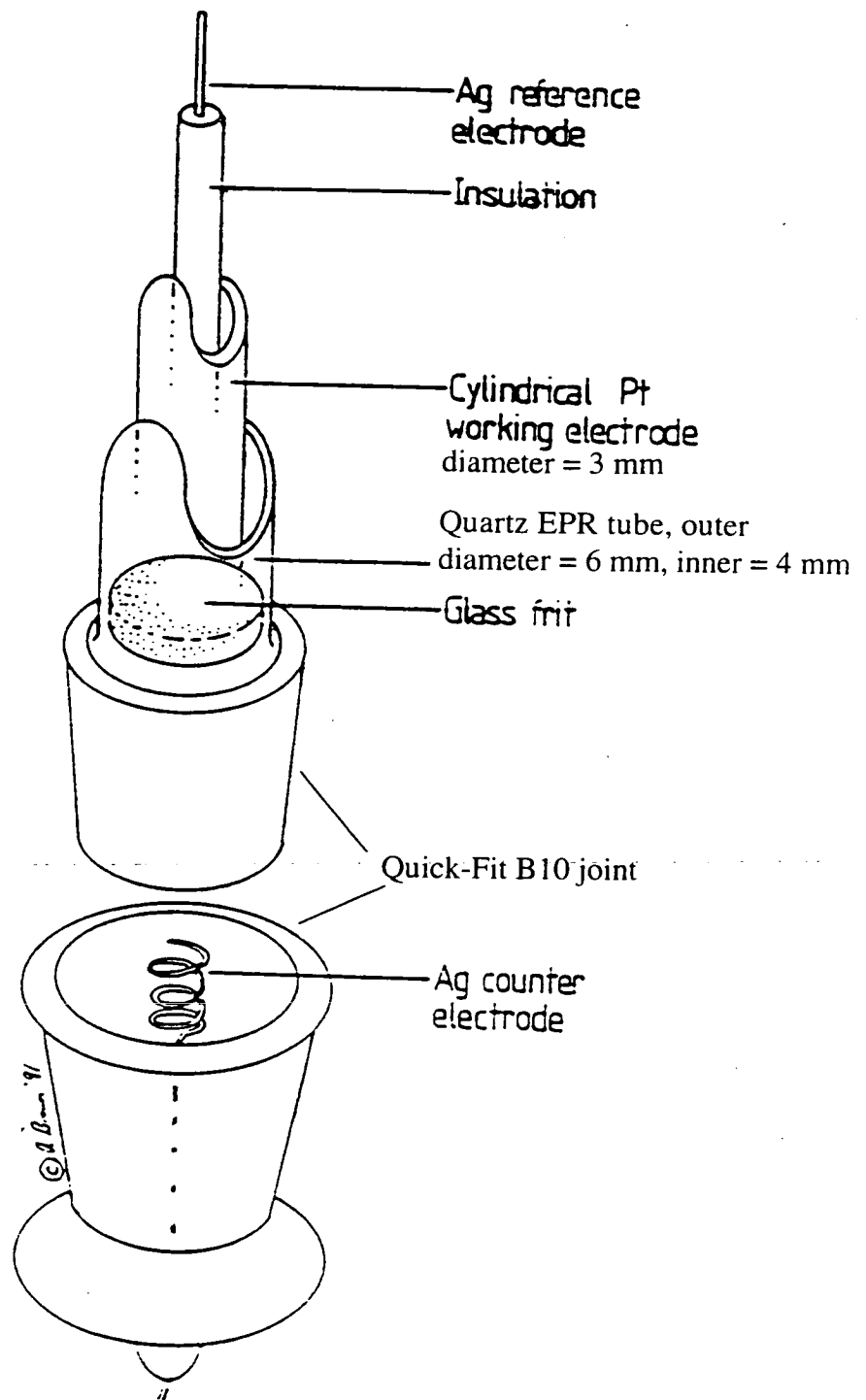
1.7   References

1. J. F. Hunsberger, *Handbook of Chemistry and Physics, 59th Ed'n*, CRC Press, **1978**, D-193.

2. P. W. Atkins, *Physical Chemistry*, 3rd Ed., Oxford University Press, **1986**.

3. D. F. Shriver, P. W. Atkins and C. H. Langford, *Inorganic Chemistry, 2nd Ed.*, Oxford Univesity Press, **1994**.

4. G. A. Heath, L. J. Yellowlees and P. S. Braterman, *J. Chem. Soc. Chem. Commun.*, **1981**, 287.

5. L. J. Yellowlees, PhD thesis, University of Edinburgh, **1982**.

6. C Creutz and N. Sutin, *Inorg. Chem.*, **1976**, 15, 496.

7. B. Durham, W. J. Dressick and T. J. Meyer, *J. Chem. Soc. Chem. Commun.*, **1979**, 381.

8. U. Laschish, M. Ottolenghi and J. Rabani, *J. Am. Chem. Soc.*, **1977**, 99, 8062.

9. V. Balzani, F. Bolletta, M. T. Gandolfi and M. Maestri, *Top. Curr. Chem.*, **1978**, 75, 1.

10. J. E. Huheey, *Inorganic Chemistry, 3rd Ed.*, Harper & Row, **1983**.

11. S. Otsuka, T. Yamanaka, *Metalloproteins, Chemical Properties and Biological Effects*, Elsevier, **1988**.

12. T. Yamanaka, *Advan. Biophys.*, **1972**, 3, 227.

13. R. P Ambler, M. Daniel, J. Hermoso, T. E. Meyer, R. G. Bartsch and M. D. Kamen, *Nature*, **1979**, 278, 659.

14. R. Haser, M. Pierrot, M. Frey, F. Payon, M. Bruschi and J. Le Gall, *Nature*,

1979, 282, 806.

15. V. T. Coombe, PhD thesis, University of Edinburgh, **1985**.

16. W. R. Heinemann, R. W. Murray and G. W. O'Dom, *Anal. Chem.*,

1969, 39, 1666.

17. L. J. Yellowlees, unpublished results, **1992**.

18. S. A. Macgregor, E. McInnes, R. J. Sorbie and L. J. Yellowlees,

Molecular Electrochemistry of Inorganic, Bioinorganic and Organometallic

Compounds, A. J. L. Pombeiro and J. A. McCleverty (eds),

Kluwer Academic Publishers, **1993**, 503.

19. M. R. Low, PhD thesis, University of Edinburgh, **1987**.

The following works were also referred to extensively in the preparation of this introductory chapter.

A. J. Bard and L. R. Faulkner, *Electrochemical methods, Fundamentals and Applications*, Wiley, **1980**.

J. Koryta, J. Dvorak and L. Kavan, *Principles of Electrochemistry, 2nd Edition*, Wiley, **1993**.

2 Tetracyanoethylene and Tetracyanoquinodimethane Complexes of Ruthenium and Osmium

2.1 Introduction

Tetracyanoethylene (tcne) was discovered in 1956 by Cairns and McGee of Du Pont[1], while tetracyanoquinodimethane (tcnq) was first reported in 1960 by Acker et al[2]. The structure of tcne is given in Figure 2.1.[3], that of tcnq in Figure 2.2.[4]

Tcne and tcnq are readily reduced to form radical anions, the additional electron entering a π* LUMO. Reduction of these molecules is sufficiently facile that they readily form brightly coloured charge transfer complexes with electron-rich aromatic compounds such as hexamethylbenzene and naphthalene. Conducting polymeric charge transfer complexes of tcnx (x = e, q) with tetrathiafulvalene (ttf) and its derivatives have also been reported, ttf-tcnq for example showing conductivity similar to that observed in graphite[5].

There have been a considerable number of metal - tcnx species reported in the literature, revealing a wide variety of interactions between the tetranitrile ligand and the metal centre. A brief overview, giving a small number of examples of each reported type of reaction between tcnx and metal centres is given below. Further information regarding the coordination chemistry of tcne and tcnq is available in a recent review by Kaim and Moscherosch[6].

Figure 2.1 Structure of tetracyanoethylene, showing bond lengths (in angstroms) and angles (in degrees) as quoted in reference 3.
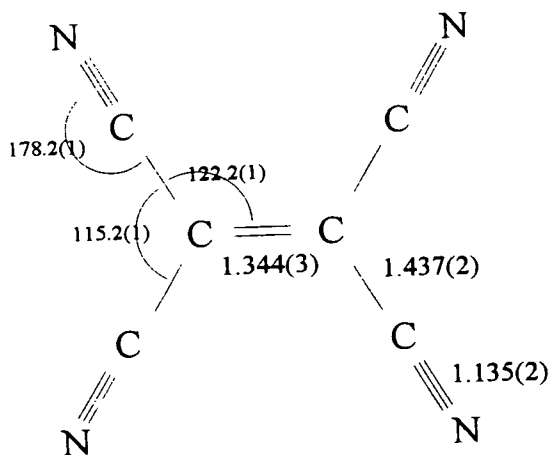
Figure 2.2 Structure of tetracyanoquinodimethane with data quoted from reference 4.
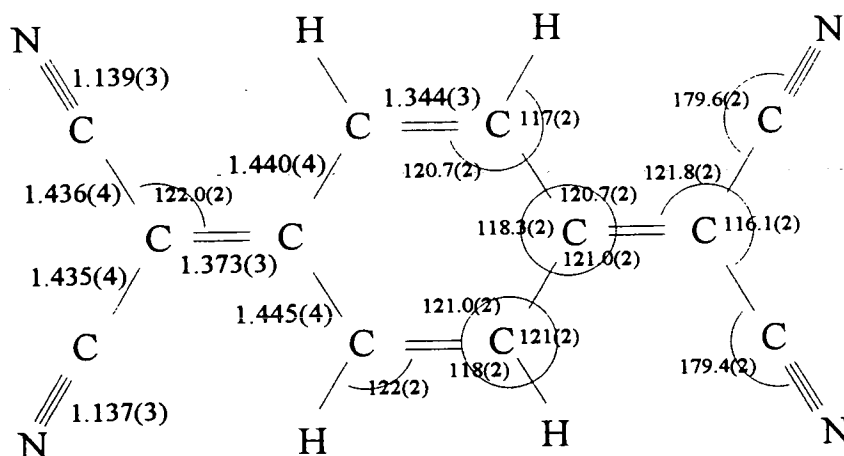
2.1.1   Salt Formation

Tcnx, being readily reduced, may act as a counter ion following electron transfer from a metal centre to give M^+tcnx^-. Examples reported in the literature include salts of alkali metals (Li^+ [tcnq]$^-$ has been used as a standard in epr spectroscopy[7]).

Transition metal salts of tcnx are well known. Kathirgamanathan and Rosseinsky, for example, have carried out conductivity studies on a considerable range of transition metal salts of tcnq[8]. The species tested included salts such as $Fe_2(tcnq)_3.5H_2O$, $Mn(tcnq).2/3MeCN$ and $Ni_2(tcnq)_3.6H_2O$, which include $(tcnq)^{2-}$; and salts of relatively unreactive transition metals such as $Ag(tcnq)$. Interestingly, single crystals of $Cu(tcnq)$ were found to exhibit conductivity comparable to that observed for metals ($784 \ \Omega^{-1}cm^{-1}$)[8].

The cobaltocinium salt of tcne, $[(Cp)_2Co]^+[tcne]^-$ has been reported[9]. A more impressive indication of the π-acidity of the tetranitriles is given by reports of $[Co(Cp^*)_2]^+_2[tcne]^{2-}$, in which the dianion of tcne has been formed by the relatively mild reducing agent[10].

An interesting group of tcnx salts are those of metallocenes and related complexes of transition metals (usually 1st row) with d^5 electronic configurations. Examples of the species reported include $[Cr(C_6H_xMe_{6-x})_2][tcnq]$ (x = 0, 3, 6)[11], $[Mn(Cp^*)_2][tcnq]$[12] and $[Fe(C_5Et_5)_2][tcnx]$ (x = e, q)[13]. All of these salts exhibit ferromagnetic coupling of the metal centres and many show "low dimensional"

packing effects, in which...[D][A][A][D][D][A][A][D]... is a common structural motif (where [D] is the electron donating metal complex and [A] is the electron accepting tetranitrile). Diamagnetic coupling of radical anion pairs is often observed[11,12]. Similar ruthenium salts have been reported, notably by Ward and coworkers, including examples in which the above structural motif is enforced by use of cyclophane ligands to link two metal centres[14].

2.1.2   Charge Transfer Complex Formation

In the case of charge transfer complex formation, electron transfer from metal to tcnx is incomplete. An example of charge transfer complex formation occurs when tcne is reacted with ferrocene, resulting in formation of [Fe(Cp)$_2$.tcne][15]. Interestingly, reaction of tcne or tcnq with decamethylferrocene results in formation of the salts [Fe(Cp*)$_2$]$^+$[tcne]$^{-(16)}$ and [Fe(Cp*)$_2$]$^+$[tcnq]$^{-(17)}$, which exhibit ferromagnetic behaviour as described in 2.1.1.

Reactions of tcne and tcnq with various species related to ferrocene have been reported in the literature, the products being salts or charge transfer complexes, depending on the electronic properties of the metal centre. Of particular interest is the tendency of these complexes to form "low dimensional solids", in which the physical properties of the species show an extremely high degree of anisotropy. Good examples of this behaviour are found in the species [(Cp*Ru)$_2$(1,4-

cyclophane)][tcnq]$_x$, x = 2 or 4, for which a number of low dimensional phases have been reported.[14,18].

2.1.3   Metal-Alkene Bound π-Complex Formation

Examples of this type have not been found for tcnq but it is the most commonly reported mode of bonding between tcne and transition metal centres. For tcne, bonding of this type is reported as involving a σ-bond from the alkene π-orbital to the metal and strong π-back bonding from the the metal to the alkene π* -orbital, as a result of the electron withdrawing -CN groups. The back bonding is sufficiently strong that the bonding may alternatively be considered to consist of σ-bonds between the metal and the two olefinic carbon atoms, forming a 3 membered chelate ring. In this mode of bonding the alkene C=C bond is considerably longer than in the free ligand, usually being of a length normally associated with C-C single bonds. Furthermore the planarity of the ligand is lost (the C-CN bonds point away from the metal atom) and therefore the facile, reversible tcne-based reduction that appears in other types of metal-tcne complex is not normally observed for the case of π-bound tcne. Examples of π-complexes reported in the literature include [IrBr(CO)(PPh$_3$)(tcne)][19], [Rh(bpy)(tcne)][20], [RuCl(NO)(PPh$_3$)$_2$(tcne)][21];   [(MeO)Ir(CO)(PPh$_3$)$_2$(tcne)][22], [Mo(≡CCH$_2$Bu^t)(η^2-tcne)(P{OMe}$_3$)(η^5-Cp)][23],   [Ni(tcne)(CN-Bu^t)$_2$][24]   and [{Ir(μ-SBu^t)(CO)(P{OMe}$_3$)}$_2$(η^2-tcne)][25]. In the examples above (where crystal

structures were reported), the "C=C" bond lengths vary from $1.476(5)^{24}$ to $1.539(17)$ Å[22]. No examples of osmium complexes exhibiting this coordination mode of tcne have yet been reported.

It is interesting to note that in recent years there have been several cases of metal-tcne complexes which were originally reported as π-bound (often on the basis of IR data) but subsequently shown to be M-N σ-complexes of the type discussed in section 2.1.4. Notable examples of such complexes include complexes of formula [(L)(CO)$_2$Mn(tcne)], where L = C$_5$H$_5$, C$_5$H$_4$Me or C$_5$Me$_5$[26,27], for which the original, erroneous, reports were published in 1968 and 1972[28].

2.1.4   Metal-Nitrogen σ-bound Complex Formation

In this mode of bonding the geometry of the ligand is generally similar to that of the free tetranitrile therefore the electronic characteristics after coordination are also similar to those of the free ligand. Complexes of this type involve σ-donation from nitrogen to the metal centre and strong π-back bonding to the tcnx π^* LUMO. In this mode of coordination, the tetranitrile ligand may be bound as the neutral ligand or the radical anion but there are cases in which the frontier orbitals have substantial contributions from metal and ligand, resulting in "intermediate oxidation states" for tcnx. Although not capable of acting as a polydentate ligand in the classical sense, tcnx may bind through its -CN groups to more than one metal centre, making formation of organometallic polymers a possibility.   "Ligand

stacking" is also reported in a significant number of cases, resulting in relatively strong intermolecular interactions in the solid state. Examples of complexes in which tcnx is bound to the metal via nitrogen include (in addition to the σ-complexes mentioned in 2.1.3 above) [Os(S$_2$PMe$_2$)$_2$(PPh$_3$)(tcne)], in which ligand and metal appear to be in "intermediate" oxidation states[29]; [{Re$_2$Cl$_4$(dppm)$_2$}$_2$(tcnq)], in which tcnq acts as a bridging ligand between two bimetallic fragments[30]; [Ru(PPh$_3$)$_2$(tcnq)]$_2$, in which two anionic tcnq ligands act as bridges between two Ru(I) centres[31], and [{(Cp*)(CO)$_2$Mn}$_4$(tcnx)], in which tcnx is σ-bound to 4 metal centres[32]. In the examples given above, for which structural data is reported (the exceptions being the tetranuclear Mn complexes), "ligand stacking" is observed in all complexes except for [{Re$_2$Cl$_4$(dppm)$_2$}$_2$(tcnq)].

2.1.5   Ligand Based Reactions

There is a considerable variety of reported reactions between tcne and other ligands, and of metal bound tcne with organic species in solution. The most commonly reported reactions include insertions into metal-ligand bonds (usually M-H, M-C or M-N), "2+2" and "2+4" cycloaddition reactions (tcne is an excellent dieneophile), rearrangements and reactions involving combinations of the above.

A particularly interesting example of a complex formed by ligand-based reactions of tcnx is [Ru{C[=C(CN)$_2$]CPh=C(CN)$_2$}(dppe)(Cp)] (shown in Figure 2.3), in which a 2+2 cycloaddition reaction between tcne and a (C≡CPh)$^-$ ligand

occurs then the product of the cycloaddition undergoes ring opening to yield a novel organic anion[33] (this paper also reports several other products of 2+2 cycloadditions between tcne and Ru-bound acetylides, where ring opening of the product does not take place). An example of insertion into an M-C bond is observed when tcne is reacted with [Ru(CO)$_2$(PR$_3$)L], where L is η^4-2,3-dimethylbuta-1,3-diene (η^4-2,3-(CH$_3$)$_2$C$_4$H$_4$) and R = Ph or OMe, giving the product shown in Figure 2.4 overleaf[34].

Figure 2.3 Reaction of tcne with [Ru(C$_2$Ph)(dppe)(Cp)] to form [Ru{C[=C(CN)$_2$]CPh=C(CN)$_2$}(dppe)(Cp)].
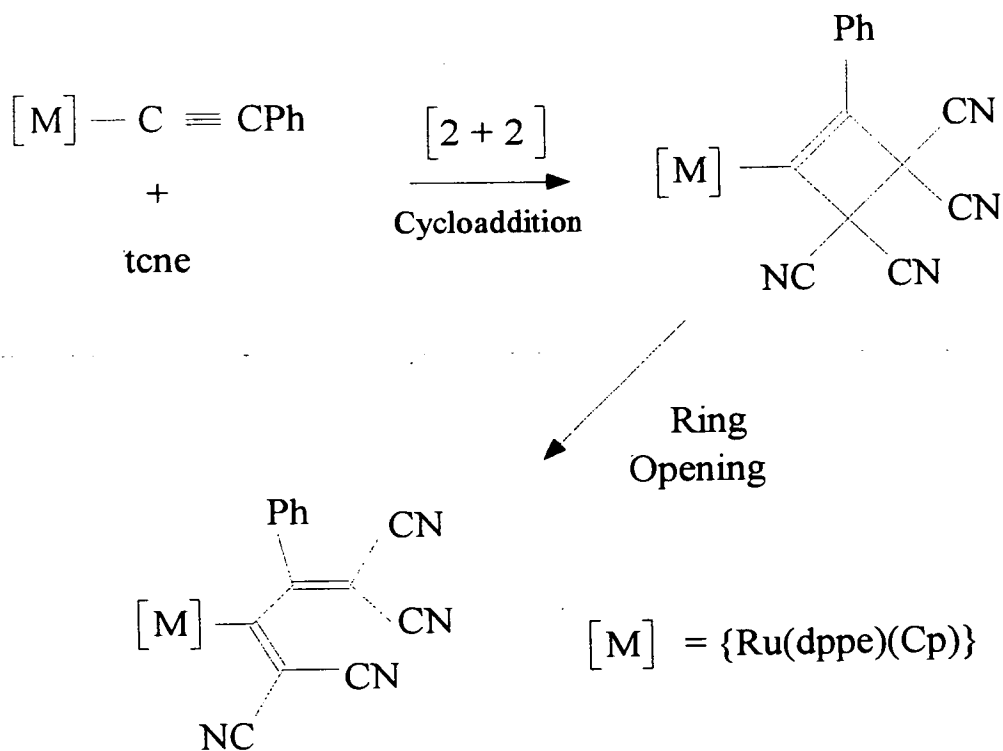
Figure 2.4 Product of reaction between tcne and [Ru(CO)$_2$(PR$_3$)L], L = η^4-2,3-(CH$_3$)$_2$C$_4$H$_4$.
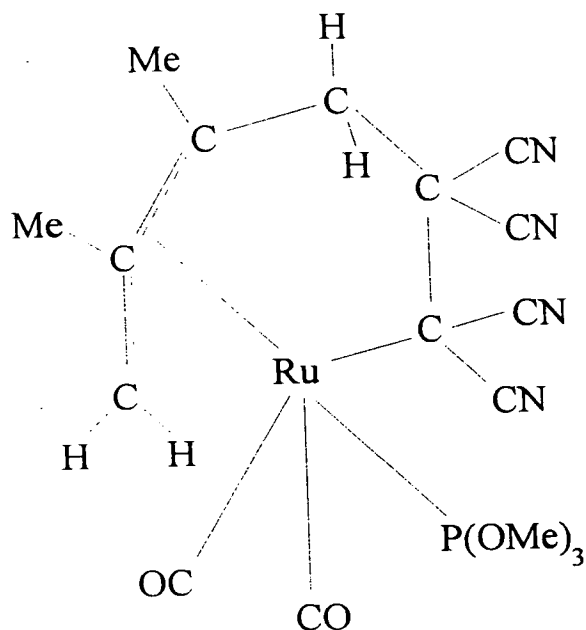
The intended objective of this work was to extend the known transition metal chemistry of tcne and tcnq, characterising the products primarily by study of their electronic properties (and by crystallographic methods, if possible) and comparing and contrasting the behaviour of the tetranitrile ligands. It was decided to concentrate efforts on complexes of ruthenium and osmium, largely as a result of the ability of these metals to adopt a wide variety of oxidation states as required by their immediate environment. In particular, three groups of starting complexes, all subjects of previous work within this department, were selected for reaction with tcnx:

1   Bipyridyl complexes of ruthenium, in particular cis-[RuCl$_2$(bpy)$_2$].

44

2   Haloosmate complexes, in particular $[OsCl_6]^{2-}$, $[OsBr_6]^{2-}$ and $[OsCl_5(py)]^-$.

3   Halo-phosphine complexes of osmium and ruthenium, specifically of the type $[MX_n(PRR'R'')_3]$, n = 2 or 3, X = Cl⁻ or Br⁻, R, R' and R'' are alkyl or aryl groups.

The third of these reactions will be covered in Chapter 3. Reactions of tcne with complexes from 1 and 2 above are discussed in the following pages.

2.2 Results and Discussion

2.2.1   Ligands

Before embarking on a study of the behaviour of metal bound tcne and tcnq, it is important to study the ligands themselves in order that the effects of the metal centre on the properties of the tetranitrile may be better understood.

2.2.1.1   Electrochemistry

Two one-electron reductions are observed during voltammetric studies of tcne. At room temperature the first reduction is reversible in most solvents but the second is quasi-reversible. In CH_2Cl_2, these reductions occur at +0.40 V and -0.7 V relative to Ag/AgCl. There is a small variation in the potentials from solvent to solvent (eg. in CH_3CN, the reductions occur at +0.34 V and -0.7 V). A cyclic voltammogram of tcne in CH_2Cl_2 is shown in Figure 2.5.

Tcnq has been found to have two reversible one- electron reductions at room temperature. In CH_2Cl_2 (Figure 2.6), the $E_{1/2}$ values for these are +0.39 V and -0.18 V versus Ag/AgCl, the reduction potentials shifting to +0.33 V and -0.20 V when the electrochemistry is studied in CH_3CN.

Electrochemical data were reported for both species in CH_3CN in Kaim's review[6]. No reference electrode was quoted, therefore direct comparisons of potentials is impossible, but the published figures show a larger gap between the first and second reductions than that observed in these experiments. This increased gap may have arisen from a higher internal resistance in the cell system used.

Figure 2.5 Cyclic voltammogram of tcne in CH_2Cl_2, 285 K.

Figure 2.6 Cyclic voltammogram of tcnq in CH_2Cl_2, 285 K.

Potential vs. Ag/AgCl
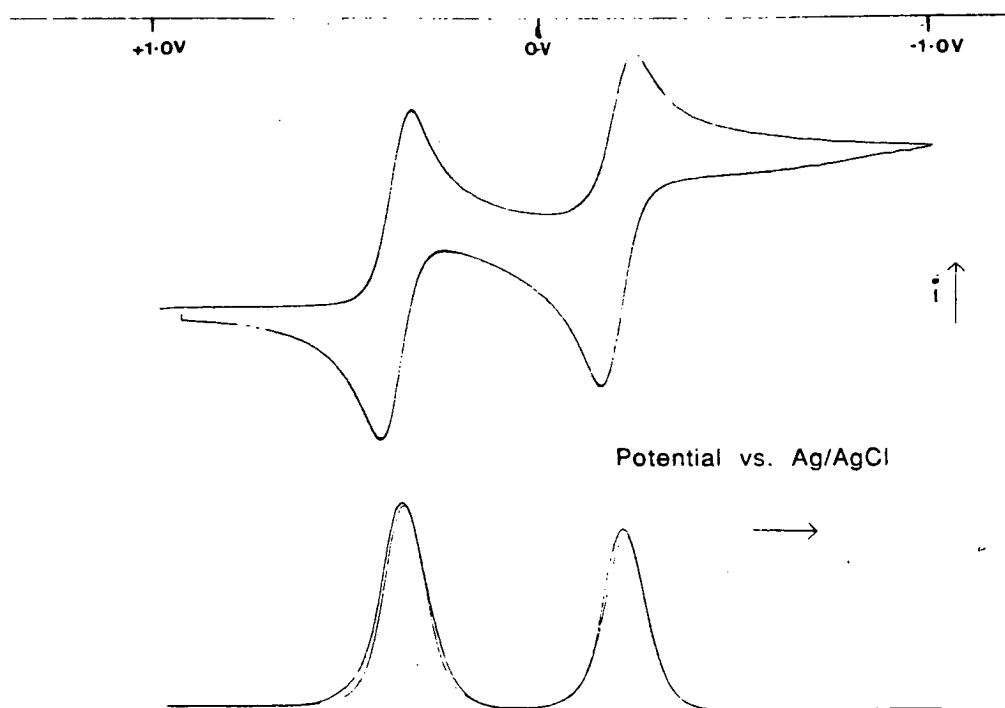
2.2.1.2   Electronic Absorption Spectroelectrochemistry

Several previous studies of the UV/visible spectra of the reduction products of

tcne and tcnq have been conducted, including that of Van Duyne and

coworkers[35,36]. The results of our own *in situ* spectroelectrochemical studies of

tcne and tcnq, which are in general agreement with those published previously, are

described below.

The first reduction of tcne (at 233 K, in CH_2Cl_2) is shown in Figure 1.9 in

chapter 1. This is a simple, reversible, one step process resulting in replacement of

the band at 39000 cm^{-1} arising from the first π to π^* transition in the neutral

47

molecule by the corresponding band for the anion at 23000 cm^{-1}. The change in energy of the transition is predominantly due to a shift to lower energy of the LUMO when an electron is added. Vibrational fine structure is observed in the band for both the neutral ligand and the radical anion.

The second reduction (Figure 2.7) resulted in collapse of the band at 23000 cm^{-1}, as would be expected given that the former LUMO is now fully occupied. A new band appeared at very high energies (>40000 cm^{-1}) but there was also significant decomposition of the tetranitrile, with the result that it was only possible to regenerate about 50% of the original quantity of radical anion, therefore the validity of any attempt to assign this band would be questionable.

Figure 2.7 Changes in the absorption spectrum accompanying reduction of tcne$^-$ in CH$_2$Cl$_2$ at 233 K, at -0.9 V versus Ag/AgCl.
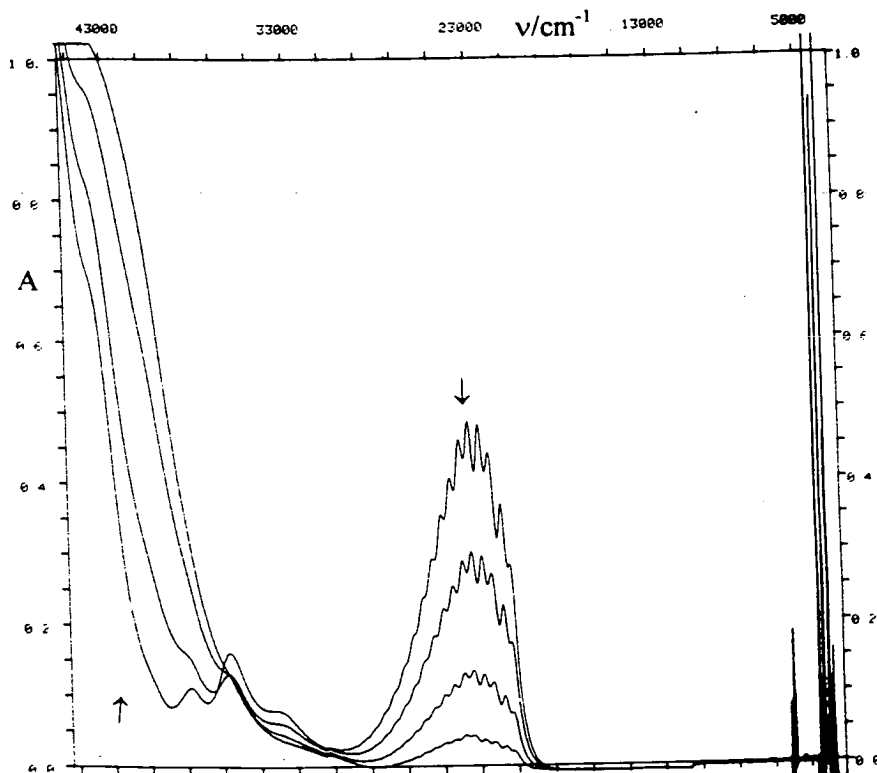
In the case of tcnq, studied in CH_2Cl_2 at 273 K, the first reduction (Figure 2.8) again induced a shift of the first allowed transition to lower energy, the spectrum showing collapse of the intense band at 25000 cm^{-1} ($\varepsilon = 70000$ M^{-1}cm^{-1}), and growth of new bands at 12000 cm^{-1} and 24000 cm^{-1}. Vibrational fine structure (more complex than in tcne$^-$) was again visible in the spectrum of the radical anion. Further reduction resulted in collapse of the bands corresponding to the radical anion and corresponding growth of new bands at 30500 cm^{-1} and 42000 cm^{-1} (as shown in Figure 2.9). On this occasion the dianion was much more stable and (even at this higher temperature) it was possible to regenerate about 90% of the radical anion. A small peak which also appeared during the second reduction, at 20000 cm^{-1}, but remained on reoxidation was assigned as a band arising from the decomposition product.

2.2.1.3 Infrared Spectroelectrochemistry

Tcne and tcnq are well suited to study by infrared spectroscopy as vibrational excitation of their cyano groups is induced by absorption of radiation at approximately 2200 cm^{-1}, normally a "quiet" region of IR spectra. Raman studies of tcne have also revealed a C=C stretch at 1569 cm^{-1}[37]. Infrared data for the tetranitriles and their anions, in a variety of environments, is given in Table 2.1 below.

Figure 2.8 Absorption spectral changes during reduction of tcnq to tcnq⁻ (E_{app} = +0.2 V) at 273 K in CH_2Cl_2
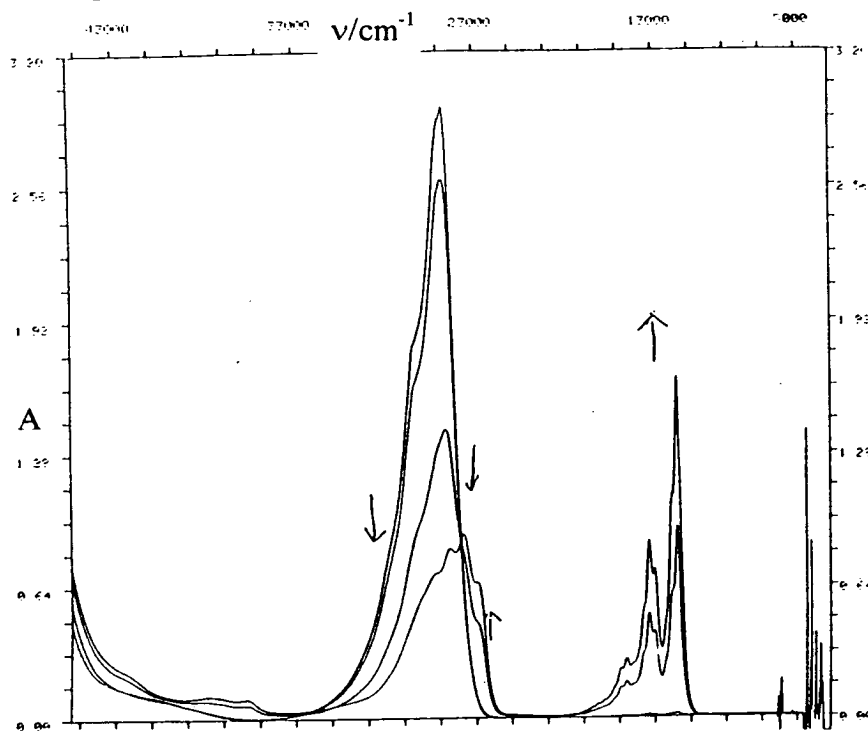
Figure 2.9 Absorption spectral changes accompanying reoxidation of $tcnq^{2-}$ to $tcnq^-$ (E_{app} = 0 V vs Ag/AgCl) in CH_2Cl_2, 273 K
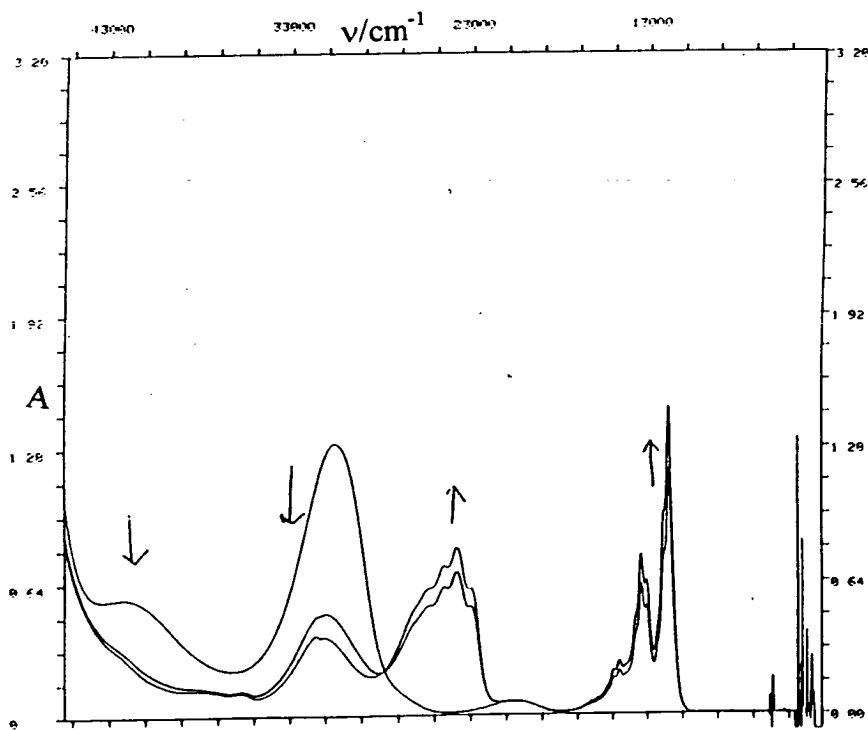
It should be noted that there is a significant decrease in the $C\equiv N$ and $C=C$ stretching energies upon addition of an electron to the antibonding π^* orbital. This is potentially useful in assigning redox processes in metal-tcnx complexes as metal or ligand-based.

Table 2.1: Selected IR data for tcnx and tcnx⁻.

		Stretches/cm⁻¹	
Species	Medium	C≡N	C=C
tcne	KBr disc	2262, 2228	IR inactive
	CH₂Cl₂	2260w, 2215m	" "
	(CH₃)₂CO	2240m, 2210s	" "
tcne⁻	CH₂Cl₂	2180, 2140	1370m
tcnq	CH₂Cl₂	2220s	Not assigned
tcnq⁻	CH₂Cl₂	2180s	" "

2.2.1.4   EPR Spectroscopy

While the neutral tetranitriles and their dianions are, unsurprisingly, EPR silent, the spectra of the radical first reduction products have been reported on several occasions. Both show spectra typical of organic radicals, with g values very close to g_e (g = 2.0028 in tcne⁻[38], 2.003 in tcnq⁻[39]), with coupling to ^{14}N and, in the case of tcnq⁻, ^1H nuclei (A_N = 1.57 G in tcne⁻[38], A_N = 0.52 G, A_H = 0.72 G in tcnq⁻[39]).

Much attention has focused on epr spectra of concentrated samples of tcnq salts (ie. powders and single crystals), as a result of the tendency to form low dimensional solids (reference 39 is an early example of such a study). In the solid, the anions readily undergo spin-spin exchange interactions, giving rise, at temperatures in excess of 20 K, to high concentrations of "triplet excitons", thus removing zero-field splitting and giving a single line spectrum. The hyperfine coupling constants given above were determined at 4 K[39].

2.2.2 Reactions of tcne and tcnq with Bipyridyl Complexes of Ruthenium

Bipyridyl complexes of ruthenium have been the subject of intensive study in recent years, primarily as a result of a long lived electronically excited state in $[Ru(bpy)_3]^{2+}$ (bpy = 2,2'-bipyridyl), which can be achieved by absorption of visible light ($v_{max} = 22000 \text{ cm}^{-1}$[40]). Several studies, notably one in which electrochemical studies were successfully correlated with electronic absorption spectra (including those of oxidation and reduction products)[40,41], have shown that the excited state arises from transfer of an electron from Ru to one of the bipyridyl ligands, ie:

$$[Ru^{II} (bpy)^0_3]^{2+} \xrightarrow{\quad h\nu \quad} {}^*[Ru^{III} (bpy)^0_2(bpy)^-]^{2+}$$
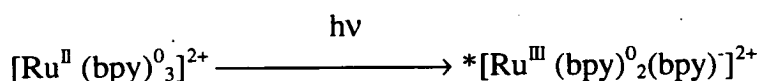
The above studies revealed that, upon reduction, the added electron was trapped within a single bipyridyl ligand (ie. the bpy ligands do not interact with each

other). Similarly the excited state is best thought of as having the promoted electron localised on one bpy ligand and thus the long life of the excited state was primarily a result of loss of symmetry within the complex upon excitation[41].

As can be seen above, electronic excitation of $[Ru(bpy)_3]^{2+}$ produces a species in which there are two highly reactive centres - the electron deficient Ru^{III} and the electron rich (bpy)⁻ radical anion. As a result, in addition to simple relaxation, $*[Ru(bpy)_3]^{2+}$, readily undergoes reaction with "quenchers" such as paraquat (PQ^{2+}, giving PQ^+ and $[Ru(bpy)]^{3+})^{[42]}$ and europium(II) (giving Eu^{3+} and $[Ru(bpy)_3]^+)^{[43]}$, thus constituting a useful source of reactive intermediates. Particular interest has focused on the possibility of using $[Ru(bpy)_3]^{2+}$ as a means of converting solar energy to chemical energy since it was shown that the excited state is thermodynamically capable of splitting water to give H_2 and O_2, although the process has been shown to be very inefficient[44].

A great deal of attention focused subsequently on production of new Ru-bipyridyl species with long lived electronically excited states but modified electronic properties, hence altering the chemical reactions which can be induced by the quenching process. In particular, three routes have been taken in these "fine tuning" studies:-

(i) Complexes of substituted bipyridyls, in which the electronic properties of the ligand are altered by attaching electron donating or withdrawing groups to the aromatic rings. Much of this work has involved complexes in which the bipyridyl ligands have ester substituents in the position *para* to nitrogen, with variations in

the organic groups attached to the ester enabling control of the solubility etc. of the complexes[45,46].

(ii) Polynuclear complexes, in which two or more non-equivalent metal centres are linked by bridging ligands (for example, (CN)$^-$ and aromatic N-donors such as 4,4'-bipyridyl). The general principal in this case is that photo-excitation at one metal centre induces transfer of energy or electrons between the excited centre and the others, via the bridging ligands. Recent examples of such species include $[(bpy)_2Ru(tpt)Ru(trpy)]^{4+}$ (trpy = 2,2',6',2"-terpyridine, tpt = tris(2-pyridyl)-1,3,5-triazine)[47] and $[NCRu(bpy)_2CNRu(bpy)_2CN]^{+}$[48].

(iii) Lower symmetry complexes, in which the metal centre is typically bound to two bipyridyl (or bipyridyl derived) ligands and a variety of other ligands, such as phosphines[49], carbonyls[50], cyanides[51] and a wide range of aromatic N-donors[52]. A popular starting material in the preparation of such species is cis-RuCl$_2$(bpy)$_2$, from which one or both chlorides can be removed, thus facilitating coordination of the new ligand(s).

As much of the interest in bipyridyl and related complexes of Ru relates to potential use of its excited states in chemical reactions, characterisation of the frontier orbitals of these complexes has been a major component of published work. There exists, therefore, a considerable database of electrochemical and UV/visible spectroscopic data relating to bipyridyl compounds of Ru, and their oxidation and reduction products. Consequently, studies of the frontier orbitals of new bipyridyl

complexes of ruthenium are made much easier by the wealth of related species with which comparisons may be made.

The objectives of this research were to synthesise new bipyridyl complexes of Ru containing tcne and tcnq, characterise these species, with particular reference to the elucidation of the nature of the frontier orbitals, and compare them with previously reported bipyridyl and tcnx complexes. One of the particular objectives which caused bipyridyl complexes to be chosen was the desire to synthesise a Ru^{II} tcne complex in which the other ligands were also π-acceptors (previous work within this department having involved the preparation of tcne complexes of Ru and Os in which the other ligands were potent π-donors)[29].

Apart from brief, unsuccessful, attempts to form a tcne or tcnq charge transfer complex with $[Ru(bpy)_3]^{2+}$, all experiments involved reaction of tcne or tcnq with cis-$[RuCl_2(bpy)_2]$, or its more reactive derivative $[RuCl(\{CH_3\}_2CO)(bpy)_2]^+$.

The products of these reactions were characterised by spectroscopic and electrochemical methods. Attempts to obtain crystals suitable for single crystal X-ray diffraction were unsuccessful.

The reactions carried out essentially consisted of removal of Cl^- from the starting complex by $AgBF_4$ and subsequent reaction with tcnx. This was carried out by 2 methods:

(i) "One pot" reactions, in which all three reagents were added to a deaerated solution of CH_2Cl_2.

(ii)   Reaction of AgBF$_4$ with [RuCl$_2$(bpy)$_2$] in acetone, forming [RuCl({CH$_3$}$_2$CO)(bpy)$_2$]$^+$, followed by removal of the precipitated AgCl and addition of the tetranitrile. Early experiments with this method tended to yield the binuclear [{RuCl(bpy)$_2$}$_2$]$^{2+}$ complex but this problem was circumvented by reducing the time allowed for the initial removal of chloride. This method of activating [RuCl$_2$(bpy)$_2$] is discussed in reference 49.

The most heavily studied complexes were [N1] and [N2], dark green species which were prepared by reaction of [RuCl({CH$_3$}$_2$CO)(bpy)$_2$]$^+$ with 3-fold excesses of tcne and tcnq respectively, excess tetranitrile being extracted after reaction with toluene. On the basis of the results given below, [N1] is believed to be [RuCl(bpy)$_2$(tcne)]$^+$, where tcne is σ-bound via N, and [N2] appears to be the analagous tcnq complex. These species were reasonably stable, decomposing over a period of several months in the solid state, or 2-3 weeks if left in solution, although rapid decomposition occurred during all attempts to purify the complexes by chromatographic methods.

Brief mention will also be made of [N3], prepared by direct reaction of [RuCl$_2$(bpy)$_2$] with excesses of AgBF$_4$ and tcne. This sparingly soluble complex was dark blue but decomposed over a period of 3 days to a pale green species. The identity of [N3] was never successfully established, beyond showing that tcne had reacted but [N1] had not been formed. UV/visible and IR data for [N3] are listed but not discussed in detail.

<u>Fast Atom Bombardment Mass Spectrometry</u>

FAB mass spectrometry data are given in Table 2.2 below for complexes [N1] and [N2] (in the case of [N2], data are given for the species before and after extraction of unreacted tcnq with toluene). In the case of [N3], no useful data were obtained.

For [N1] and [N2], the spectra appear to confirm formation of $[RuCl(bpy)_2(tcne)]^+$ and $[RuCl(bpy)_2(tcnq)]^+$ respectively. In the case of [N2], it is interesting to note that prior to removal of excess tcnq, there appears to be a significant quantity of the binuclear complex $[\{RuCl(bpy)_2\}_2(tcnq)]^{2+}$, although this species has all but disappeared after Soxhlet extraction with toluene. This appears to indicate that the binuclear complex is thermally unstable and decomposes rapidly upon contact with hot toluene allowing reaction of the released $\{Ru(bpy)_2Cl\}^+$ fragments with unextracted tcnq to form more of the mononuclear complex.

Table 2.2: Mass spectrometry data for [N6] and [N7].

NB - In the table below, L = 2,2'-bipyridyl.

Species	m/z*	Assignment	Expected Mass#	Intensity
[N1]	578	$[RuClL_2(tcne)]^+$	577	28.2
	491			23.2
	477	$[RuClL_2(NC)]^+$	475	47.4
	449	$[RuClL_2]^+$	449	100
	413	$[RuL_2]^+$	414	72.2
	257	$[RuL]^+$	258	58.4
[N2]^a	1102	$[\{RuClL_2\}_2(tcnq)]^+$	1102	2.7
	740	$\{[RuClL_2(tcnq)][BF_4]\}^+$	740	2.1
	653	$[RuClL_2(tcnq)]^+$	653	8.7
	474	$[RuClL_2(NC)]^+$	475	16.8
	449	$[RuClL_2]^+$	449	100
	413	$[RuL_2]^+$	414	56.3
[N2]^b	1102	$[\{RuClL_2\}_2(tcnq)]^+$	1102	0.4
	740	$\{[RuClL_2(tcnq)][BF_4]\}^+$	740	1.7
	653	$[RuClL_2(tcnq)]^+$	653	10.4
	474	$[RuClL_2(NC)]^+$	475	17.2
	449	$[RuClL_2]^+$	449	100
	413	$[RuL_2]^+$	414	56.9

Notes:-

* - Only the most intense peak of each group is quoted.

- The expected mass is calculated for the isotopes of greatest abundance (ie. ^{102}Ru, ^{35}Cl etc.).

a,b - Before and after removal of unreacted tcnq respectively.

<u>Infrared Spectroscopy</u>

The energies of the IR active C≡N stretching modes in [N1], [N2] and [N3] are given in Table 2.3 below. Although, in most modes of coordination, the C=C stretching mode of vibration should now be IR active, assignment of tcne-based C=C stretches proved to be impossible as several modes of vibration associated with the bipyridyl ligands absorb in the same region of the spectrum.

Comparison with the spectra of the free ligands suggests that the shift to lower energy of the CN stretches is insufficient to correspond to tcnx⁻. The change is, however, consistent with Ru-N σ-coordination, in which back donation from Ru to the π*-orbital of the tetranitrile results in general weakening of the C≡N bonds.

Table 2.3: Selected IR data for [N1], [N2] and [N3]

<u>Complex</u>	<u>Medium</u>	<u>ν of C≡N stretches /cm^{-1}</u>
[N1]	KBr disc	2200m; 2160s
[N2]	KBr disc	2190m; 2150s; 1970m,br
[N3]	KBr disc	2215w; 2120-2175m

2.2.2.3   Electronic Absorption Spectroscopy

UV/visible data for [N1], [N2], [N3] and related precursors are given in Table 2.4. below.

By analogy with the starting materials, the bands at 35000 - 36500 cm^{-1} were assigned to bpy π to π^* transitions, as were those at 41500 cm^{-1}.

Replacement of the π-donor Cl$^-$ ligand by π-accepting tcnx would be expected to reduce the electron density at Ru, with a consequent lowering of the energy of the metal- based HOMO. Thus it is reasonable to expect that the Ru to bpy charge transfer bands observed at 18100 cm^{-1} and 26500 cm^{-1} in the starting complex would be shifted to higher energy on replacement of a Cl$^-$ ligand by tcnx. On this basis the bands at 24000 - 26000 cm^{-1} were provisionally assigned as Ru to bpy MLCT bands (the second transition is believed to have shifted such that it is superimposed upon the much stronger bpy π to π^* transition). The splitting of this band, as compared with the starting complex, is thought to arise from the reduced symmetry about the metal centre, and subsequent loss of equivalence of the bpy ligands. It should be noted that in the case of [N2], the bands in this region of the spectrum may also contain a component from internal tcnq transitions, as observed in the free ligand. It should be noted that the sample of [N2] used to record the spectrum shown in Figure 2.11 still contained some unreacted tcnq.

Table 2.4: Selected EAS data

Species	Solvent	v/cm^{-1} $(10^{-4}\varepsilon/M^{-1}cm^{-1})$
2,2'-bipyridyl	CH_2Cl_2	35700(3.7), 42500(2.2)
cis-[Ru(bpy)$_2$Cl$_2$]	CH_2Cl_2	18100(0.67), 26500(0.69)
		33700(3.8), 41500(1.76)
[RuCl(bpy)$_2$({CH$_3$}$_2$CO)]$^{+\#}$	(CH$_3$)$_2$CO*	19500(0.71), 28000(0.79)
[N1]^a	CH_2Cl_2	13600(0.12),24000(0.41),
		25130(0.42), 36100(4.2),
		37500(3.9)
[N2]^b	CH_3CN	12800(0.75), 25000(1.3),
		27000sh(1.1), 34900(4.2),
		41500(2.5)
[N3]$^\#$	CH_2Cl_2	14200(0.72), 26000(0.80),
		36300(6.4)

Notes:-

* - In acetone no bands are observable above 30000 cm^{-1}, as a result of strong absorption by the solvent.

a - See Figure 2.10. ε calculated for MW = 577.

b - See Figure 2.11. ε calculated for MW = 653.

- Extinction coefficients were not obtained, therefore values are given in arbitrary absorption units, to show relative intensities of bands within a complex. The consistent intensity of the bpy π to π* band (at 36300 cm^{-1} in [N2]) suggests approximate extinction coefficients of 4500, 5000 and 40000 dm^{3}mol^{-1}cm^{-1}, in order of increasing energy.

Figure 2.10 UV/visible Spectrum of [N1] in CH_2Cl_2
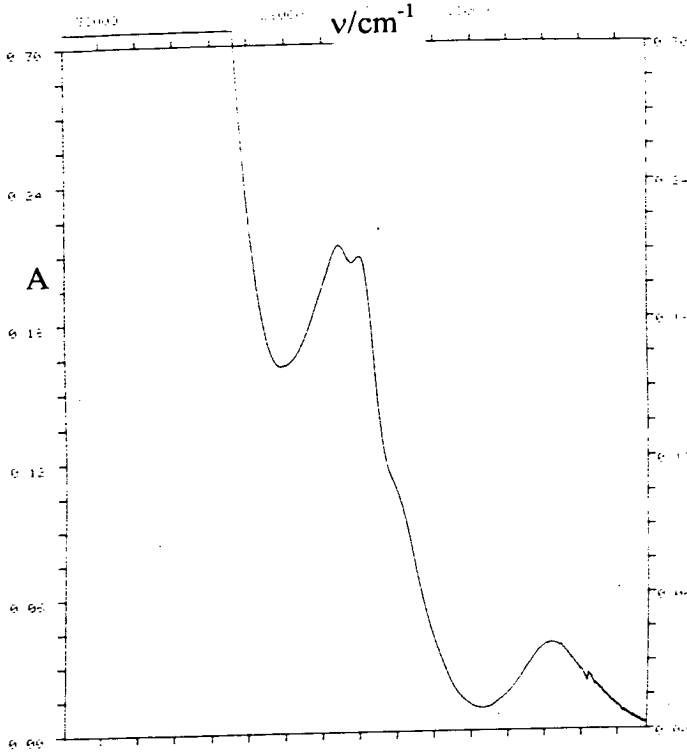
Figure 2.11 UV/visible spectrum of [N2] in CH_3CN
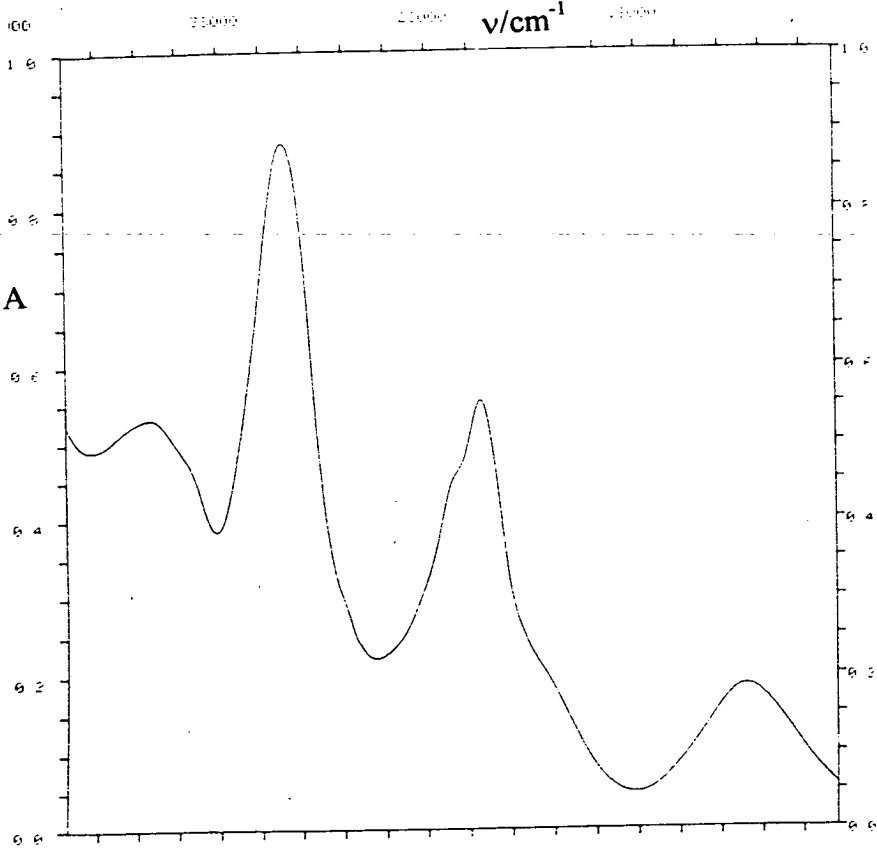
By elimination, the bands at 13000 - 14000 cm^{-1} were assigned as Ru to tcnx MLCT bands. This is not an unreasonable deduction as the π-accepting behaviour of the tetranitrile ligands is indicative of a low lying ligand-based LUMO, therefore any Ru to tcnx transition would be expected to occur at relatively low energy.

Further UV/visible spectroscopic studies were carried out, particularly with [N1]. The progress of the reaction between tcne and [RuCl(bpy)$_2$({CH$_3$}$_2$CO)]$^+$ was monitored by UV/visible spectroscopy (Figure 2.12). This appeared to show some formation of tcne$^-$ (some vibrational structure, similar to that in tcne$^-$, is observed in the range 20000 -24000 cm^{-1}), suggesting that the reaction mechanism involves reduction of tcne followed by coordination of the radical anion. Similar phenomena have been observed previously in reactions of tcne with, for example, dithiolate complexes of Ru and Os[53]. The most likely source of this reduction would appear to be [RuCl(bpy)$_2$({CH$_3$}$_2$CO)]$^+$, giving an ion pair as a reactive intermediate in the formation of [Ru(bpy)$_2$Cl(tcne)]$^+$.

To assist in assignment of the charge transfer bands, a brief study of the solvent dependence of the charge transfer bands in [N1] was also carried out. Essentially, because charge transfer involves a change in dipole moment within the complex, the solvent molecules in the outer coordination sphere must rearrange, a process which requires energy. The energy required for solvent reorganisation will vary according to the coordinating strength (and dipole moment) of the solvent, therefore the energy of the band associated with the charge transfer process will also vary from solvent to solvent. The results of this study, given in Table 2.5, show that the

energy of the first charge transfer band increases as the donor number increases (although not in a linear fashion), while solvent has little effect on the position of the second band. Previous studies with related species have shown that Ru to bpy charge transfer bands often exhibit very small changes in energy with solvent[54] therefore these results support the provisional assignments given earlier.

The low energy of the Ru to tcnx charge transfer band is consistent with a low-lying ligand-based LUMO. This, coupled with the similar nature of the spectra obtained for the tcne and tcnq complexes, suggests that the tetranitrile ligands are coordinating to Ru via nitrogen.

Figure 2.12 Formation of [N1], in acetone.
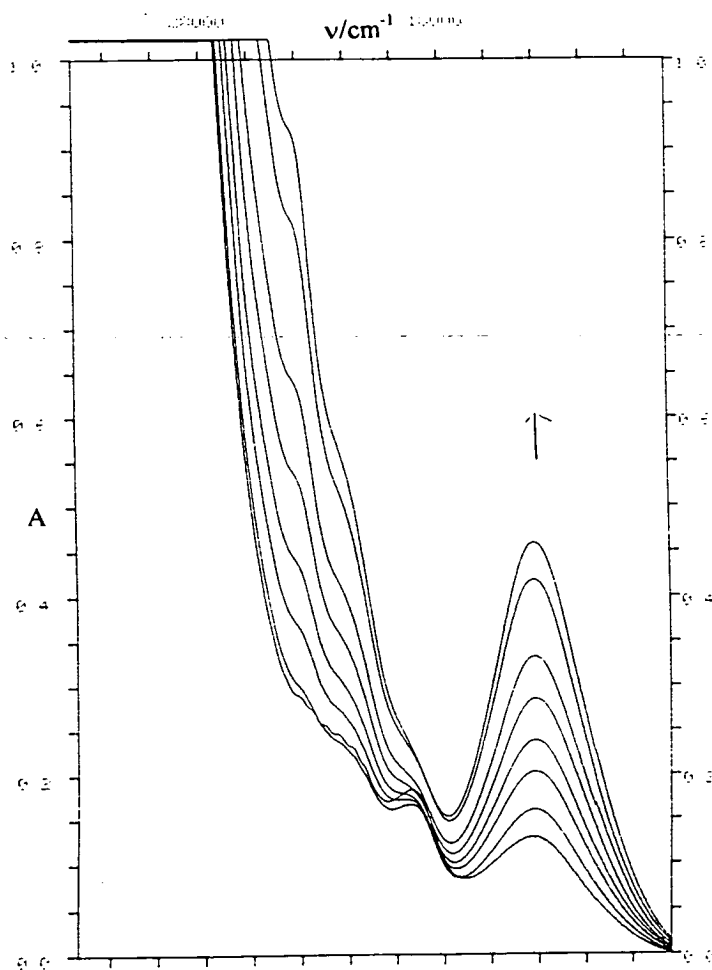
Table 2.5   Effect of solvent donor strength on the energy of the charge transfer

bands in [N1].

Solvent	$DN^{\#}$	v_1/cm^{-1}	v_2/cm^{-1}	v_3/cm^{-1}
CH_2Cl_2	-	13600	24000	25130
$PhNO_2$	4.4	13750	N/A*	N/A*
PhCN	11.9	13850	24000	25350
CH_3CN	14.1	14080	24200	25400
$(CH_3)_2CO$	17.0	14150	24000	25400
DMF	26.6	15000^a	24200	25400
DMSO	29.8	15750^a	24000	25150

Notes:

- DN is the donor number of the solvent, a measure of the electron donating

strength of the solvent. Values for DN were obtained from reference 55.

* - Values for v_2 and v_3 were not obtained as $PhNO_2$ absorbs in the relevant region

of the spectrum

a - Values of v_1 in DMF and DMSO are less precise, as there was some merging of

this peak and more intense higher energy bands.

2.2.2.4   Electrochemistry

Voltammetric studies were carried out on [N1] and [N2], with results as listed in Table 2.6.

Table 2.6:   Redox data for [N1], [N2] and $RuCl_2(bpy)_2$.

Complex	Solvent	Oxidations/V[#]	Reductions/V[#]
cis-[RuCl_2L_2]	CH_2Cl_2	+0.50_r	-1.54_q
[RuClL_2Ac]^+	$(CH_3)_2CO$	+0.94_r	Not observed*
[N1]	CH_2Cl_2	+1.31_r	+0.52_r, -1.17_q, -1.4_i
[N2]	CH_3CN	+1.18_r	+0.52_r,_-0.18_r, -1.4_i

Notes:

L = 2,2'-bipyridyl, Ac = Acetone

- All potentials are quoted relative to the Ag/AgCl reference electrode, versus which $E_{1/2}$ for the oxidation of ferrocene occurs at +0.55V. The suffixes describe the redox process:- r = reversible, q = quasi-reversible and i = irreversible.

* - The "solvent window" of the acetone used did not extend to sufficiently negative potentials to permit study of the bipyridyl based reductions.

As demonstrated by the shift in oxidative potential when Cl⁻ is replaced by acetone, replacing a π-donor ligand with a π-acceptor results in a shift of any

metal-based processes to more positive potentials (by way of further comparison, in [Ru(bpy)$_2$(CN)$_2$], in CH$_2$Cl$_2$, the Ru- based oxidation has an E$_{1/2}$ value of +1.02 V[56]). Thus it is reasonable to assign the oxidative processes in [N1] and [N2] as Ru$^{II/III}$ couples. Comparison of redox potentials with the dicyano complex listed above gives a striking indication of the π-withdrawing power of the tetranitrile ligands.

Previous work involving tcne[26,27,29] has indicated that there is generally a fairly small change in the position of the tcne$^{0/-}$ couple on σ-coordination to a metal centre, therefore the reductive processes observed at +0.5 V in [N1] and [N2] were assigned as tetranitrile- based reductions. The irreversible reductions at -1.4 V were assigned as bipyridyl based by analogy with the starting complex.

In previous studies the tetranitrile based reduction was often shifted to more negative potentials upon σ-coordination to a metal centre (an extreme example being [Os(S$_2$PMe$_2$)$_2$(PPh$_3$)(tcne)], in which the tcne$^{0/-}$ reduction is at -0.18 V versus Ag/AgCl[29]) but in the cases of [N1] and [N2] the shift was to more positive potentials. This suggests that the back-bonding from metal to ligand is weaker in [N1] and [N2] than those previously synthesised within this department.

Attempts to obtain electrochemical data for [N3] were thwarted by a combination of low solubility and instability.

2.2.2.5   Electronic Absorption Spectroelectrochemistry

The UV/visible spectroelectrochemistry of [N1] and [N2] was studied at 243 K in CH_3CN. The behaviour of the complexes was extremely similar and is discussed below. Figures are shown representing oxidation and reduction of [N2]. Both reduction and oxidation were found to be fully reversible, "one step" processes (as made evident by the presence of several isosbestic points in both series of spectra).

Oxidation of [N2] (Figure 2.13) results in several changes to the UV/visible spectrum. Charge transfer bands are now observed at 14000 cm^{-1} (ε = 3500 $mol^{-1}dm^3cm^{-1}$) (the corresponding band appears at 14500 cm^{-1} in [N1]) and 25500 cm^{-1} (ε = 14000), while the bipy π - π^* band at 35000 cm^{-1} is much reduced in intensity and a new band has appeared at 32000 cm^{-1}.

The higher energy bands (at 32000 and 35000 cm^{-1}) are relatively simple to assign as bpy π - π^* bands. Oxidation to Ru^{III} has been shown to split the first bpy π - π^* band into two weaker bands in, for example, $[Ru(bpy)_{3-n}(py)_{2n}]^{2+/3+}$ (n = 0, 1 or 2) and cis-$[Ru(bpy)_2Cl_2]^{0/+}$.[41] In all the above cases the new π - π^* band appears at approximately 32000 cm^{-1}.

Assignment of the lower energy bands is more complicated. There are three possible LMCT processes in the Ru^{III} complex, involving excitation of tcnq, bipyridyl or Cl^- based electrons.

Figure 2.13 Absorption spectral monitoring of oxidation of [N2] in CH$_3$CN, 243 K, E_{app} = +1.4 V versus Ag/AgCl.
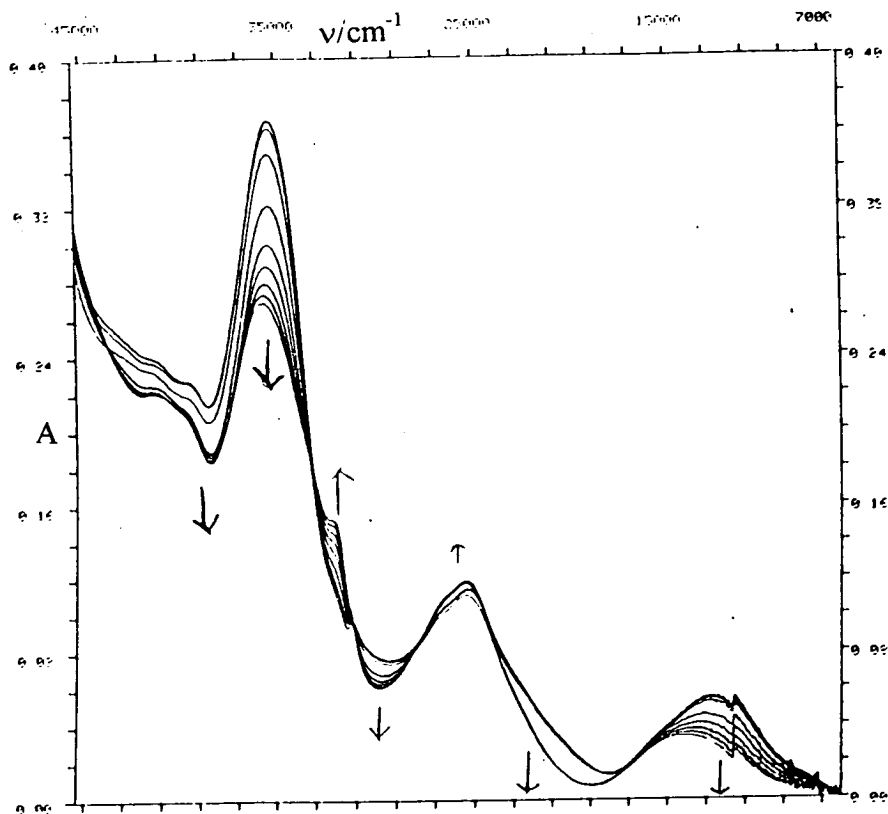
Some assistance is afforded by comparison with the spectrum of cis-[Ru(bpy)$_2$Cl$_2$]$^+$, which contains charge transfer bands at 18000 (ε = 500 mol^{-1}dm^{3}cm^{-1}), 21900(2700) and 26500(6400) cm^{-1}.[41] The charge transfer bands in cis-[Ru(bpy)$_2$Cl$_2$]$^+$ were assigned, in order of increasing energy, as a bpy - Ru^{III} LMCT band, a Ru^{III} - bpy MLCT band and a Cl$^-$ - Ru^{III} LMCT band[41]. It is interesting to note that the bpy - Ru LMCT band has a relatively low extinction coefficient; this is also the case in the spectra of, for example, [Ru(bpy)$_3$]$^{3+}$ (ν = 15000 cm^{-1}, ε = 700 mol^{-1}dm^{3}cm^{-1}) and cis-[Ru(bpy)$_2$(py)$_2$]$^{3+}$ (ν = 14900 cm^{-1}, ε =

450 mol^{-1}dm^{3}cm^{-1})^{41}. It is not unreasonable, therefore, to expect that the analogous band in [Ru(bpy)$_2$Cl(tcnx)]$^{2+}$ will also be relatively weak.

Replacement of a π-donor ligand such as Cl$^-$ with a π-acceptor such as tcnq would be expected to cause the metal based HOMO to shift to lower energy. We therefore predict that, compared with the spectrum of [Ru(bpy)$_2$Cl$_2$]$^+$, the spectrum of [Ru(bpy)$_2$Cl(tcnx)]$^{2+}$ will contain MLCT bands at higher energy and LMCT bands at lower energy. We suggest that the band at 25500 cm^{-1} in the spectrum of [N2] arises from a combination of Cl$^-$ to Ru^{III} LMCT, Ru^{III} to bpy MLCT and possibly tcnq to Ru^{III} LMCT processes, while the lower energy band at 14000 cm^{-1} is a combination of bpy to Ru^{III} LMCT and Ru^{III} to tcnq MLCT processes.

Reduction (Figure 2.14) results in a shift of the Ru - tcnx MLCT band to lower energy, with the maximum of the new Ru - tcnx$^-$ band at 9500 cm^{-1} in [N2], 10200 cm^{-1} in [N1]. This shift to lower energy is to be expected, as introducing an electron to the tcnx-based π* LUMO will normally result in a lowering of the energy of that orbital. A number of other changes were also observed in the spectrum, the bulk of which are similar to those observed on reduction of free tcnq (collapse at 25000 cm^{-1} accompanied by growth at slightly lower energy), plus a possible shift of the Ru-bpy charge transfer bands to slightly lower energy (concomittant with a small increase in electron density at Ru).

Figure 2.14 Absorption spectral monitoring of reduction of [N2] in CH₃CN at 243

K, E_{app} = +0.2 V versus Ag/AgCl.
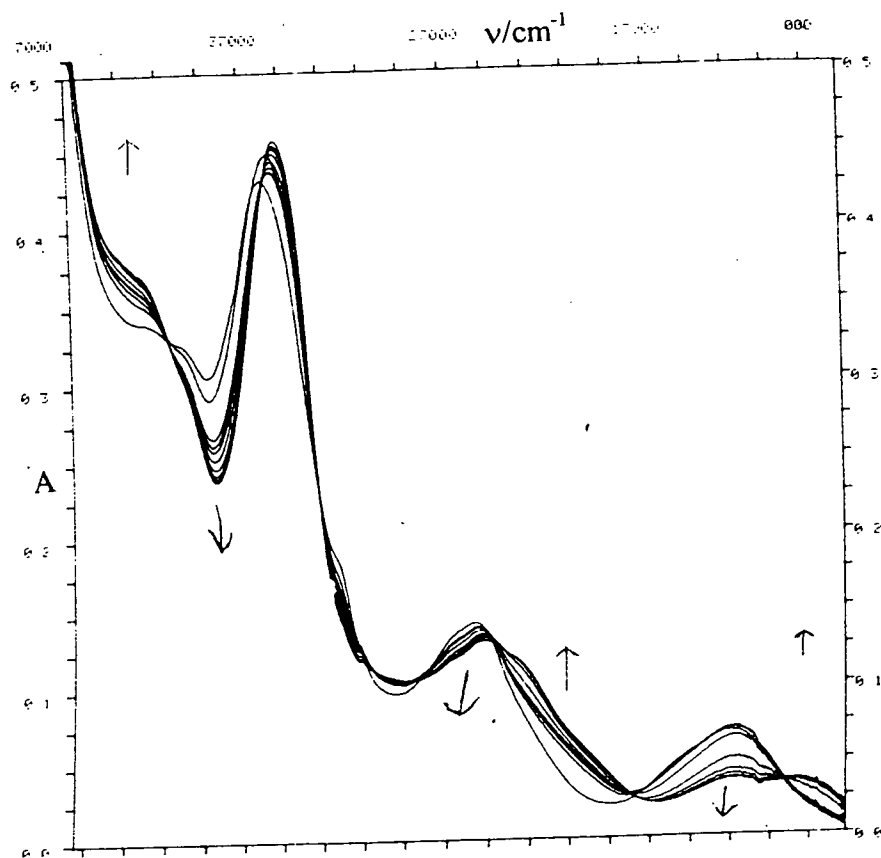
2.2.2.6   Summary

The experimental data reported above, particluarly the similarity of the results

obtained for [N1] and [N2], indicate that [N1] and [N2] are the Ru-N σ-bound

complexes [RuCl(bpy)₂(tcne)]⁺ and [RuCl(bpy)₂(tcnq)]⁺ respectively. The data also

shows that the tetranitriles are coordinated as neutral ligands. Electrochemical

studies show that the complexes are very electron deficient, as exemplified by the

ligand-based reductions at +0.52 V versus Ag/AgCl, only 40 mV less positive than

the $[Fe(Cp)_2]^{0/+}$ oxidation. This is not surprising given that the other ligands, with

the exception of Cl⁻, are also π-acceptors. Some evidence of binuclear complexes

being formed as a minor, thermally unstable, product of the reaction between

$[RuCl(bpy)_2(OC\{CH_3\}_2)]^+$ and tcnq was also obtained. The proposed structure of

[N1] is shown in Figure 2.15.

Figure 2.15 The proposed structure of [N1]
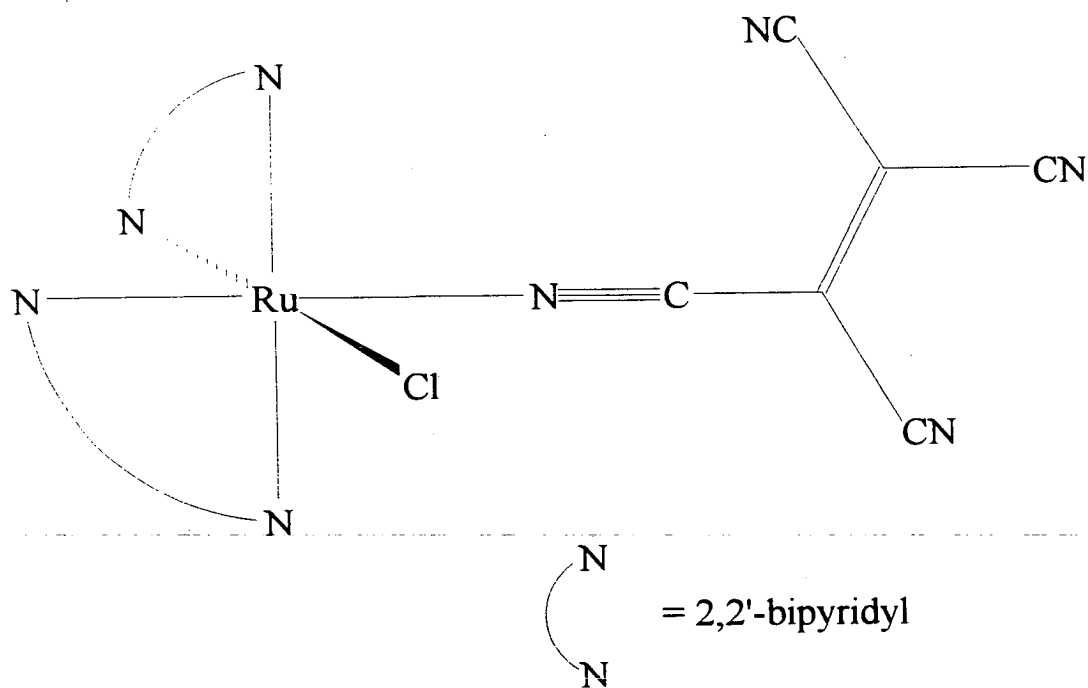
Given the paucity of data, the precise identity of [N3] remains a matter of

speculation, although it is clear that tcne has reacted with $[Ru(bpy)_2Cl_2]$ but [N1]

has not been formed. One possibility is that a π-complex of formula

[RuCl(bpy)$_2$(tcne)]$^+$ has been formed (see Figure 2.16). An interesting precedent for such behaviour is reported by Roth and Kaim. This is the case of [W(CO)$_5$(tcne)], for which the π-complex and the isomeric W-N σ-complex have both been reported[62]. Rapid rearrangement of the π-complex to give the σ-complex occurs upon reduction to the monoanion, a reaction which can be reversed by oxidation of the σ-complex.

Figure 2.16 Possible structure of [N3]
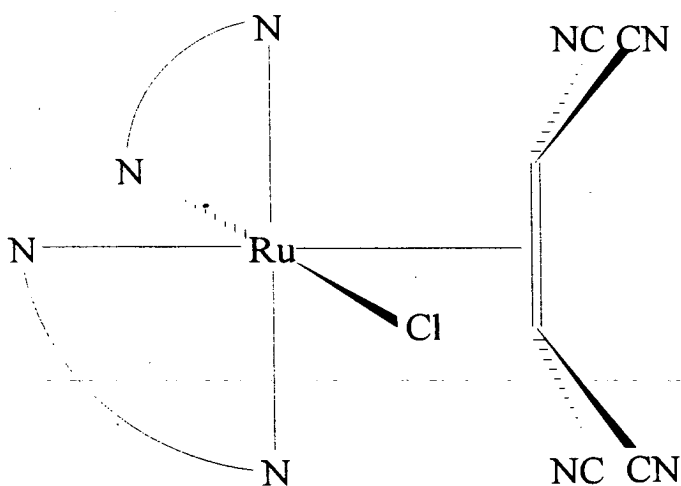
2.2.3   Reactions of Haloosmate(IV) Complexes with tcne

Recently, within this department, a comprehensive study of complexes of general formula $[OsX_{6-n}(py)_n]^{z+}$, n = 0-6, X = Cl, Br, I, was conducted[57,58]. During the course of this work, a great deal of kinetic, electrochemical and UV/visible spectroelectrochemical data were collected for a considerable number of species with osmium oxidation states ranging from +2 to +5. These previously unreported species were prepared by either "conventional" or electrosynthetic methods.

The result of the above study was that any subsequent work involving haloosmate complexes would be able to draw on a considerable database of spectroscopic and electrochemical evidence in any discussions of the frontier orbitals of related species. Also of interest was the discovery that, during electrochemical preparations of the type

$$[OsX_6]^{2-} + e^- \, [OsX_6]^{3-} \xrightarrow[\;k_f\;]{L} [OsX_5L]^{2-} + X^-$$
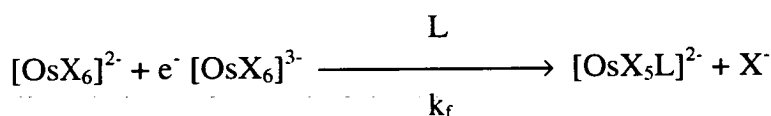
the pseudo-first order rate constant, k_f, is independent of L, where L is a π-accepting ligand, and hence the rate determining step was deduced to be loss of X^- (the rate of halide loss increasing as one progresses down the periodic table from Cl^- to I^-). This has significant implications in that it suggests that reaction can be

induced between $[OsX_6]^{2-}$ and *any* π-accepting ligand in solution by the simple expedient of reducing the starting complex.

It was also discovered in the course of the work described above[57,58] that the redox behaviour of the complexes generally obeyed the "ligand parameterisation" and "ligand additivity" rules for electrochemistry proposed by Lever[59] and Bursten[60] (similar hypotheses have also been put forward for a wide variety of spectroscopic techniques, as summarised in Bursten's review[60]). Essentially the concept behind the hypotheses of ligand parameterisation and additivity is that if the potential of the $M^{n/n+1}$ couple is known for species related to the complex under study then it should be possible to accurately predict the potential of the same couple in the complex under study. For example, if the $Os^{III/IV}$ couples for $[OsCl_6]^{2-}$ and $[OsCl_5(py)]^-$ are known, then it should be possible to predict the potential at which the $Os^{III/IV}$ process occurs in $[OsCl_4(py)_2]$. In practice this was found to be the case, although for the $Os^{II/III}$ couples it was found that the predictions only held for the *trans* isomer of the disubstituted species[57]. This isomeric dependence is incorporated in Bursten's model[60], which predicts, for the $Os^{II/III}$ couple in the system $[OsX_{6-n}(py)_n]^{z+}$ a linear plot of $E_{1/2}$ against n for n = 0, 1 and the *trans* isomer of n = 2. Lever's model, on the other hand, does not make allowances for geometrical isomerism[59], but its predictions were also found to agree well with experimental data for the *trans* disubstituted complexes[57].

As a means of extending the known chemistry of tcne, tcnq and haloosmate complexes a number of reactions between tcnx and haloosmate complexes were

studied electrosynthetically. Relative to the above study, there is one complication in these systems in that the π-accepting ligands are generally more readily reduced than the metal complexes, therefore, these electrosyntheses represent attempts to induce reaction between $[OsX_6]^{3-}$ and the *reduction products* of π-accepting ligands (the monoanion in the case of tcne, the dianion in the case of tcnq). These reactions were monitored, and their products studied, by electrochemical and spectroscopic methods, enabling deductions to be made about whether the above mechanistic conclusions still held for the tetranitrile ligands (ie. whether the tetranitrile anions reacted in a manner typical of π-acceptor ligands), The nature of the frontier orbitals of the reaction products and intermediates was also investigated.

2.2.3.1 Reaction of tcne with $[OsCl_6]^{2-}$

This reaction was a three step electrosynthesis (as shown schematically overleaf), monitored by electrochemistry, UV/visible spectroscopy and IR spectroscopy. Coulometric studies confirmed that all three steps in the reaction were one electron processes.

$$[OsCl_6]^{2-} + tcne \xrightarrow{\text{+0.2 V}} [OsCl_6]^{2-} + tcne^-$$

$$\downarrow \text{-0.7 V}$$

$$[OsCl_6]^{3-} + tcne^-$$

$$\downarrow$$

$$[OsCl_5(tcne)]^{2-} \xleftarrow{\text{+0.3 V}} [OsCl_5(tcne)]^{3-} + Cl^-$$
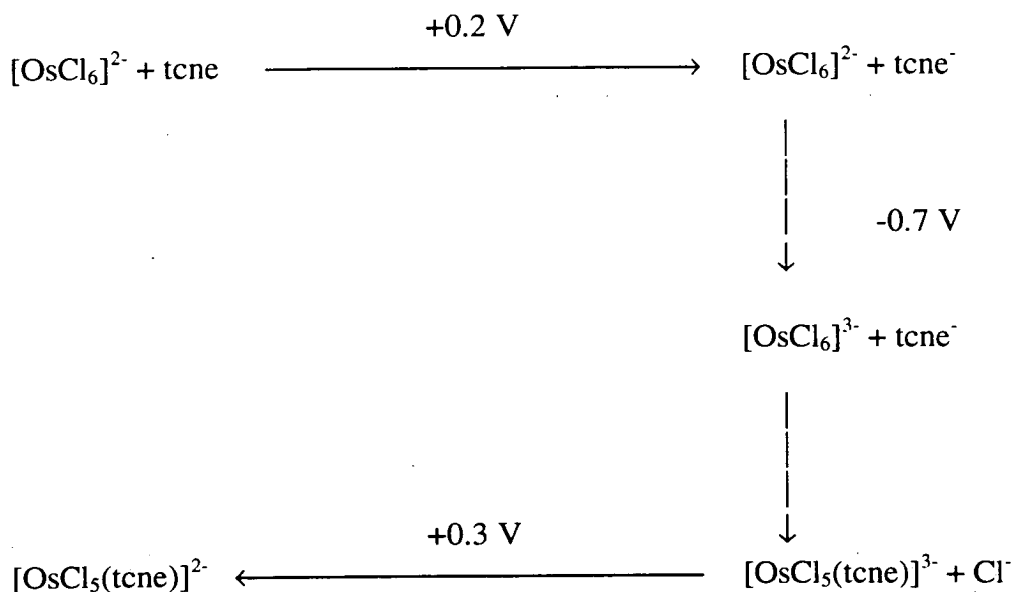
Electrosynthetic reaction of $[OsCl_6]^{2-}$ with tcne.

Figure 2.17 shows the cyclic voltammogram of the starting solution, namely tcne and $[Bu_4N]^+_2[OsCl_6]^{2-}$ in CH_2Cl_2 containing $[Bu_4N]^+[BF_4]^-$ (0.5 moldm^{-3}) as supporting electrolyte. The reversible $Os^{IV/V}$ couple is observed at +1.39 V (once again, all redox potentials are quoted versus Ag/AgCl), while the $Os^{IV/III}$ reduction is at -0.56 V[57] and thus partially superimposed upon the quasi-reversible second reduction of tcne. Figure 2.18 shows the corresponding electronic absorption spectrum, the intense bands at 27000 (ε = 9000 M^{-1}cm^{-1}) and 29000 cm^{-1} (ε = 11000 M^{-1}cm^{-1}) arising from Cl$^-$ to Os charge transfer processes. The IR spectrum showed the anticipated C≡N stretches at 2260 and 2215 cm^{-1}, corresponding to uncoordinated tcne.

Figure 2.17 CV of $[OsCl_6]^{2-}$ and tcne in CH_2Cl_2.
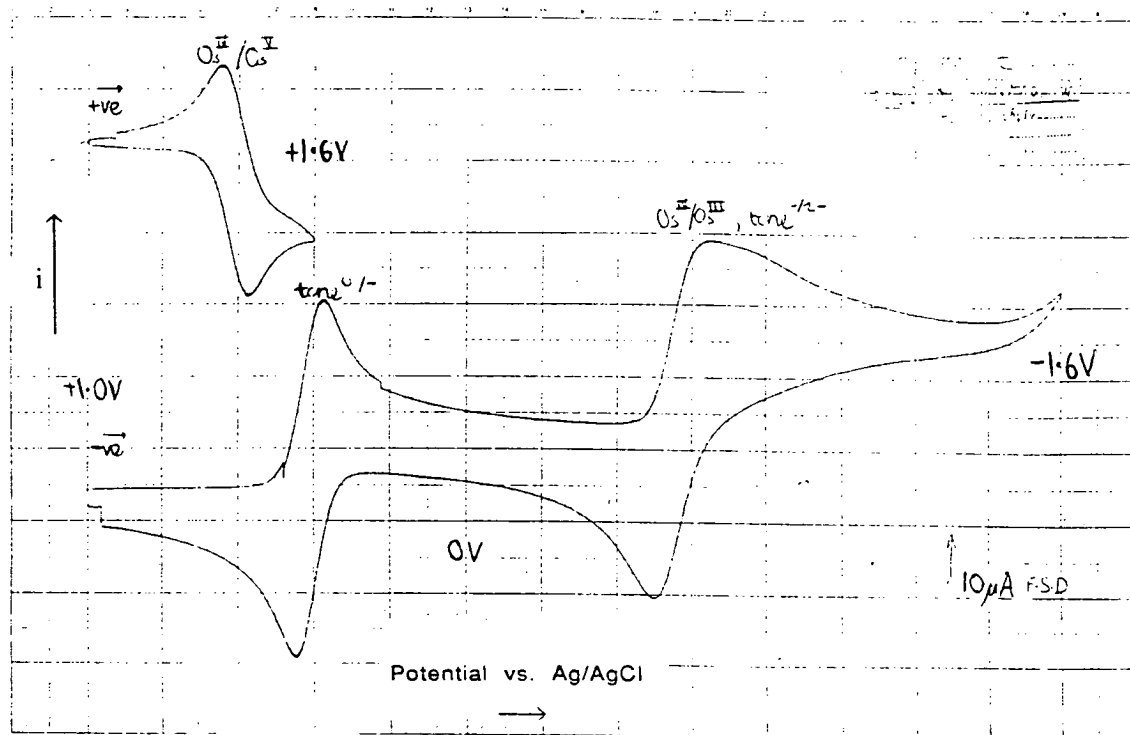
Figure 2.18 Electronic absorption spectrum of $[OsCl_6]^{2-}$ and tcne in CH_2Cl_2.
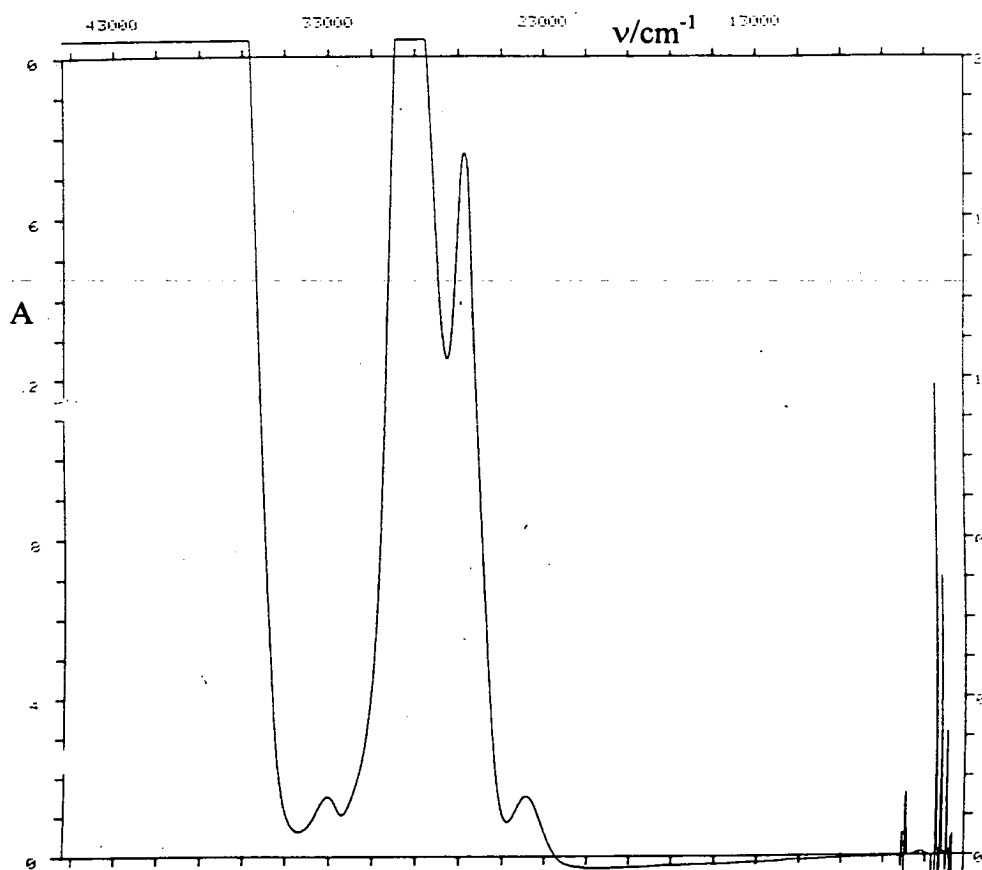
The first step in the synthesis was reduction of tcne. This induced no changes in the cyclic voltammogram of the solution (although, as anticipated, the stirred voltammogram showed that the tcne$^{-/0}$ process at +0.40 V was now an oxidation), while the UV/visible/NIR spectrum (Figure 2.19) showed the expected collapse of the strong, high energy bands observed for neutral tcne accompanied by growth of those normally observed in the spectrum of the radical anion at 23000 cm^{-1} (the new bands are largely masked by the LMCT bands of [OsCl$_6$]$^{2-}$). The IR spectrum showed C$\equiv$N stretching modes at 2180 and 2140 cm^{-1}, consistent with the presence of free tcne^{-}.

Figure 2.19 Electronic absorption spectrum of [OsCl$_6$]$^{2-}$ and tcne^{-} in CH$_2$Cl$_2$
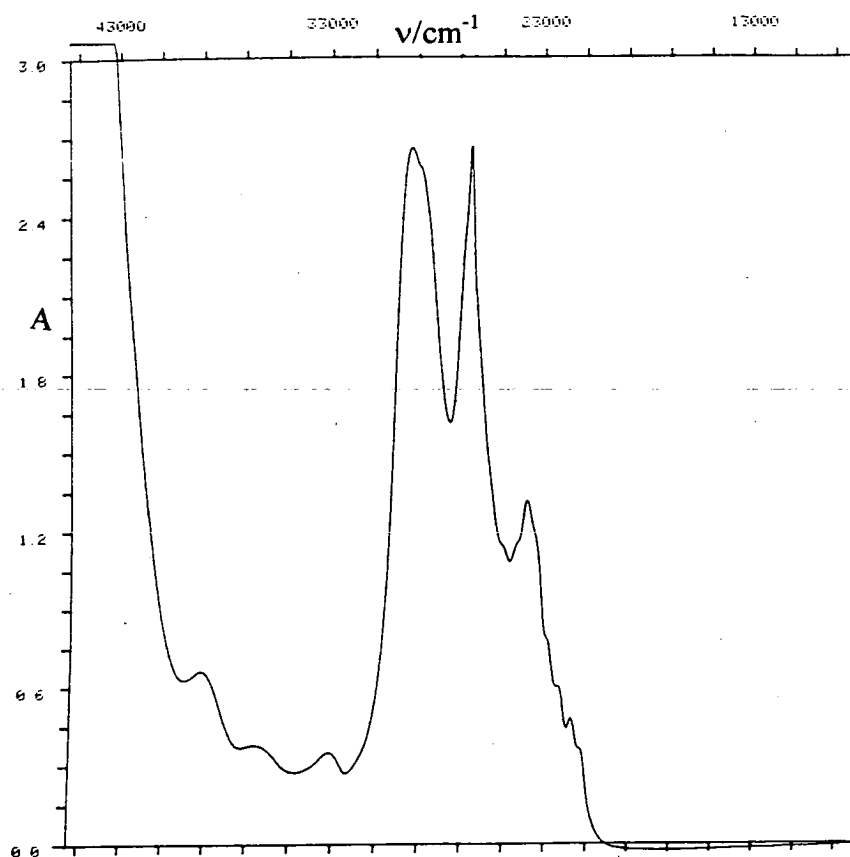
$[OsCl_6]^{2-}$ was now reduced, with a resultant colour change from yellow to an intense blue. As mentioned earlier, it has been shown that reduction of $[OsCl_6]^{2-}$ induces loss of Cl^-, enabling the complex to react with π-acceptor ligands. There was a change in the observed electrochemistry (Figure 2.20), which now showed (in addition to small couples arising from traces of unreacted starting materials), an irreversible oxidation at +1.35 V indicating the presence of free chloride ions in solution, a partially reversible oxidation at +0.78 V and a reversible oxidation at +0.09 V provisionally assigned as the $Os^{III/IV}$ couple and a σ-bound $tcne^{-/0}$ process respectively, and a quasi-reversible reduction at -0.95 V, which may be either a $tcne^{-/2-}$ process or an $Os^{III/II}$ reduction.

The electronic absorption spectrum (Figure 2.21) also revealed substantial changes after this step, with a general collapse of the previously observed bands, and new absorbances at 13000, 17000, 21000, 33000 and 38500 cm^{-1}. Assignment of this spectrum and that obtained after the final step will be dicussed later.

The IR spectrum now revealed sharp bands at 2175 and 2140 cm^{-1}, plus a weaker, broader band at 1810cm^{-1}.

Figure 2.20 CV of $[OsCl_5(tcne)]^{3-}$ in CH_2Cl_2
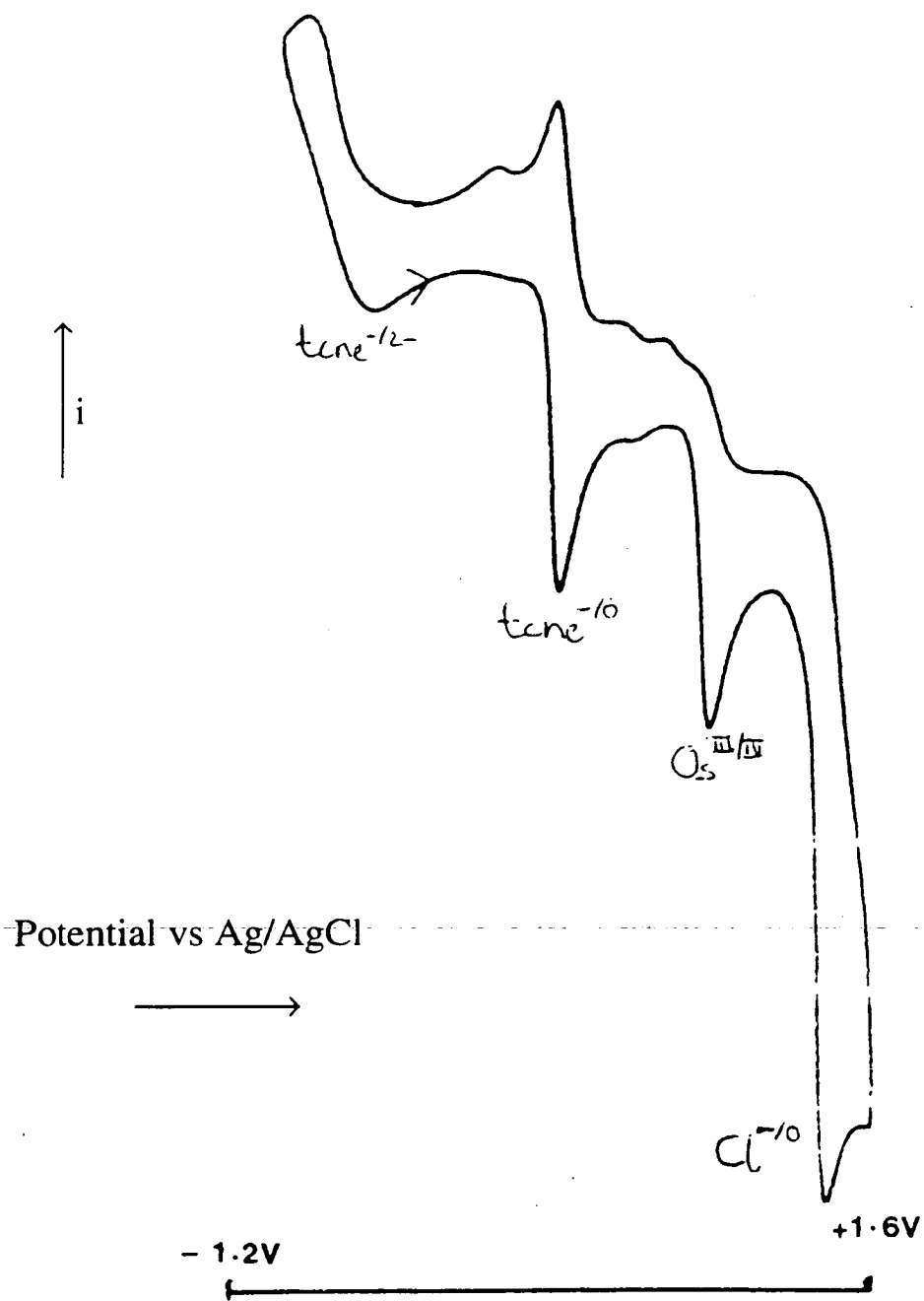
Figure 2.21 Electronic absorption spectrum of $[OsCl_5(tcne)]^{3-}$ in CH_2Cl_2.
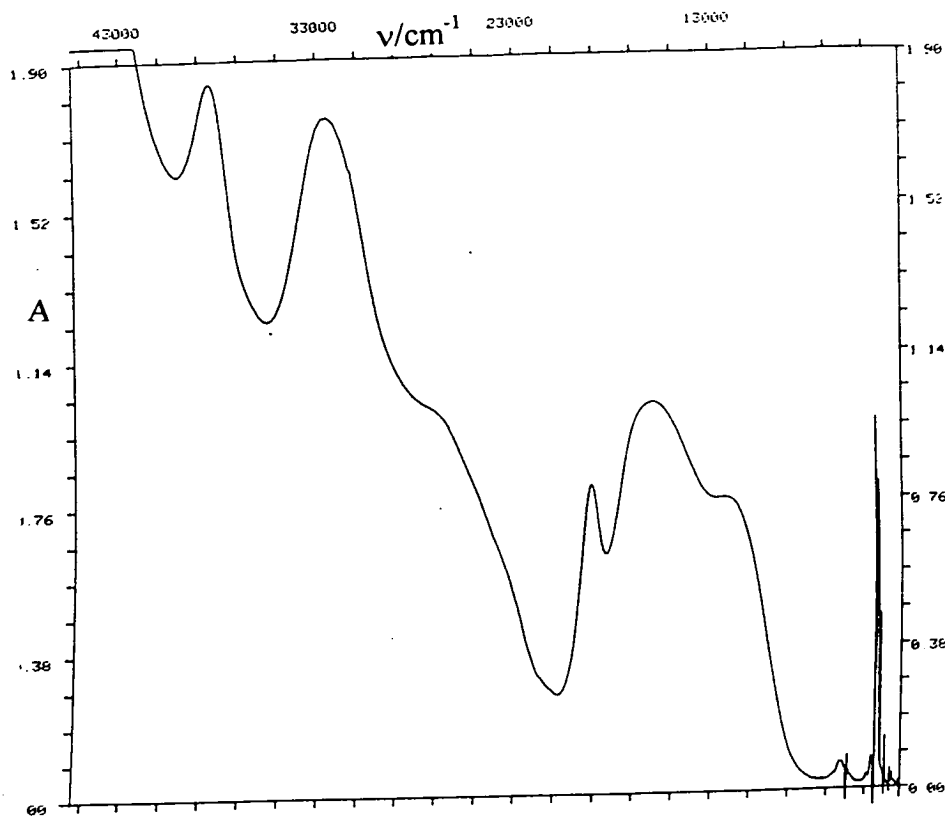
The third and final process involved electrooxidation of the solution, at +0.3 V.

IR spectroscopy of the green product showed $C\equiv N$ stretches at 2195(s),

2180(m,br) and 2040(w) cm^{-1}, this change further suggesting that the process at

+0.09V was tcne-based. The cyclic voltammogram was unaffected by this

oxidation.

In the UV/visible/NIR spectrum (Figure 2.22), the maxima were now at 6500,

9000, 13000, 25000 and 27500 cm^{-1}.

The product was found to be air stable as a solid but attempts to purify it by

chromatographic methods resulted in rapid decomposition.

Figure 2.22 Electronic absorption spectrum of $[OsCl_5(tcne)]^{2-}$ in CH_2Cl_2.
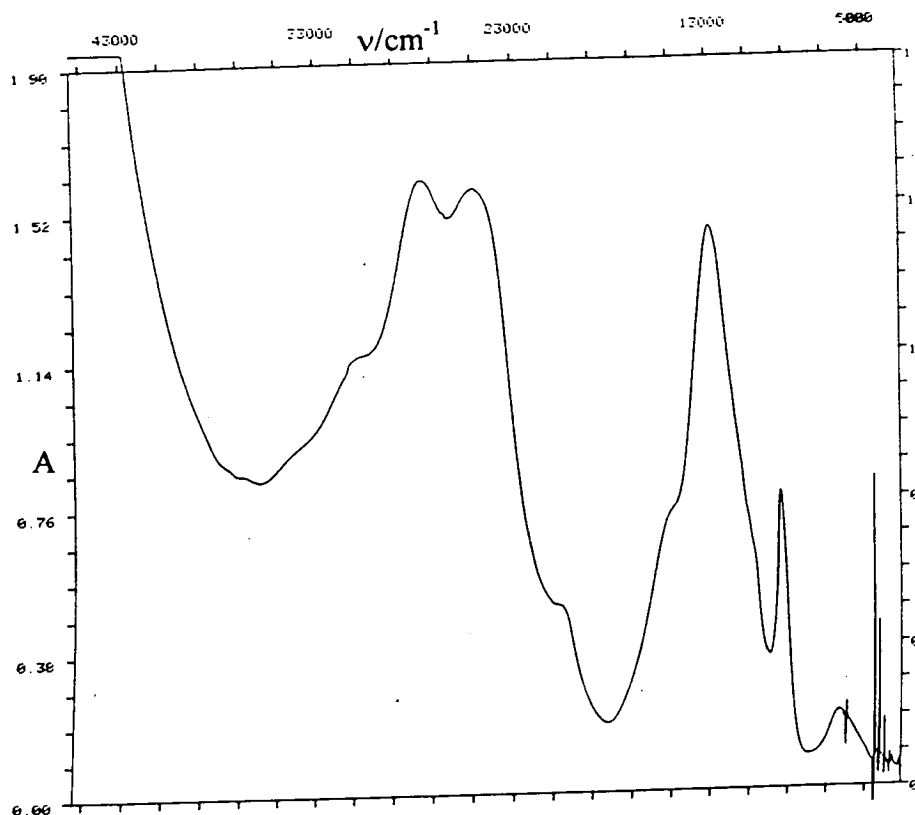
As a result of the electrochemical and spectroscopic evidence obtained, it is believed that the green product of this electrosynthesis was the Os-N σ-bound complex $[OsCl_5(tcne)]^{2-}$, with tcne formally bound as the neutral ligand. Formation of this compound by the method employed shows that tcne can act as a π-accepting ligand, a further example of the π-acidity of the tetranitrile. Evidence of the π-accepting power of tcne is also obtained by comparison of the observed redox behaviour with previously synthesised complexes of formula $[OsCl_5L]^{n-}$, where n = 1, 2[57]. The $Os^{III/IV}$ couple in complexes of the form $[OsCl_5L]^{n-}$ generally occurs at modest potentials. For example, when L = PhCN, $E_{1/2}$ = +0.16 V vs Ag/AgCl, compared to $E_{1/2}$ = +0.78 V when L = tcne. When L is the strong

π-acceptor CO, however, the $Os^{III/IV}$ process is observed at +1.06 V. The negative

shift of the $tcne^{0/-}$ couple from +0.40 V to +0.09 V upon coordination shows that

there is considerable electron tranfser from Os^{III} to tcne, presumably by π-back

bonding.

UV/visible spectroscopic data for $[OsCl_6]^{2-}$, $[OsCl_5(tcne)]^{2-}$ and $[OsCl_5(tcne)]^{3-}$

are collected in Table 2.7 for ease of reference.

Table 2.7 UV/visible data for $[OsCl_6]^{2-}$, $[OsCl_5(tcne)]^{2-}$ and $[OsCl_5(tcne)]^{3-}$.

Complex	v_{max}/cm^{-1} ($10^{-3}\varepsilon$/mol^{-1}cm^{-1}dm^3)
$[OsCl_6]^{2-}$	27000(9), 29000(11)
$[OsCl_5(tcne)]^{2-}$	6260(0.4), 13000(4.6), 17000(6.1), 21000(4.8), 33000(10.5), 38500(11)
$[OsCl_5(tcne)]^{3-}$	6320(0.8), 9000(4.7), 13000(9.1), 25000(9.8), 27500(10)

In the UV/visible spectrum of $[OsCl_5(tcne)]^{2-}$, the bands at 25000 and 27500

cm^{-1} were assigned, after comparison with related species such as $[OsCl_5(py)]^{2-}$, as

arising from Cl^- to Os^{III} LMCT transitions. The series of peaks at approximately

13000 cm^{-1} were attributed to tcne to Os^{III} charge transfer processes. The weak

band at 6300 cm^{-1} is thought to be a forbidden metal-based transition which arises

from the lost degeneracy of the t_{2g} orbitals. A similar band has been observed, for

example, in the electronic absorption spectrum of $[Os(bpy)_2Cl(PPh_3)]^+$, in which $\nu_{max} = 6990$ cm^{-1} ($\varepsilon = 150$ mol^{-1}dm^{3}cm^{-1})[61].

Assignment of the spectrum of $[OsCl_5(tcne)]^{3-}$ is significantly more difficult. It was suggested above that the first reduction is tcne based, resulting in formation of $[Os^{III}Cl_5(tcne^-)]^{3-}$. If this hypothesis is correct then we might expect reduction to induce a small shift in the positions of the Cl$^-$ to Os^{III} charge transfer bands to higher energy, consistent with a small increase in electron density at Os. In the observed spectra however, addition of an electron induces an blue-shift of at least 8000 cm^{-1} in the band positions to 33000 and 38000 cm^{-1}. We must also assign the bands in the vicinity of 17000 cm^{-1}.

An internal redox process from tcne$^-$ to Os^{III} is unlikely, given the electrochemistry of the complexes, where the relative positions and reversibilities of the two observed reductions both support the theory that these processes are tcne-based, and by the fact that bands apparently related to the expected Cl$^-$ to Os^{III} are observed. The energies of the maxima are considerably higher than expected but in Os^{II} complexes, Cl$^-$ to Os charge transfer processes are not normally observable at moderate energies.

The most likely explanation, therefore, is that reduction of tcne in the formation of $[OsCl_5(tcne)]^{3-}$ results in a lowering in energy of the (tcne)$^-$ SOMO such that it lies close to that of the Os^{III} SOMO allowing extensive mixing of the two orbitals in question. This would result in a new, unoccupied orbital with substantial metal character, at considerably higher energy than the SOMO of

85

[OsCl$_5$(tcne)]$^{2-}$ and a corresponding new HOMO, at lower energy. The molecular orbital diagram in Figure 2.23 below attempts to explain the shift in the "Cl$^-$ to Os^{III}" charge transfer band, and the origins of the band observed at low energy, which can now be assigned to electron transfer between the two new molecular orbitals.

Figure 2.23 Effect on Os and tcne-based MO's of reduction of [OsCl$_5$(tcne)]$^{2-}$ to [OsCl$_5$(tcne)]$^{3-}$.
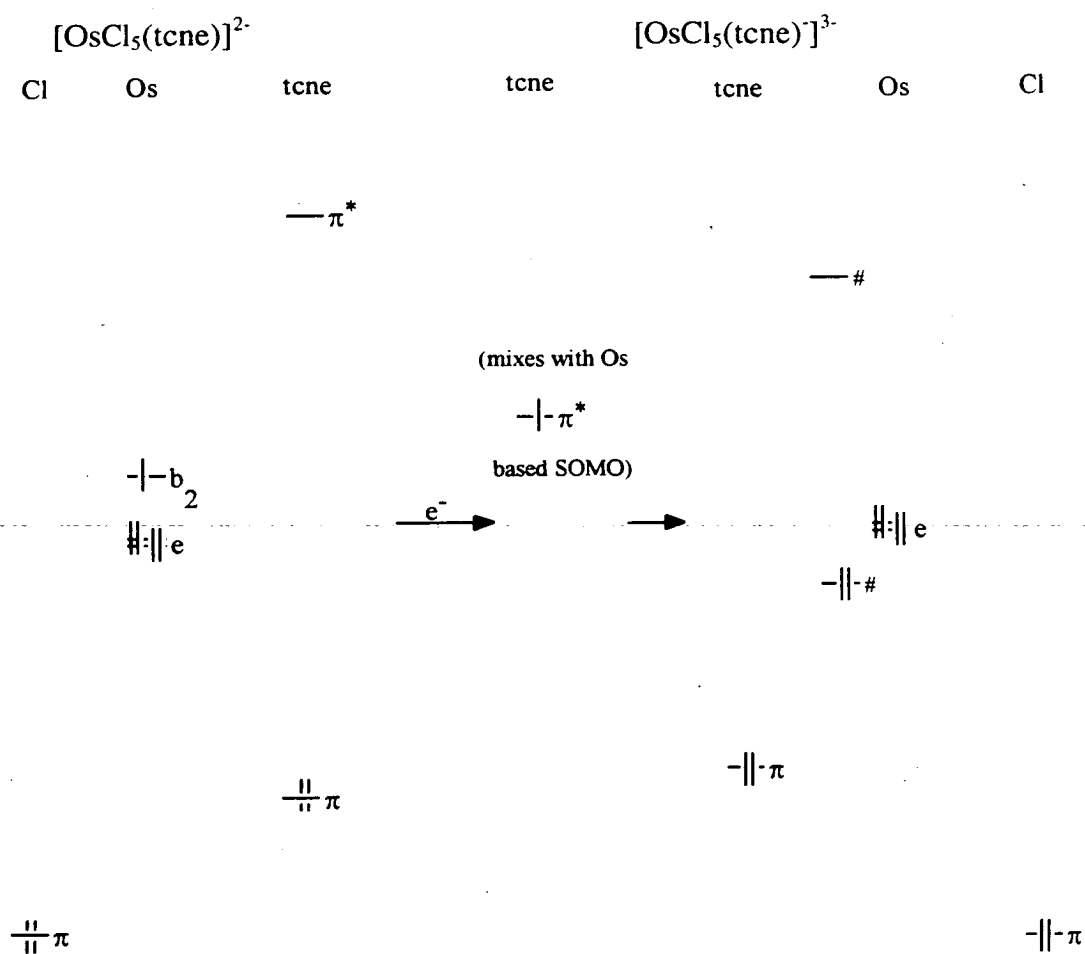
#: These orbitals have significant Os **and** tcne character

86

In order to obtain more information about the above reaction the electrosynthesis was repeated in the OTE cell, in CH_2Cl_2 at 273 K. Reduction of tcne (shown in Figure 2.24) induced collapse of the π to π^* bands at 37000 and 39000 cm^{-1} and growth of the corresponding bands for the same transition in the radical anion at 23000 cm^{-1}. An isosbestic point was observed at 35500 cm^{-1}, as had been the case when only tcne was studied (Figure 1.8), thus confirming that no reaction between metal and ligand was occurring at this stage.

Figure 2.24 Absorption spectral monitoring of reduction of tcne in the presence of $[OsCl_6]^{2-}$, at 273 K in CH_2Cl_2, E_{app} = +0.2 V.
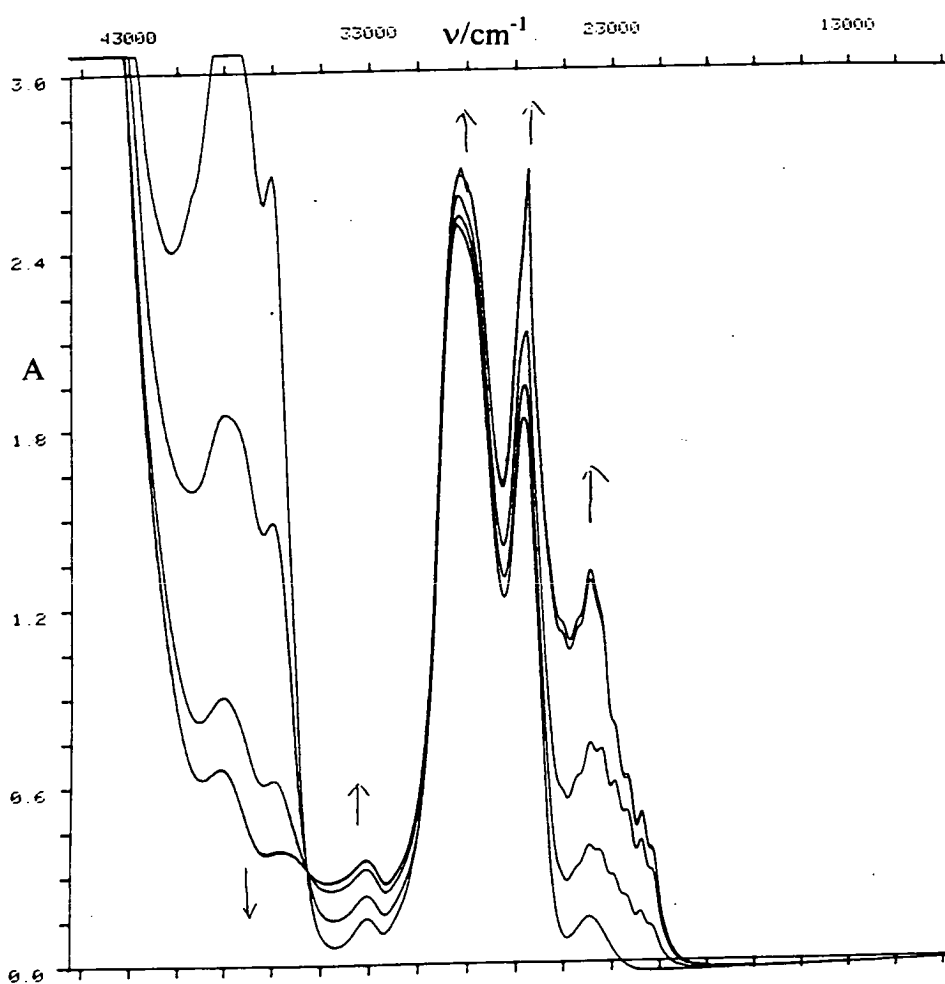
Reduction of $[OsCl_6]^{2-}$ followed and spectra monitoring progress of the reduction are shown in Figure 2.25. It should be noted that electrogeneration had not gone to completion when the recording of the series of spectra ended. This induced collapse of the original (Cl^- to Os^{IV}) LMCT and tcne$^-$ π - π^* bands, accompanied by growth at higher and lower energies as seen previously in the bulk electrosynthesis. Isosbestic points were observed at 21000 and 31000 cm^{-1}. This suggests that there are no significant intermediates in this reaction, ie. that the loss of chloride takes place rapidly compared with the electrogeneration that induced it, and the subsequent coordination of tcne$^-$ is also a very rapid process. This is consistent with the observations made during the electrosynthetic reaction of $[OsCl_6]^{2-}$ with pyridine and implies a similar mechanism of formation[57].

The reoxidation of the product is shown in Figure 2.26. It should be noted however that the spectrum also shows some regeneration of unreacted $[OsCl_6]^{2-}$, a phenomenon not observed when the reaction was carried out in a conventional coulometry cell (presumably because of the more efficient mass transport afforded by stirring the solution in the coulometric cell). In this case the "crossover points" at 15000 and 31000 cm^{-1} were not isosbestic (an isosbestic point was observed, however, at 20000 cm^{-1}), because electrogeneration of more than one species was taking place simultaneously.

Figure 2.25 Absorption spectra showing reduction of $[OsCl_6]^{2-}$ in the presence of tcne⁻, in CH_2Cl_2 at 273 K, E_{app} = -0.7 V.
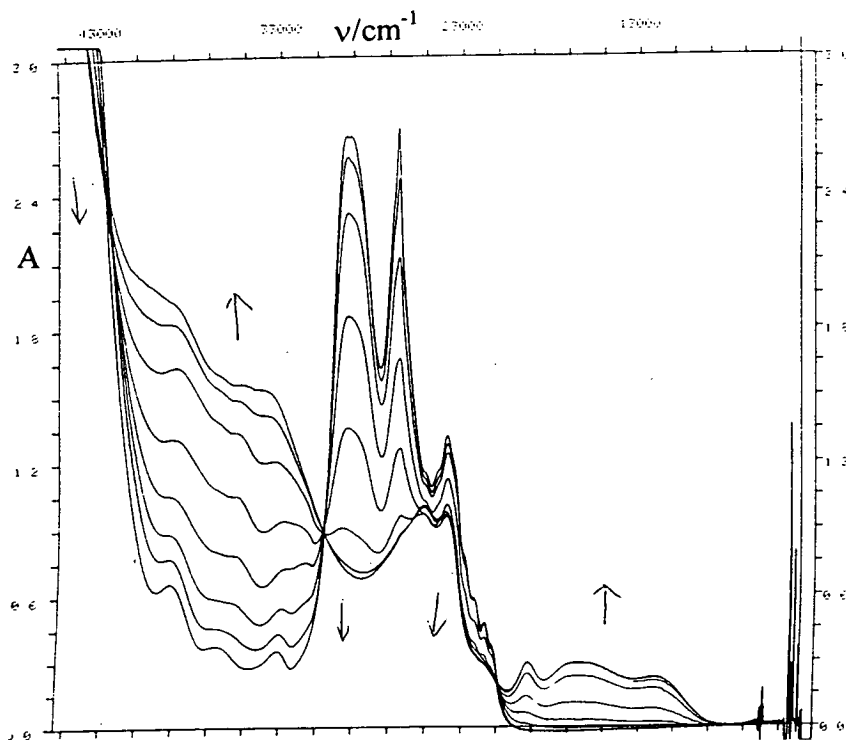
Figure 2.26 Absorption spectral monitoring of oxidation of $[OsCl_5(tcne)]^{3-}$ in CH_2Cl_2 at 273 K, E_{app} = +0.3 V.
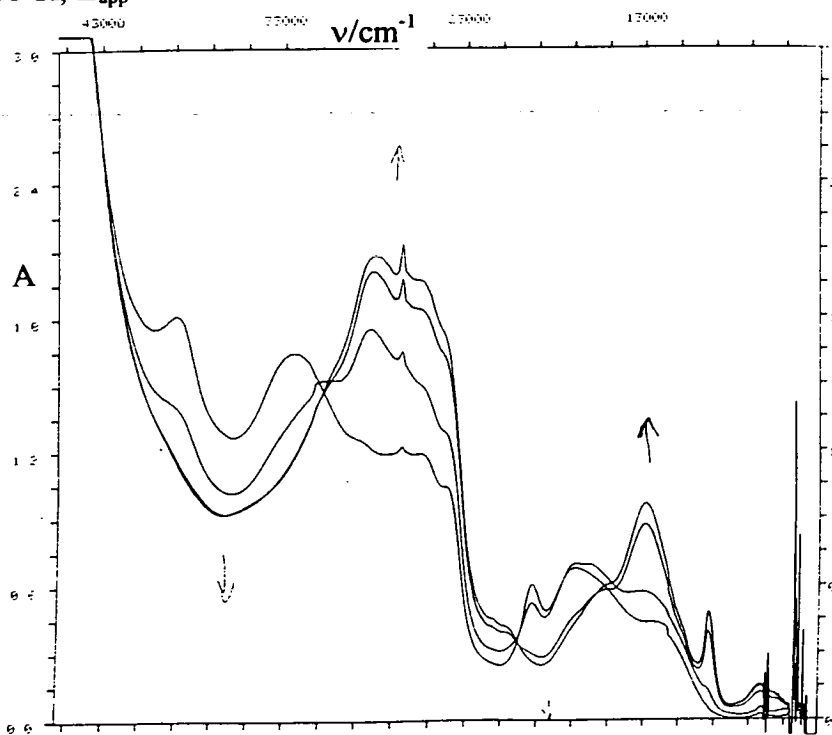
The data obtained in the above experiments suggest strongly that the product of the electronically induced reaction of tcne with $[OsCl_6]^{2-}$ is the Os-N σ-bound complex $[OsCl_5(tcne)]^{2-}$. The first reduction of the product complex, at +0.09 V versus Ag/AgCl, appears to be tcne-based, suggesting that the tetranitrile is bound as the neutral ligand and osmium has an oxidation state of +3, although there is significant electron transfer from metal to tcne, via back-bonding into the π^* LUMO, hence the negative shift of the ligand-based reduction. Product formation involves reaction of $[OsCl_6]^{3-}$ with tcne⁻, which appears to follow a similar mechanism to reaction of $[OsCl_6]^{3-}$ with other π-accepting ligands such as pyridine[57,58].

2.2.3.2   Reaction of tcne with $[OsBr_6]^{2-}$

This reaction was carried out in order to allow comparison with the similar experiment carried out using $[OsCl_6]^{2-}$ above, particularly with regard to electrochemical and spectroscopic behaviour, where comparisons might assist and confirm assignments.   Figure 2.27 shows a cyclic voltammogram of the starting mixture of $[Bu_4N]^+_2[OsBr_6]^{2-}$ and tcne in CH_2Cl_2, which immediately reveals a significant advantage of $[OsBr_6]^{2-}$ over its hexachloro analogue. In the case of the hexabromo complex, the $Os^{IV/III}$ couple has an $E_{1/2}$ value of -0.42 V versus Ag/AgCl, 0.14 V more positive than $[OsCl_6]^{2-}$, therefore the second reduction of tcne is not partially superimposed on the osmium-based reduction.

90

Figure 2.27 CV of [OsBr$_6$]$^{2-}$ and tcne in CH$_2$Cl$_2$.
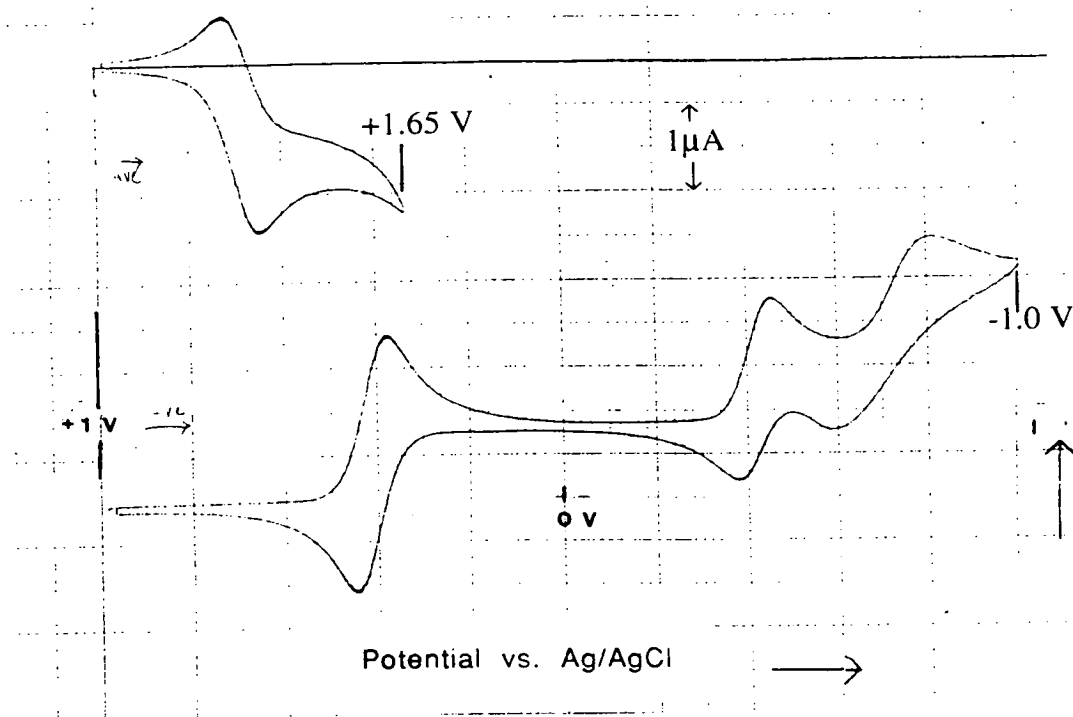
Reduction of tcne had no effect on the CV, and the UV/visible/NIR spectrum again shows a simple superposition of the tcne$^-$ π - π* bands on those arising from the Br$^-$ to Os LMCT (Figure 2.28). The LMCT bands are at lower energy than in the corresponding hexachloro complex (the first group are at 20000, 22000 and 24000 cm^{-1}). For ease of reference, electronic spectral data for [OsBr$_6$]$^{2-}$, [OsBr$_5$(tcne)]$^{3-}$ and [OsBr$_5$(tcne)]$^{2-}$ are collected in Table 2.8.

Reduction of osmium again induced halide loss, with subsequent coordination of tcne. The electrochemistry of the product complex (Figure 2.29) showed reversible oxidations at +0.15 V (assigned to bound tcne) and +0.84 V (assigned as the Os$^{III/IV}$ couple). The smaller wave at +0.40 V shows the presence of a small

amount of unreacted tcne (the CV of the starting solution reveals an apparent excess of the ligand). An irreversible process, arising from oxidation of free Br⁻ ions was observed at +1.3 V.

The electronic absorption spectrum (Figure 2.30) now shows bands at 16500 and 27000 cm^{-1}, provisionally assigned as tcne⁻ to Os^{III} and Br⁻ to Os^{III} LMCT bands respectively. The IR spectrum showed $C{\equiv}N$ stretches at 2180(s), 2140(w) and 2100(w) cm^{-1}.

Figure 2.28 Electronic absorption spectrum of tcne⁻ and $[OsBr_6]^{2-}$ in CH_2Cl_2.
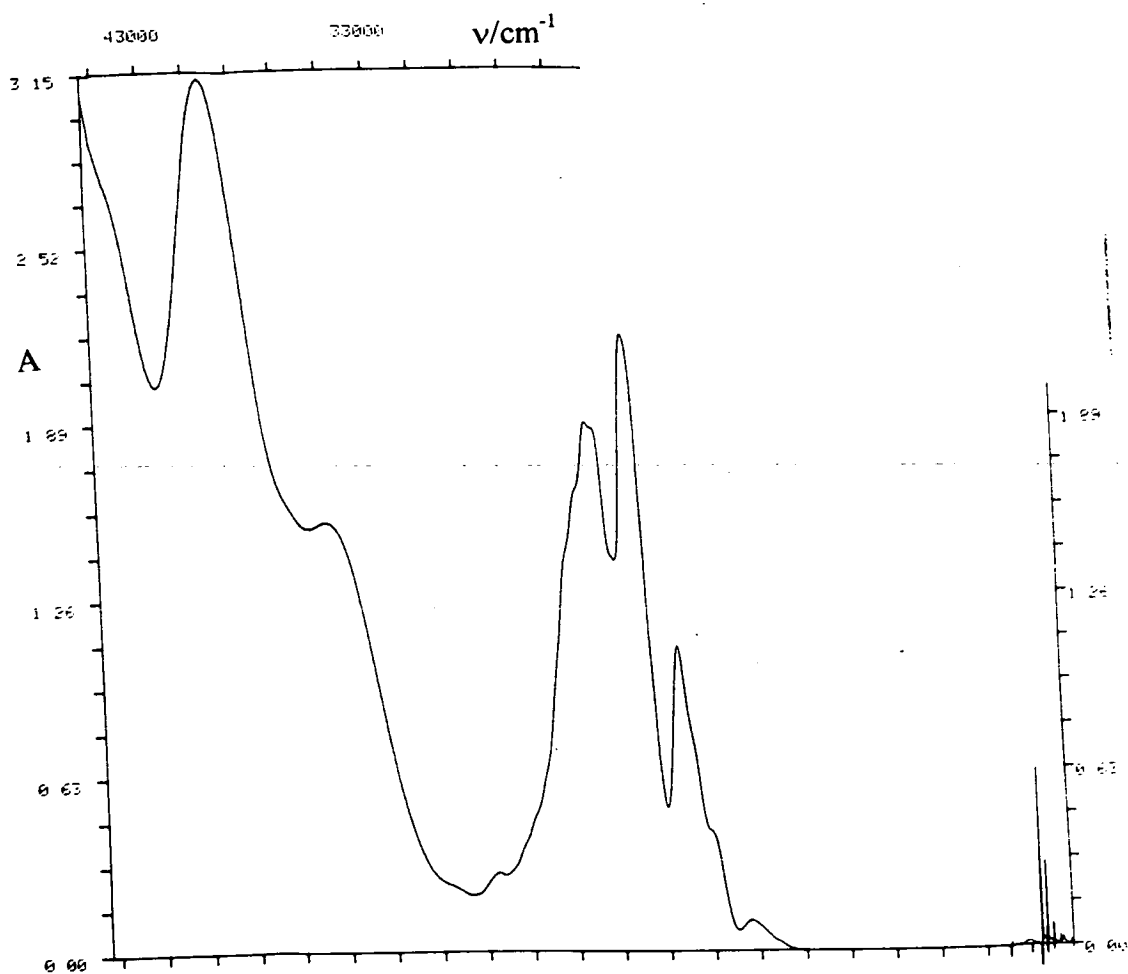
Figure 2.29 A.c. voltammogram of $[OsBr_5(tcne)]^{3-}$ (plus unreacted $tcne^-$) in CH_2Cl_2.
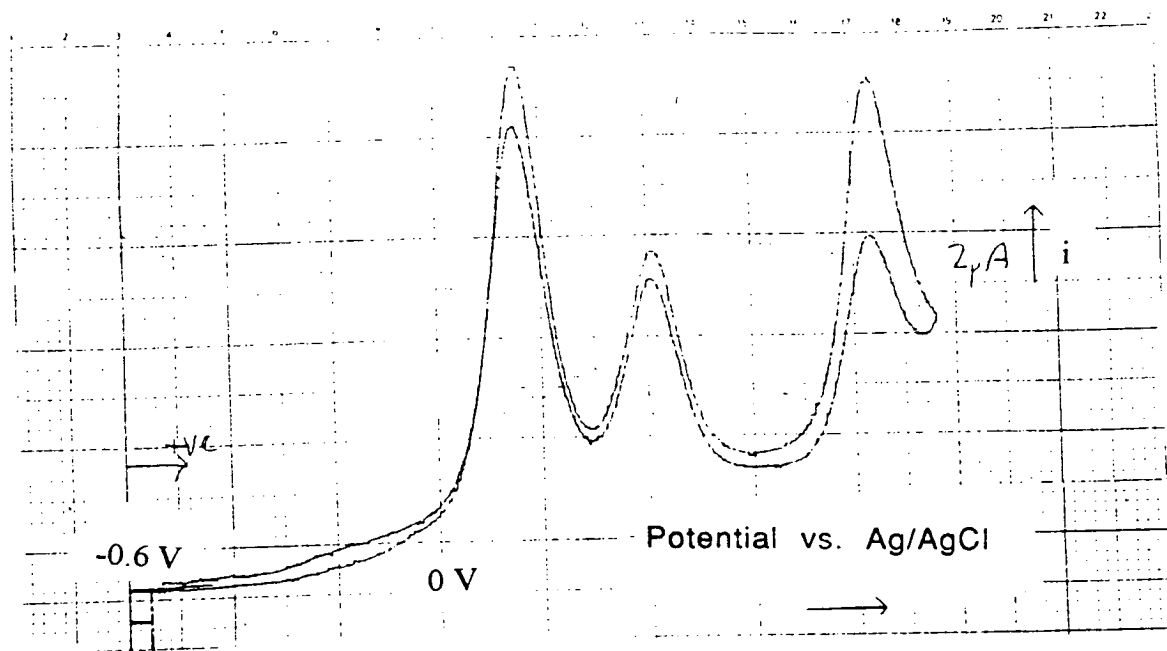
Figure 2.30 Electronic absorption spectrum of $[OsBr_5(tcne)]^{3-}$ in CH_2Cl_2.
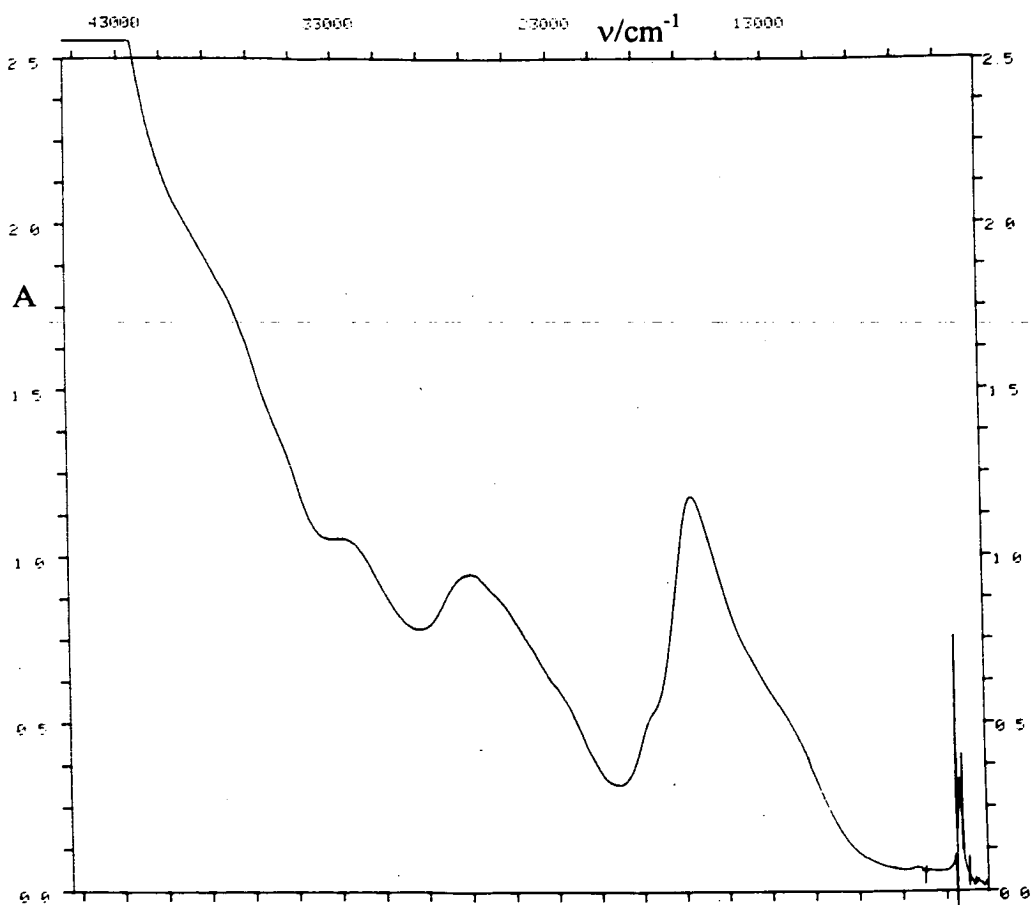
Reoxidation of tcne again caused no observable change in the cyclic voltammetry of the complex. The UV/visible/NIR spectrum (Figure 2.31) showed bands at 6200, 9000, 12300, 15000 and 27000 cm^{-1}. In the IR spectrum, the C≡N stretching modes are observed at 2195(s), 2140(vw) and 2100(m,br) cm^{-1}.

Table 2.8 UV/visible data for [OsBr$_6$]$^{2-}$, [OsBr$_5$(tcne)]$^{3-}$ and [OsBr$_5$(tcne)]$^{2-}$.

Complex	ν_{max}/cm^{-1} ($10^{-3}\varepsilon$/mol^{-1}dm^{3}cm^{-1})
[OsBr$_6$]$^{2-}$	20000(8.0), 22000(12), 23500(7.0), 35000(10), 40000(22)
[OsBr$_5$(tcne)]$^{3-}$	16500(12), 27000(9.5), 33000(10.6)
[OsBr$_5$(tcne)]$^{2-}$	6150(1.9), 9050(4.4), 12300(11), 15000(11), 27000(12)

The data aquired clearly shows that [OsBr$_6$]$^{2-}$ has reacted with tcne in the same fashion as [OsCl$_6$]$^{2-}$, to give the product [OsBr$_5$(tcne)]$^{2-}$, featuring Os in the +3 oxidation state and neutral, σ-bound tcne. In this case, however, the green product was less stable than when the analogous reaction was carried out with [OsCl$_6$]$^{2-}$.

2.2.3.3   Reaction of tcne with [OsCl$_5$(py)]$^-$

This reaction was studied briefly with the primary objective of obtaining more evidence for the mechanism of reaction between halo-osmate complexes and tcne. In this example, unlike those above, reduction of osmium (E$_{1/2}$ for the Os$^{IV/III}$ couple

is at +0.02 V versus Ag/AgCl) does not induce rapid reaction with tcne⁻. Instead, after 2 hours, voltammetric studies of the reaction mixture showed that less than 50% of the starting complex had been consumed. The electrochemistry of the product complex (assumed to be [OsCl₄(py)(tcne)]⁻) showed a bound tcne$^{0/-}$ couple at +0.23 V, and an irreversible chloride oxidation at +1.35 V. The metal-based oxidation was not observed, suggesting that it lay at a more positive potential than the Cl⁻ oxidation.

Figure 2.31 Electronic absorption spectrum of [OsBr₅(tcne)]$^{2-}$ in CH₂Cl₂.
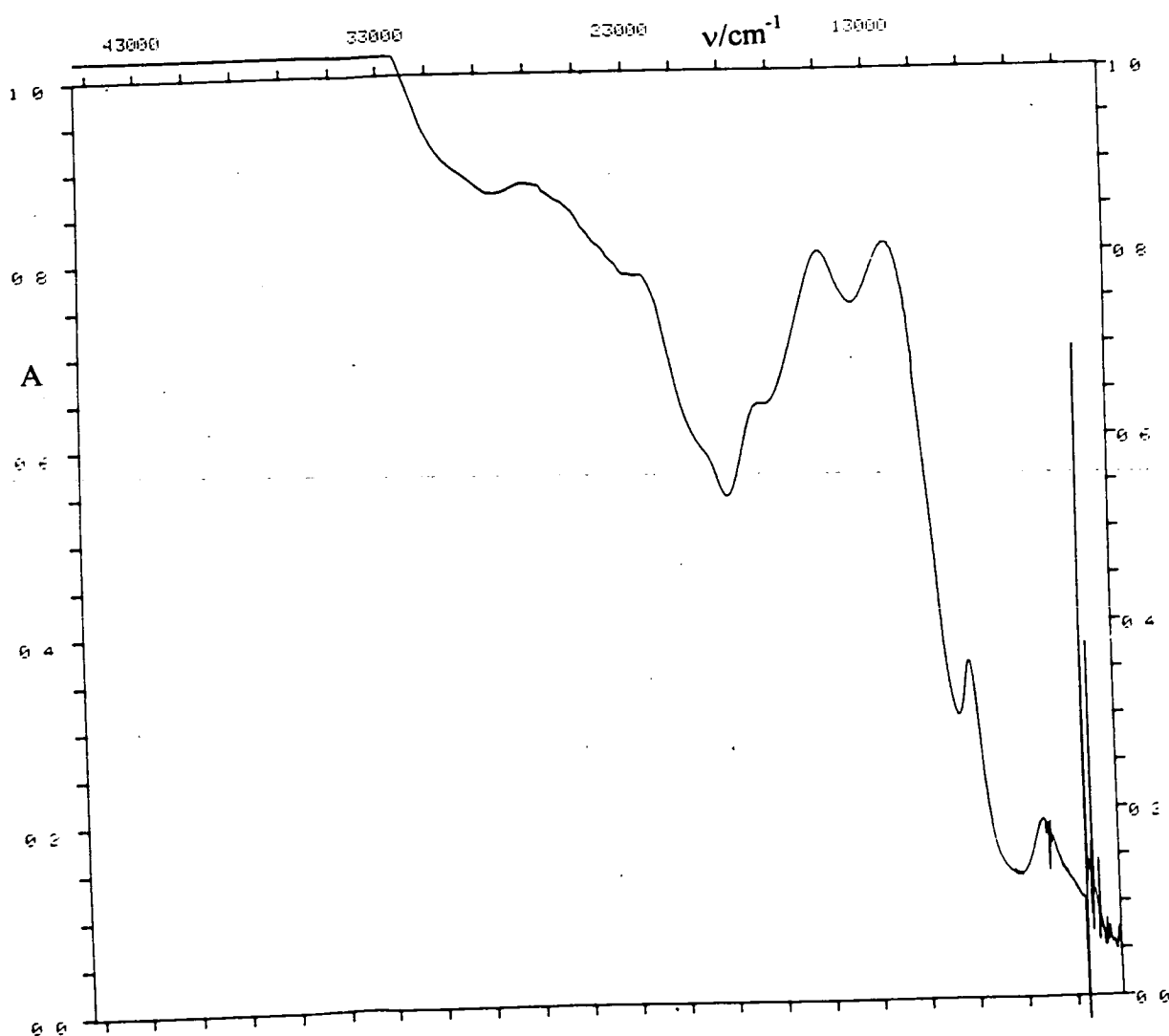
Previous studies have revealed that reduction of $[OsCl_5(py)]^-$ to form the Os^{III} complex does not induce rapid halide loss, unlike reduction of the hexahalo complexes[57,58]. Thus the greatly reduced reaction rate shows that loss of halide is the rate determining step in the electrochemically induced reaction between $[OsCl_5(py)]^{2-}$ and tcne$^-$, and, by extension, in the reactions of hexahaloosmate complexes with tcne$^-$. This implies that the reaction proceeds by a dissociative mechanism in which halide loss must occur before tcne is able to coordinate to osmium. Similar behaviour was observed in previous studies of electrosynthetic reactions of haloosmate complexes with π-accepting ligands[57,58].

2.2.3.4   Attempted Reaction Between $[OsCl_6]^{2-}$ and tcnq

Attempts were made to induce reaction between these species by electrochemical means. In this case, however, the second reduction of tcnq occurs at a more positive potential than the $Os^{IV/III}$ couple, therefore it was necessary to electrogenerate the dianion of the tetranitrile prior to reduction of osmium. In the event, no reaction was observed between tcnq^{2-} and $[OsCl_6]^{3-}$, presumably because formation of the dianion, giving a fully occupied π^* LUMO, destroys the π-accepting character of tcnq and effectively removes the possibility of the reaction following the general $[OsCl_6]^{3-}$/L mechanism observed previously (L is any π-accepting ligand).

2.2.3.5   Conclusions

The complexes $[OsCl_5(tcne)]^{2-}$, $[OsBr_5(tcne)]^{2-}$ and $[OsCl_4(py)(tcne)]^-$ were all prepared by electrosynthetic methods, reaction taking place in all three cases between $tcne^-$ and the reduction product of the starting complex. All three reactions appeared to proceed in a manner typical of reactions of halo-osmate complexes with π-acceptor ligands, the rate determining step apparently being loss of halide, followed by rapid attack of $tcne^-$. The redox data, and UV/visible and IR data are consistent with the $[OsX_5(tcne)]^{2-}$ containing neutral, σ-bound tcne. It is reasonable to assume that the same coordination mode of tcne is adopted in the pyridine complex.

The potency of tcne as a π-acceptor is made evident by the extremely large positive shifts in the potentials of the Os-based redox processes - pentahalo osmium complexes in which the stable oxidation state of Os is +3 are very unusual.

In the case of $[OsCl_4(py)(tcne)]$, the $Os^{III/IV}$ couple was not observed in the CV of the product. It was assumed that this is because of the Cl^- oxidation at +1.35 V. The principles of ligand additivity proposed by Bursten[60] and Lever[59] may be used to test this assumption, as it was found in previous studies of haloosmate complexes that, unlike the $Os^{II/III}$ couples, the $Os^{III/IV}$ couples were not affected by geometrical isomerism[57,58]. Lever's general equation for prediction of the $E_{1/2}$ is given overleaf, where E_{calc} is the predicted $E_{1/2}$ value, S_M and I_M are constants for a specific redox couple of a given metal (assuming spin state remains unchanged),

ΣE_L is the sum of the contributions made by each ligand to the electrochemistry of the metal centre (in general, for π-donors $E_L < 0$ and for π-acceptors $E_L > 0$) and C_{ref} is a correction term dependent on the reference electrode in use (for the system used in this research, $C_{ref} = -0.105$).

$$E_{calc} = S_M (\Sigma E_L) + I_M + C_{ref} \qquad (I)$$

The values of E_L for Cl^- and py were reported by Lever to be -0.24 V and +0.25 V respectively[59], while previous work within this department[57] determined values for $Os^{III/IV}$ couples of $S_M = 1.05$ and $I_M = 1.095$. Given these values it is possible to predict that the $Os^{III/IV}$ couple in $[OsCl_6]^{2-}$ will be at

$$
\begin{aligned}
E_{calc} &= (1.05 \times 6 \times -0.24) + 1.095 - 0.105 \\
&= -0.52 \text{ V vs Ag/AgCl}
\end{aligned}
$$

which is a reasonable approximation to the experimentally determined value. Applying the same equation, it is possible to calculate an approximate value for E_{tcne} in the M-N σ-bound mode of coordination. In the cyclic voltammogram of $[OsCl_5(tcne)]^{2-}$, the $Os^{III/IV}$ couple was observed at +0.78 V. Inserting this value into equation (i) gives

$$
\begin{aligned}
0.78 &= (1.05 \times (5 \times -0.24 + E_{tcne})) + 1.095 - 0.105 \\
&= (1.05 \times E_{tcne}) - 0.27
\end{aligned}
$$

therefore,

$$E_{tcne} = (0.78 + 0.27)/1.05 = 1.00$$

This figure is not unreasonable for a strong π-acceptor ligand such as tcne. Using the approximate value of E_{tcne} (a more accurate determination would require comparison of a series of related tcne complexes), it is possible to predict $E_{1/2}$ for the $Os^{III/IV}$ couple in $[OsCl_4(py)(tcne)]^-$.

$$E_{calc} = (1.05 \times (4 \times -0.24 + 0.25 + 1.00) + 1.095 - 0.105$$

$$= +1.29 \text{ V vs Ag/AgCl}$$

If the above estimate of $E_{1/2}$ is reasonable, then the oxidation of the Os centre would be superimposed upon that of Cl^- in the cyclic voltammogram.

A further test of the validity of the approximate value of E_{tcne} can be obtained by comparing predicted and experimental $E_{1/2}$ values for $[OsBr_5(tcne)]^{2-}$. Given that $E_{Br} = -0.22 \text{ V}^{59}$,

$$E_{calc} = 1.05 \times (1.00 - 5 \times 0.22) + 1.095 - 0.105$$

$$= +0.885 \text{ V}$$

which compares fairly well with the experimental value of +0.84 V and thus shows that the approximate value of E_{tcne} is not unreasonable.

In the case of tcnq, reaction with $[OsCl_6]^{2-}$ did not take place. This is presumably because it is necessary to reduce tcnq to its dianion before electroreduction of $[OsCl_6]^{2-}$ could take place, thus fully populating the low lying LUMO of the neutral tetranitrile and removing its π-accepting character. Preparation of a haloosmate tcnq complex would presumably require a starting complex which could be reduced at a more positive potential than the $E_{1/2}$ value for

the tcnq$^{/2-}$ potential. In principle this could be achieved in reaction with [OsCl$_5$(py)]$^-$, although reaction would probably be extremely slow as the starting complex does not readily lose Cl$^-$ on reduction.

2.3 Experimental

HPLC grade CH$_2$Cl$_2$ was purified by standing over KOH pellets for 1 week, followed by distillation, over P$_2$O$_5$, under nitrogen immediately prior to use. Hexane was purified by distillation over Na wire. Other solvents were used as supplied with the exception of diethyl ether, which was stored over sodium.

RuCl$_3$.xH$_2$O (x $\approx$ 3), 2,2'-bipyridyl, LiCl, tcne, tcnq and AgBF$_4$ were used as supplied. Tetrabutylammonium salts of [OsCl$_6$]$^{2-}$ and [OsBr$_6$]$^{2-}$ were prepared within this department by K. J. Taylor[58].

Voltammetric and coulometric studies were carried out as discussed in Chapter 1, using the appropriate cells connected to a PAR 170 electrochemistry system or a Hi-Tek PPR1 waveform generator, and recorded on a Hewlett-Packard 7045A X-Y recorder. UV/visible spectra and spectroelectrochemical studies were carried out in a Perkin-Elmer λ9 UV/Visible/NIR spectrophotometer. The spectroelectrochemical studies used the OTE cell described in Chapter 1, and the potential source was a Metrohm E506 potentiostat. IR spectra were recorded using a Perkin-Elmer 598 IR spectrometer. All mass spectra were recorded on a Kratos-50TC spectrometer, using 3-nitrobenzylalcohol as the matrix.

Preparation of [Bu$_4$N][BF$_4$]

HBF$_4$ solution (40%, 100 cm^3) was diluted with 1 litre of distilled water, and neutralised by addition of Bu$_4$NOH solution (40%). The white precipitate formed by this reaction was filtered off and recrystallised from water/methanol. The purified product was dried *in vacuo* at 350 K for a minimum of 48 hours before use.

cis-[Ru(bpy)$_2$Cl$_2$]

This was prepared using the method reported by Sullivan, Salmon and Meyer[49]. RuCl$_3$.xH$_2$O (1.60 g), 2,2'-bipyridyl (2.00 g) and LiCl (1.76 g) were refluxed in DMF (15 cm^3) for 8 hours under nitrogen. After the solution cooled to room temperature, acetone (75 cm^3) was added and the mixture was cooled to 255 K overnight. The microcrystalline product was filtered, washed with water and ether and dried in vacuo. The yield was approximately 65%. The identity and purity of the product were checked by recording of UV/visible and IR spectra, and by cyclic voltammetry.

[Ru(bpy)$_2$Cl({CH$_3$}$_2$CO)][BF$_4$]

In a typical preparation *cis*-[Ru(bpy)$_2$Cl$_2$] (200 mg) and AgBF$_4$ (80 mg) were stirred under nitrogen, in the dark, in deaerated acetone (30 cm^3) for 80 minutes then filtered under gravity to remove the AgCl

formed, yielding the acetone solution of the product complex. The resultant red solution was immediately used in a subsequent reaction. The purity of the product was assured by the very low solubility of the starting complex in acetone[49].

[Ru(bpy)₂Cl(tcne)][BF₄] ([N1])

Tcne (180 mg) was added to a freshly prepared solution of [Ru(bpy)₂Cl({CH₃}₂CO)][BF₄] in acetone (see above) and stirred for 8 hours under nitrogen. The UV/visible spectrum of a sample of the reaction mixture was monitored during the 2nd and 3rd hours. After reaction, the volume was reduced by evaporation and the product precipitated by addition of nitrogen purged hexane (50 cm³). Excess tcne was removed by shaking the product with toluene (five 20 cm³ fractions). Attempts to further purify the dark green product by chromatography resulted in its decomposition.

[Ru(bpy)₂Cl(tcnq)][BF₄] ([N2])

This was prepared similarly to the tcne complex above, but tcnq (250 mg) was substituted for tcne. After precipitation of the product, excess tcnq was removed by a Soxhlet extraction, using toluene.

Complex [N3]

Cis-[Ru(bpy)₂Cl₂] (150 mg), tcne (38 mg) and AgBF₄ (130 mg) were added to N₂ purged CH₂Cl₂ (40 cm³), in darkness. The mixture was stirred under

N$_2$ for 24 hours. Filtration (on the Schlenk line) yielded a blue solution from which the product was precipitated by addition of n-hexane, which was isolated by filtration and dried in vacuo. The isolated yield was only 43 mg, partly as a result of some product being removed by the first filtration (the purpose of which was to remove AgCl).

[Bu$_4$N][OsCl$_5$(py)]

Following the method developed by K. J. Taylor[57], [Bu$_4$N]$_2$[OsCl$_6$] (50 mg) and pyridine (5 mg) were added to an argon purged 0.5 moldm^{-3} solution of [Bu$_4$N][BF$_4$] in CH$_2$Cl$_2$ (10 cm^3) in an electrosynthetic cell (see Chapter 1 for details). Electrogeneration at -0.70 V versus Ag/AgCl, under argon, induced reduction of osmium, resulting in loss of one chloride ligand and coordination of pyridine. When the reaction had gone to completion (monitored by cyclic voltammetry) the product was reoxidised by electrogeneration at +0.20 V. The product was purified by elution from a silica column with CH$_2$Cl$_2$. The yield after purification was 90%.

[Bu$_4$N]$_2$[OsCl$_5$(tcne)]

[Bu$_4$N]$_2$[OsCl$_6$] (33.2 mg) and tcne (4.8 mg) were added to an argon purged CH$_2$Cl$_2$ solution of [Bu$_4$N][BF$_4$] (0.5 moldm^{-3}, 10 cm^3) in an electrogenerative cell. Electrogeneration was conducted at +0.20 V vs Ag/AgCl to reduce tcne. Once reduction of tcne was complete, electrogeneration at -0.70 V

was used to reduce osmium, thus inducing loss of Cl⁻ and coordination of tcne⁻. The final synthetic step was electrogeneration at +0.30 V, oxidising the coordinated tcne⁻. Coulometric studies showed all electrogenerations to be one electron steps. The cyclic voltammetry, IR and UV/visible spectra were recorded at each stage of the synthesis. After the final electrogeneration the voltammetric, coulometric and spectroscopic data suggested a yield of 85 - 90%. Attempts were made to purify the green product (in particular, to separate it from the supporting electrolyte) by thin layer chromatography, but these resulted in decomposition.

[Bu$_4$N]$_2$[OsBr$_5$(tcne)]

[Bu$_4$N]$_2$[OsBr$_6$] (36.9 mg) and tcne (4.1 mg) were added to an argon purged solution of [Bu$_4$N][BF$_4$] (0.5 moldm^{-3}) in CH$_2$Cl$_2$ (10 cm^3) in an electrosynthetic cell. Electrogenerations were carried out (each step monitored by electrochemical and spectroscopic means as above) at +0.20 V, -0.60 V, then +0.30 V. Although the dark green product complex appeared to be stable in the solid state, attempts to purify it by chromatography resulted in rapid decomposition.

[Bu$_4$N][OsCl$_4$(py)(tcne)]

[Bu$_4$N][OsCl$_5$(py)] (23 mg) and tcne (4.3 mg) were dissolved in a deaerated solution of [Bu$_4$N][BF$_4$] (0.5 moldm^{-3}) in CH$_2$Cl$_2$ (10 cm^3) as above. Tcne was reduced as before, then the osmium complex was reduced by electrogeneration at -0.25 V vs Ag/AgCl. After electrogeneration had gone to completion, the potential was held at -0.25 V, except during brief interruptions to monitor the progress of the reaction by cyclic voltammetry. After 6 hours, when the yield of product had reached 35-40% as judged from the cyclic voltammograms, electrogeneration at +0.40 V was used to reoxidise the bound tcne$^-$.

Attempted reaction of tcnq with [OsCl$_6$]$^{2-}$

Tcnq (5.3 mg) and [Bu$_4$N]$_2$[OsCl$_6$] (23 mg) were dissolved in an argon purged solution of [Bu$_4$N][BF$_4$] (0.5 moldm^{-3}) in CH$_2$Cl$_2$ (10 cm^3) in a coulometric cell, as above. Electrogenerations were carried out, in order, at +0.20 V, -0.40 V and -0.70 V versus Ag/AgCl. The cyclic voltammetry of the solution was recorded at each stage, and remained unchanged throughout the experiment.

2.4 References

1. (a) T. L. Cairns and E. G. McGeer, *Pat. App. 757773*, **1956**. (b) T. L. Cairns,
   R. H. Carboni, D. D. Coffmann, V. A. Englehardt, R. E. Heckert, E. L. Little,
   E. G. McGeer, B. C. McKusick, W. J. Middleton, R. M. Scribner,
   C. W. Theobald and H. E. Winberg, *J. Am. Chem. Soc.*, **1958**, <u>80</u>, 2775.

2. D. S. Acker, R. J. Harder, W. R. Hertler, W. Mahler, L. R. Melby,
   R. E. Benson and W. E. Mochel, *J. Am. Chem. Soc.*, **1960**, <u>82</u>, 6408.

3. R. G. Little, D. Pautler and P. Coppens, *Acta Cryst.*, **1971**, <u>B27</u>, 1493.

4. R. E. Long, R. A. Sparks and K. N. Trueblood, *Acta Cryst.*, **1965**, <u>18</u>, 932.

5. J. Ladik, A. Karpfen, G. Stollhof and P. Fulde, *Chem. Phys.*, **1975**, <u>7</u>, 267.

6. W. Kaim and M. Moscherosch, *Coord. Chem. Rev.*, **1994**, <u>129</u>, 157.

7. H. Sakurai, K. Tsuchiya and K. Migita, *Inorg. Chem.*, **1988**, <u>27</u>, 3877.

8. P. Kathirgaman and D. R. Rosseinsky, *J. Chem. Soc. Chem. Commun.*,
   1980, 839.

9. R. L. Brandon, J. H. Osiek and A. Ottenburg, *J. Org. Chem.*, **1966**, <u>31</u>, 1214.

10. D. A. Dixon and J. S. Miller, *J. Am. Chem. Soc.*, **1987**, <u>109</u>, 3656.

11. J. S. Miller, D. M. O'Hare, A. Chakraborty and A. J. Epstein,
    J. Am. Chem. Soc., **1989**, <u>111</u>, 7853.

12. W. E. Broderick, J. A. Thompson, E. P. Day and B. M. Hoffman, *Science*,
    1990, <u>249</u>, 401.

13. K.-M. Chi, J. C. Calabrese, W. M. Reiff and J. S. Miller, *Organometallics*,

1991, <u>10</u>, 688.

14. M. D. Ward, P. J. Fagan, J. C. Calabrese and D. C. Johnson,

    J. Am. Chem. Soc., **1989**, <u>111</u>, 1719.

15. M. Rosenblum, R. W. Fish and C. Bennett, *J. Am. Chem. Soc.*,

    1964, <u>86</u>, 5166.

16. J. S. Miller, J. C. Calabrese, A. J. Epstein, R. W. Bigelow, J. H. Zhang and

    W. M. Reiff, *J. Chem. Soc. Chem. Commun.*, **1986**, 1026.

17. G. A. Candela, L. Swarzenbruder, J. S. Miller and M. J. Rice,

    J. Am. Chem. Soc., **1979**, <u>101</u>, 2755.

18. M. D. Ward, *Synth. Met.*, **1988**, <u>27</u>, B211.

19. J. A. McGinnetty and J. A. Ibers, *J. Chem. Soc. Chem. Commun.*, **1968**, 235.

20. G. Mestroni, A. Camus and G. Zassinovich, *J. Organomet. Chem.*,

    1974, <u>65</u>, 119.

21. O. Gandolfi, B. Giovannitti, M. Ghedini and G. Dolcetti,

    J. Organomet. Chem., **1976**, <u>129</u>, 207.

22. T. S. Janik, K. A. Bernard, M. R. Churchill and J. D. Atwood,

    J. Organomet. Chem., **1987**, <u>323</u>, 247.

23. M. Bottrill, M. Green, A. G. Orpen, D. R. Saunders and I. D. Williams,

    J. Chem. Soc. Dalton Trans., **1989**, 511

24. J. K. Stalick and J. A. Ibers, *J. Am. Chem. Soc.*, **1970**, <u>92</u>, 5333.

25. A. Maisonnat, J.-J. Bonnet and R. Poilblanc, *Inorg. Chem.*, **1980**, <u>19</u>, 3168.

26. H. Braunwarth, G. Huttner and L. Zsolnai, *J. Organomet. Chem.*,

1989, <u>372</u>, C23.

27. B. Olbrich-Deussner, W. Kaim and R. Gross-Lannert, *Inorg. Chem.*,

1989, <u>28</u>, 3113.

28. (a) M. Herberhold, *Angew. Chem.*, **1968**, <u>80</u>, 314; (b) *idem, ibid,*

1972, <u>84</u>, 773.

29. A. E. D. McQueen, A. J. Blake, T. A. Stephenson, M. Schroder and

L. J. Yellowlees, *J. Chem. Soc. Chem. Commun.*, **1988**, 1533.

30. S. L. Bartley and K. R. Dunbar, *Angew. Chem. Int. Ed. Engl.*, **1991**, <u>30</u>, 448.

31. L. Ballester, M. C. Barral, A. Gutierrez, R. Jiminez-Aparicio,

J. M. Martinez-Muyo, M. F. Perpinan, M. A. Monge and C. Ruiz-Valero,

J. Chem. Soc. Chem. Commun., **1991**, 1397.

32. (a) R. Gross-Lannert, W. Kaim and B. Olbrich-Deussner, *Inorg. Chem.*, **1990**,

<u>29</u>, 5046; (b) W. Kaim, T. Roth, B. Oblrich-Deussner, R. Gross-Lannert,

J. Jordanov and E. K. H. Roth, *J. Am. Chem. Soc.*, **1992**, <u>114</u>, 5693.

33. M. I. Bruce, T. W. Hambley, M. R. Snow and A. G. Swincer,

Organometallics, **1985**, <u>4</u>, 501.

34. K. L. Amos and N. G. Connelly, *J. Organomet. Chem.*, **1980**, <u>194</u>, C57.

35. D. L. Jeanmaire, M. R. Suchanski and R. P. Van Duyne,

J. Am. Chem. Soc., **1975**, <u>97</u>, 1699.

36. D. L. Jeanmaire and R. P. Van Duyne, *J. Am. Chem. Soc.*, **1976**, <u>98</u>, 4029.

37. J. J. Hinkel and J. P. Devlin, *J. Chem. Phys.*, **1973**, <u>58</u>, 4750.

38. J. A. A. de Boer, D. N. Reinhoudt, J. W. H. M. Uiterwijk and S. Harkema,

J. Chem. Soc. Perkin Trans. II, **1986**, 377.

39. I. M. Brown and M. T. Jones, *J. Chem. Phys.*, **1969**, <u>51</u>, 4687.

40. G. A. Heath, L. J. Yellowlees and P. S. Braterman,

    J. Chem. Soc. Chem. Commun., **1981**, 287.

41. L. J. Yellowlees, PhD thesis, University of Edinburgh, **1982**.

42. C. Creutz and N. Sutin, *J. Am. Chem. Soc.*, **1976**, <u>98</u>, 6384.

43. C. R. Bock, T. J. Meyer and D. G. Whitten, *J. Am. Chem. Soc.*,

    1974, <u>96</u>, 4710.

44. U. Lashisch, M. Ottolenghi and J. Rabani, *J. Am. Chem. Soc.*, **1977**, <u>99</u>, 8062.

45. C. M. Elliot, *J. Chem. Soc. Chem. Commun.*, **1980**, 261.

46. P. J. Delaive, J. T. Lee, H. Abruna, H. W. Sprintschnik, T. J. Meyer and

    D. G. Whitten, *Inorg. and Org. Photochem.*, **1978**, 28.

47. S. Chirayil, V. Hodge, Y. Zahng and R. P. Thummel, *Inorg. Chem.*,

    1991, <u>30</u>, 2821.

48. C. A. Bignozzi, S. Roffia, C. Chiorboli, J. Davila, M. T. Indelli and

    F. Scandola, *Inorg. Chem.*, **1989**, <u>28</u>, 4351.

49. B. P. Sullivan, D. J. Salmon and T. J. Meyer, *Inorg. Chem.*, **1978**, <u>17</u>, 3334.

50. D. Choudhardy, D. J. Cole-Hamilton, R. F. Jones and G. Smith,

    J. Chem. Soc. Dalton Trans., **1982**, 1143.

51. F. Barigelletti, A. Juris, V. Balzani, P. Belser and A. von Zewelesky,

    J. Phys. Chem., **1987**, <u>91</u>, 1095.

52. R. A. Krause, *Inorg. Chim. Acta*, **1977**, <u>22</u>, 209.

53. A. E. D. McQueen, PhD Thesis, University of Edinburgh, **1989**.

54. S. J. Milder, *Inorg. Chem.*, **1989**, <u>28</u>, 868.

55. A. B. P. Lever, *Inorganic Electronic Spectroscopy*, Elsevier, **1984**, 211.

56. P. Usher, unpublished results, University of Edinburgh, **1992**.

57. K. J. Taylor and L. J. Yellowlees, *Molecular Electrochemistry of Inorganic,*
    Bioinorganic and Organometallic Compounds, A. J. L. Pombeiro and
    J. A. McCleverty (eds), Kluwer Academic Publishers, **1993**, 69

58. K. J. Taylor, PhD Thesis, University of Edinburgh, **1991**

59. A. B. P. Lever, *Inorg. Chem.*, **1990**, <u>29</u>, 1271.

60. B. E. Burstein and M. R. Green, *Prog. Inorg. Chem.*, **1988**, <u>36</u>, 474.

61. E. M. Kober, K. A. Goldsby, D. N. S. Narayana and T. J. Meyer,
    J. Am. Chem. Soc., **1983**, <u>105</u>, 4303.

62. T. Roth and W. Kaim, *Inorg. Chem.*, **1992**, <u>31</u>, 1930.

3.1 Introduction

This chapter discusses reactions of tcne and tcnq with complexes of the general formula $[MX_n(PR_2R')_3]$, where M = Ru or Os, X = Cl or Br, n = 2 or 3, R and R' are alkyl or aryl groups and may be equivalent. Complexes of formula $[OsX_3(PR_2R')_3]$ were first reported by Chatt and coworkers in 1968[1]. Subsequent studies have shown that these complexes will readily react (usually under reductive conditions, which induce elimination of Cl⁻) to give a variety of complexes of general formula $[OsX_2(PR_2R')_3L]$ or $[OsX_2(PR_2R')_2L_2]$, most products featuring the metal centre in the +2 oxidation state. Examples of reactions of $[OsX_3(PR_2R')_3]$ are shown in Figure 3.1. The reactivity of the analogous Ru complexes is generally similar.

Many of the reactions listed below have also been initiated by electrochemical reduction, although it was found that the product of electrochemical reaction sometimes formed in a different configuration to that observed during chemical reaction. In general, the *trans* isomer of $[OsX_2(PR_3)_3L]$ is the kinetically favoured product but the *cis* isomer is thermodynamically favoured[8,9]. Additionallly, compounds of general formula $[OsX_2(PR_3)_3(solv)]$ can be formed by electrochemical reduction in coordinating solvents such as MeCN, DMF (products featuring N-bound and O-bound DMF were both isolated) and DMSO[8,9].

Figure 3.1 Reactions of [OsX$_3$L$_3$]; X = Cl, Br; L = PR$_2$R'.

mer-[OsL$_3$Cl$_2$(N$_2$)][2]

[OsL$_3$Cl$_2$(NCR)][3]   Zn,N$_2$ [OsL$_3$Cl$_2$(CO)][3]

Zn,RCN   Zn,CO

[OsL$_3$Cl$_2$(NH$_3$)][4]   [OsL$_3$Cl$_2$(NH$_2$R)]

                NH$_3$ + [OsL$_3$Cl$_2$(N$_2$H$_4$)][4]

                                            RNH$_2$

                N$_3$

mer-[OsL$_3$Cl$_2$(N$_3$)][5] ⟵——— [OsL$_3$X$_3$] ——⟶ $trans$-[OsL$_2$X$_2$(CO)$_2$][3]

                                    CO,Zn/Hg

S$_2$PR$_2$ S$_2$CNR$_2$

cis-[OsL$_2$(S$_2$PR$_2$)$_2$][6] cis-[OsL$_2$(S$_2$CNR$_2$)$_2$][6]

                        NaBH$_4$

                        [OsL$_3$H$_4$][7]
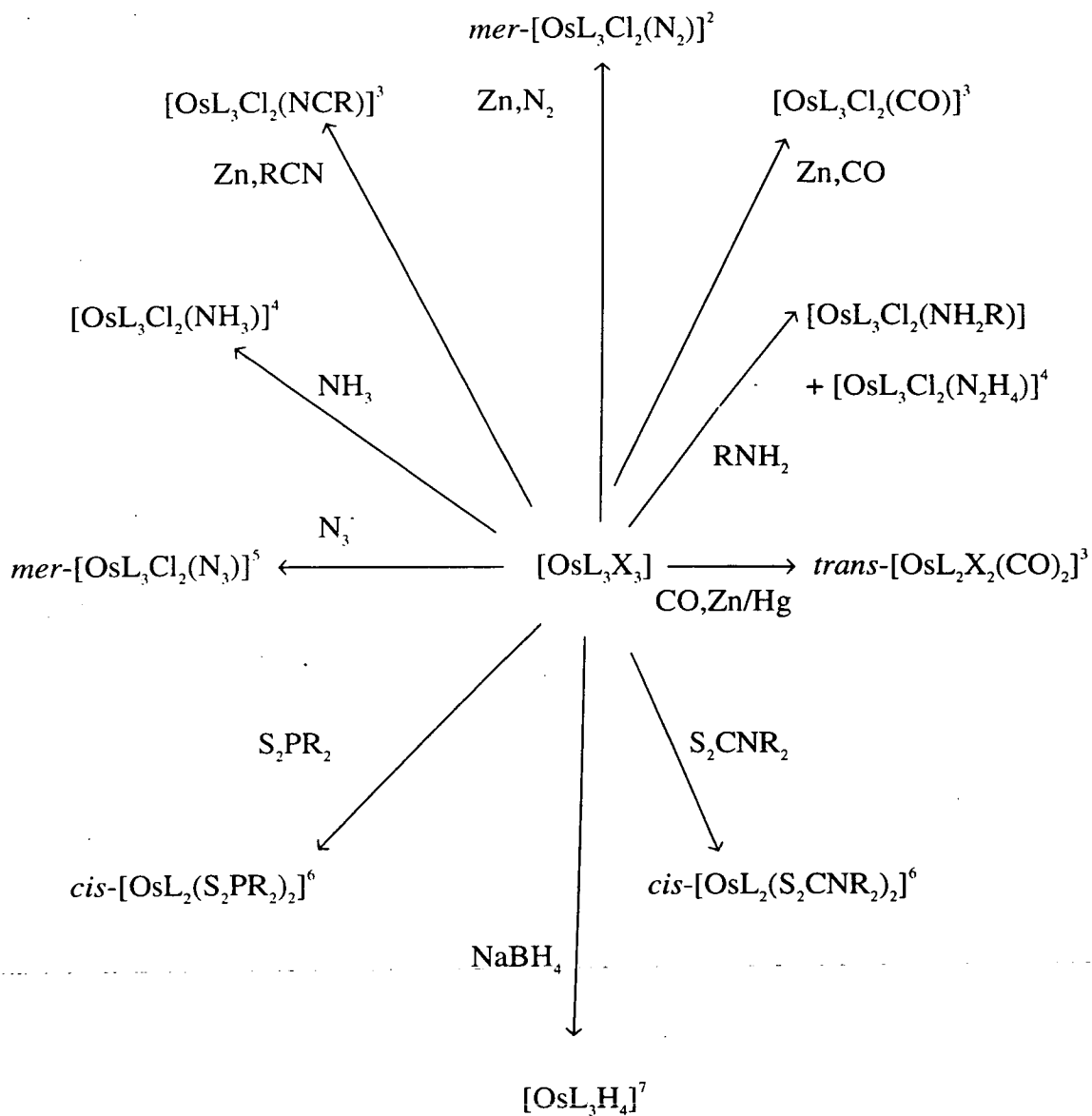
With bulky phosphines such as PPh$_3$, the five coordinate [MX$_2$(PR$_3$)$_3$] is stabilised[10,11] (the "vacant" coordination site undergoes agostic interactions with H atoms in the ortho position on the phenyl groups of the phosphines[12]). As a result these species have a reactive site already available without the use of "halide stripping" methods, thus simplifying reactions with π-acceptor ligands such as tcne. It is, however, possible that steric factors would prevent reaction with tcne or tcnq.

A further advantage of working with phosphine complexes of Ru and Os is that the electrochemical and spectroscopic behaviour of the starting complexes and many of the products mentioned above has been reported and assigned[8,9], thus simplifying assignment of spectra and voltammograms of new species.

The objectives of this work were to study the reactions of tcne and tcnq with halo-phosphine complexes of ruthenium and osmium, employing chemical and electrochemical synthetic routes, thus extending the known chemistry of the halo-phosphine complexes and the tetranitriles. The intention was to characterise the products by both structural and electrochemical methods, with particular emphasis on elucidation of the nature of the frontier orbitals.

3.2 Results and Discussion

The principal results obtained during the research described in this chapter relate to the reaction of tcne with *mer*-[OsCl$_3$(PEt$_2$Ph)$_3$]. This reaction yielded, via an intermediate complex, the unexpected product *trans*-[OsCl$_2$(PEt$_2$Ph)$_3$(NC{CN}C=C{OH}CN)], the first reported example of

tricyanovinyl alcohol (tcva) as a ligand bound to a transition metal centre. The bulk of this chapter therefore concentrates on the structural and electrochemical characterisation of this complex (hereafter referred to as [P1]), and discussions of the mechanism by which it was formed. Other reactions of tcnx with phosphine complexes of Ru and Os are subsequently compared and contrasted with the above system.

3.2.1   Reactions of tcne with *mer*-[OsCl$_3$(PEt$_2$Ph)$_3$]

In THF, *mer*-[OsCl$_3$(PEt$_2$Ph)$_3$] reacted rapidly with tcne upon addition of AgBF$_4$, forming a dark blue-grey solution which reacted further, over a period of 30 minutes, to give a purple-pink solution of [P1], from which the product complex was isolated in high yield. If the reaction was carried out in CH$_2$Cl$_2$, it was possible to isolate the intermediate complex (subsequently referred to as [P2]), although this complex proved to be extremely reactive, converting readily to [P1] in solution.

3.2.1.1   Structural Characterisation of [P1]

FAB mass spectrometry, conducted in thioglycerol, gave a peak for the molecular ion at m/z = 879, plus a series of breakdown peaks corresponding to loss of various ligands, as detailed in Table 3.1.

Table 3.1 Selected FAB mass spectrometric data for [P1]

m/z	Intensity	Assignment	Expected m/z
879	4.8	$[M]^+$	879
843	4.0	$[M - Cl]^+$	844
760	100	$[OsCl_2(PEt_2Ph)_3]^+$	760
725	12	$[OsCl(PEt_2Ph)_3]^+$	725
594	98	$[OsCl_2(PEt_2Ph)_2]^+$ $([A]^+)$	594
555	18	$[OsCl(PEt_2Ph)_2]^+$	559
		$[A - C_3H_3]^+$	555
525	12	$[Os(PEt_2Ph)_2]^+$	524
429	30	$[OsCl_2(PEt_2Ph)]^+$	428
393	20	$[OsCl(PEt_2Ph)]^+$	393
167	202	$[PEt_2Ph]^+$	166

IR spectroscopy of a KBr disc doped with [P1] showed, in addition to a large number of modes associated with PEt_2Ph and absorbances at 325 and 310 cm^{-1} corresponding to Os-Cl stretching vibrations, $C{\equiv}N$ stretching vibrations at 2225 (sh), 2220 (m) and 2185 cm^{-1} (m), plus an O-H stretch at 3250 cm^{-1} (m,br) (the O-H stretches associated with water normally appear in the range 3400 - 3600 cm^{-1}). A band at 1610 cm^{-1} (s) was tentatively assigned as a C=C stretch (in free tcne the C=C stretch is observed by Raman spectroscopy at 1569 cm^{-1})[13].

Experimental and expected elemental analysis data for [P1] is listed in Table 3.2. providing further evidence of the nature of the product complex.

Table 3.2. CHN data for [P1]

Experimental	%C = 48.2, %H = 5.28, %N = 4.88
[OsCl$_2$(PEt$_2$Ph)$_3$(tcne)]	%C = 48.7, %H = 5.03, %N = 6.31
[OsCl$_2$(PEt$_2$Ph)$_3$(tcva)]	%C = 47.8, %H = 5.23, %N = 4.78

A single crystal X-ray diffraction study of [P1] yielded the structural data listed in Table 3.3. Views of [P1] are shown in Figure 3.2. The complex cocrystallised with THF as [P1].0.5THF. This is the first reported case of tcva acting as a ligand. In addition, the structure exhibits a number of other noteworthy features.

Compared with Os-tcne complexes studied previously, the Os-N bond is relatively long at 2.06 Å (in [Os(S$_2$PR$_2$)$_2$(PPh$_3$)(tcne)], when R = Me the Os-N bond length is 1.899(7) Å, and when R = Ph, Os-N = 1.858(10) Å[14]), suggesting that the π-back bonding from Os[II] to tcva is weaker in this case than the tcne complexes reported previously. This may be due in part to the tcva in [P1] being *trans* to a π-accepting phosphine ligand whereas tcne is *trans* to π-donor ligands such as dithiophosphinates in the previously reported examples.

Figure 3.2 Views of [P1], obtained by single crystal X-ray diffraction.
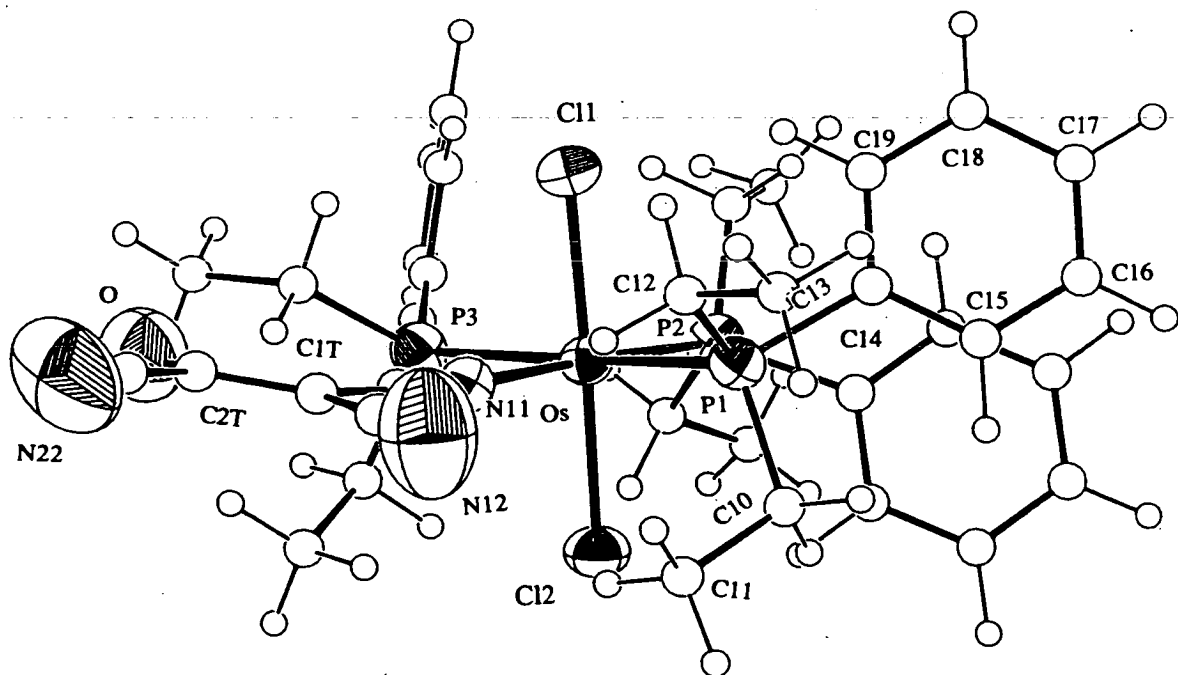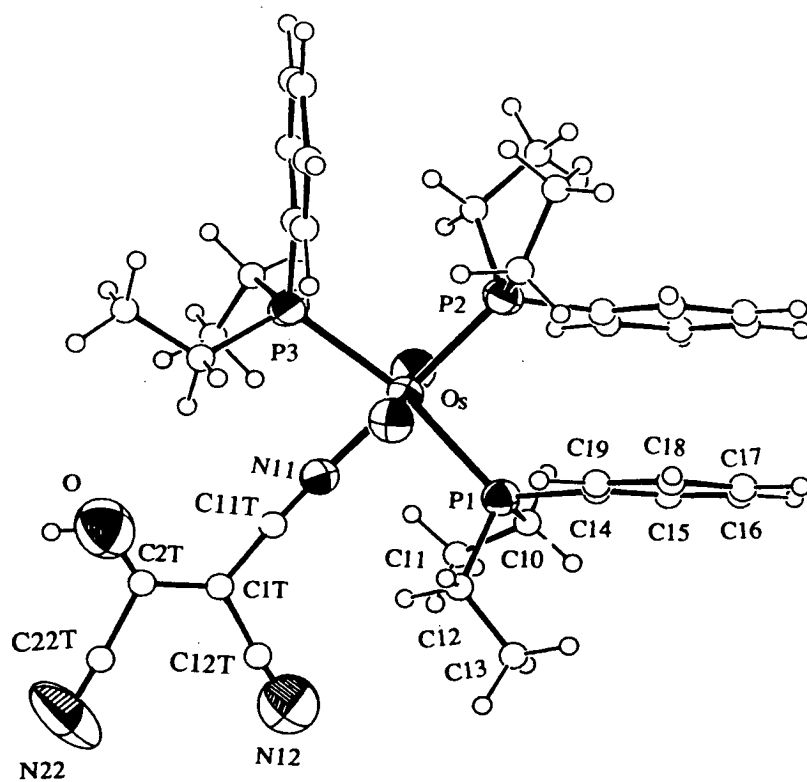
Table 3.3   Selected structural data for [P1]

(i) Bond lengths

Os	−N(11)	2.064(4)		P(1)	−C(12)	1.829(5)
Os	−Cl(1)	2.3488(11)		P(1)	−C(14)	1.824(3)
Os	−Cl(2)	2.3448(12)		C(10)	−C(11)	1.544(8)
Os	− P(1)	2.4270(12)		C(12)	−C(13)	1.523(8)
Os	− P(2)	2.3763(12)		P(2)	−C(20)	1.842(6)
Os	− P(3)	2.4501(12)		P(2)	−C(22)	1.843(5)
N(11)	−C(11T)	1.151(6)		P(2)	−C(24)	1.831(3)
C(11T)	−C(1T)	1.406(7)		C(20)	−C(21)	1.513(8)
C(1T)	−C(12T)	1.451(9)		C(22)	−C(23)	1.535(9)
C(1T)	−C(2T)	1.328(9)		P(3)	−C(30)	1.833(5)
C(12T)	−N(12)	1.056(12)		P(3)	−C(32)	1.838(5)
C(2T)	− O(1)	1.178(10)		P(3)	−C(34)	1.837(3)
C(2T)	−C(21T)	1.534(12)		C(30)	−C(31)	1.518(8)
C(21T)	−N(22)	1.160(12)		C(32)	−C(33)	1.531(8)
P(1)	−C(10)	1.837(5)				

(ii) Bond angles

N(11) −	Os	−Cl(1)	87.92(10)		C(10) −	P(1)	−C(12)	103.34(22)
N(11) −	Os	−Cl(2)	89.87(10)		C(10) −	P(1)	−C(14)	104.92(19)
N(11) −	Os	− P(1)	85.32(10)		C(12) −	P(1)	−C(14)	100.93(18)
N(11) −	Os	− P(2)	177.60(10)		P(1) −	C(10)	−C(11)	111.9(4)
N(11) −	Os	− P(3)	85.09(10)		P(1) −	C(12)	−C(13)	115.9(4)
Cl(1) −	Os	−Cl(2)	177.66(4)		P(1) −	C(14)	−C(15)	121.70(22)
Cl(1) −	Os	− P(1)	88.45(4)		P(1) −	C(14)	−C(19)	118.27(21)
Cl(1) −	Os	− P(2)	94.46(4)		Os −	P(2)	−C(20)	111.40(18)
Cl(1) −	Os	− P(3)	87.54(4)		Os −	P(2)	−C(22)	111.58(17)
Cl(2) −	Os	− P(1)	92.13(4)		Os −	P(2)	−C(24)	118.91(11)
Cl(2) −	Os	− P(2)	87.75(4)		C(20) −	P(2)	−C(22)	107.54(24)
Cl(2) −	Os	− P(3)	91.51(4)		C(20) −	P(2)	−C(24)	100.99(20)
P(1) −	Os	− P(2)	94.99(4)		C(22) −	P(2)	−C(24)	105.42(20)
P(1) −	Os	− P(3)	169.73(4)		P(2) −	C(20)	−C(21)	118.6(4)
P(2) −	Os	− P(3)	94.75(4)		P(2) −	C(22)	−C(23)	117.9(4)
Os	−N(11)	−C(11T)	173.6(4)		P(2) −	C(24)	−C(25)	118.26(23)
N(11) −	C(11T)	−C(1T)	176.7(5)		P(2) −	C(24)	−C(29)	121.48(24)
C(11T) −	C(1T)	−C(12T)	114.3(5)		Os −	P(3)	−C(30)	110.75(18)
C(11T) −	C(1T)	−C(2T)	123.8(5)		Os −	P(3)	−C(32)	114.38(17)
C(12T) −	C(1T)	−C(2T)	121.6(6)		Os −	P(3)	−C(34)	119.74(11)
C(1T) −	C(12T)	−N(12)	176.4(9)		C(30) −	P(3)	−C(32)	104.17(24)
C(1T) −	C(2T)	− O(1)	126.7(7)		C(30) −	P(3)	−C(34)	100.80(20)
C(1T) −	C(2T)	−C(21T)	111.8(6)		C(32) −	P(3)	−C(34)	105.14(20)
O(1) −	C(2T)	−C(21T)	121.4(7)		P(3) −	C(30)	−C(31)	115.4(4)
C(2T) −	C(21T)	−N(22)	176.9(9)		P(3) −	C(32)	−C(33)	114.4(4)
Os −	P(1)	−C(10)	115.41(16)		P(3) −	C(34)	−C(35)	118.43(24)
Os −	P(1)	−C(12)	111.05(16)		P(3) −	C(34)	−C(39)	121.53(24)
Os −	P(1)	−C(14)	119.15(10)					

Table 3.3(continued)

(iii) Torsion angles

C(11T)-C(1T)	-C(2T)	- O(1)	6.7(12)		C(22)	- P(2)	-C(24)	-C(25)	-173.5(3)
C(11T)-C(1T)	-C(2T)	-C(21T)	-174.7(6)		C(22)	- P(2)	-C(24)	-C(29)	0.9(3)
C(12T)-C(1T)	-C(2T)	- O(1)	-179.7(8)		P(2)	-C(24)	-C(25)	-C(26)	174.48(24)
C(12T)-C(1T)	-C(2T)	-C(21T)	-1.1(9)		C(29)	-C(24)	-C(25)	-C(26)	0.0(5)
C(12)	- P(1)	-C(10)	-C(11)	56.1(4)		P(2)	-C(24)	-C(29)	-C(28)	-174.28(24)
C(14)	- P(1)	-C(10)	-C(11)	161.5(3)		C(25)	-C(24)	-C(29)	-C(28)	0.0(5)
C(10)	- P(1)	-C(12)	-C(13)	54.4(4)		C(24)	-C(25)	-C(26)	-C(27)	-0.1(5)
C(14)	- P(1)	-C(12)	-C(13)	-54.0(4)		C(25)	-C(26)	-C(27)	-C(28)	-0.1(5)
C(10)	- P(1)	-C(14)	-C(15)	8.1(3)		C(26)	-C(27)	-C(28)	-C(29)	0.1(5)
C(10)	- P(1)	-C(14)	-C(19)	-169.7(3)		C(27)	-C(28)	-C(29)	-C(24)	0.0(5)
C(12)	- P(1)	-C(14)	-C(15)	115.2(3)		C(32)	- P(3)	-C(30)	-C(31)	-56.6(5)
C(12)	- P(1)	-C(14)	-C(19)	-62.5(3)		C(34)	- P(3)	-C(30)	-C(31)	52.2(4)
P(1)	-C(14)	-C(15)	-C(16)	-177.68(22)		C(30)	- P(3)	-C(32)	-C(33)	-52.2(4)
C(19)	-C(14)	-C(15)	-C(16)	0.0(4)		C(34)	- P(3)	-C(32)	-C(33)	-157.8(4)
P(1)	-C(14)	-C(19)	-C(18)	177.77(22)		C(30)	- P(3)	-C(34)	-C(35)	57.1(3)
C(15)	-C(14)	-C(19)	-C(18)	0.0(4)		C(30)	- P(3)	-C(34)	-C(39)	-121.1(3)
C(14)	-C(15)	-C(16)	-C(17)	0.0(4)		C(32)	- P(3)	-C(34)	-C(35)	165.2(3)
C(15)	-C(16)	-C(17)	-C(18)	0.0(4)		C(32)	- P(3)	-C(34)	-C(39)	-13.0(3)
C(16)	-C(17)	-C(18)	-C(19)	0.0(4)		P(3)	-C(34)	-C(35)	-C(36)	-178.28(24)
C(17)	-C(18)	-C(19)	-C(14)	0.0(4)		C(39)	-C(34)	-C(35)	-C(36)	0.0(5)
C(22)	- P(2)	-C(20)	-C(21)	78.9(5)		P(3)	-C(34)	-C(39)	-C(38)	178.21(24)
C(24)	- P(2)	-C(20)	-C(21)	-31.3(5)		C(35)	-C(34)	-C(39)	-C(38)	0.1(5)
C(20)	- P(2)	-C(22)	-C(23)	-35.0(5)		C(34)	-C(35)	-C(36)	-C(37)	0.0(5)
C(24)	- P(2)	-C(22)	-C(23)	72.2(5)		C(35)	-C(36)	-C(37)	-C(38)	-0.1(5)
C(20)	- P(2)	-C(24)	-C(25)	-61.7(3)		C(36)	-C(37)	-C(38)	-C(39)	0.1(5)
C(20)	- P(2)	-C(24)	-C(29)	112.7(3)		C(37)	-C(38)	-C(39)	-C(34)	-0.1(5)

The 'alkene' C=C bond is, at 1.328(9) Å, the same, to within experimental error, as in free tcne (1.344(3) Å[15]). It is therefore reasonable to expect that the C=C bonds will be of similar strength, a fact which appears to validate the assignment of the C=C stretching mode in the IR spectrum given above. This is consistent with the observations regarding the long Os-N bond length and relatively low π-back

bonding, as it has been shown for tcne σ-complexes that weakening (ie. lengthening) of the C=C bond is related to the extent of back-donation into the tcne π*-LUMO[14,16,17]. This weakening is most easily observed in the IR spectra, which has in some cases (where the C=C band was observed in the range 1400 - 1420 cm^{-1}) been used to assign N-bound tcne complexes as containing anionic tcne[16,17]. Crystallographic studies are rather more ambiguous in this area, primarily as a result of the large standard deviations normally reported for the alkene bond length. For example, in $[Os(S_2PPh_2)_2(PPh_3)(tcne)]$ the tcne C=C bond length is reported as 1.401(19) Å[14], a distance which, given the large standard deviation reported, is not significantly different from the C=C bond length in free tcne[15]. The IR spectrum of $[Os(S_2PPh_2)_2(PPh_3)(tcne)]$, however, contains a C=C stretch at 1430 cm[-1(14)], indicating significant weakening of the C=C bond.

The C-O bond in tcva is unusually short for a single bond at 1.178(10) Å (the hydroxylic proton was "found" and not simply refined in a calculated position). This is, however, consistent with structural studies of salts $([(Cp)_2Fe]_{1.5}[C_5N_3O]$[18] and the N(6),N(6)-dimethyladeninium salt[19]) of the deprotonated anion of tcva (X-ray data for the free ligand have not been published), in which C-O bonds of 1.15(2) to 1.246(7) Å have been reported[18,19]. In the deprotonated anion it is thought that both resonance forms are important, hence the short C-O distance[18]. In Os-bound tcva, similar interactions appear to be taking place between oxygen and the olefinic π-orbitals.

Two of the phenyl groups on adjacent phosphine ligands (P1 and P2 as labelled) lie in parallel planes to within 1.6°. The perpendicular separation is 3.3 Å and the centres of the phenyl groups are separated by 3.8 Å, suggesting interactions similar to those encountered in graphite. Similar phenomena have been observed in other species such as $[OsCl_2(PMe_2Ph)_4]^{+(20)}$. The phosphorous *trans* to the tcva ligand is also significantly closer to osmium than the other two, possibly as a result of the interaction between the phenyl rings.

There are four [P1] molecules per unit cell, as shown in the packing diagram in Figure 3.3. Unlike some of the previously reported tcne and tcnq complexes[14,21,22], [P1] does not exhibit "ligand stacking".

[P1] was not sufficiently soluble to yield useful nmr data.

3.2.1.2   Electrochemical Characterisation of [P1]

Although structural data may provide indirect evidence as to the nature of the frontier orbitals, a more rigorous study requires the acquisition of more direct evidence. This may be achieved by utilisation of electrochemical and spectroelectrochemical techniques and is particularly useful in cases where the species under study has more than one redox active centre.

Figure 3.3 Packing of [P1], viewed along "a" axis
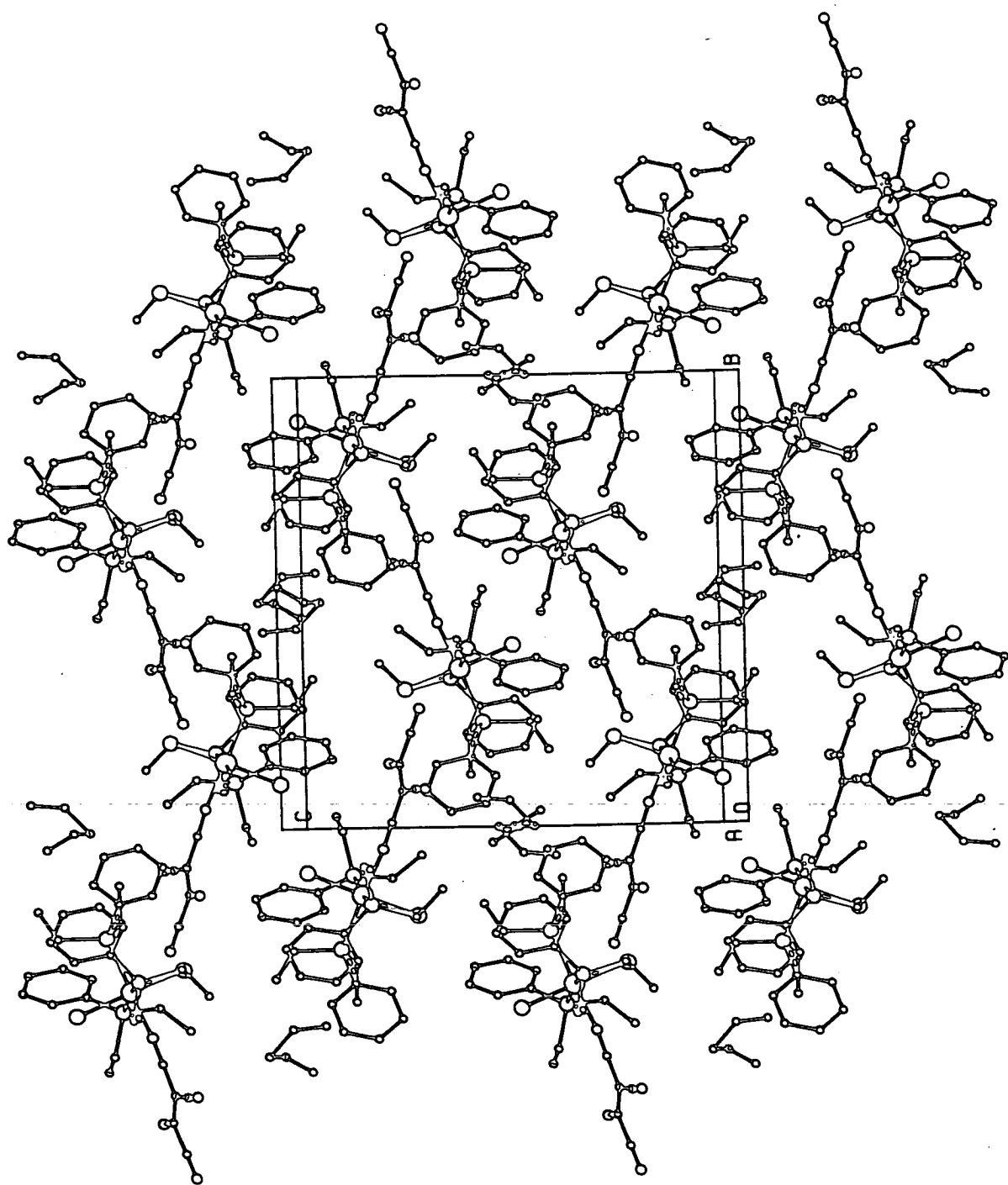
In the specific case of [P1], interest centres around the interactions and oxidation states of Os and tcva. As stated earlier, when tcne is σ-bound to metal centres the ligand may be neutral or anionic, or there may be extensive mixing of the metal and tcne-based orbitals, such that both HOMO and LUMO have considerable metal and ligand character and extensive electron delocalisation between metal and tcne occurs. Comparison of structural and IR data with tcne complexes, as mentioned above, suggests that there is relatively little electron transfer from the Os dπ orbitals into the tcva LUMO (ie. the complex is best decribed as $M^{II}L^{0}$). An investigation of the electrochemical properties of [P1] was carried out in order to determine the nature of the frontier orbitals in this tcva complex.

3.2.1.2.1 Redox Behaviour

Voltammetric studies of mer-[OsCl$_3$(PEt$_2$Ph)$_3$] were carried out in CH$_2$Cl$_2$ at room temperature, revealing a reversible Os$^{III/IV}$ oxidation at +1.05 V versus Ag/AgCl and a partially reversible Os$^{II/III}$ reduction at -0.40 V. At +0.22 V in the return scan, there is a peak associated with the oxidation of the 5 coordinate daughter product. The cyclic voltammogram of mer-[OsCl$_3$(PEt$_2$Ph)$_3$] is shown in Figure 3.4.

Figure 3.5 shows the electrochemical response of [P1] in CH$_2$Cl$_2$, revealing a reversible oxidation at +1.43V, a reversible reduction at +0.09V and an irreversible

reduction at -1.0 V. Coulometric experiments showed that the reversible couples are all one-electron processes.

As discussed in the previous chapter, replacement of a π-donor ligand with a π-acceptor normally results in a large anodic shift in the potential of any metal-based redox couples, therefore the process at +1.43 V in [P1] was provisionally assigned as an $Os^{II/III}$ couple. Unfortunately, no redox data for free tcva was found in the literature. By analogy with the electrochemistry of tcne complexes, the reversible reduction and irreversible reduction were provisionally assigned as based on the tcva ligand.

In order to confirm the provisional assignments given above, a study of the spectroelectrochemical behaviour of [P1] was conducted.

Figure 3.4 Cyclic voltammogram of *mer*-OsCl₃(PEt₂Ph)₃

Potential vs. Ag/AgCl

--------> -0.6V

+1.2V
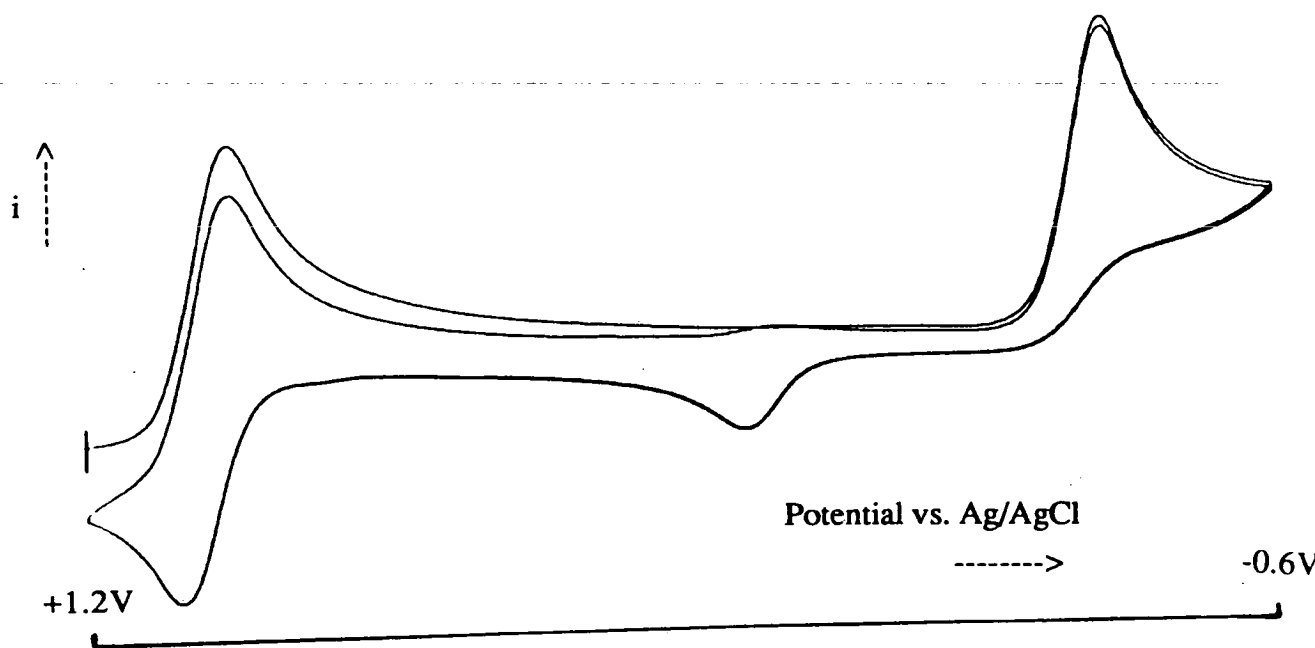
Figure 3.5 Cyclic and a.c. voltammograms of [P1]

+0.5V

+1.8V

Potential vs. Ag/AgCl

-------->

i

+0.5V   0V   -1.2V
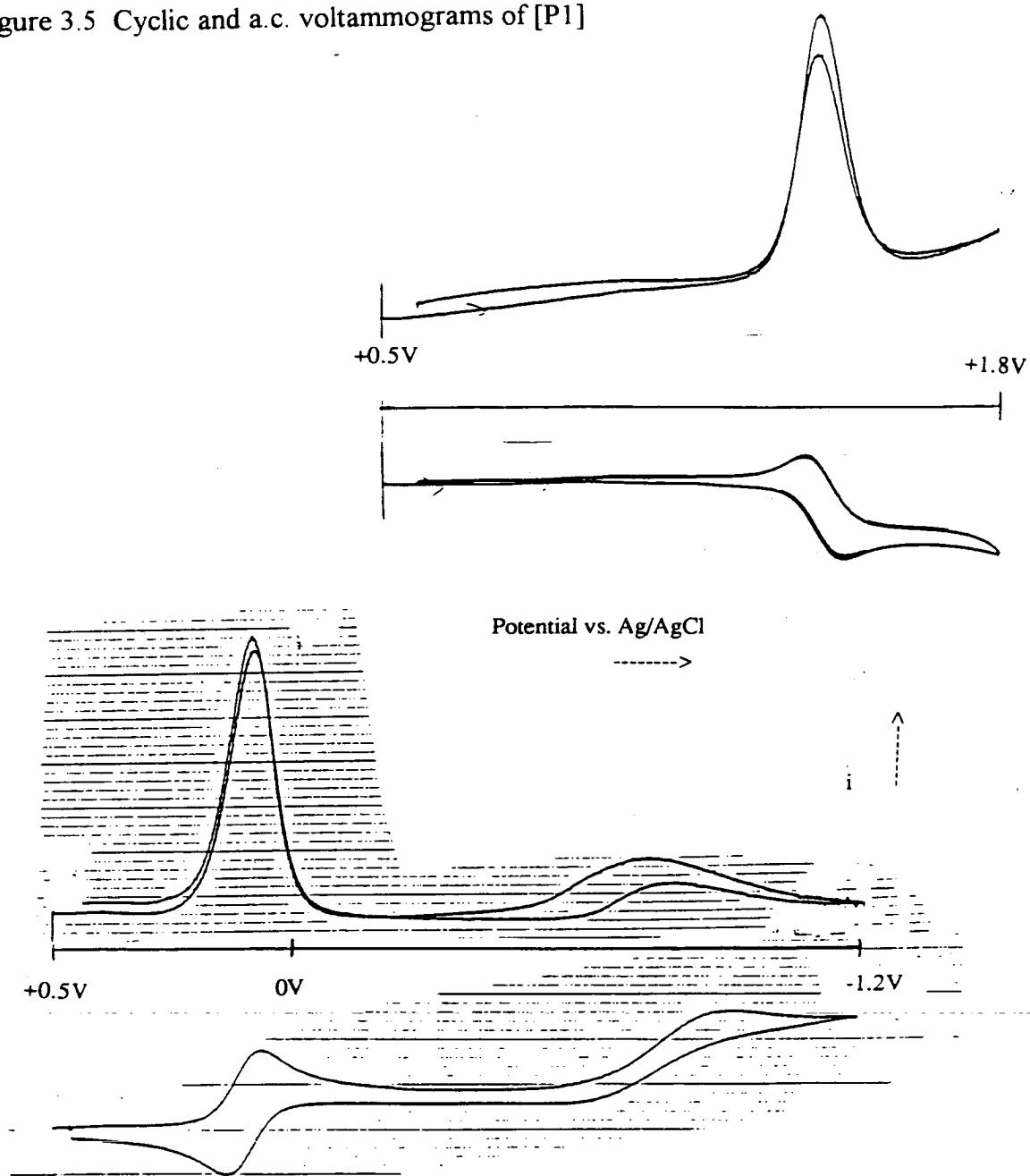
3.2.1.2.2 IR Spectroelectrochemistry

Upon reduction of [P1] to give the monoanion it was found that the $C \equiv N$

stretching modes in CH_2Cl_2 shifted from 2225, 2220 and 2185 cm^{-1} to 2180, 2140

and 2105 cm^{-1}, stretching energies similar to those observed in free tcne$^-$ (2180 and 2140 cm^{-1}; see Chapter 2). Unfortunately, it was impossible to determine the energy of the C=C stretching mode upon reduction, due to strong absorption in the relevant area of the spectrum by the supporting electrolyte. The above shift represents a significant weakening of the C≡N bonds and is consistent with the first reduction of [P1] being tcva-based.

3.2.1.2.3 EPR Spectroelectrochemistry

[P1] and its oxidation product were EPR silent at all temperatures down to 77 K. Studies of the frozen glass of [P1]$^-$ in MeCN gave spectra such as that shown in Figure 3.6. The relatively small peak width and closeness of the g-value to g$_e$ (for [P1], g = 2.012, $\Delta_{1/2}$ = 23 G) are consistent with the spectrum expected for an organic radical (in the case of tcne$^-$, g = 2.0028[23]), thus confirming that the first reduction (and hence the LUMO) of [P1] is tcva-based. Close inspection of spectra of [P1]$^-$ reveals shoulders on the peak, probably due to coupling with ^{14}N nuclei (in tcne$^-$ the ^{14}N coupling constant has been reported as 1.57 G[23]). Attempts to obtain more sharply resolved spectra of [P1]$^-$ were, however, unsuccessful.

The oxidation was assigned as osmium-based. The lack of an observed signal in the EPR study of [P1]$^+$ may be a result of rapid relaxation, due to a multiply degenerate (or near degenerate) electronic ground state.

126

Figure 3.6 EPR spectrum of [P1]⁻ in CH₃CN, 120 K

g = 2.012
SW = 500G
CF = 3300G
T = 120K
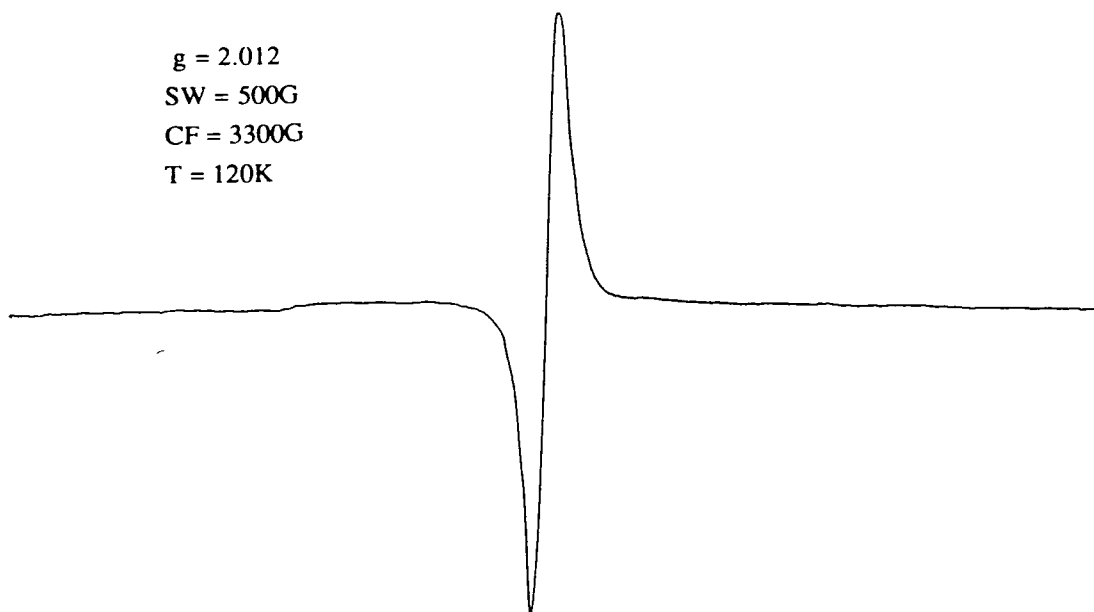
3.2.1.2.4 UV/visible Spectroelectrochemistry

In THF at room temperature, the UV/visible spectrum of mer-[OsCl₃(PEt₂Ph)₃]

shows peaks at 18900 (ε = 700 dm³mol⁻¹cm⁻¹), 23100 (1700), 29500 (shoulder,

1400), 33400 (2600) and 39500 cm⁻¹ (13500) (see Figure 3.7). In 1970, Leigh and

Mingos reported the spectrum of the similar mer-[OsCl₃(PBuⁿ₂Ph)₃], recorded in

CHCl₃.[24] This contained maxima at 18500 (800), 22800 (1540), 28700 (shoulder),

33100 (shoulder) and 38500 (15200) cm⁻¹, positions and intensities very similar to

those which we found for mer-[OsCl₃(PEt₂Ph)₃]. Leigh and Mingos assigned the

four lower energy bands as Cl⁻ to Os(t₂g) bands and the highest energy band to a Cl⁻

to Os(eg*) process.[24] The assignment of the highest energy band is, however, called

into question by the spectra of two other reported species. In the spectrum of

mer-[OsBr₃(PEt₂Ph)₃], although the four lower energy bands have moved to 17300,

19200, 20700 and 24900 cm⁻¹, the highest energy band is unaffected by the change

127

of halide[24]. Clearly the highest energy absorbance does not arise from halide to metal charge transfer processes. Further light is shed by the spectrum of *mer*-[OsCl$_3$(PPr$^n_3$)$_3$], which contains four bands similar to the lower energy ones in *mer*-[OsCl$_3$(PBu$^n_2$Ph)$_3$] (at 19100, 23900, 26100(shoulder) and 32700cm^{-1}) but has no high energy band[24]. As the most significant change in the complex is the replacement of a dialkylphenyl phosphine with a trialkylphosphine we propose that the band at 38500 cm^{-1} arises from an intra-ligand transition associated with the phenyl group of the PBu$_2$Ph. In *mer*-[OsCl$_3$(PEt$_2$Ph)$_3$], therefore, we assigned the four lower energy bands as Cl$^-$ to Os^{III} charge transfer processes and the highest energy band to an internal transition in the phenyl group of PEt$_2$Ph.

The spectrum of [P1] in CH$_2$Cl$_2$ (Figure 3.8), has peaks at 17400 (600), 20400 (900), 32500 (5500) and 39000 cm^{-1} (14200). The two lower energy bands exhibit significant solvent dependence - in THF, for example, the maxima are at 18100, 20900, 32500 and 39000 cm^{-1}. An obvious effect of this is that while the complex is purple-pink in THF it is a deep red in many other solvents.

The band at 39000 cm^{-1} was again assigned as an intraligand band. From the IR and EPR studies, which indicate a ligand based LUMO and metal based HOMO, one would predict an Os^{II} to tcva MLCT band at relatively low energy. In light of this the bands at 17400 and 20400 cm^{-1} were provisionally assigned to such MLCT processes. The band at 32500 cm^{-1} was, in light of its solvent independence, tentatively assigned as a tcva-based intraligand band.

Figure 3.7 UV/visible spectrum of *mer*-[OsCl₃(PEt₂Ph)₃], THF
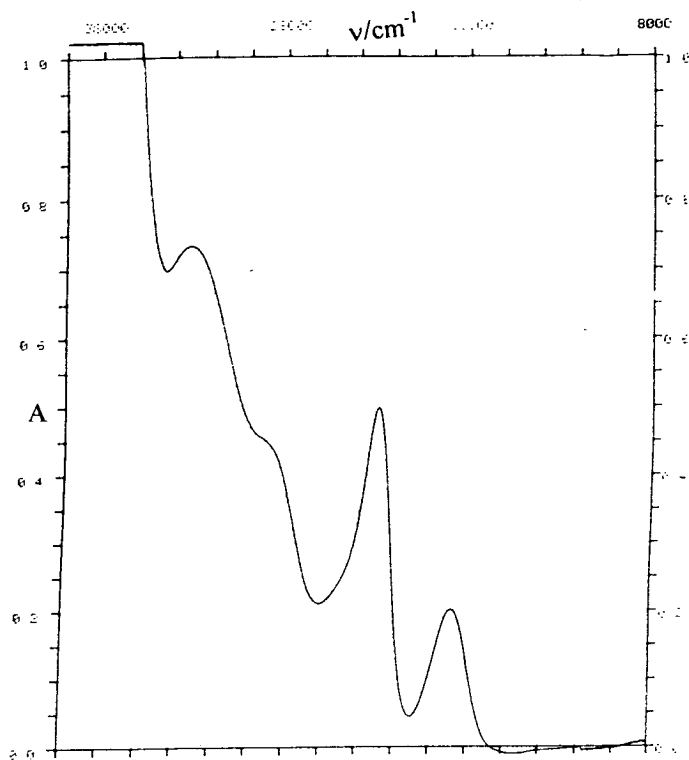
Figure 3.8 UV/visible spectrum of [P1] in CH₂Cl₂
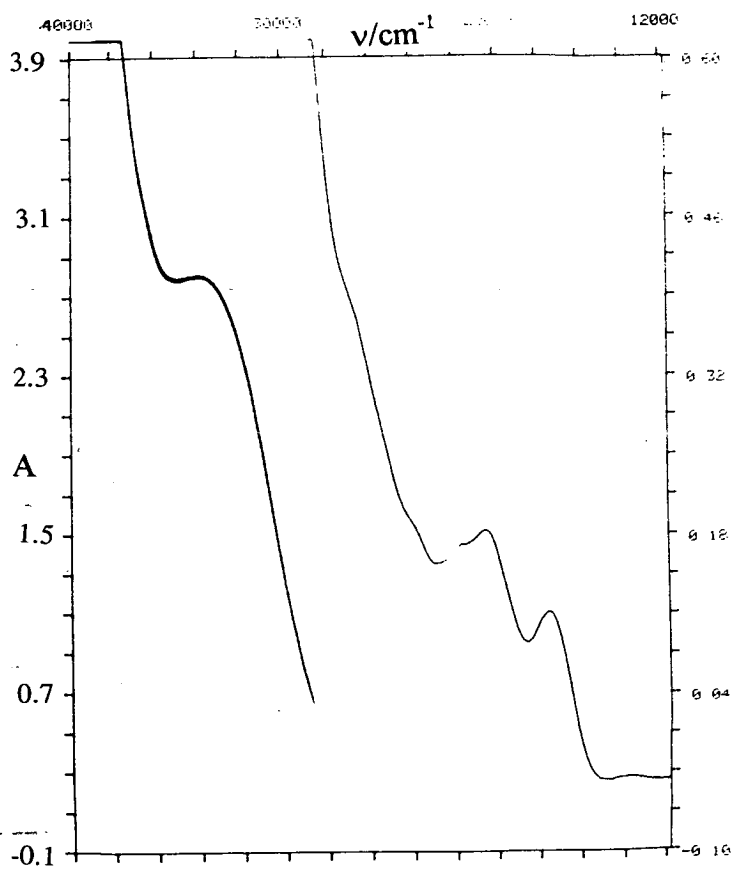
Reduction of [P1], (Figures 3.9 and 3.10) conducted in CH_2Cl_2 at 260 K, induces collapse of the lowest energy band, confirming its assignment as an Os to tcva MLCT band. This is accompanied by the growth of a new band at 24000 cm^{-1}, a frequency comparable with that of the π - π^* band observed in the spectrum of tcne$^-$. This fact led to assignment of the new band as an internal π - π^* transition in Os-bound tcva$^-$. Isosbestic points were observed at 20000, 30000, 31500 and 36000 cm^{-1}, although changes in the spectrum at higher energies were minor. The first reduction was fully reversible at 260 K.

Figure 3.9 UV/visible spectra, showing reduction of [P1] in CH_2Cl_2 at 260 K, E_{app} = -0.1 V.
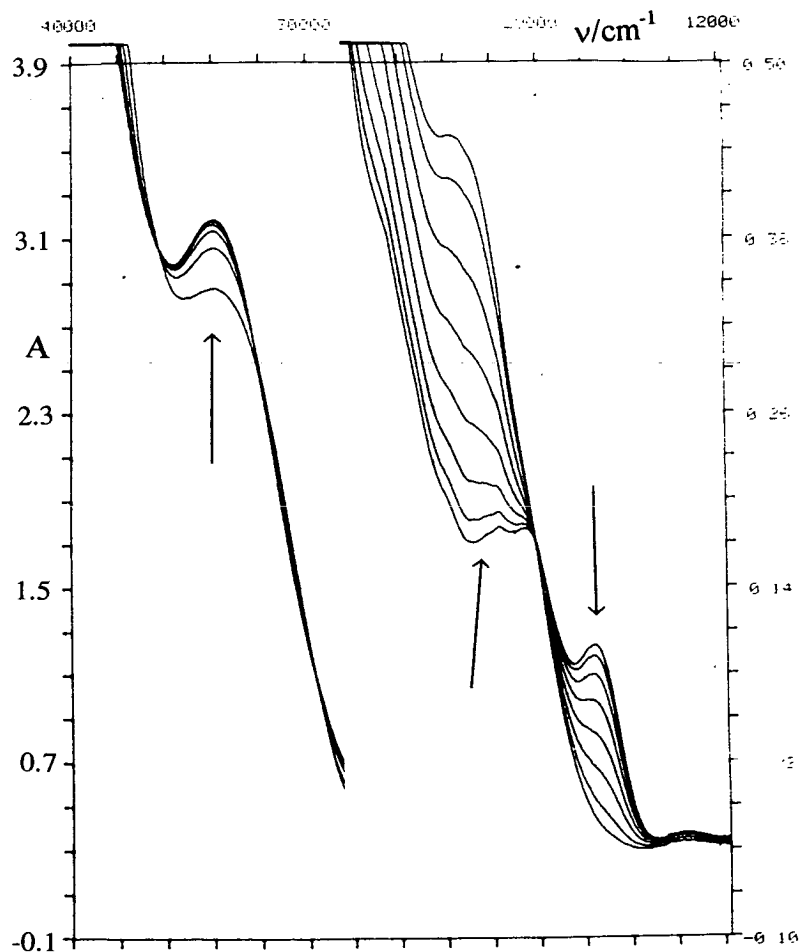
Figure 3.10 Absorption spectrum of [P1]⁻, CH_2Cl_2, 260 K.
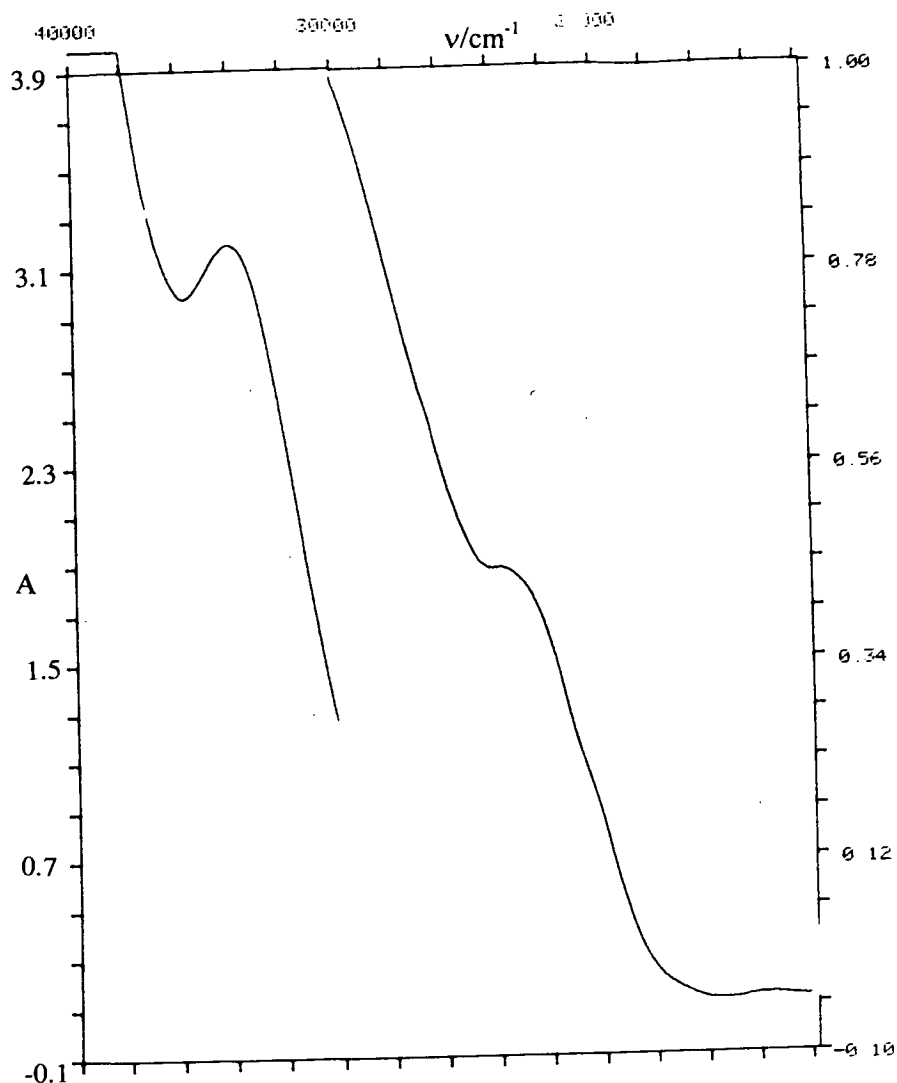
Oxidation of [P1] (the re-reduction to the parent species is shown in Figure 3.11) resulted in the growth of a new peak at 13900 cm⁻¹, collapse of the peak at 20400 cm⁻¹, and growth of another peak at 23700 cm⁻¹. A shoulder is also observed at 17000 cm⁻¹. At higher energies, a strong band was seen at 36000 cm⁻¹ ($\epsilon \approx$ 14000 $dm^3mol^{-1}cm^{-1}$). Isosbestic points were observed at 18000, 21500, 24500 and 26500 cm⁻¹.

After comparison with the spectrum of *mer*-[OsCl₃(PEt₂Ph)₃], we have

assigned the shoulder at 17000 cm⁻¹ and the band at 23700 cm⁻¹ as Cl⁻ to Osᴵᴵᴵ LMCT

bands. The band at 13900 cm⁻¹ was assigned to a tcva to Osᴵᴵᴵ transition. The band

at 36000 cm⁻¹ was assigned, as a result of its similar extinction coefficient, as the

phosphine-based π-π* transition. It is thought that the tcva-based π-π* band is

superimposed upon the stronger phosphine band. As with the first reduction, the

oxidation of [P1] was found to be fully reversible at 260 K.

Figure 3.11 Absorption spectra showing reduction of [P1]⁺ in CH₂Cl₂ at 260 K, E_app

= +1.3 V.
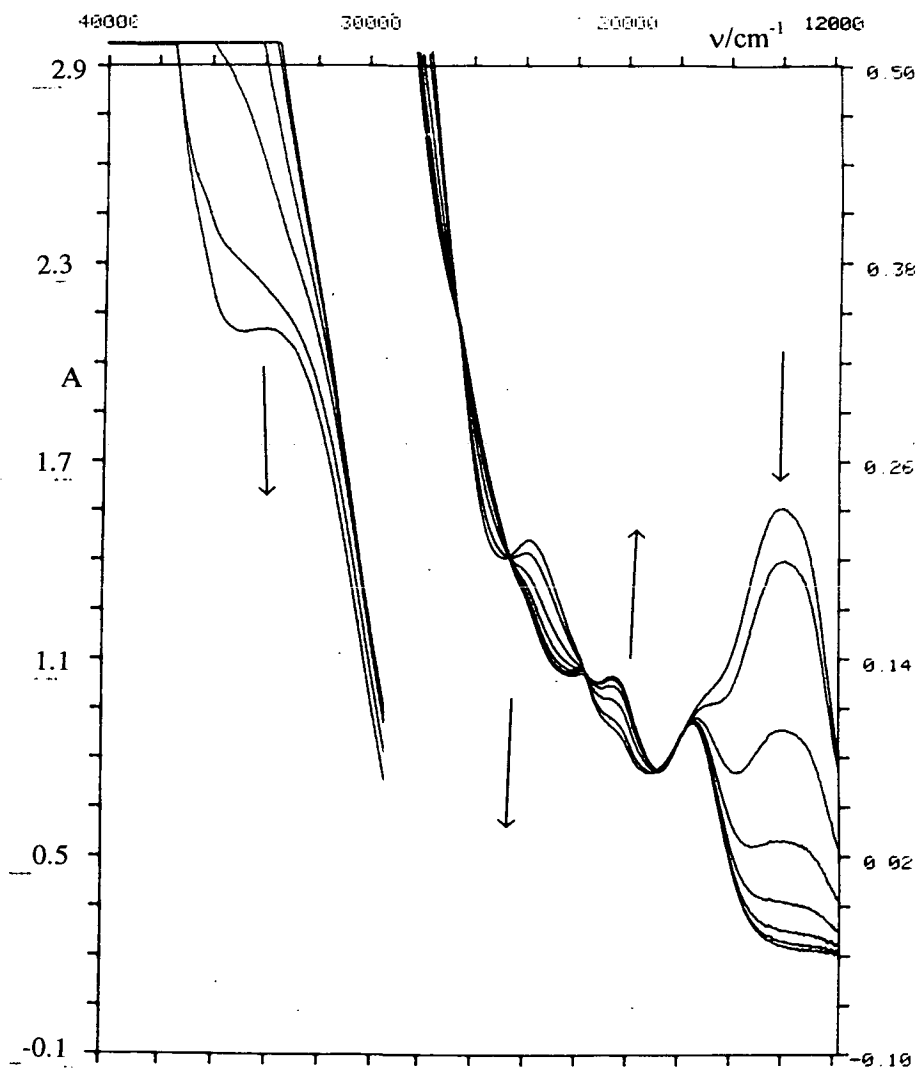
3.2.1.2.5 Summary

The electrochemical and spectroelectrochemical data obtained is generally consistent with [P1] having a tcva-based LUMO and an Os-based HOMO. Thus, [P1] is best described as $[Os^{II}(tcva)^{0}Cl_{2}(PEt_{2}Ph)_{3}]$, while $[P1]^{+}$ and $[P1]^{-}$ are best described as $[Os^{III}(tcva)^{0}Cl_{2}(PEt_{2}Ph)_{3}]^{+}$ and $[Os^{II}(tcva)^{-}Cl_{2}(PEt_{2}Ph)_{3})]^{-}$ respectively.

3.2.1.3   Mechanistic Studies of [P1]

The reaction of $[OsCl_{3}(PEt_{2}Ph)_{3}]$ with tcne and $AgBF_{4}$ to form [P1] is a multi-step process. In addition to the expected removal of Cl⁻ from the Os complex by $AgBF_{4}$ and subsequent binding of a π-accepting ligand (either tcne or tcva), there is also a nucleophilic substitution reaction resulting in the replacement of CN⁻ group with OH⁻, and a metal-based reduction process, giving the Os^{II} product. It is clearly desirable to deduce when and how these various steps take place during the course of the formation of [P1] if we are to conduct controlled syntheses of [P1] and related complexes.

Initial observations, from the structural and electrochemical data reported earlier, suggest that initial coordination to the metal centre is via unsubstituted tcne. This is based on the speed of the reaction (free tcne will react slowly with water, in neutral or acidic conditions to form tcva, and preparation of tcva is generally carried out by boiling an aqueous suspension of tcne until evolution of HCN ceases[25]). The hypothesis that Os-bound tcne undergoes hydrolysis is also

supported by the selectivity of substitution (for the position *cis* to the CN group bound to Os). As with the free ligand, the most likely source for the substitution is water, probably absorbed by THF from the atmosphere during the short interval between distillation and use in the reaction. This hypothesis is supported by the fact that it is possible to convert a CH_2Cl_2 solution of the freshly prepared intermediate complex, [P2], into [P1] by the simple expedient of adding a small quantity of water.

Another possible source of moisture was $AgBF_4$ which is known to be hygroscopic. In light of this attempts were made to prepare the intermediate complex using $TlBF_4$ to remove Cl^- from the starting complex. These attempts, however, failed to induce any observable reaction within 1 week, as compared with the few seconds required to produce the intermediate when silver was employed. This suggests that $AgBF_4$ may be involved in a manner other than mere "halide stripping" in the formation of [P1].

Identifying the intermediate complex [P2] is obviously crucial if a mechanism of formation for [P1] is to be deduced. Successful isolation of this blue-grey species was problematic and redissolution for spectroscopic purposes usually resulted in conversion to [P1], although the solid intermediate was relatively stable. Attempts to obtain FAB mass spectra of [P2] also resulted in conversion to [P1] when the matrix (3-nitrobenzylalcohol or thioglycerol) was added to the sample. As a result, the only reliable data obtained by conventional means were a UV/visible spectrum in CH_2Cl_2 (see Figure 3.12), which showed a charge transfer band at 13800 cm^{-1} and the strong band at 39000 cm^{-1} associated with PEt$_2$Ph (the

ratio of these peaks was 1:10, implying an extinction coefficient for the lower energy band of approximately 1400 $dm^3mol^{-1}cm^{-1}$), and an IR spectrum of a doped KBr disc which showed $C\equiv N$ stretching modes at 2215 (sh), 2205 (sh), 2195 (m) and 2100 cm^{-1} (w,br), thus confirming that tcne had reacted in the formation of [P2]. OH stretches were not observed in the IR spectrum, indicating that [P2] contains tcne, not tcva.

Figure 3.12 UV/visible spectrum of [P2], CH_2Cl_2
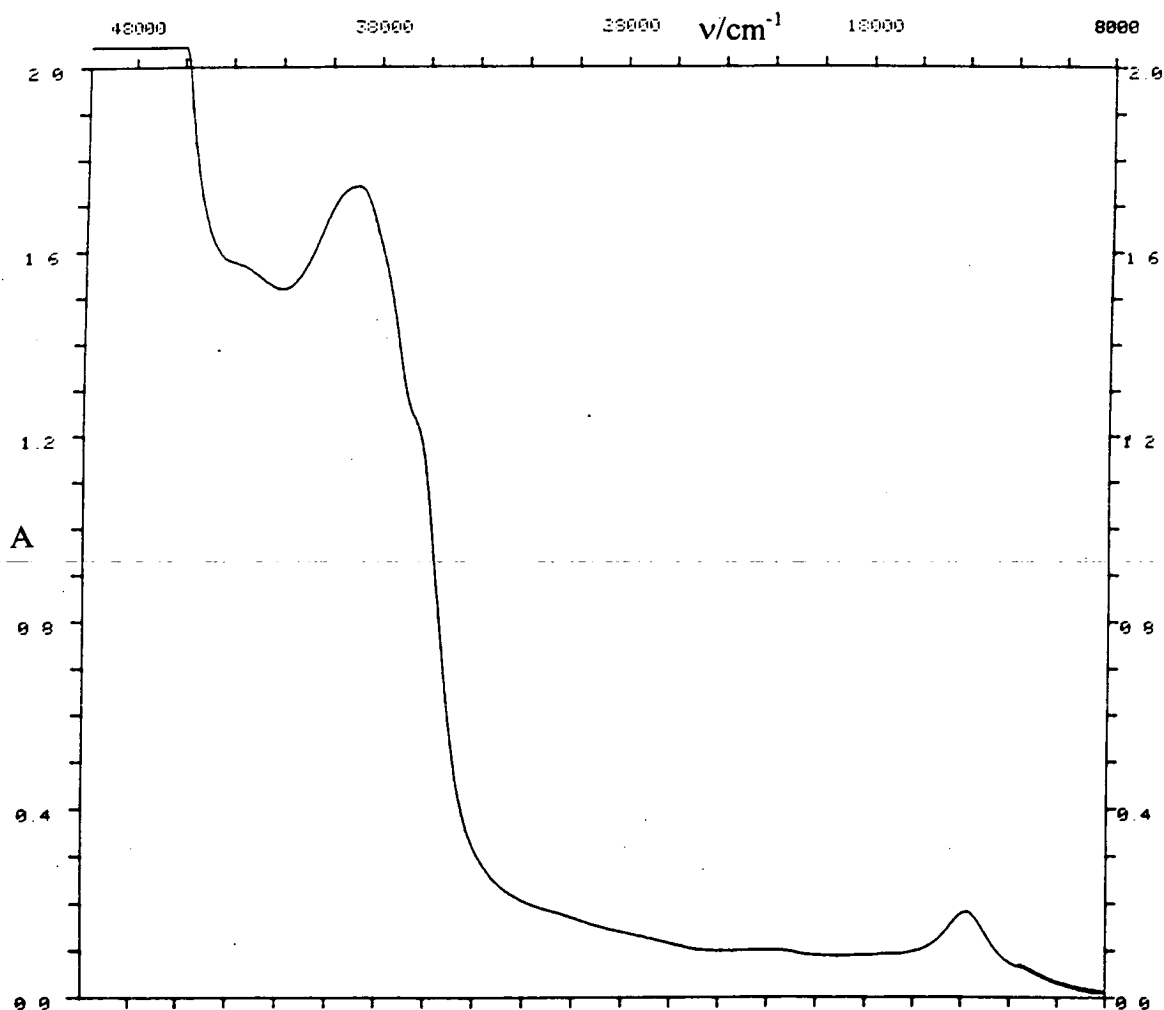
To circumvent the problems of isolation and redissolution it was decided to synthesise [P2] within a voltammetric cell, allowing direct electrochemical investigation of the intermediate.

Initial experiments involved a repetition of the preparative method employed previously. Figure 3.13 shows a cyclic voltammogram of the starting mixture of tcne and $[OsCl_3(PEt_2Ph)_3]$ in CH_2Cl_2. It is worth noting that the osmium-based reduction now has two daughter products associated with it on the return wave, the second one possibly due to oxidation of a tcne containing daughter product (the first daughter product arises from oxidation of the five coordinate daughter product, as observed when only $[OsCl_3(PEt_2Ph)_3]$ is studied).

Figure 3.13 CV of tcne and *mer*-$[OsCl_3(PEt_2Ph)_3]$ in CH_2Cl_2
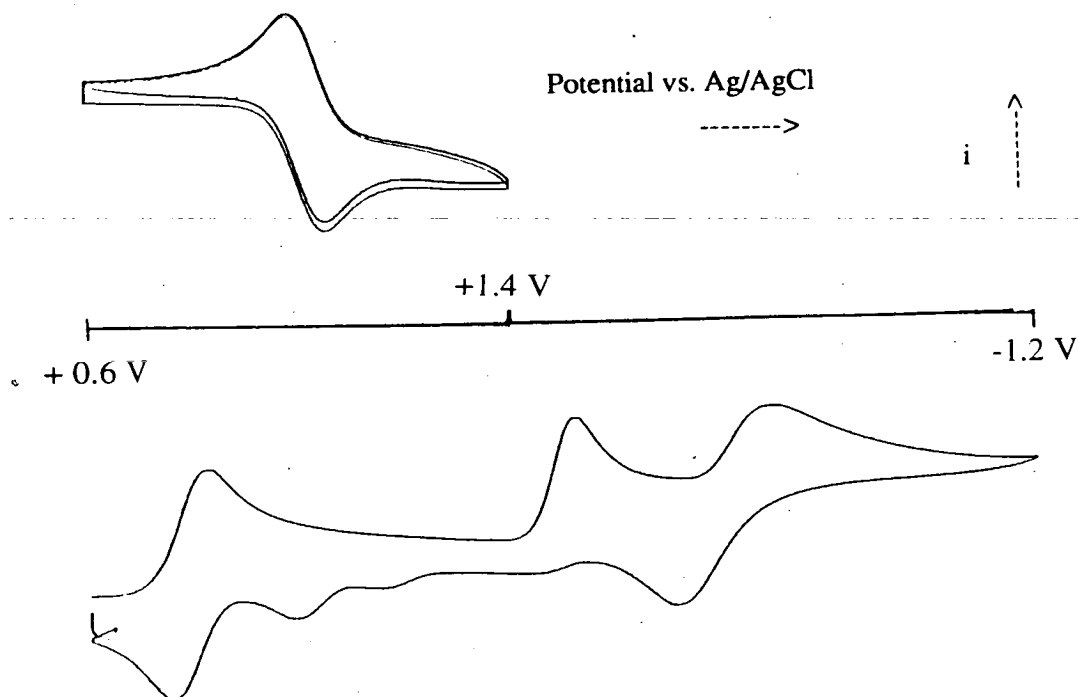
Upon addition of AgBF$_4$ the UV/visible spectrum changed to one matching the spectra recorded for [P2] previously. The electrochemical response after addition of AgBF$_4$ is shown in Figure 3.14. In addition to couples associated with excess unreacted tcne, the cyclic voltammogram of the product contains a reversible reduction at +0.19 V vs Ag/AgCl and an oxidation at +1.52 V. The position and nature of these couples may, however, have been affected by coating of the working electrode associated with the Ag$^{+/0}$ sorption/desorption process at +1.0 V.

Figure 3.14 CV of [P2] (plus AgBF$_4$) in CH$_2$Cl$_2$

+1.7 V –   +0.6 V   -1.4 V
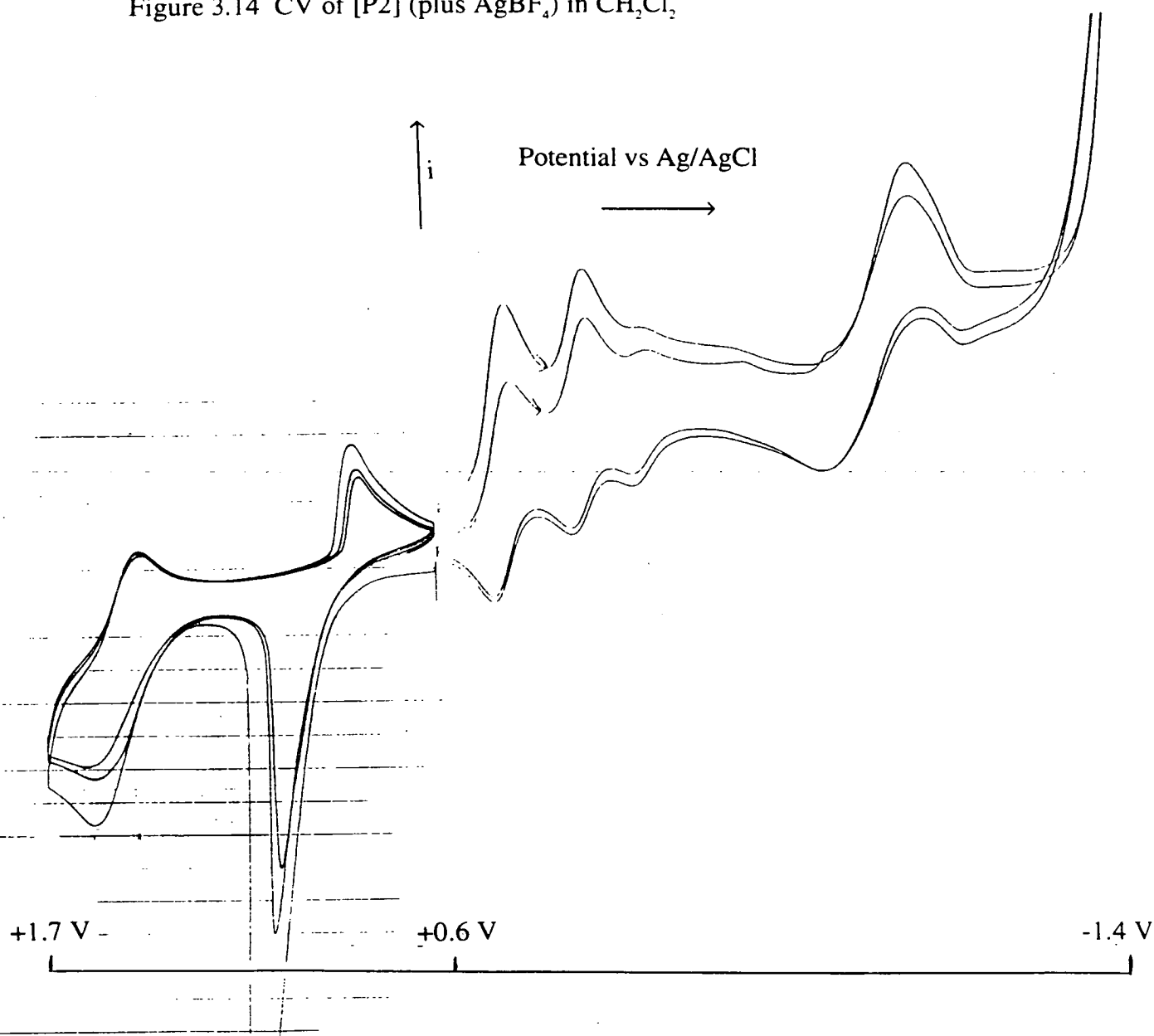
To check the validity of the observed electrochemistry of the product mixture in the above experiment it was clearly important to prepare [P2] in the absence of silver. To that end attempts were made to produce [P2] by electrosynthesis. The reaction consisted of three one electron electrogeneration reactions, reduction of tcne, reduction of Os^{III} inducing loss of Cl$^-$ and coordination of tcne, then oxidation of the product complex (this reaction scheme is shown in Figure 3.15). Although the yield of product was decreased when [P2] was prepared electrochemically, electrochemical study of the solution after reaction showed couples in identical positions to those observed when [P2] was prepared by chemical methods. The electronic absorption spectrum of the product mixture was consistent with a mixture of [P2], mer-[OsCl$_3$(PEt$_2$Ph)$_3$] and tcne$^-$ (see Figures 3.16 and 3.17).

Figure 3.15 Reaction scheme for electrosynthesis of [P2].

$$[OsCl_3(PEt_2Ph)_3] + tcne \xrightarrow{\ +0.2\ V\ } [OsCl_3(PEt_2Ph)_3] + tcne^-$$

$$\Big\downarrow\ -0.55\ V$$

$$[OsCl_3(PEt_2Ph)_3]^- + tcne^-$$

$$\Big\downarrow$$

$$[OsCl_2(PEt_2Ph)_3(tcne)], \text{ complex [P2]} \xleftarrow{\ +0.40\ V\ } [OsCl_2(PEt_2Ph)_3(tcne)]^-$$
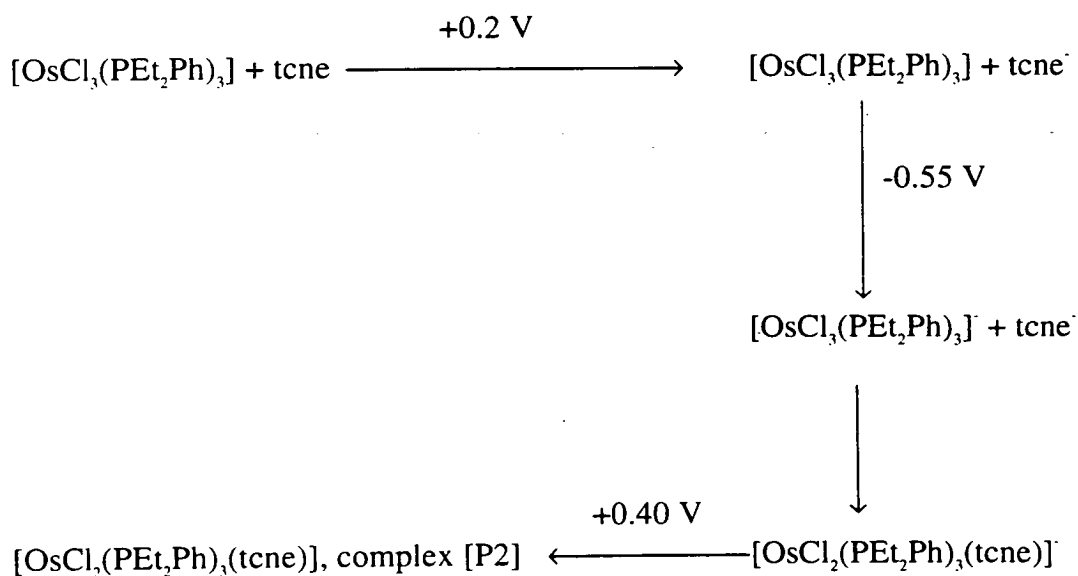
Figure 3.16 UV/visible spectrum of [P2]·, tcne· and "[OsCl$_3$(PEt$_2$Ph)$_3$]·" in CH$_2$Cl$_2$

ABSCISSA	ORDINATE	
+5745.6	0.334	A
+5991.9	0.334	A
+6092.2	0.301	A
+6142.5	0.289	A
+8833.9	0.381	A
+13624	0.339	A
+25126.	0.649	A
+39249	4.274	A
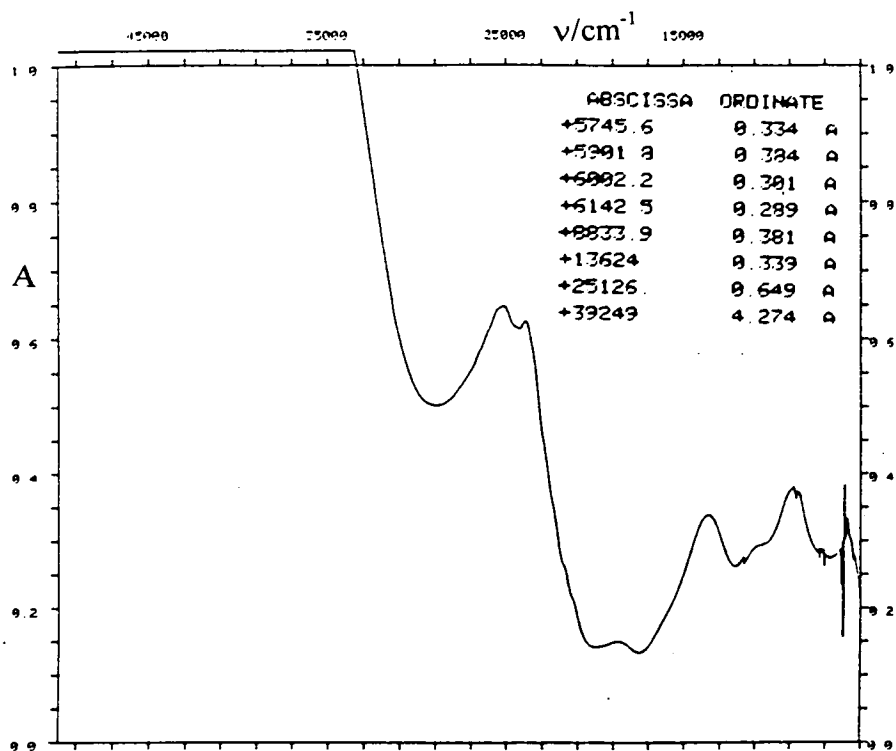
Figure 3.17 Absorption spectrum of [P2], tcne· and [OsCl$_3$(PEt$_2$Ph)$_3$] in CH$_2$Cl$_2$

ABSCISSA	ORDINATE	
+5744.3	−0.193	A
+5834.9	−0.198	A
+5998.4	−0.142	A
+6092.2	−0.225	A
+8417.5	−0.221	A
+25497.	0.272	A
+37426.	3.765	A
+38522.	4.343	A

139
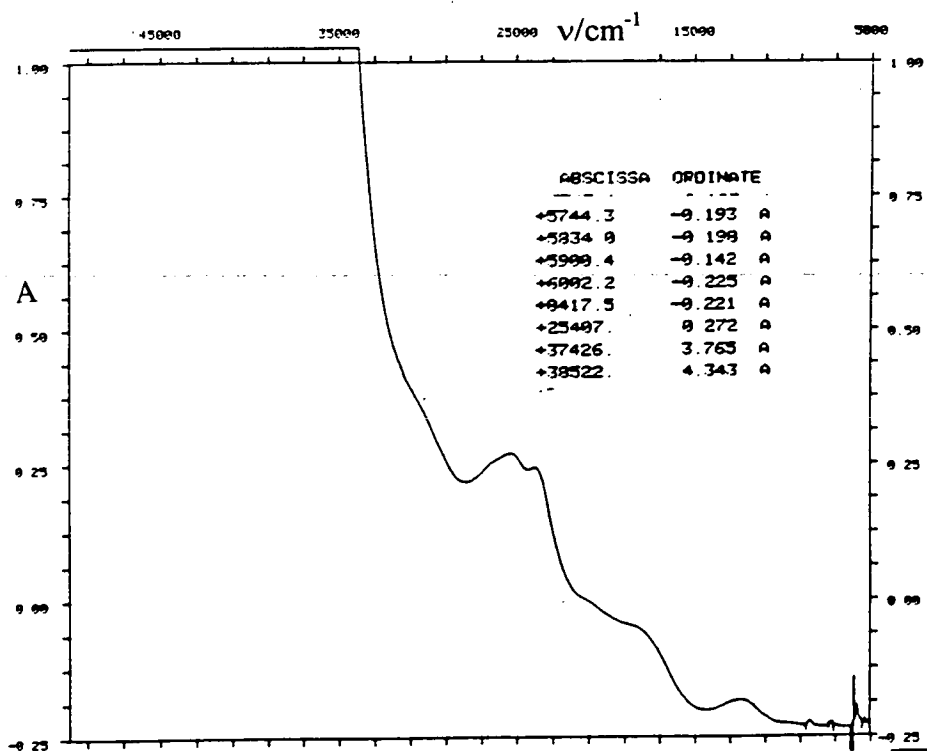
In considering the electrochemistry of [P2], it is useful to make comparisons with [P1], as the cyclic voltammograms have marked similarities. Both exhibit an oxidation in the region of +1.5 V and a reduction at a small positive potential. This suggests that in [P2], as in [P1], the oxidation and reduction processes may be assigned as metal and ligand-based respectively. If a -CN group on tcne were replaced by an -OH group, one would expect a reduction in the electron withdrawing capacity of the ligand. This would therefore result in a small increase in electron density at the metal centre and a corresponding shift of any metal-based oxidations to less positive potentials. Comparing the oxidations in [P2] and [P1], it can be seen that formation of [P1] results in a small negative shift from +1.52 V to +1.43 V. This suggests strongly that [P2] is [OsCl$_2$(PEt$_2$Ph)(tcne)]. The increase in electron density on replacement of (CN)$^-$ with (OH)$^-$ would be expected to make ligand-based reductions more difficult, resulting in a shift to more negative redox potentials of any such processes. Comparing the voltammetric behaviour of [P2] and [P1] again shows this to be the case, supporting the hypothesis that [P2] is in fact [OsCl$_2$(PEt$_2$Ph)$_3$(tcne)]. Reduction of Os during the formation of [P2] is also implied by the nature of the electrosynthetic preparation of [P2], during which two one-electron reductions but only one (apparently ligand-based) oxidation took place, as shown in the reaction scheme in Figure 3.15.

It is worth noting at this point that attempts to prepare [P2] by addition of tcne to a solution of the reduction product of [OsCl$_3$(PEt$_2$Ph)$_3$] were invariably unsuccessful. This suggests, as observed with various other reactions described in this thesis and elsewhere[26], that the species which actually attacks the metal centre

is tcne⁻. In the chemical formation of [P2], this presumably means a reaction in which tcne⁻ attacks $[Os^{III}Cl_2(PEt_2Ph)_3]^+$, once Cl⁻ had been removed by Ag⁺, and the product then undergoes a rapid "internal redox" reaction in which an electron is transferred from ligand to metal to form $[Os^{II}Cl_2(PEt_2Ph_2)(tcne)^0]$. It should be noted that although the redox properties of $[OsCl_3(PEt_2Ph)_3]$ suggest that tcne⁻ would not be able to reduce Os^{III} in the starting complex, it is more than adequate to reduce Os^{III} after coordination, as a result of the very large positive shift in the potential of the $Os^{III/II}$ couple.

Assuming the above to be the case, the search is now for an agent capable of reducing tcne, not the starting complex (this is logical, given that tcne is more easily reduced than $[OsCl_3(PEt_2Ph)_3]$ and $[OsCl_2(PEt_2Ph)_3]^+$). It was observed during the electrochemical experiments that formation of [P2] occurred in higher yield if a substantial excess of $AgBF_4$ was employed. Given the earlier observation that $TlBF_4$ was unable to induce formation of [P2], this suggests that silver may be involved in the reductive process.

Reduction of tcne by Ag^I to give tcne⁻ and Ag^{II} or Ag^{III} is perhaps the most obvious possibility. It is, however, questionable whether tcne would be capable of oxidising Ag^I. A less obvious possibility is suggested by reports of $Ag^+(tcne)^{-}$[27] and $Ag^+(tcnq)^{-}$[28], which imply that tcne is capable of oxidising Ag^0. As a large excess of $AgBF_4$ is required to prepare [P2] in high yield it is possible that small amounts of Ag^0 in the fluoroborate salt are responsible for reduction of tcne to its radical anion. At present we have been unable to determine which oxidation state of silver is involved. It is, however, clear that silver is responsible for reduction of

tcne prior to attack of Os^{III} by the radical anion.   To conclude, it would appear that formation of [P1] proceeds by the following route. AgBF$_4$ is added to a solution of tcne and [OsCl$_3$(PEt$_2$Ph)$_3$], resulting in removal of Cl$^-$ from Os and reduction of tcne. This causes attack of Os^{III} by tcne$^-$, followed by an internal redox reaction to give [Os^{II}Cl$_2$(PEt$_2$Ph)$_3$(tcne)], the intermediate complex.   This subsequently reacts with small quantities of H$_2$O in solution to give [Os^{II}Cl$_2$(PEt$_2$Ph)$_3$(tcva)]. This is detailed in Figure 3.18.

Figure 3.18 Mechanism of formation of [OsCl$_2$(PEt$_2$Ph)$_3$(tcva)]

[OsCl$_3$(PEt$_2$Ph)$_3$] + tcne   [OsCl$_2$(PEt$_2$Ph)$_3$(tcva)], [P1]

          ↓ fast   H$_2$O   ↑ slow

AgBF$_4$

                               [Os^{II}Cl$_2$(PEt$_2$Ph)$_3$(tcne^0)], [P2]

                                        ↑

                     Internal redox   fast

[OsCl$_2$(PEt$_2$Ph)$_3$]$^+$ + tcne$^-$ ⟶ [Os^{III}Cl$_2$(PEt$_2$Ph)(tcne$^-$)]
                           fast
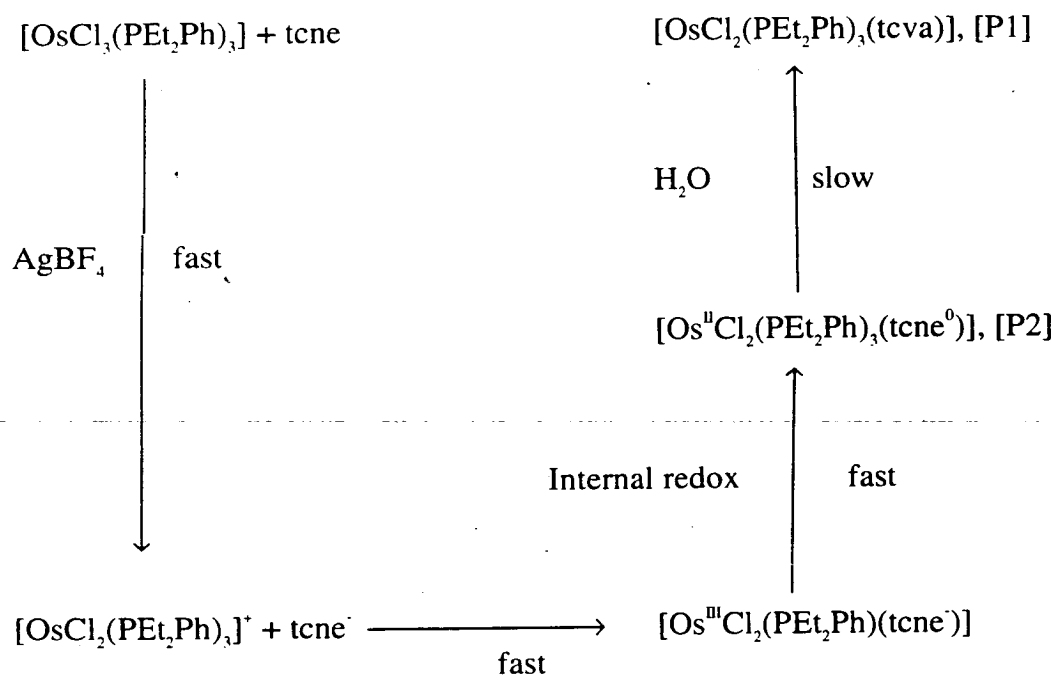
A small number of unsuccessful attempts were made to induce other substitution reactions of Os-bound tcne. In these, [P2] was prepared in CH_2Cl_2 then a small quantity of a nucleophile such as methanol or ethanol was introduced to the system, but either [P1] was isolated or the complex decomposed without giving isolable products.

3.2.1.4   Conclusions

Mer-[OsCl$_3$(PEt$_2$Ph)$_3$] reacts with tcne and AgBF$_4$ to give trans-[OsCl$_2$(PEt$_2$Ph)$_3$(tcne)] ([P2]), which subsequently reacts with water to give trans-[OsCl$_2$(PEt$_2$Ph)$_3$(tcva)] ([P1]). It appears that the reaction proceeds via attack of [OsCl$_2$(PEt$_2$Ph)$_3$]$^+$ by tcne$^-$, tcne having apparently been reduced by silver.

In both complexes, the HOMO is Os-based and the LUMO is nitrile based (ie the complex is best described as Os^{II}L^0). It would appear that back donation to tcva's π^*-LUMO in [P1] is relatively low. This is best exemplified by the short tcva C=C distance and high energy of the C=C stretching vibration in the IR spectrum. Back donation appears to be greater in the case of [P2]. This is shown, for example, by the fact that the Os-based oxidation is at a more positive potential than in [P1] and in the slightly lower energies of the C≡N stretching modes in [P2].

143

Reactions were carried out between tetranitriles and a number of halo-phosphine complexes of Ru and Os. Subsequent to obtaining the results reported in 3.2.1, one of the primary objectives of this work was to investigate the extent and ease of reaction of metal bound tcnx to give the tricyano alcohol ligand. The reactions carried out are listed below.

Mer-[OsCl$_3$(PEt$_2$Ph)$_3$] was reacted with tcnq and AgBF$_4$ in THF, yielding a dark blue product [P3], which exhibited very low solubility in almost all solvents, making characterisation difficult. It is believed that a polymeric species may have been formed.

Tcne was reacted with AgBF$_4$ and [OsBr$_3$(PMe$_2$Ph)$_3$]. This reaction was conducted in THF and in CH$_2$Cl$_2$, enabling comparison of the dark red/brown products, designated [P4] and [P4c] respectively. No significant differences were observed in the results for [P4] and [P4c] and no evidence was found of hydrolysis of bound tcne. [P4] was found to be [Os^{II}Br$_2$(PMe$_2$Ph)$_3$(tcne^0)], in which we suggest that tcne is N-bound to Os.

Reaction was also carried out between tcne and [RuCl$_2$(PPh$_3$)$_3$], again in THF and in CH$_2$Cl$_2$, yielding the bright blue [P5] and [P5c]. Again, no evidence of hydrolysis was found, and the product of both reactions is believed to be [RuCl$_2$(PPh$_3$)$_3$(tcne)], featuring neutral, N-bound tcne.

An attempt was made to prepare a binuclear complex by reaction of [P5] with [RuCl$_2$(PPh$_3$)$_3$] in THF, giving another blue complex, [P6]. Although the

experimental evidence was not conclusive, this attempt appears to have been successful, yielding [{RuCl$_2$(PPh$_3$)$_3$}$_2$(tcne)].

The complexes reported in this section showed a high degree of stability in the solid state, to the extent that spectra recorded several months after synthesis were the same as those obtained from the freshly isolated reaction products. They all underwent rapid decomposition, however, when attempts were made to purify the products by chromatography.

3.2.2.1   IR Spectroscopy

Spectra were recorded of KBr discs of all the complexes, and the energies of the C≡N stretching modes (and, when assigned, the tcnx based C=C stretches) are listed in Table 3.4. It should be noted that none of the spectra showed an OH stretch similar to that observed in [P1]. Additionally, in the case of [P3], the expected bands associated with (PEt$_2$Ph) were not observed, implying that reaction of the phosphine ligands had taken place. Comparison of spectra of products of the same reaction conducted in different solvents (ie. [P4], [P4c]; and [P5], [P5c]) showed no differences in the IR spectra of the products, suggesting that the same product is obtained from the syntheses in THF and CH$_2$Cl$_2$. Furthermore, in the cases when AgBF$_4$ was used to abstract Cl⁻ or Br⁻ from the starting complexes, there was no evidence of the broad, strong bands, centred at 1084 cm⁻¹, which are observed in spectra of [BF$_4$]⁻ salts. It is reasonable to conclude, therefore, that

neutral complexes have been formed, as observed in the reactions between tcne and
$[OsCl_3(PEt_2Ph)_3]$.

The differences between the spectra of [P5] and [P6] are not inconsistent with
tcne forming a bridge between two $[RuCl_2(PPh_3)_3]$ centres. It is to be expected that
binding of tcne to two metal centres would result in a greater degree of π-back
donation from the Ru dπ orbitals into the tcne π^* LUMO than coordination to a
single metal. Previous studies have shown that the extent of π-back donation is
related to the weakening of the C=C bond[14,16,17], as is observed on formation of [P6]
from [P5].

Table 3.4   Selected IR data for [P3], [P4], [P5] and [P6].

Complex	$\nu^{C\equiv N}$/cm^{-1}	$\nu^{C=C}$/cm^{-1}
[P3]	2200m, 2190m, 2180w	not assigned
[P4]	2205sh, 2194m, 2108w,br	" "
[P5]	2199m, 2124s	1460m,br
[P6]	2200m, 2180sh, 2115s,br	1405m,br

3.2.2.2   FAB Mass Spectrometry

Mass spectrometric data is given in Table 3.5. As with the IR spectroscopic data there are no significant differences between spectra of products of reactions conducted in THF and CH_2Cl_2. Unfortunately, most of the spectra did not contain a peak corresponding to the expected molecular ion (the exception to this is [P5]), although they generally correspond well to breakdown of the expected metal-tcnx adducts. The spectrum of [P6] was particularly disappointing, showing no significant peaks above m/z = 653 (which corresponds to $[RuCl(PPh_3)_2]^+$), implying that the complex may have been decomposed by the matrix (although changing the matrix employed did not significantly alter the observed mass spectrum). The lower m/z peaks in the spectrum of [P6] were generally indistinguishable from those of [P5].

In addition to the data above, a high m/z spectrum was obtained for [P3], which contained peaks corresponding to, for example, $[\{OsCl_2(PEt_2Ph)_3\}_4tcnq]^+$ (m/z = 3244), $[\{OsCl_2(PEt_2Ph)_3\}_3tcnq]^+$ (m/z = 2485) and $[\{OsCl_2(PEt_2Ph)_3\}_4(tcnq)_2]^+$ (m/z = 3450), plus significant peaks at even higher m/z which were not successfully assigned. This suggests that [P3] is a polynuclear, and possibly polymeric, species, which is consistent with its extremely low solubility.

Table 3.5   Selected FAB-MS data for [P3], [P4], and [P5].

Complex	m/z	Assignment	Intensity
[P3]	1373		13
	760	$[OsCl_2(PEt_2Ph)_3]^+$	35
	725	$[OsCl(PEt_2Ph)_3]^+$	10
	594	$[OsCl_2(PEt_2Ph)_2]^+$	100
	557	$[OsCl(PEt_2Ph)_2]^+$	25
	529		25
	499/501		15
[P4]	764	$[OsBr_2(PMe_2Ph_3)]^+$	65
	685	$[OsBr(PMe_2Ph)_3]^+$	40
	626	$[OsBr_2(PMe_2Ph)_2]^+$	100
	546	$[OsBr(PMe_2Ph)_2]^+$	35
	468	$[Os(PMe_2Ph)_2]$	20
[P5]	1087	$[RuCl_2(PPh_3)_3(tcne)]^+$	23
	696	$[RuCl_2(PPh_3)_2]^+$	25
	653	$[RuCl(PPh_3)_2]^+$?	100
	625	$[Ru(PPh_3)_2]^+$	60
	547	$[Ru(PPh_3)(PPh_2)]^+$	40
	519		70
	363	$[RuPPh_3]^+$	50

3.2.2.4   Redox Behaviour

The cyclic voltammetric behaviour of [OsBr$_3$(PMe$_2$Ph)$_3$] in CH$_2$Cl$_2$ shows a reversible Os$^{III/IV}$ couple at +1.08 V versus Ag/AgCl, while the reduction is, like that of [OsCl$_3$(PEt$_2$Ph)$_3$], partially reversible, occuring at -0.10 V, with the oxidation of the daughter product observed at +0.15 V on the return sweep.

Voltammetric studies of [P4], in CH$_2$Cl$_2$, reveal a reversible reduction at +0.23 V, and a quasi-reversible oxidation at +1.48 V. By analogy with [P1] and [P2], the charge transfer processes were assigned as tcne and osmium-based respectively. The cyclic voltammogram of [P4] is shown in Figure 3.19.

Figure 3.19 Cyclic voltammogram of [P4] in CH$_2$Cl$_2$.

Potential vs Ag/AgCl

+1.65

-1.2

+0.6
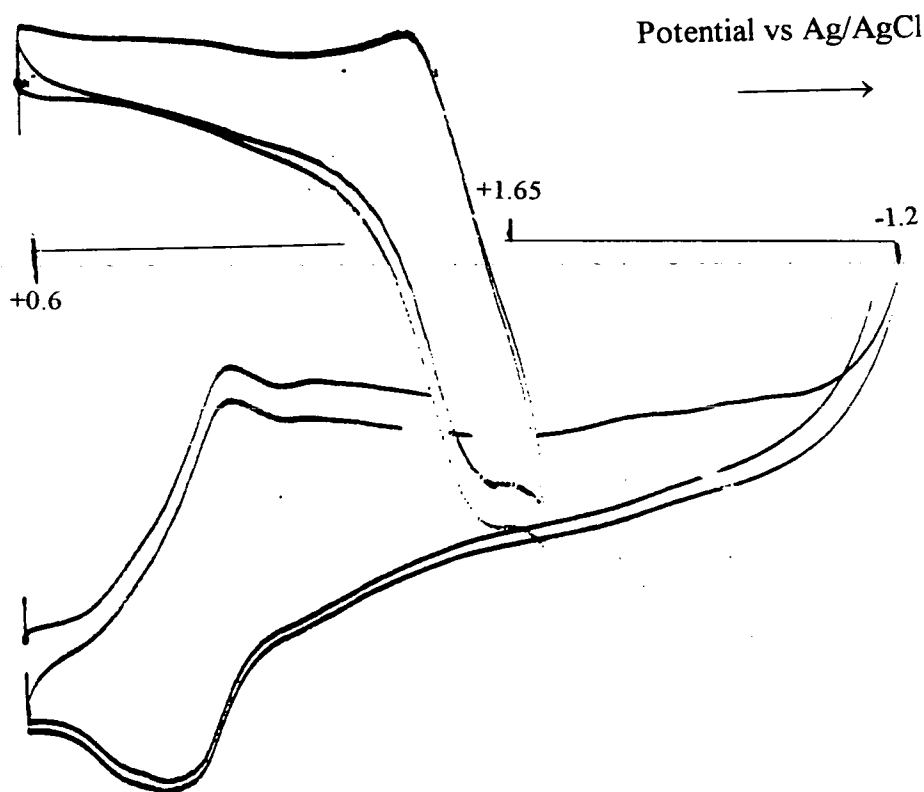
The voltammetric response of [RuCl$_2$(PPh$_3$)$_3$] in CH$_2$Cl$_2$ was time dependent. Initially, a partly reversible oxidation was observed at +0.83 V versus Ag/AgCl, but over a period of 90 minutes this was replaced by a reversible oxidation at +0.58 V. Both species also showed a quasi- reversible reduction at -1.25 V (believed to be PPh$_3$ based).

The signal to noise ratio in cyclic voltammograms of [P5] in CH$_2$Cl$_2$ and in THF, was rather poor due to solubility problems. The study in CH$_2$Cl$_2$ did, however, apppear to show a reversible reduction at +0.26 V (confirmed by a.c. voltammetry) and a quasi-reverible oxidation at +1.65 V.

Similar solubility problems were encountered with [P6], which appeared to show a reduction at +0.22 V and an oxidation at +1.57 V, when it was studied in CH$_2$Cl$_2$. Coulometric studies of this complex were not conducted, therefore it is not known whether the oxidation is a one or two-electron process.

[P3] was insufficiently soluble to permit study of its redox behaviour.

In [P4], [P5] and [P6], the observed redox behaviour is generally similar to that observed for [P1] and [P2], thus suggesting that the complexes contain N-bound polynitrile ligands coordinated to M^{II} centres (M = Ru, Os). Given the lack of the OH stretch in the IR spectra, and the fact that the reductions occur at more positive potentials than in [P2], it seems reasonable to conclude that the polynitrile bound to the metal centres is tcne, ie. there is no evidence of the rapid hydrolysis observed when tcne is reacted with [OsCl$_3$(PEt$_2$Ph)$_3$].

Comparison of the voltammograms of [P5] and [P6] shows differences which are not inconsistent with [P6] containing tcne which is bound to 2 metal centres. Coordination of tcne to a second metal would be expected to increase the electron density in tcne's π^*-LUMO, thus making reduction of the ligand more difficult. Simultaneously, it is reasonable to expect that electron withdrawal by tcne from the *individual* Ru centres would be reduced, therefore one would also expect the metal-based oxidation to shift to a less positive potential. The lack of coulometric data for [P6] makes it impossible to know if there are significant metal-metal interactions in the binuclear complex.

3.2.2.5 UV/visible Spectroelectrochemistry

Data obtained from the electronic absorption spectra of [P4], [P5], [P6] and their precursors are given in Table 3.6. Spectra were also recorded of solutions of [P3] but the low solubility resulted in a poor signal to noise ratio (the best spectra were recorded in CH_2Cl_2 and DMF). The spectra obtained for [P3] were invariably dominated by a band at 25000 cm^{-1} arising from π to π^* transitions within tcnq. In DMF, bands consistent with the corresponding transition in tcnq$^-$ were also observed although these were much weaker than the bands associated with the neutral tetranitrile which were observed in the same spectrum. A band assigned to a charge transfer process was also observed (at 15000 cm^{-1} in CH_2Cl_2, 17500 cm^{-1} in DMF).

151

Table 3.6   UV/visible spectroscopic data

Complex	Solvent	ν_{max}/cm^{-1} $(10^{-3}\varepsilon/mol^{-1}cm^{-1}dm^3)$
$[OsBr_3(PMe_2Ph)_3]$	CH_2Cl_2	13500(0.3), 17500(1.3), 21100(1.4), 39300(14)
	THF	13500(0.3), 18000(1.3), 20600(1.5), 39300(14)
[P4]	CH_2Cl_2	16300(0.9), 20900(1.2), 23600(1.0), 40000(17)
	THF	16800(0.9), 21000(1.2), 24000(1.0), 40000(17)
[P5]	CH_2Cl_2	13000(7.0), 36500(38)
	THF	13500(7.0), 36500(38)
[P6]	THF	11800(5.5), 15400(4.6), 37000(41)

Spectra of [P4] and [P4c] recorded in CH_2Cl_2 were identical, and there were no significant differences between spectra of [P5] at [P5c], although it should be noted that in some of the spectra the peak at 36500 cm^{-1} is more highly resolved, showing three closely spaced bands. Spectra of [P4], [P5] and [P6] are shown in Figures 3.20 - 3.22.

Figure 3.20 UV/visible spectrum of [P5], in CH$_2$Cl$_2$.
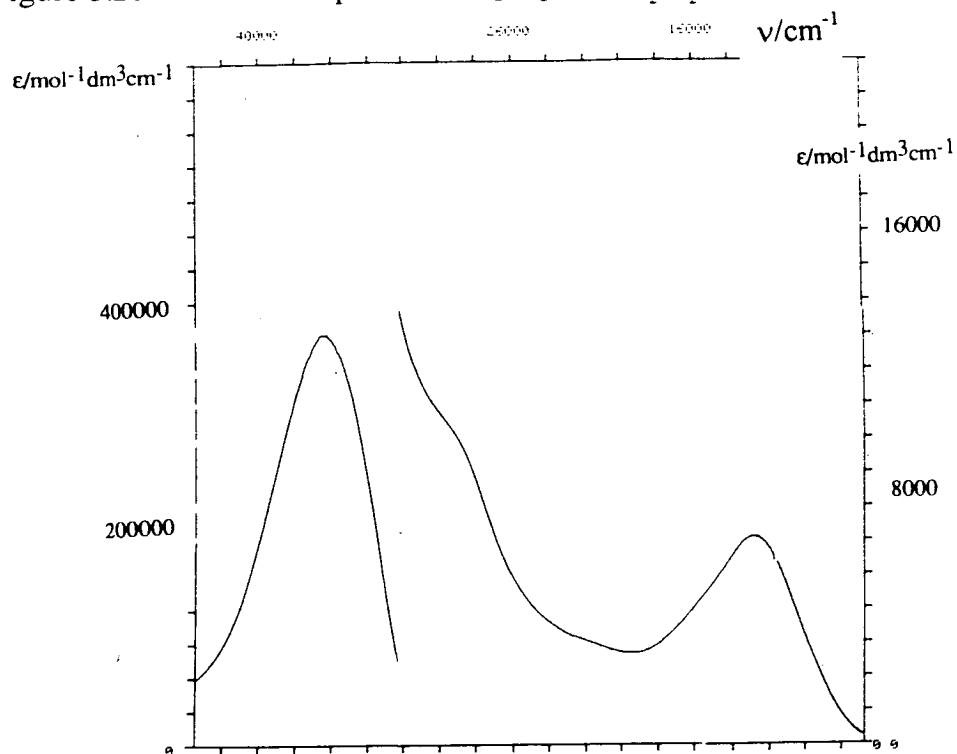
Figure 3.21 UV/visible spectrum of [P6], in THF.
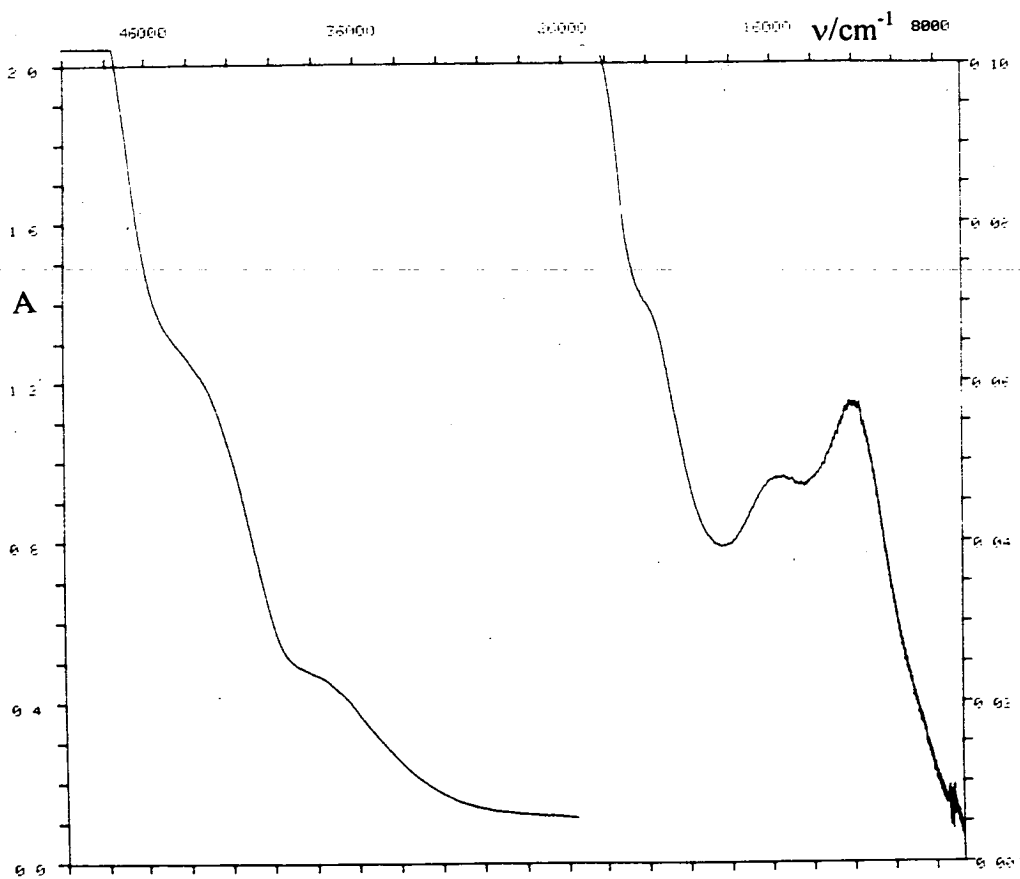
The UV/visible spectroelectrochemistry of [P4] was studied at -20°C in CH$_2$Cl$_2$.

Reduction of [P4] (Figure 3.23) was found to be reversible at this temperature, with isosbestic points observed in the record of the electrogeneration at 23000 and 36000 cm^{-1}. The spectrum of [P4]$^-$ (Figure 3.24) shows a broad, weak peak at 16000 cm^{-1} and a series of bands similar to those observed for free tcne$^-$ between 23000 and 25000 cm^{-1}. Oxidation of [P4] was found to be irreversible at 253 K. The spectrum of the oxidation product (Figure 3.25) contained a broad peak at 23000 cm^{-1}

Figure 3.22 UV/visible spectrum of [P4], in THF.
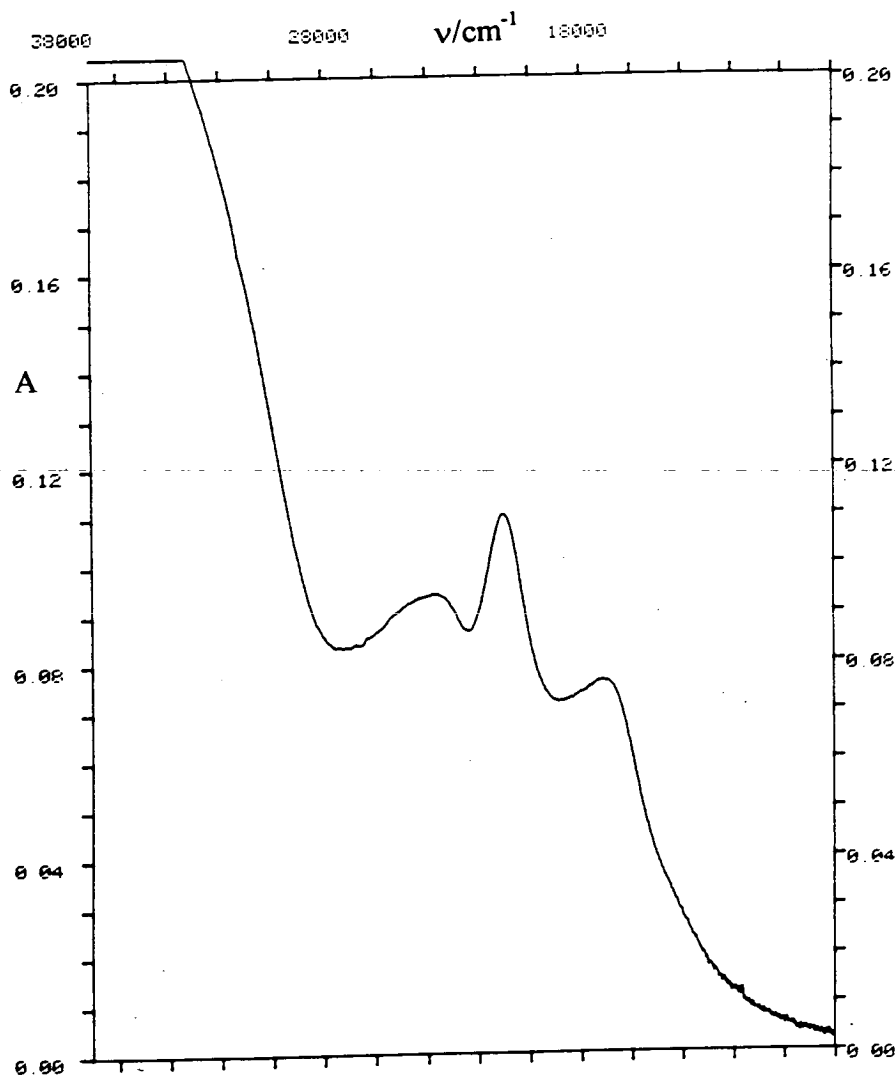
Figure 3.23 UV/visible spectrum of [P4]⁻ in CH_2Cl_2, 253 K.
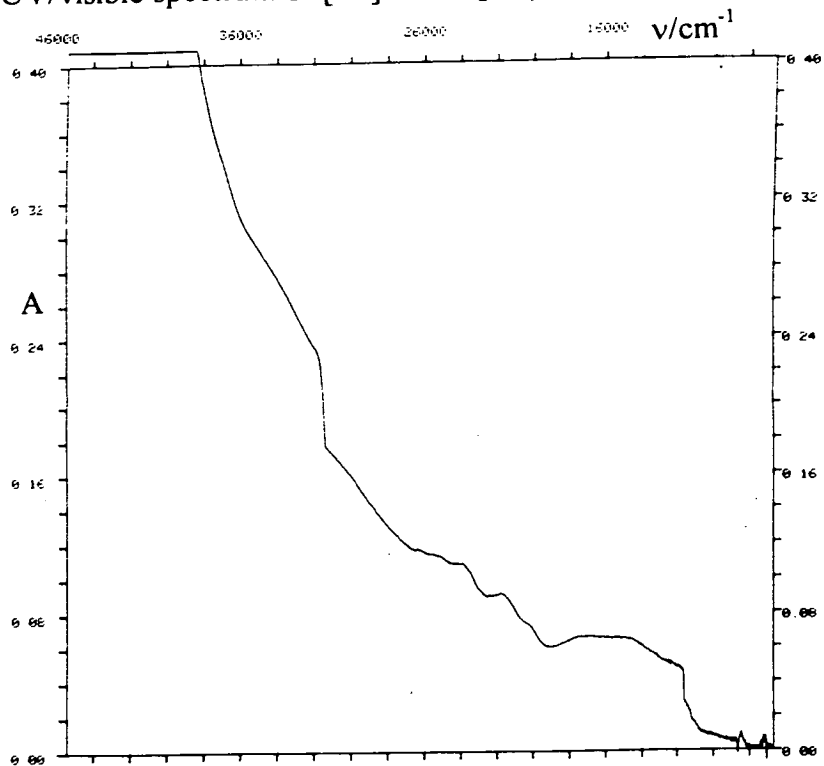
Figure 3.24 UV/visible spectral monitoring of reoxidation of [P4]⁻ in CH_2Cl_2, 253

K, E_{app} = +0.5 V.
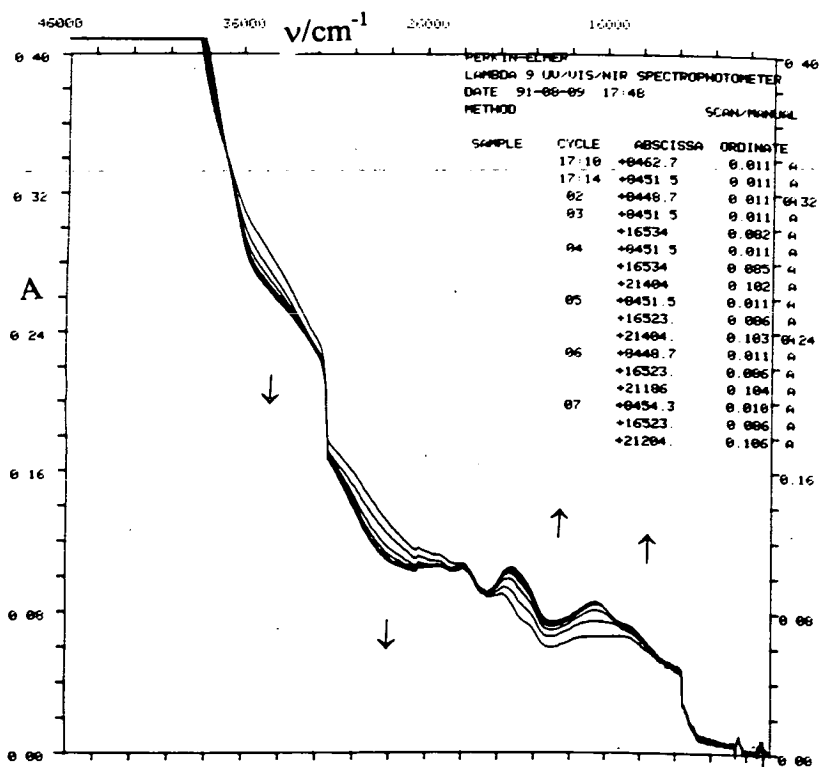
Figure 3.25 UV/visible spectrum of oxidation product of [P4], in CH$_2$Cl$_2$ at 253 K.
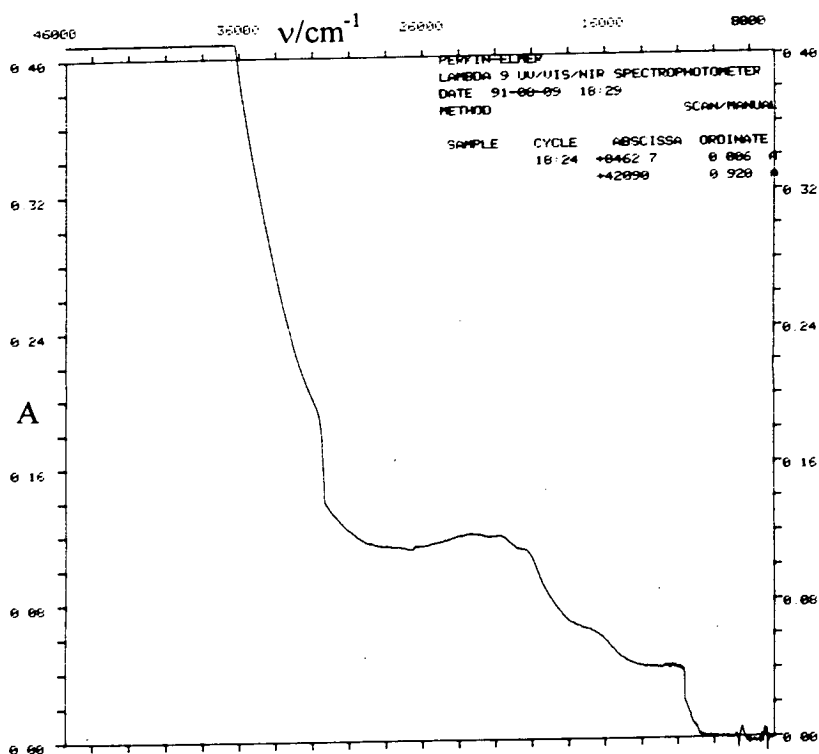
The spectroelectrochemistry of [P5] was also studied in CH$_2$Cl$_2$ at 250 K. In this case it was possible to reverse both the reduction and the oxidation. [P5] showed a broad charge transfer band at 16000 cm^{-1} (approximate ε = 5000 mol^{-1}cm^{-1}dm^3), while reduction also induced small changes in the relative intensities of the high energy bands above 30000 cm^{-1}. Oxidation resulted in the collapse of the original charge transfer band, accompanied by growth between 20000 and 27000 cm^{-1}. The UV/Visible spectroelectrochemistry of [P5] is shown in Figures 3.26 - 3.29.

Figure 3.26 Absorption spectral monitoring of reduction of [P5] in CH_2Cl_2, 250 K

$E_{app} = 0$ V.
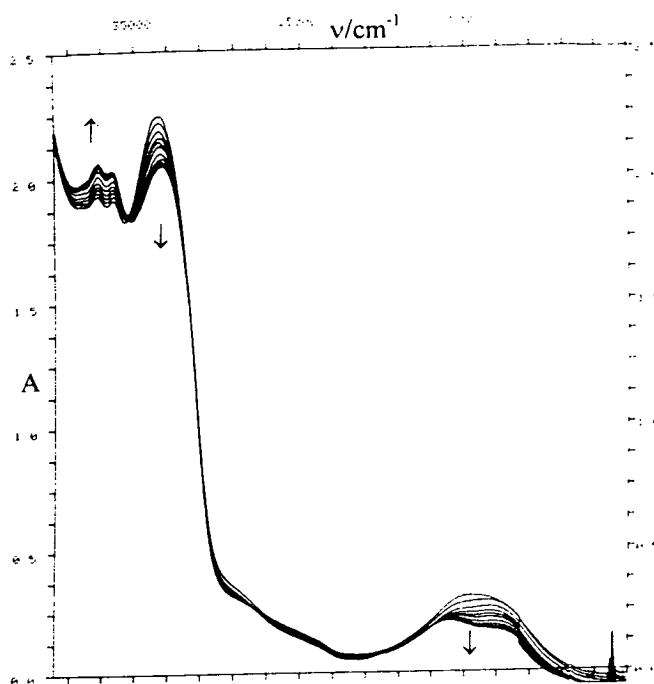
Figure 3.27 Absorption spectrum of [P5] in CH_2Cl_2, 250 K
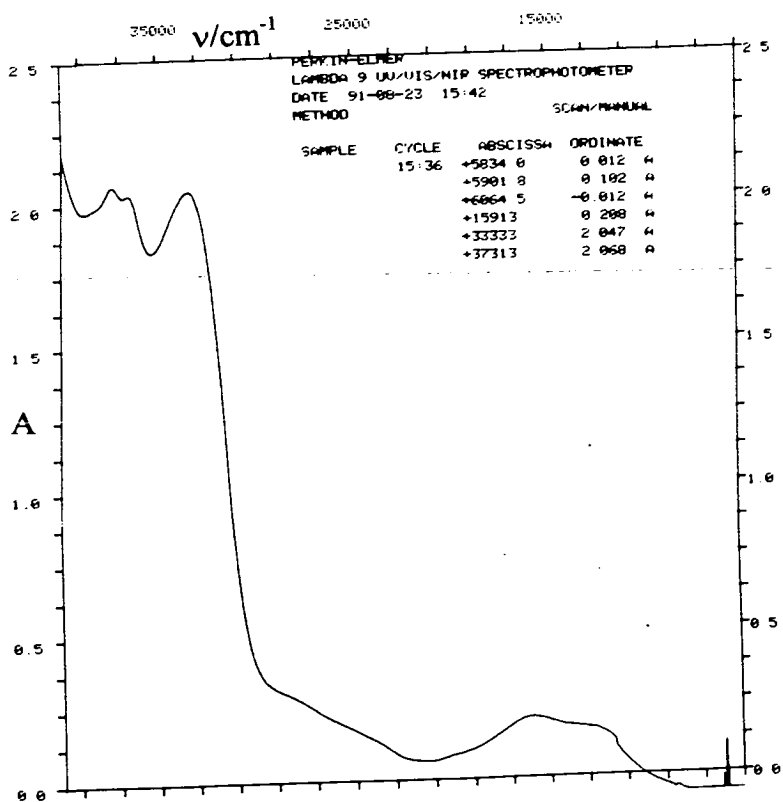
Figure 3.28 Absorption spectra showing oxidation of [P5] in CH_2Cl_2 at 250 K, E_{app} = +1.8 V.
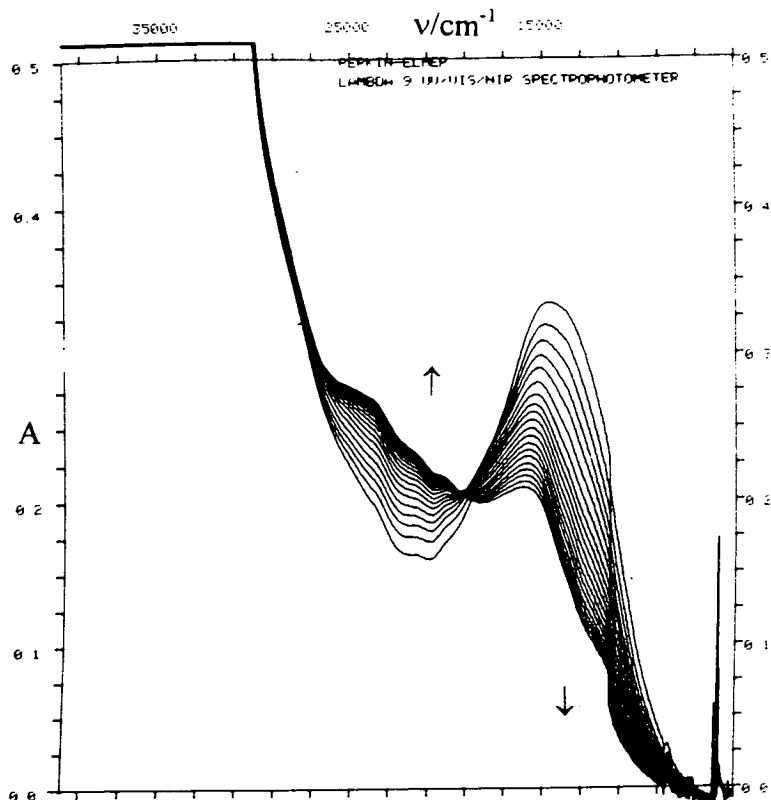
Figure 3.29 Absorption spectrum of [P5]$^+$ in CH_2Cl_2, 250 K.
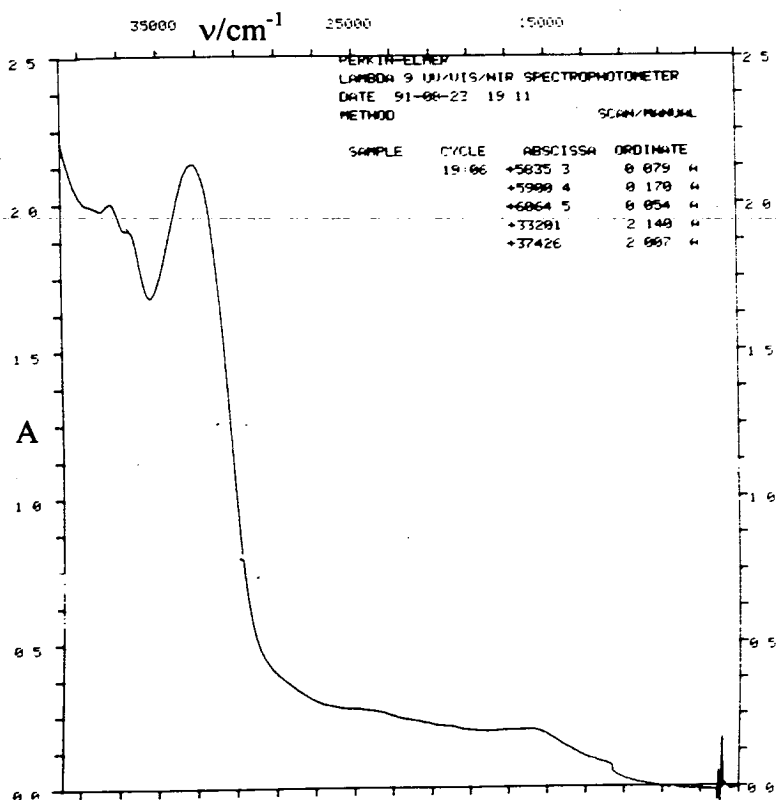
3.2.2.6   Conclusions

In the cases of [OsBr$_3$(PMe$_2$Ph)$_3$] and [RuCl$_2$(PPh$_3$)$_3$], the experimental evidence strongly suggests that the products of reaction with tcne are [OsBr$_2$(PMe$_2$Ph)$_3$(tcne)] ([P4]) and [RuCl$_2$(PPh$_3$)$_3$(tcne)] ([P5]) respectively, both complexes containing N-bound tcne. Identical products were obtained when the reactions were carried out in THF instead of CH$_2$Cl$_2$, and there was no evidence of hydrolysis of metal bound tcne.

Addition of a further equivalent of [RuCl$_2$(PPh$_3$)$_3$] to [P5] appears to result in formation of the binuclear complex [{RuCl$_2$(PPh$_3$)$_3$}$_2$(tcne)], [P6]. Although no experimental evidence of the stereochemistry of the product was obtained, steric factors make it reasonable to conclude that the 1,2-*trans* complex was formed. Again, there was no evidence of tcne hydrolysis.

The case of [P3] is rather perplexing. The low solubility and mass spectra suggest that a polymeric species may have been formed, but the IR data appears to indicate that reaction of the phosphine ligands has occurred.

At present, [OsCl$_2$(PEt$_2$Ph)$_3$(tcne)] is the only complex in which rapid hydrolysis of tcne has been observed. The reasons for this unique status are currently unclear and we intend to conduct further investigations of this matter.

3.3 Experimental

In addition to the solvents used in chapter 2, which were treated as before, THF was purified by distillation under N_2, from sodium wired solvent to which benzophenone had been added. [OsBr$_3$(PMe$_2$Ph)$_3$] and [RuCl$_2$(PPh$_3$)$_3$] were prepared by others within this department (see references 1 amd 11 respectively). [OsO$_4$] and PEt$_2$Ph were supplied in sealed ampoules of known mass.

In general, equipment was similar to that used in Chapter 2, except as specified below. EPR spectra were recorded using a Bruker ER-200D-SRC spectrometer and the EPRESISE cell, with a Metrohm E506 potentiostat used as the potential source. Some IR spectra were recorded on a Perkin-Elmer series 1600 FTIR spectrometer, the others being recorded on the Perkin-Elmer 598 IR spectrometer. The matrix used for all reported FAB mass spectra was thioglycerol.

mer-[OsCl$_3$(PEt$_2$Ph)$_3$]

This was prepared by a method similar to that reported by Chatt _et al_[1]. Concentrated HCl (1 cm^3) and PEt$_2$Ph (2 g) were added under nitrogen to nitrogen purged ethanol (50 cm^3). [OsO$_4$] (1 g) was then added and the reaction mixture was refluxed for 15 minutes. After cooling, the crude product was isolated by filtration. The product was purified ([Os$_2$(μ-Cl)$_3$(PEt$_2$Ph)$_6$]$^+$Cl$^-$ being the main impurity) by elution with CH$_2$Cl$_2$ from a column of silica (the binuclear impurity was successfully isolated in pure form by subsequent elution with ethanol).

Typical yields of the purified product were 60%, with yields of the impurity in the range 20 - 30%.

trans-[OsCl₂(PEt₂Ph)₃(tcva)] ([P1])

In a typical synthesis, *mer*-[OsCl₃(PEt₂Ph)₃] (140 mg) and tcne (45 mg) were dissolved in deaerated THF (30 cm³) under N₂. To this was added a solution of AgBF₄ (40 mg) in THF (10 cm³). The reaction mixture was left to stand in the dark to allow the AgCl precipitate time to settle, which was then removed by filtration under gravity. The volume of solvent was reduced to approximately 10 cm³ and the product was precipitated by addition of n-hexane (25 cm³). The isolated product usually required no purification and 80% was a typical yield. A sample of the product was dissolved in CH₂Cl₂, and n-hexane was overlaid and allowed to diffuse into the solution, yielding crystals of the product complex suitable for single crystal X-ray diffraction studies.

Crystallographic Data for *trans*-[OsCl₂(PEt₂Ph)₃(tcva)]

$C_{37}H_{50}N_3O_{1.5}P_3Cl_2Os$; MW = 914.9; Monoclinic; Space group $\underline{P}2_1/n$ (Alternate no. 14 of $\underline{P}2_1/c$); a = 12.8579(14), b = 18.3131(22), c = 17.1444(20) Å, $\alpha = \gamma = 90°$, $\beta = 94.349(11)°$, V = 4025.4 Å³ (from θ values of 23 reflections measured at $\pm\omega$ such that $14 < \theta < 16°$, $\lambda = 0.71074$ A); Z = 4, $D_c = 1.509$ gcm⁻³; Deep red lath of dimensions 0.16x0.25x0.54 mm; μ(Mo-Kα) = 34.55 cm⁻¹; F(000) = 1840.

Data Collection and Processing

The crystal was mounted on a STADI-4 diffractometer and data were collected at 298 K in the $\omega - 2\theta$ mode using graphite-monochromated Mo-Kα radiation. Of 5446 unique reflections measured ($2.5° < \theta < 22.5°$; h = -13 to 13, k = 0 to 18, l = 0 to 18), 4593 with F > 4σ(F) were used in all calculations. An initial absorption correction was made[29] (maximum and minimum correction factors were 0.4207 and 0.3102 respectively). No observable crystal decay occurred during data collection.

Structure Analysis and Refinement

Structure solution and refinement were carried out using SHELX76[30], the Os atom of the asymmetric unit being located by Patterson synthesis. All other non-H atoms were located by iterative least squares refinement and difference Fourier syntheses. Scattering factors for Os were obtained from reference 31. All non-H atoms except those within the cocrystallised solvent were refined anisotropically. A final absorption correction was made using DIFABS[32] (maximum and minimum correction factors of 1.188 and 0.913). The C atoms of the phenyl rings were constrained to refine as regular hexagons, using the AFIX command. All H atoms were refined in fixed calculated positions (using AFIX), with the exception of the H atom of tricyanovinyl alcohol, the position of which was constrained by use of DFIX commands. The weighting scheme $w^{-1} = \sigma^2(F) + 0.000244F^2$ gave satisfactory agreement analysis. At convergence $(\Delta/\sigma)_{max}$ in the final cycle was 0.24 and the final values of R and R$_w$

Table 3.7 Atomic coordinates for [P1], with isotropic thermal parameters (esds in parentheses).

	x	y	z	U_{iso}
Os	0.069300(10	0.149110(10	0.125200(10	0.03837(14)
N(11)	0.0421(3)	0.04762(21)	0.17214(21)	0.0453(22)
C(11T)	0.0228(3)	-0.0108(3)	0.1914(3)	0.047(3)
C(1T)	-0.0066(4)	-0.0804(3)	0.2156(3)	0.061(3)
C(12T)	-0.1131(7)	-0.0850(4)	0.2380(4)	0.098(5)
N(12)	-0.1905(6)	-0.0846(4)	0.2552(5)	0.146(7)
C(2T)	0.0528(7)	-0.1394(4)	0.2121(4)	0.087(5)
O(1)	0.1395(6)	-0.1414(3)	0.1949(4)	0.117(5)
C(21T)	-0.0044(9)	-0.2087(4)	0.2360(5)	0.138(7)
N(22)	-0.0430(7)	-0.2625(4)	0.2544(5)	0.156(7)
Cl(1)	0.02882(9)	0.09824(6)	0.00080(6)	0.0526(7)
Cl(2)	0.11090(9)	0.19505(7)	0.25134(6)	0.0558(7)
P(1)	-0.11572(9)	0.16977(7)	0.13485(7)	0.0430(6)
C(10)	-0.1529(4)	0.1975(3)	0.2317(3)	0.060(3)
C(11)	-0.1317(5)	0.1365(3)	0.2935(3)	0.081(4)
C(12)	-0.1902(4)	0.?959(3)	0.1150(3)	0.058(3)
C(13)	-0.3075(4)	0.0917(3)	0.1213(4)	0.081(4)
C(14)	-0.18486(24)	0.23280(16)	0.06684(15)	0.050(3)
C(15)	-0.23894(24)	0.29298(16)	0.09290(15)	0.063(3)
C(16)	-0.29399(24)	0.33844(16)	0.03910(15)	0.079(4)
C(17)	-0.29492(24)	0.32370(16)	-0.04079(15)	0.082(4)
C(18)	-0.24084(24)	0.26352(16)	-0.06687(15)	0.076(4)
C(19)	-0.18580(24)	0.21808(16)	-0.01305(15)	0.058(3)
P(2)	0.10294(10)	0.26764(6)	0.07667(7)	0.0489(7)
C(20)	0.2314(4)	0.3018(3)	0.1155(4)	0.070(4)
C(21)	0.2505(5)	0.3834(3)	0.1157(4)	0.088(5)
C(22)	0.1020(5)	0.2682(3)	-0.0310(3)	0.068(3)
C(23)	0.1609(6)	0.3300(4)	-0.0690(4)	0.101(5)
C(24)	0.0182(3)	0.34327(15)	0.10118(20)	0.054(3)
C(25)	0.0126(3)	0.36099(15)	0.17988(20)	0.069(4)
C(26)	-0.0438(3)	0.42210(15)	0.20069(20)	0.093(5)
C(27)	-0.0946(3)	0.46551(15)	0.14279(20)	0.097(5)
C(28)	-0.0890(3)	0.44781(15)	0.06408(20)	0.095(5)
C(29)	-0.0326(3)	0.38669(15)	0.04327(20)	0.076(4)
P(3)	0.24791(9)	0.10501(7)	0.11628(7)	0.0489(7)
C(30)	0.2483(4)	0.0072(3)	0.0935(3)	0.066(3)
C(31)	0.3555(5)	-0.0261(3)	0.0860(4)	0.090(5)
C(32)	0.3314(4)	0.1124(3)	0.2078(3)	0.064(3)
C(33)	0.3018(5)	0.0610(4)	0.2728(3)	0.085(4)
C(34)	0.32672(24)	0.14121(19)	0.04017(17)	0.057(3)
C(35)	0.29434(24)	0.12732(19)	-0.03791(17)	0.074(4)
C(36)	0.35378(24)	0.15221(19)	-0.09727(17)	0.091(5)
C(37)	0.44563(24	0.19096(19)	-0.07851(17)	0.100(5)
C(38)	0.47800(24)	0.20484(19)	-0.00043(17)	0.0?3(5)
C(39)	0.41856(24)	0.17996(19)	0.05891(17)	0.072(4)
C(1S)	-0.0431(21)	0.0584(14)	0.4841(15)	0.082(7)
C(2S)	0.0152(10)	0.0000(7)	0.4319(7)	0.097(3)
C(3S)	-0.0223(18)	0.0655(13)	0.5585(14)	0.090(6)
C(4S)	0.1103(17)	-0.0006(11)	0.4728(13)	0.084(6)
C(5S)	0.0710(14)	-0.0352(10)	0.5310(10)	0.103(6)

163

Table 3.8 Atomic coordinates for H atoms in [P1].

	x	y	z	U_{iso}
H(1)	0.1783	-0.1808	0.2216	0.0800
H(10A)	-0.2350	0.2105	0.2276	0.0800
H(10B)	-0.1085	0.2453	0.2502	0.0800
H(11A)	-0.1546	0.1551	0.3494	0.0800
H(11B)	-0.0497	0.1233	0.2983	0.0800
H(11C)	-0.1762	0.0885	0.2757	0.0800
H(12A)	-0.1604	0.0449	0.1561	0.0800
H(12B)	-0.1776	0.0686	0.0563	0.0800
H(13A)	-0.3435	0.0394	0.1084	0.0800
H(13B)	-0.3397	0.1318	0.0800	0.0800
H(13C)	-0.3225	0.1082	0.1799	0.0800
H(15)	-0.2382	0.3044	0.1547	0.0800
H(16)	-0.3358	0.3850	0.0593	0.0800
H(17)	-0.3375	0.3589	-0.0824	0.0800
H(18)	-0.2416	0.2521	-0.1287	0.0800
H(19)	-0.1439	0.1715	-0.0332	0.0800
H(20A)	0.2890	0.2771	0.0812	0.0800
H(20B)	0.2432	0.2834	0.1754	0.0800
H(21A)	0.3287	0.3945	0.1401	0.0800
H(21B)	0.1953	0.4101	0.1506	0.0800
H(21C)	0.2411	0.4038	0.0565	0.0800
H(22A)	0.0216	0.2710	-0.0540	0.0800
H(22B)	0.1357	0.2172	-0.0483	0.0800
H(23A)	0.2336	0.3093	-0.0876	0.0800
H(23B)	0.1764	0.3735	-0.0272	0.0800
H(23C)	0.1140	0.3506	-0.1191	0.0800
H(25)	0.0519	0.3274	0.2247	0.0800
H(26)	-0.0481	0.4358	0.2616	0.0800
H(27)	-0.1382	0.5128	0.1589	0.0800
H(28)	-0.1283	0.4814	0.0193	0.0800
H(29)	-0.0282	0.3730	-0.0177	0.0800
H(30A)	0.2026	-0.0008	0.0386	0.0800
H(30B)	0.2122	-0.0213	0.1394	0.0800
H(31A)	0.3472	-0.0835	0.0725	0.0800
H(31B)	0.4024	-0.0195	0.1404	0.0800
H(31C)	0.3929	0.0010	0.0397	0.0800
H(32A)	0.3270	0.1679	0.2289	0.0800
H(32B)	0.4105	0.1004	0.1951	0.0800
H(33A)	0.3547	0.0690	0.3241	0.0800
H(33B)	0.3067	0.0051	0.2533	0.0800
H(33C)	0.2232	0.0726	0.2870	0.0800
H(35)	0.2232	0.0973	-0.0524	0.0800
H(36)	0.3287	0.1415	-0.1577	0.0800
H(37)	0.4916	0.2102	-0.1245	0.0800
H(38)	0.5491	0.2348	0.0141	0.0800
H(39)	0.4437	0.1907	0.1194	0.0800

Table 3.9 Anisotropic thermal parameters for [P1].

	U_{11}	U_{22}	U_{33}	U_{23}	U_{13}	U_{12}
Os	0.03945(14)	0.03726(15)	0.03816(14)	-0.00055(7)	0.00287(9)	-0.00178(7)
N(11)	0.0424(21)	0.0447(23)	0.0485(22)	-0.0012(18)	0.0042(16)	-0.0008(17)
C(11T)	0.043(3)	0.051(3)	0.046(3)	-0.0008(22)	0.0037(20)	0.0067(22)
C(1T)	0.082(4)	0.042(3)	0.058(3)	0.0108(23)	0.001(3)	0.001(3)
C(12T)	0.100(6)	0.101(5)	0.093(5)	0.017(4)	0.021(4)	-0.051(5)
N(12)	0.122(6)	0.122(6)	0.196(9)	0.044(5)	0.035(6)	0.009(5)
C(2T)	0.105(6)	0.078(5)	0.079(5)	0.008(3)	0.001(4)	0.010(4)
O(1)	0.129(5)	0.106(4)	0.115(4)	0.021(3)	0.021(4)	0.006(3)
C(21T)	0.212(10)	0.075(5)	0.121(7)	0.031(5)	-0.047(6)	-0.034(6)
N(22)	0.227(9)	0.074(4)	0.161(7)	0.046(4)	-0.039(6)	-0.039(5)
Cl(1)	0.0592(7)	0.0524(7)	0.0459(6)	-0.0096(5)	0.0012(5)	-0.0001(5)
Cl(2)	0.0579(7)	0.0640(7)	0.0446(6)	-0.0093(5)	-0.0026(5)	-0.0020(6)
P(1)	0.0415(6)	0.0454(6)	0.0416(6)	0.0011(5)	0.0018(5)	-0.0002(5)
C(10)	0.055(3)	0.074(3)	0.051(3)	0.006(3)	0.0102(23)	0.016(3)
C(11)	0.085(4)	0.106(5)	0.052(3)	0.018(3)	0.023(3)	0.015(4)
C(12)	0.049(3)	0.050(3)	0.075(3)	0.0073(24)	-0.0049(25)	-0.0105(23)
C(13)	0.044(3)	0.076(4)	0.123(5)	0.005(4)	-0.001(3)	-0.012(3)
C(14)	0.041(3)	0.051(3)	0.057(3)	0.0054(22)	-0.0032(21)	0.0014(21)
C(15)	0.059(3)	0.061(3)	0.069(3)	0.004(3)	0.006(3)	0.010(3)
C(16)	0.069(4)	0.068(4)	0.098(5)	0.010(3)	0.000(3)	0.024(3)
C(17)	0.074(4)	0.091(4)	0.080(5)	0.023(4)	-0.002(3)	0.019(4)
C(18)	0.072(4)	0.089(4)	0.064(3)	0.019(3)	-0.007(3)	0.012(3)
C(19)	0.051(3)	0.068(3)	0.055(3)	0.010(3)	-0.0005(23)	0.0045(25)
P(2)	0.0510(7)	0.0421(6)	0.0541(7)	0.0014(5)	0.0119(6)	-0.0036(5)
C(20)	0.058(3)	0.055(3)	0.097(4)	-0.004(3)	0.008(3)	-0.015(3)
C(21)	0.085(4)	0.073(4)	0.106(5)	-0.011(4)	0.014(4)	-0.033(4)
C(22)	0.083(4)	0.059(3)	0.063(3)	0.012(3)	0.023(3)	0.001(3)
C(23)	0.124(6)	0.097(5)	0.083(5)	0.017(4)	0.038(4)	-0.023(4)
C(24)	0.058(3)	0.035(3)	0.068(3)	0.0062(22)	0.019(3)	-0.0046(21)
C(25)	0.075(4)	0.053(3)	0.081(4)	-0.005(3)	0.024(3)	-0.005(3)
C(26)	0.106(5)	0.067(4)	0.106(5)	-0.021(4)	0.045(4)	-0.005(4)
C(27)	0.097(5)	0.049(4)	0.147(7)	0.003(4)	0.042(5)	0.013(3)
C(28)	0.092(5)	0.057(4)	0.137(6)	0.028(4)	0.026(4)	0.013(3)
C(29)	0.075(4)	0.052(3)	0.100(4)	0.016(3)	0.018(3)	0.004(3)
P(3)	0.0406(7)	0.0540(8)	0.0521(7)	0.0021(6)	0.0053(5)	0.0016(5)
C(30)	0.063(3)	0.058(3)	0.078(4)	-0.003(3)	0.012(3)	0.011(3)
C(31)	0.078(4)	0.073(4)	0.119(5)	-0.005(4)	0.020(4)	0.029(3)
C(32)	0.052(3)	0.083(4)	0.056(3)	0.011(3)	-0.0014(24)	0.004(3)
C(33)	0.086(4)	0.104(5)	0.065(4)	0.020(3)	-0.002(3)	0.023(4)
C(34)	0.044(3)	0.062(3)	0.065(3)	0.0025(24)	0.014(3)	-0.0067(23)
C(35)	0.061(4)	0.096(4)	0.065(4)	0.002(3)	0.017(3)	0.016(3)
C(36)	0.078(5)	0.125(6)	0.072(4)	0.022(3)	0.031(4)	0.025(4)
C(37)	0.086(5)	0.124(6)	0.094(5)	0.044(5)	0.052(4)	0.031(4)
C(38)	0.054(4)	0.104(5)	0.123(6)	0.041(4)	0.038(4)	0.008(3)
C(39)	0.051(3)	0.074(4)	0.092(4)	0.012(3)	0.008(3)	0.003(3)

were 0.026 and 0.038 respectively for 393 parameters, S = 1.234. The final Fourier synthesis showed no important features and the maximum and minimum residual electron densities were 0.58 and -0.44 eÅ^{-3} respectively.

[OsCl$_2$(PEt$_2$Ph)$_3$(tcne)] ([P2])

In a typical preparation, AgBF$_4$ (30 mg) was added to a solution of *mer*-[OsCl$_3$(PEt$_2$Ph)$_3$] (100mg) and tcne (35 mg) in N$_2$ purged CH$_2$Cl$_2$ (25 cm^3) in a flask shielded from the light. The mixture was stirred for 10 minutes then allowed to stand in the dark for 3 hours under N$_2$. The accumulated AgCl precipitate was removed by filtration, the solvent volume was reduced and deaerated hexane (30 cm^3) was added to precipitate the product.

The *in situ* synthesis of [P2] in an electrochemical cell was conducted by a similarly. In this case 10 mg of AgBF$_4$ was added to an argon purged solution of tcne (6 mg) and [OsCl$_3$(PEt$_2$Ph)$_3$] (28 mg) in CH$_2$Cl$_2$ (10 cm^3 with [Bu$_4$N][BF$_4$] 0.5 moldm^{-3} as supporting electrolyte) in a voltammetric cell.

The electrosynthesis of [P2] was conducted as follows. Tcne (4.5 mg) and *mer*-OsCl$_3$(PEt$_2$Ph)$_3$ (24 mg) were dissolved in a deaerated solution of [Bu$_4$N][BF$_4$] (0.5 moldm^{-3}) in CH$_2$Cl$_2$ (10 cm^3), in the working electrode compartment of a coulometric cell (see Chapter 1). A potential of +0.1 V versus Ag/AgCl was applied at the working electrode to reduce tcne. When electrogeneration had gone to completion (deduced by current measurements), the applied potential was altered to -0.55 V in order to reduce the osmium complex. In this case electrogeneration was continued for 10 minutes after the reduction had gone to completion, to allow

tcne⁻ time to react with Os^{II}. Electrogeneration was then carried out at +0.40 V versus Ag/AgCl to reoxidise the bound tcne. Voltammetric studies suggsted yields in the region of 50 - 60% with respect to the starting complex.

Complex [P3]

This was prepared similarly to [P1] but tcnq (80 mg) replaced tcne. After addition of AgCl, the expected colour change occurred but was followed by spontaneous precipitation of the blue product.

[OsBr$_2$(PMe$_2$Ph)$_3$(tcne)] ([P4]/[P4c])

[P4] prepared similarly to [P1] but *mer-*[OsBr$_3$(PMe$_2$Ph)$_3$] (160 mg) replaced *mer-*[OsCl$_3$(PEt$_2$Ph)$_3$].

In the preparation of [P4c], CH$_2$Cl$_2$ (50 cm^3) replaced THF.

CHN analysis.   Found: C = 36.8%, H = 3.62%, N = 5.70%.

Calculated for C$_{30}$H$_{33}$Br$_2$N$_4$OsP$_3$:   C = 40.4%, H = 3.73%, N = 6.28%

[RuCl$_2$(PPh$_3$)$_3$(tcne)] ([P5]/[P5c])

Tcne (100 mg) was added to a nitrogen purged solution of [RuCl$_2$(PPh$_3$)$_3$] (250 mg) in THF (50 cm^3). After one hour the solvent volume was reduced and the blue product precipitated from solution by addition of deaerated hexane (50 cm^3). Yields were essentially quantitative.

[P5c] was prepared by addition of tcne (40 mg) to a deaerated solution of [RuCl$_2$(PPh$_3$)$_3$] (100 mg) in CH$_2$Cl$_2$ (40 cm^3), followed by reduction of solvent volume and precipitation with hexane as above.

CHN analysis.   Found: C = 65.5%, H = 4.87%, N = 5.15%.

Calculated for C$_{60}$H$_{45}$N$_4$Cl$_2$P$_3$Ru: C = 66.3%, H = 4.17%, N = 5.15%.

[{RuCl$_2$(PPh$_3$)$_3$}$_2$(tcne)] [P6]

[RuCl$_2$(PPh$_3$)$_3$] (50 mg) and [P5] (55 mg) were stirred in THF (20 cm^3) under N$_2$ for one hour. The volume of solvent was reduced and the product precipitated by addition of hexane. The yield of crude product was 90%.

3.4 References

1. J. Chatt, G. J. Leigh, D. M. P. Mingos and R. M. Paske, *J. Chem. Soc. (A)*, **1968**, 2636.

2. J. Chatt, G. Leigh and R. L. Richards, *J. Chem. Soc. (A)*, **1970**, 2243.

3. J. Chatt, D. P. Melville and R. L. Richards, *J. Chem. Soc. (A)*, **1971**, 1169.

4. J. Chatt, G. Leigh and R. M. Paske, *J. Chem. Soc. (A)*, **1969**, 854.

5. B. Bell, J. Chatt, J. R. Dilworth and G. Leigh, *Inorg. Chim. Acta*, **1972**, <u>6</u>, 635.

6. D. J. Cole-Hamilton and T. A. Stephenson, *J. Chem. Soc. Dalton Trans.*,

    1976, 2396.

7. G. Leigh, J. J. Levison and S. D. Robinson, *J. Chem. Soc. Chem. Commun.*,

    1969, 705.

8. V. T Coombe, G. A. Heath, T. A. Stephenson, J. D. Whitelock and

    L. J. Yellowlees, *J. Chem. Soc. Dalton Trans.*, **1985**, 947.

9. V. T. Coombe, PhD thesis, University of Edinburgh, **1985**

10. T. A. Stephenson and G. Wilkinson, *J. Inorg. Nucl. Chem.*, **1966**, <u>28</u>, 945.

11. P. S. Hallman, T. A. Stephenson and G. Wilkinson, *Inorg. Synth.*,

    1970, <u>12</u>, 237.

12. S. J. La Placa and J. A. Ibers, *Inorg. Chem.*, **1965**, <u>4</u>, 778.

13. J. J. Hinkel and J. P. Devlin, *J. Chem. Phys.*, **1973**, <u>58</u>, 4750.

14. A. E. D. McQueen, A. J. Blake, T. A. Stephenson, M. Schroder and

    L. J. Yellowlees, *J. Chem. Soc. Chem. Commun.*, **1988**, 1533.

15. R. G. Little, D. Pautler and P. Coppens, *Acta Cryst.*, **1971**, <u>B27</u>, 1493.

16. M. F. Rettig and R. M. Wing, *Inorg. Chem.*, **1969**, <u>8</u>, 2685.

17. R. Gross and W. Kaim, *Angew. Chem. Int. Ed. Engl.*, **1987**, <u>26</u>, 251.

18. B. W. Sullivan and B. M. Foxman, *Organometallics*, **1983**, <u>2</u>, 187.

19. T. Dahl, *Acta Chem. Scand. A*, **1983**, <u>37</u>, 353.

20. R. J. Sorbie, PhD thesis, University of Edinburgh, **1989**.

21. H. Braunwarth, G. Huttner and L. Zsolnai, *J. Organomet. Chem.*,

1989, <u>372</u>, C23.

22. J. P. Cornelissen, J. H. van Diemen, L. R. Groeneveld, J. G. Haasnoot,

A. L. Spek and J. Reedijk, *Inorg. Chem.*, **1992**, <u>31</u>, 199.

23. J. A. A. de Boer, S. Harkema, D. N. Reinhoudt and J. W. H. M. Uiterwijk,

J. Chem. Soc. Perkin Trans II, **1986**, 377.

24. G. J. Leigh and D. M. P. Mingos, *J. Chem. Soc. (A)*, **1970**, 587.

25. W. J. Middleton, E. L. Little, D. D. Coffmann and V. A. Englehardt,

J. Am. Chem. Soc., **1958**, <u>80</u>, 2795.

26. A. E. D. McQueen, PhD thesis, University of Edinburgh, **1989**.

27. M. Lenarda, R. Ros, O. Traverso, W. D. Pittis, W. H. Baddley and M. Graziani,

Inorg. Chem., **1977**, <u>17</u>, 3178.

28. P. Kathirgaman and D. R. Rosseinsky, *J. Chem. Soc. Chem. Commun.*,

1980, 839.

29. A. C. T. North, D. C. Phillips and F. S. Matthews, *Acta Cryst.*, **1968**, <u>A24</u>, 351.

30. SHELX76 "A program for crystal structure and refinement", G. M. Sheldrick,

University of Cambridge, England, **1976**.

31. D. T. Cromer and J. L. Mann, *Acta Cryst.*, **1968**, <u>A24</u>, 321.

32. DIFABS, N. Walker and D. Stuart, *Acta Cryst.*, **1983**, <u>A39</u>, 158.

4   Trinuclear Mixed-Valence Complexes of Ruthenium

4.1   Introduction

This chapter relates to the study of metal-metal interactions in a group of mixed-valence complexes containing three ruthenium atoms in a linear arrangement.

Complexes containing two or more metal atoms have been the source of much interest in recent years, with the emphasis on study of the extent and nature of any metal-metal interactions. One particularly fruitful area of study has been that of binuclear complexes in which the two metal centres have different formal oxidation states, as these are among the simplest systems in which metal-metal interactions and intramolecular electron transfer can be studied. A brief introduction to the study of polynuclear complexes and metal-metal bonding is given in the following pages.

While the extent of interaction (and electron delocalisation) varies considerably from complex to complex, it has been shown that the properties of mixed-valence complexes, especially the degree of electron delocalisation between the metal atoms, are strongly related to the relative symmetries of the ligand fields of the constituent metal ions. Symmetry was used as the mainstay of the categorisation of mixed-valence compounds into three classes by Robin and Day in 1967[1] as listed below.

Class I complexes are "valence trapped", i.e. there is no interaction between the metal centres. Generally the metal centres occupy very different coordination environments (eg. one metal with a tetrahedral arrangement of ligands, the other

with an octahedral arrangement). The spectra of such complexes are essentially superpositions of the spectra of the constituent ions. Examples of class I mixed-valence complexes include $[(\eta-C_5H_5)Co(CO)_2.HgCl_2]^2$ and $[(o-C_6H_4CH_2NPh)_2Rh(\mu-Cl)_2Rh(CO)_2]^3$.

Class II complexes contain metal centres that are similar but not identical (the metal centres are distinguishable by crystallographic and other means). In these complexes the metal centres interact weakly - the degree of delocalisation of the valence electrons between the metal centres is of the order of 10%. The spectra of class II complexes are similar to, but not identical to superpositions of the spectra of the constituent ions. In addition to bands associated with the constituent ions, the electronic absorption spectra of class II complexes exhibit a broad intervalence charge transfer (IVCT) band at low energies (this will be discussed in more detail later in this introduction). Examples of reported class II mixed-valence complexes include $[(NH_3)_5Ru(fmn)Ru(NH_3)]^{5+}$ (fmn = fumaronitrile)[4], $[(bpy)_2ClRu(pyz)RuCl(bpy)_2]^{3+}$[5] (pyz = pyrazine), $[(bpy)_2ClRu(pyz)OsCl(bpy)_2]^{3+}$[6] and $[(PBu_3)_3Ru(\mu-Cl)_3RuCl_2(PBu_3)]^7$.

In class III complexes the metal centres are *not* distinguishable. Full delocalisation of electrons between the metal centres occurs (ie. an $M^{+2}-M^{+3}$ class III complex can be more informatively represented as M_2^{5+}, in which each metal has an effective oxidation state of +2.5), including the phenomenon of metal-metal bonding when the metal centres are in direct contact. In the case of class III mixed-valence complexes the spectra obtained are not generally similar to superpositions of spectra of the constituent ions. The electronic absorption spectrum again contains bands at

low energy, which are discussed below. Examples of class III mixed-valence complexes include $[(NH_3)_5Ru(pyz)Ru(NH_3)_5]^{5+}$, often referred to as the Creutz-Taube complex[8], $[Ru_2(O_2CPr)_4Cl]_n$[9], $[(PMe_2Ph)_3Ru(\mu-Cl)_3Ru(PMe_2Ph)_3]^{2+(10)}$, and $[L_2ClRu(\mu-Cl)_3RuClL_2]$, L = PMe_3, PMe_2Ph[7].

Potential energy diagrams representing the three classes of mixed-valence complexes are shown in Figure 4.1.[11] It should be noted, however, that although the definitions of Robin and Day remain extremely useful more than twenty five years after their formulation they do not manage to cover all cases. In particular they effectively exclude the possibility of metal-metal bonding between non-equivalent metal centres but several non symmetrical mixed-valence complexes exhibiting metal-metal bonds have been published (examples include $[(RO)_2X_2Re\equiv ReX_2(PPh_3)_2]$, R = Me, Et or Pr, X = Cl or Br[12]; $[(C_6F_5O)_4Mo\equiv Mo(OC_6F_5)(NMe_2)(HNMe_2)_2]$[13] and $[Os_2Cl_4(chp)_2(H_2O)]$, shown in Figure 4.2.[14]).

In general, however, the symmmetry considerations espoused by Robin and Day still apply. Non-equivalent metal centres generally possess d-orbitals of different energies and the extent of mixing of the orbitals is greatly reduced by energy differences. Consequently, metal-metal bonding between non-equivalent metal centres is rare.

Figure 4.1. Potential energy versus nuclear configuration for class I, II and III mixed-valence complexes.
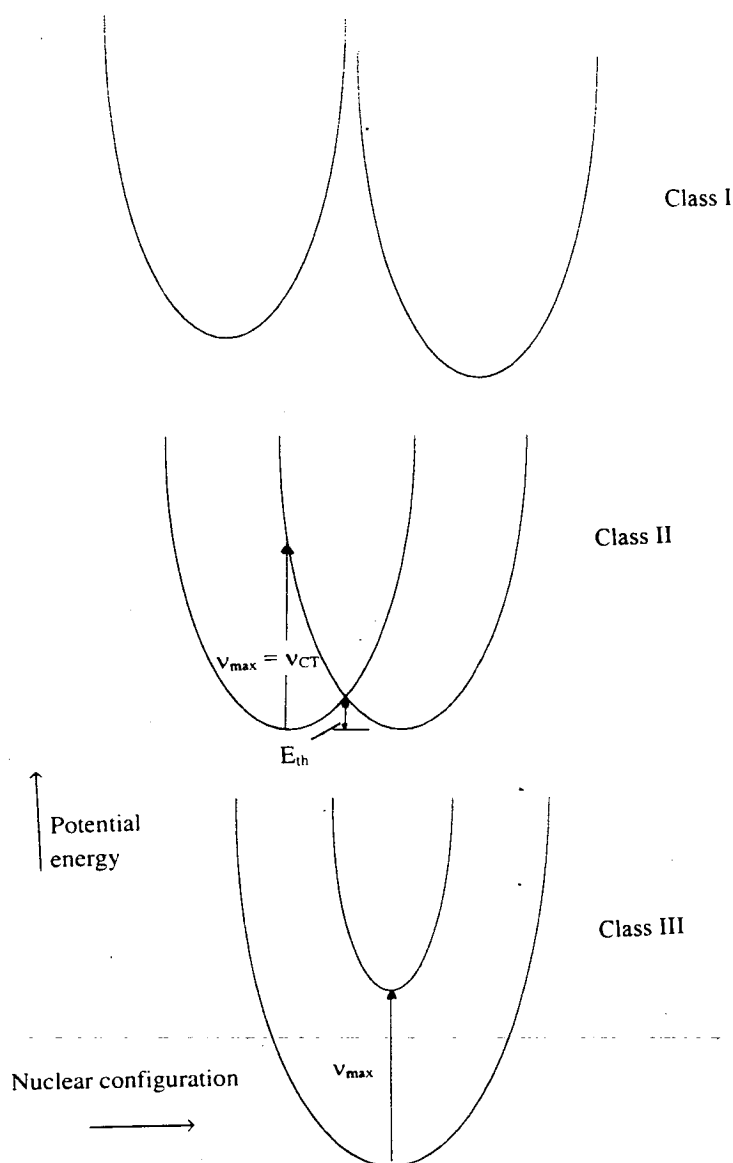
NB:- The X-axis represents the reaction coordinate for thermally induced electron transfer, in terms of the changing positions of the nuclei of the metals and ligands (the nuclear configuration) associated with the electron transfer process. The pathway for photolytic electron transfer is also shown in the class II diagram. In the diagram for class III complexes, the higher energy curve represents an electronic excited state.

174

Figure 4.2 $Os_2Cl_4(chp)_2(H_2O)$
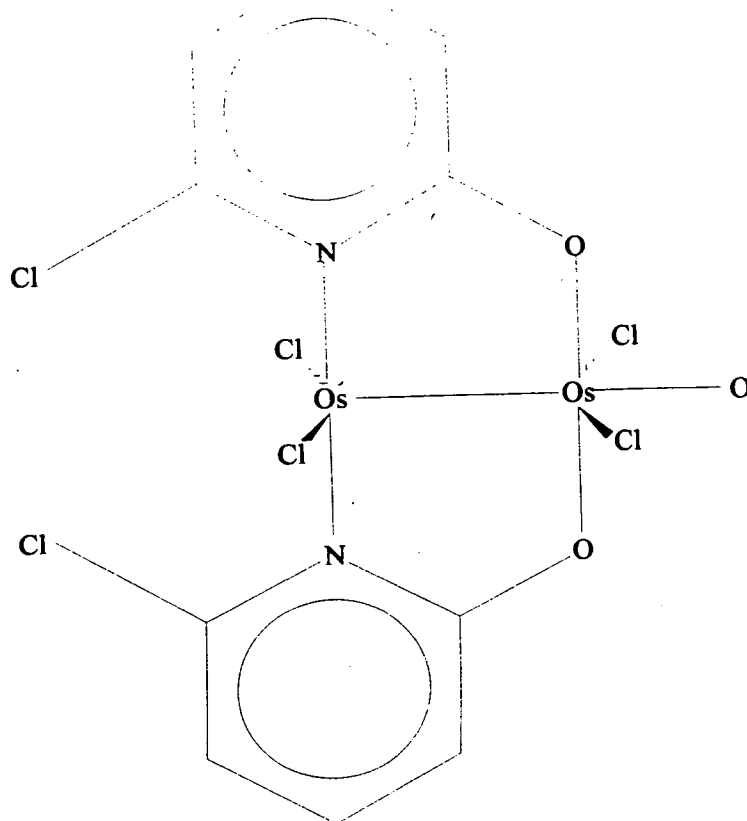
As might be expected from the potential energy diagrams, both class II and class III mixed-valence complexes have distinctive low energy bands in their electronic absorption spectra. In the case of class II complexes this band arises from an intervalence charge transfer process, during which an electron is transferred from one metal centre to the other eg.

$$M(II)M'(III) \xrightarrow{h\nu} M(III)M'(II)$$
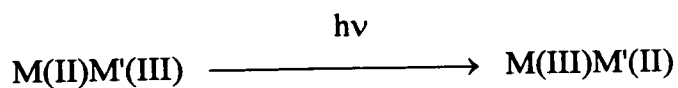
This process involves promotion of the electron from the ground state in M to a vibrationally excited state of M', then vibrational relaxation to complete the

process of electron transfer. IVCT bands tend to be fairly weak, with extinction coefficients usually less than 1000 $mol^{-1}cm^{-1}dm^{3}$ (for example, in $[(bpy)_2ClRu(pyz)RuCl(bpy)_2]^{3+}$ the IVCT band is at 7700 cm^{-1} and ε = 450 $mol^{-1}cm^{-1}dm^{3(5)}$, while $[(NH_3)_5Ru(fmn)Ru(NH_3)_5]^{5+}$, in CH_3CN, has an IVCT band with v_{max} = 10260 cm^{-1} and ε = 150 $mol^{-1}cm^{-1}dm^{3(4)}$). These bands are unusually broad; for "symmetrical" complexes such as those given above $\Delta_{1/2}$ is generally in the region of 5000 cm^{-1} ($\Delta_{1/2}$ is defined as the band width when A/A_{max} = 0.5). Electronic transitions occur far more rapidly than any structural response to that excitation (Franck-Condon Principle). The potential energy diagram indicates that it is possible to promote an electron from the vibrational ground state of M into many vibrationally excited states of M' with a considerable range of energies, hence the significant band width of IVCT bands. Vibrational structure is almost never observed in IVCT bands, but splitting due to spin-orbit coupling effects sometimes occurs with third row transition metals such as Os (an example of this phenomenon is observed with $[(bpy)_2ClOs(PPh_2CH_2Ph_2P)OsCl(bpy)_2]^{3+}$ for which broad near infrared bands are observed at 10000 cm^{-1} and 6000 $cm^{-1(15)}$).

In class III mixed-valence complexes, low energy bands normally arise from allowed transitions between "new" MOs, formed by metal-metal bonds or strong interactions with bridging ligands. These bands are generally more intense than the IVCT bands observed with class II complexes (for example the spectrum of the Creutz-Taube complex contains a maximum at 6370 cm^{-1}, with ε = 5500 $mol^{-1}cm^{-1}dm^{3(8)}$). The band widths are smaller than those observed with class II complexes

(eg. $\Delta_{1/2} = 1200$ cm^{-1} in the Creutz-Taube complex[8]). This follows from the Franck-Condon principle as the turning points of the zero point vibration of the lower potential energy surface and the upper surface are geometrically very close therefore fewer vibrational excited states of the electronic excited state are accessible from the electronic ground state (see Figure 4.1). In the case of class III complexes selection rules may permit more than one low energy transition. Vibrational structure is sometimes observed in these bands (for example in $[Tc_2Cl_8]^{3-}$ the low energy absorption band has a vibrational progression superimposed on it, the frequency of which (320 ± 5 cm^{-1}) corresponds to the $Tc{\equiv}Tc$ stretching vibration in the electronically excited state[46]).

In principle it should be possible to distinguish between class II and class III complexes by study of the low energy electronic absorption spectra. In 1967, Hush published several parameters for the spectra of binuclear class II complexes to further aid in the distinction[16]. Hush theory for binuclear complexes with identical terminal ligand sets is given below.

As shown in Figure 4.1, E_{op} corresponds to the energy of the photolytic intervalence charge transfer process, $h\nu_{CT}$. The energy barrier of the thermal electron transfer process is given by

$$4E_{th} = E_{op} \qquad (4.1)$$

where
$$E_{op} = E_{in} + E_{out} \qquad (4.2)$$

E_{in} is the Franck-Condon term and E_{out} relates to the rearrangement of the outer sphere solvent molecules about the metal centres after electron transfer occurs. The solvent reorganisation is necessitated by the change in dipole moment of the complex and the energy required for this process is given by

$$E_{out} = e^2 \left(\frac{1}{2r_1} + \frac{1}{2r_2} - \frac{1}{d} \right) \left(\frac{1}{D_{op}} - \frac{1}{D_s} \right) \qquad (4.3)$$

Where r_1 and r_2 are the radii of the coordination spheres, d is the distance between the metal centres (r and d are in Å), D_{op} is the optical dielectric constant of the solvent (equivalent to n^2 where n is the refractive index) and D_s is the static dielectric constant of the solvent.

As a result, v_{CT} varies from solvent to solvent such that a plot of hv_{CT} versus $(1/D_{op} - 1/D_s)$ should give a straight line, with the intercept close to E_{in}.

In contrast, the position of the low energy bands observed in the spectra of binuclear class III complexes should be independent of the chosen solvent (this is the case, for example, in the Creutz-Taube ion[8]) as the electron remains delocalised between the metal centres on promotion therefore excitation does not induce a change in dipole moment within the complex.

Hush theory also predicts the band halfwidth, at 298 K, as shown below[16]:

$$\Delta_{1/2}(calc) = (2310 \, v_{CT})^{1/2} \, cm^{-1} \qquad (4.4)$$

For a class II mixed-valence complex, $\Delta_{1/2}$(calc) should agree to within 10% with the experimentally obtained value of $\Delta_{1/2}$. The bandwidth of class II complexes is temperature dependent, becoming significantly narrower upon cooling, an effect which is much less pronounced in class III complexes. It should be noted, however, that the low energy bands in class III mixed-valence complexes become more intense on cooling, as a result of reduced vibrational coupling (ie. symmetry allowed transtions become "more allowed" upon cooling - this is also the case for other allowed electronic transitions in addition to the low energy bands observed for class III complexes).

The degree of delocalisation, α, within mixed-valence complexes may be obtained from the IVCT using the following equation[16]:

$$\alpha^2 = \frac{4.24 \times 10^{-4} \varepsilon \, \Delta_{1/2}}{v_{CT} d^2} \qquad (4.5)$$

In class II mixed-valence complexes $0 < \alpha < 0.25$.

By determination of the above parameters it is usually possible to deduce whether a mixed-valence complex belongs to class II or class III via study of the low energy region of its electronic absorption spectrum.

Interpretation of the chemical and spectroscopic properties of class III mixed-valence complexes clearly necessitates an understanding of metal-metal bonding within the species under study. In particular, to fully understand spectroscopic and structural data we require a valid qualitative (and preferably quantitative) representation of the frontier molecular orbitals.

179

The simplest species in which metal-metal bonding occurs are clearly the binuclear complexes, therefore a brief discussion of metal-metal bonding in binuclear complexes follows.

The most straightforward form of metal-metal bonding occurs in complexes where the constituent metal ion fragments mutually occupy "coordination sites" of the other metal ie. in the complex $[L_nMM'L'_n]$ ML_n is effectively a ligand of M' and vice versa. Examples of such complexes include $[M_2X_8]^{n-}$ species, X = Cl, Br; n = 0, 1 or 2 when M = Mo, W; n = 1, 2 or 3 when M = Re, Tc; in which the halide ligands are arranged about the metal centre in a pseudo square planar arrangement[17]. Other groups of complexes feature bidentate bridging ligands, such as the polymeric $[Ru_2(O_2CR)_4Cl]$ family, in which (in the solid state) metal-metal bound binuclear complexes are linked to each other by bridging chloride ligands (see Figure 4.3. below)[9,18,19].

Figure 4.3. $[M_2X_8]^{2-}$ and $[Ru_2(O_2CR)_4Cl]$
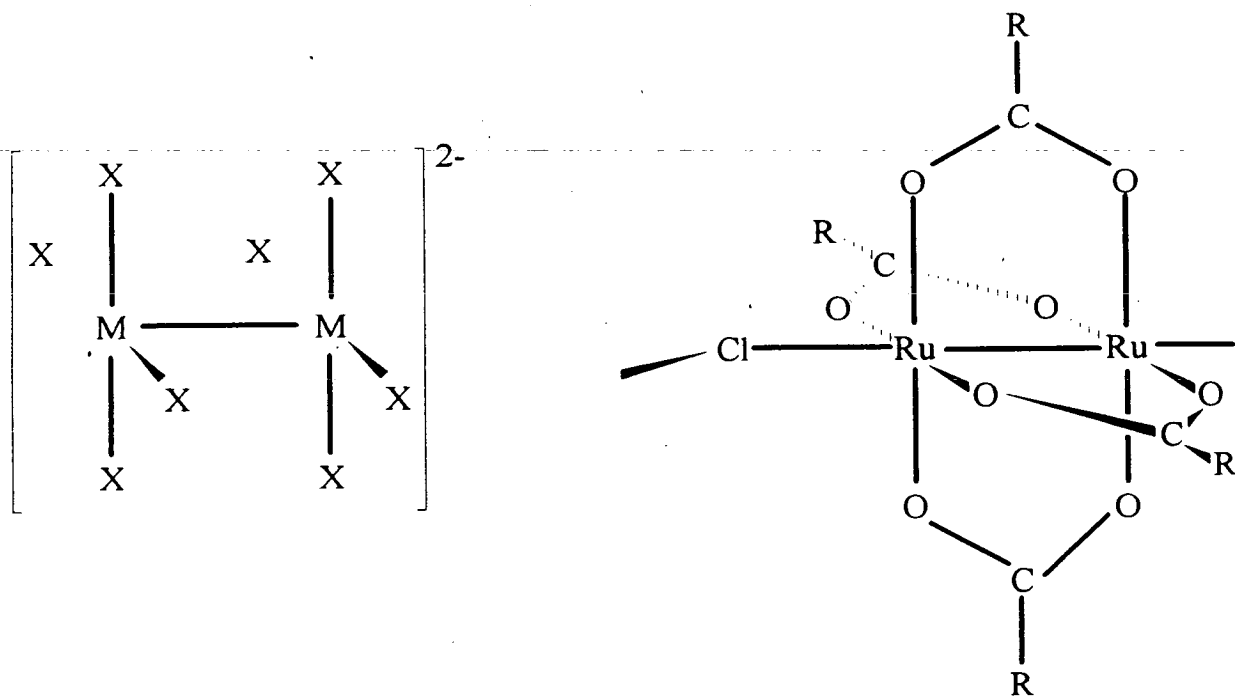
The highest possible point group for these examples is D_{4h}. It is possible to derive a reliable representation of the molecular orbitals involved in metal-metal bonding by consideration of only the metal d orbitals[17]. For these orbitals, the only interatomic mixing is of like with like ie. $d_z{}^2$ with $d_z{}^2$, d_{xy} with d_{xy} etc.

The positive overlap of the $d_z{}^2$ orbitals gives rise to a σ-bonding orbital, while the negative overlap results in the formation of the corresponding σ^* orbital. The overlaps of the degenerate d_{xz} and d_{yz} orbitals give rise to degenerate pairs of equivalent but orthogonal π-bonding and π^*-antibonding orbitals, and the overlap of the d_{xy} orbitals results in the formation of δ and δ^*-orbitals. In principle, a further pair of δ and δ^* orbitals could be formed by overlap of the $d_{x^2-y^2}$ orbitals but these are primarily involved in σ-bond formation with the ligands on their own metal atoms, hence intermetallic interaction of $d_{x^2-y^2}$ orbitals is minimal[17]. The $d_{x^2-y^2}$ orbitals also lie at significantly higher energy than the other metal d-orbitals.

In accordance with the Huckel concept that MO energies of similar pairs of orbitals are proportional to the extent of the overlap, the following ordering of the orbitals, in increasing energy, would be expected[17].

$$\sigma < \pi < \delta < \delta^* < \pi^* < \sigma^*$$

A qualitative MO diagram derived from these observations is shown in Figure 4.4. Sequential filling of the orbitals shows that formal quadruple bonds are obtained with d^4-d^4 systems (eg. $[Re_2Cl_8]^{2-}$)[17], bonding may occur in systems

containing up to 15 d-electrons (ie. in d^7-d^8 mixed-valence systems) and d^5-d^6 systems such as the Ru complexes mentioned above[9,18,19] formally have 2.5 Ru-Ru bonds. The eclipsed conformation observed in complexes of formula $[M_2X_8]^{n-}$ is caused by (and evidence for) the δ-orbital, overlap of the d_{xy} orbitals being maximised by an eclipsed conformation (the σ- and π- overlaps are not significantly affected by the conformation of the ligands with respect to those on the other metal)[17].

Figure 4.4   Qualitative MO diagram for M-M bonding in binuclear complexes with square planar metal centres (eclipsed conformation).
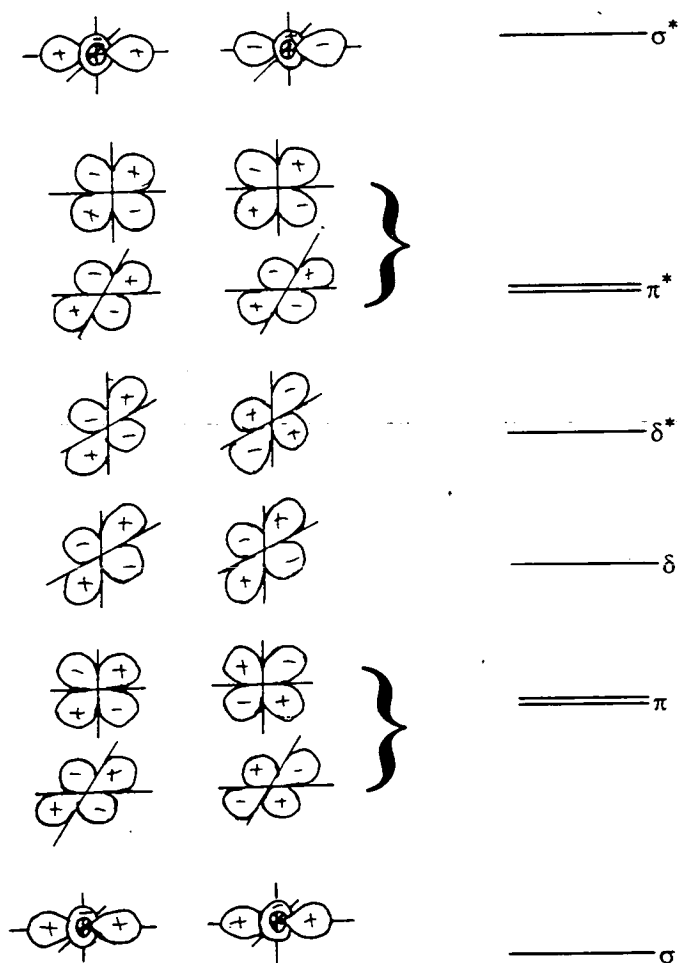
The complexity of metal-metal interactions is increased in cases when the metals do not occupy coordination sites of the other. This phenomenon is normally observed when there are two or more bridging ligands in which the atoms binding to the metal centres are not separated by one or more atoms. Of particular relevance to this work is the case of face sharing polyoctahedra.

Let us first consider the simple case of the edge sharing bioctahedron, a structural motif (shown below) known to appear both in the presence and the absence of metal-metal bonding.
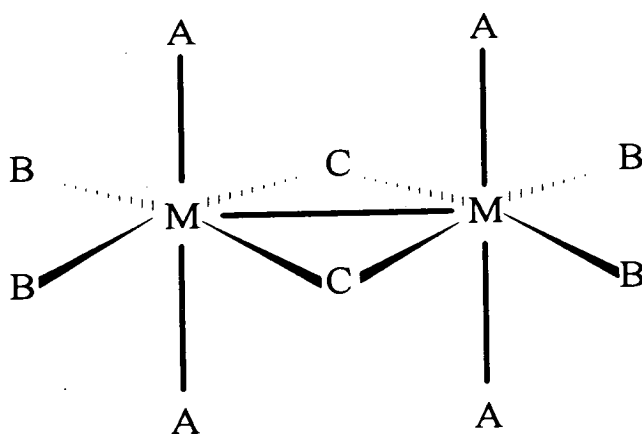
Edge sharing bioctahedral structural motif

On this occasion, the highest possible symmetry is D_{2h}. If the geometries about the metal centres are genuinely octahedral then the CMC and MCM angles will be 90°. Any substantial deviation from these angles is generally indicative of intermetallic bonding or repulsive interactions.

The metal-metal bonding of edge sharing bioctahedral complexes has been discussed by Cotton[17,20] and the relevant MO diagram is shown in Figure 4.5. The principal change in the metal-metal MO formation in this case is that there is only one π-orbital (and one π^*), as the other d-orbitals which could form π-overlaps (the $d_{x^2-y^2}$) are involved in σ-bond formation with the ligands in the $B_2MC_2MB_2$ plane (the d_{z^2} is involved with bonding to the axial A ligands). The metal-metal distance tends to be greater than those in the complexes discussed above therefore the extent of the π- and particularly the δ-overlaps is considerably reduced. One interesting feature of the bonding is the possibility of interaction between the δ-orbital with any occupied non-bonding p-orbitals on the bridging ligands (Figure 4.6). The result of this interaction is that the δ-orbital is often of higher energy than the δ^*-orbital.[20] It should be noted however, that, due to the weakness of the δ-overlap this effect does not have any important consequences for the metal-metal bonding.

It can be seen that M-M bonds may form whenever there is a total of 11 or fewer d-electrons (ie. d^5-d^6 or less) but such bonds are not always observed. Bond formation is opposed by, among other things, electrostatic repulsion between the metal centres with the result that bonding is rarely observed when the metals are in high oxidation states (+2 or greater for 1st row transition metals, +4 or greater for 2nd and third row metals)[17].

Figure 4.5   M-M bonding in edge sharing bioctahedra
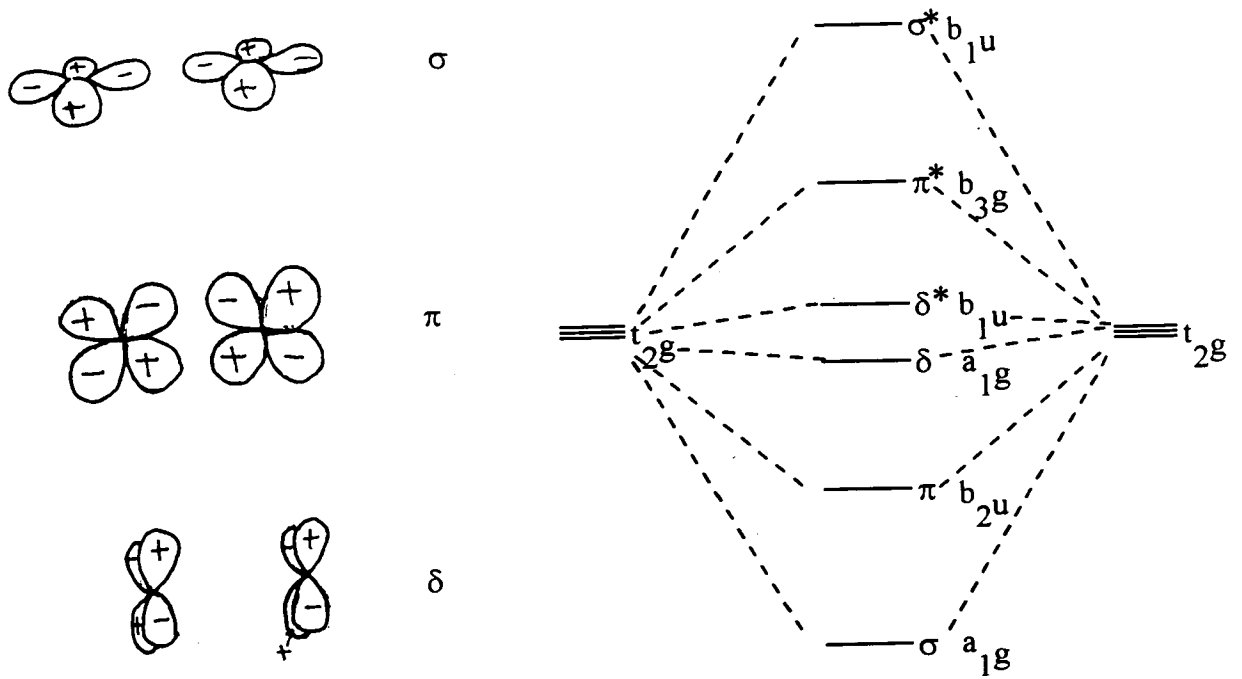
Figure 4.6   Interaction of δ-orbitals with ligand based lone pairs in edge sharing

bioctahedra
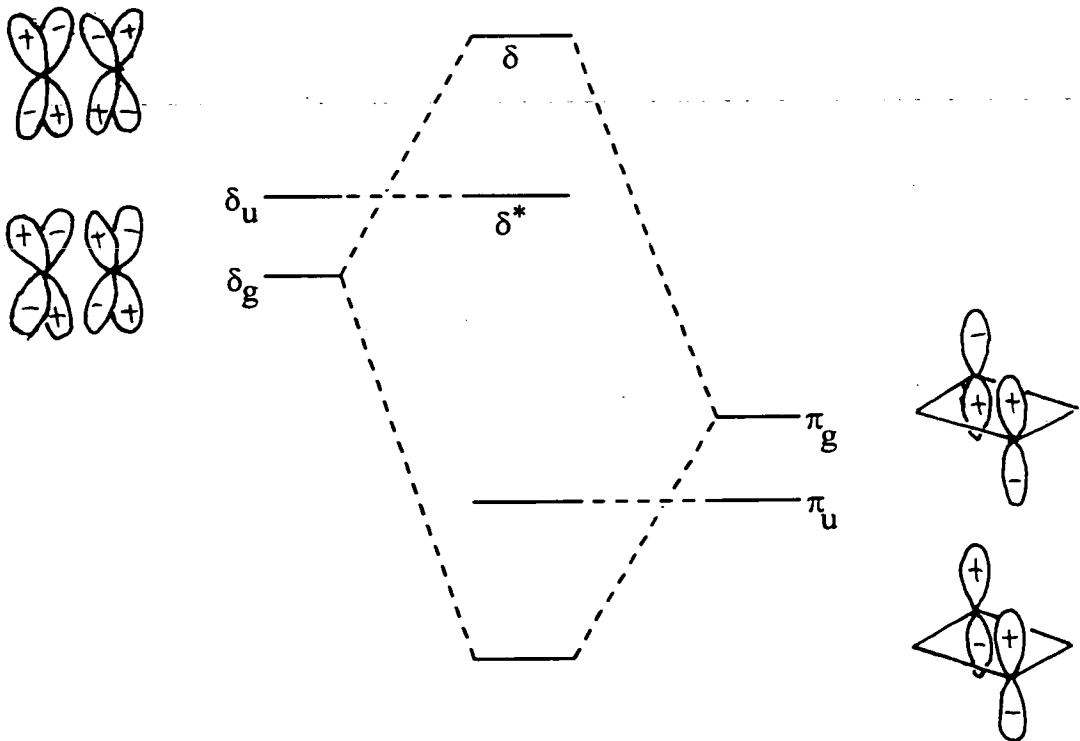
Examples of edge sharing bioctahedral complexes which exhibit metal-metal bonding include various $Ru^{III}Ru^{III}$ complexes[21-27] with Ru-Ru single bonds. Ru-Ru bond lengths range from 2.57 Å for $[Ru_2(PMe_2Ph)_2(C_5NH_4NH)_6]$[22] (shown schematically below) to 3.12 Å in $[(SnMe_3)(CO)_3Ru(\mu\text{-}SnMe_2)_2Ru(CO)_3(SnMe_3)]$[24].

N(A) = amino-N

N(P) = pyridyl-N

$[Ru_2(PMe_2Ph)_2(C_5NH_4NH)_6]$
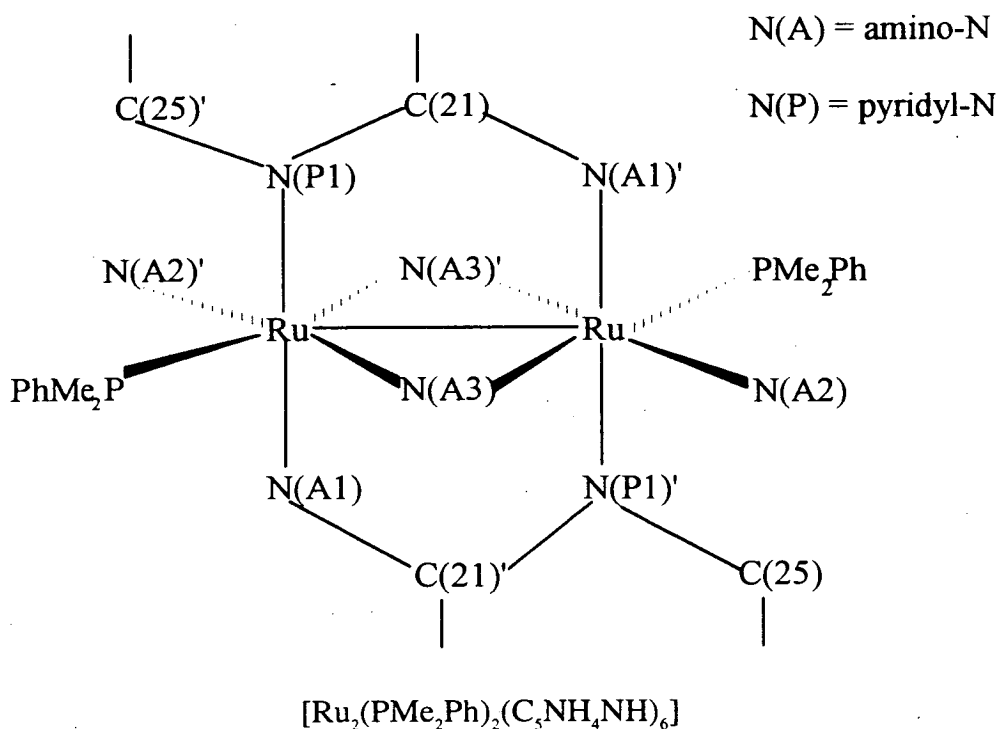
It is clear from study of the complexes above that the Ru-Ru bond length is strongly dependent upon the steric requirements of the donor atom of the bridging ligands (the shortest Ru-Ru distances are encountered in complexes with bridging N-donors[21,22], while Si, S and Cl-donors give similar bond lengths to each other[23,25-27], and the longest bonds are observed in a complex with Sn-donor[24] bridges). In the case of $[Ru_2(\mu\text{-}Cl)_2Cl_4(PR_3)_4]$[28,29] however, no bond is formed (Ru-Ru = 3.73 Å when R = Bu^n, for example[28]). Very few mixed-valence examples

of edge sharing bioctahedral complexes have been reported: electrogenerated

$[Os_2Cl_{10}]^{3-}$, for example, shows no evidence of metal-metal bonding[30].

Now consider the case of face sharing bioctahedral complexes, shown below. The highest possible symmmetry is D_{3h}. If the geometry about each metal is truly octahedral then the angle BMB is 90° and the angle MBM is 70.53° If no bond forms then repulsive forces (steric, electrostatic) will push the metals apart, substantially increasing the MBM angle and reducing the BMB angle[31].
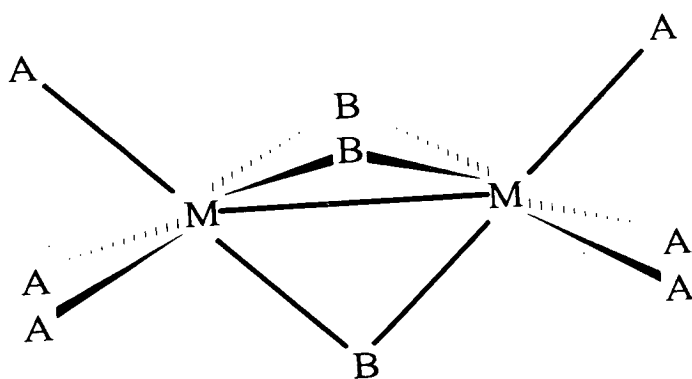
Face sharing bioctahedral structure

Several intensive studies of the MO structure of face sharing bioctahedra have been carried out[32-35], and these have revealed some surprising results. Qualitatively, one might expect that the d_{xz} and d_{yz} orbitals would be involved primarily in σ-bonding to the ligands, leaving the d_{z^2} orbitals to form molecular orbitals with σ and σ* symmetry and the d_{xy} and $d_{x^2-y^2}$ orbitals to form degenerate pairs of δ- and δ*-orbitals. In practice however, there is strong mixing between the $d_{xz,yz}$ and the d_{xy,x^2-y^2} pairs, resulting in one pair of hybrid orbitals which bind primarily to the

ligands and a second pair which participate in M-M interactions. The resultant molecular orbitals bave e' (bonding) and e" (antibonding) symmetries, with overlaps which are intermediate between π- and δ-bonding[35]. A molecular orbital diagram for face sharing bioctahedral complexes is shown in Figure 4.7. It should be noted however, that the extent of the e' and e" overlaps is very small. As a result they do not greatly influence the strength of the M-M bond. Examples include $[Mo_2Cl_9]^{3-}$, the e'-e" separation has been calculated to be 2000 cm^{-1}[34] and $[Ru_2Cl_9]^{3-}$, where the separation is reported as only 80 cm^{-1}[35]. These values compare with σ-σ* separations of 22000 cm^{-1} and 11400 cm^{-1} respectively.

As with edge sharing bioctahedral complexes, metal-metal bonding becomes important if there are fewer than 11 d electrons (ie. d^5-d^6 or less) but bonding is not always observed when it is theoretically possible.

Several Ru^{III}-Ru^{III} face sharing bioctahedral complexes have been reported[7,17,28,35-37], including the aforementioned $[Ru_2Cl_9]^{3-}$. A significant Ru-Ru interaction occurs in all cases; metal-metal distances range from 2.65 Å in $[(PMe_3)_3Ru(\mu-CH_2)_3Ru(PMe_3)_3]^{37}$ to 3.20 Å in $[(PEt_3)Cl_2Ru(\mu-Cl)_3RuCl(PEt_3)_2]^7$. The metal-metal distances are again largely dependent upon the steric requirements of the bridges. There have also been a small number of Ru^{II}-Ru^{III} compounds reported, which conform to Robin and Day's principles. Symmetrical compounds, of formula $[(PR_3)_2ClRu(\mu-Cl)_3RuCl(PR_3)_2]$, appear to exhibit Ru-Ru bonding (metal-metal distances range from 2.99-3.12 Å) while the unsymmetrical complexes, of formula $[(PR_3)_3Ru(\mu-Cl)_3RuCl_2PR_3]$, do not (Ru-Ru distances of 3.3-3.4 Å are observed)[7].

188

Figure 4.7   MO diagram for face sharing bioctahedral complexes
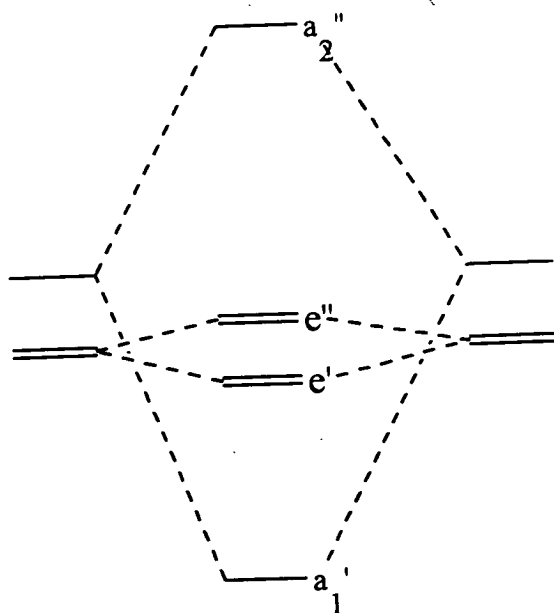
Recent work within this department[10] has involved a study of confacial bioctahedral complexes of general formula $[L_2L'M(\mu-X)_3ML_2L'']^{n+}$, M = Ru or Os; X = OH^- (Ru only), Cl^- Br^-, or I^-; L = PR_3 or $P(OMe)_aPh_{3-a}$; L',L'' = PR_3, $P(OMe)_aPh_{3-a}$, Cl^- or CS (a = 1-3) and n = 1, 2 or 3. The stable $M^{II}M^{II}$ complexes were electrochemically or chemically oxidised to the mixed-valence $M^{II}M^{III}$ and the $M^{III}M^{III}$ complexes and were characterised by spectroscopic and, in the case of $[(PEt_3)_3Os(\mu-Cl)_3Os(PEt_3)_3]^{2+}$, structural methods. It was found that, when L' = L the dicationic and tricationic species all exhibited strong metal-metal interactions consistent with intermetallic bonding, while the complex $[Cl(PPh_3)_2Ru(\mu-Cl)_3Ru(PPh_3)_2(CS)]^+$ was a class II mixed-valence complex with

189

weak intermetallic interactions. In the case of the class III systems, it was found that the strength of the metal-metal interactions in the Ru complexes was dependent upon the steric requirements of the terminal phosphine ligands (no such dependence was observed in the Os complexes).

This chapter reports the study of a group of face sharing *trioctahedral* complexes (general structure as shown in Figure 4.8) and their metal-metal interactions. The first reported complex was $[Ru_3Cl_{12}]^{4-}$[38], prepared by Cotton and Bino in 1980. A more recent paper discusses a quantitative MO study of this complex[35]. Subsequently, only three papers reporting similar complexes have been published, all by Cotton and coworkers[28,39,45]. These papers feature compounds of general formulae $[L_2ClRu(\mu-Cl)_3Ru(\mu-Cl)_3RuClL_2]^{(28,39)}$ and latterly $[L_3RuCl_3RuCl_3RuL_3]^{+(45)}$, where L is a tertiary phosphine. The above references consist primarily of structural studies and quantitative MO calculations. As a result of the relative paucity of information about such unusual complexes we resolved to systematically study several of these mixed-valence compounds (of general formula $[L_2XRuX_3RuX_3RuXL_2]$) with the primary objective being to study the nature of the metal-metal interactions within such species.

Figure 4.8.   Face sharing trioctahedral structural motif
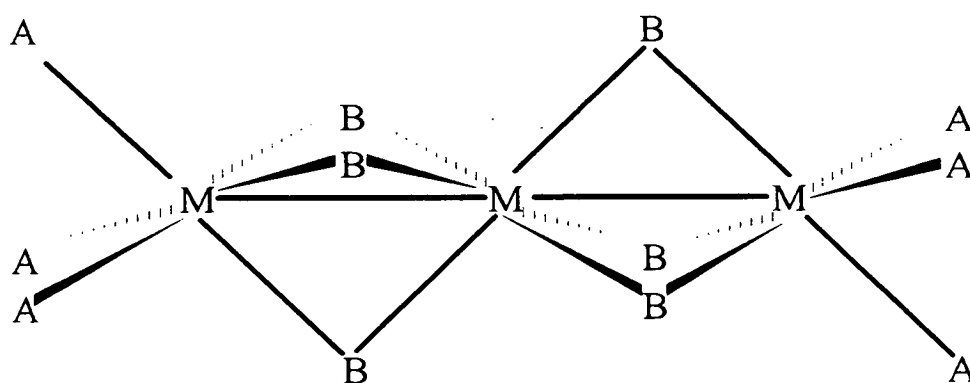
4.2   Results and discussion

4.2.1   Synthesis and Purification

In 1968 Chatt and coworkers[40] reported a tendency for binuclear complexes to be formed as side products of the syntheses of monomeric tri-halo tris phosphine compounds of ruthenium. We have found that reaction of $RuCl_3$ and PEt_2Ph, in the ratios recommended for preparation of $[RuCl_3(PEt_2Ph)_3]$,[40] resulted in a mixture of products including $[Ru_2Cl_5(PEt_2Ph)_4]$ and $[Ru_2Cl_3(PEt_2Ph)_6]^+$ but not the mononuclear compound. In addition, the trinuclear complex $[Ru_3Cl_8(PEt_2Ph)_4]$ was isolated in a yield of 20%. Purification of the trinuclear species was by column chromatography, although the (otherwise air stable) product showed a tendency to decompose during this process.

To optimise the yield of the trinuclear complex and reduce the number of side products, a brief study was conducted to find the reaction conditions most conducive to the preparation of $[Ru_3Cl_8(PEt_2Ph)_4]$. In general, it was found that the method reported by Cotton and Torralba[39] was the most effective. Thus reaction of PEt_2Ph and $RuCl_3.xH_2O$ in a 4:3 molar ratio in MeOH at room temperature gives the desired trinuclear complex in 40-50% yield. Using a small excess of phosphine (up to $PR_3:RuCl_3.xH_2O = 5:3$) was found to increase the yield of the desired product slightly, but it also increased the formation of impurities, particularly $[Ru_2Cl_5(PEt_2Ph)_4]$. A larger excess of phosphine reduced the yield of $[Ru_3Cl_8(PEt_2Ph)_4]$ while increasing formation of $[Ru_2Cl_5(PEt_2Ph)_4]$ and

$[Ru_2Cl_3(PEt_2Ph)_6]^+$. A small excess of chloride tended to increase the yield without causing formation of impurities. Heating the reaction mixture resulted in faster product formation but resulted in reduced yields and increased formation of binuclear impurities.

A number of compounds of general formula $[Ru_3Cl_8(QR_3)_4]$ were synthesised using the method of Cotton and Torralba[39]. We have prepared and studied $[Ru_3Cl_8(PEt_2Ph)_4]$, $[Ru_3Cl_8(PPr^n_3)_4]$, $[Ru_3Cl_8(PMe_3)_4]$ (previously reported by Cotton and Torralba[39]) and $[Ru_3Cl_8(AsPr^n_3)_4]$. The latter complex is the first face sharing trioctahedral complex with arsine terminal ligands. All syntheses proceeded much as described above giving the desired product in reasonable yield. All the products were stable in the solid state and only decomposed slowly in solution (over a period of several weeks).

In order to study the effects upon the trinuclear complexes of modifying the steric and electronic requirements of the terminal ligands, syntheses were also attempted using PPh_3 and $P(OMe)_3$. These syntheses were less successful than those described in the preceding paragraph, giving lower yields of $[Ru_3Cl_8L_4]$, which decomposed rapidly during purification attempts. Some data extracted from studies of the crude products are given in the following sections.

Attempts were also made to study the effects of varying the bridging ligands. This involved the attempted syntheses of complexes featuring Br⁻ bridging ligands. Preparation of $[Ru_3Br_8(PEt_2Ph)_4]$ from "RuBr₃" (obtained by reaction of $RuCl_3.xH_2O$ with excess LiBr in MeOH), gave the desired product in very low yield (less than 5%). All other attempts to isolate trinuclear complexes with Br⁻ bridging ligands

from similar preparations were unsuccessful. Unsuccessful attempts were also made to induce bromination of Cl bridged trinuclear complexes by stirring the trinuclear chloro complex with Bu_4NBr in THF.

4.2.2 IR Spectroscopy

Study of the lower energy regions of the IR spectrum of $[Ru_3Cl_8(PEt_2Ph)_4]$, in a KBr disc, reveals bands at 305 and 325 cm^{-1} which were assigned as Ru-Cl$_t$ stretches where Cl$_t$ is a terminal chloride ligand. There were also broader bands, assigned as Ru-Cl$_b$ stretching modes (Cl$_b$ is a bridging chloride) at 405 and 415 cm^{-1}. Similar behaviour was observed in all complexes featuring chloride ligands.

Spectra of KBr discs doped with $[Ru_3Br_8(PEt_2Ph)_4]$ contained bands at 355, 365 and 370 cm^{-1} which were assigned as Ru-Br$_b$ stretching modes. The positions of the Ru-Br$_t$ modes were not obtained from the spectra as absorption due to the KBr matrix commenced at 280 cm^{-1}.

4.2.3 Qualitative MO studies

The stated objectives of this research were to investigate the electronic structure of the frontier orbitals of $[Ru_3X_8L_4]$ from experimental (structural, electrochemical and spectroscopic) data. It is, however, convenient to use a

193

simplified representation of the electronic structure as a context within which to discuss the experimental observations.

A qualitative MO study of metal-metal bonding in face sharing trioctahedral complexes is presented below. It is then compared, briefly, with the quantitative studies carried out by Cotton and co-workers[35,39]. In later sections the implications of the experimental data are discussed with respect to the frontier orbitals, and refinements to the qualitative MO diagram are suggested.

Development of a reliable representation of any metal-metal bonding in face sharing trioctahedral complexes follows from consideration of two simpler systems - linear triatomic molecules and face sharing bioctahedral complexes.

As the metal atoms are in a linear arrangement in the face sharing trioctahedral complexes under study, mixing of their orbitals should follow the pattern observed in linear triatomic species. The mixing of three orbitals from the contributing atoms (one from each atom) gives rise to one bonding orbital, one non-bonding orbital and one antibonding orbital. This is shown for mixing of three d_z^2 orbitals, where the z-axis passes through all three atoms, in Figure 4.9 below.

Figure 4.9   Mixing of three d_z^2 atomic orbitals
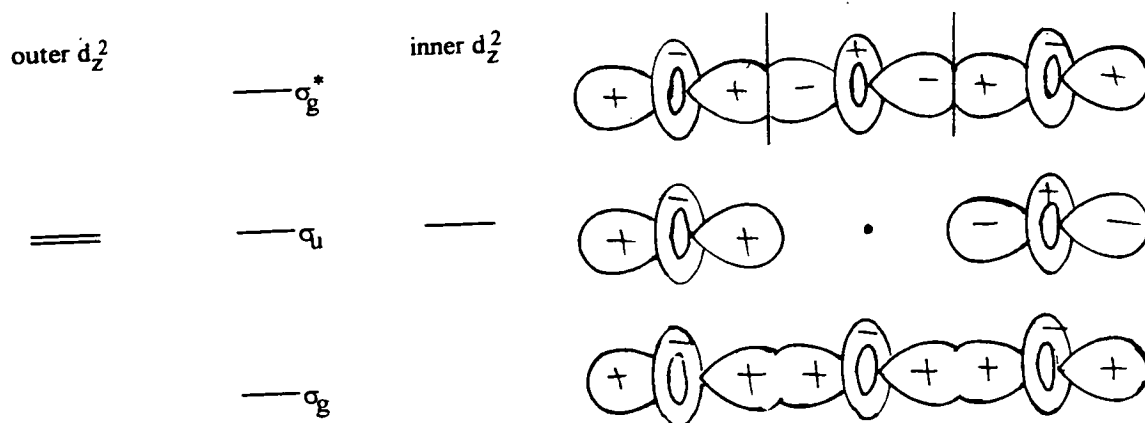
This principle is now applied to face sharing trioctahedral complexes. The highest possible symmetry for such complexes is D_{3d}. This symmetry is retained provided all ligands of a given type (ie. bridging or terminal) are equivalent. Each metal atom can be expected to contribute three orbitals to metal-metal bonding, the d_{z^2}, plus the degenerate $d_{xy}/d_{x^2-y^2}$ pair. The resultant mixing of d_{z^2} orbitals will give rise to σ-bonding, non-bonding and antibonding orbitals (one of each), while the mixing of the d_{xy} and $d_{x^2-y^2}$ will result in degenerate pairs of mutually orthogonal δ-bonding, non-bonding and antibonding orbitals. The overlap of the d_{xy} and $d_{x^2-y^2}$ orbitals will be considerably less than that of the d_{z^2} orbitals, therefore the δ-overlaps will have a much smaller effect on the metal-metal bonding.

A qualitative MO diagram showing mixing of the relevant orbitals in face sharing trioctahedral complexes, as described in the preceding paragraph, is shown in Figure 4.10. This electronic configuration can accommodate up to 18 d-electrons and positive metal-metal interactions may arise with 17 or fewer d-electrons. "Ru_3^{8+}" complexes such as those under study contribute 16 d-electrons and therefore have formal half-bonds between each pair of metals (ie. a net 3-centre 2-electron bond). It might be expected (ignoring the effects of electrostatic repulsion) that oxidation of such species would result in stronger M-M bonds consistent with removal of an electron from an antibonding orbital, while reduction would give weaker bonding. Bonding will be dominated, however, by the relative populations of the σ-bonding and σ^*-antibonding orbitals.

Figure 4.10   Simplified qualitative molecular orbital diagram for face sharing

trioctahedral complexes
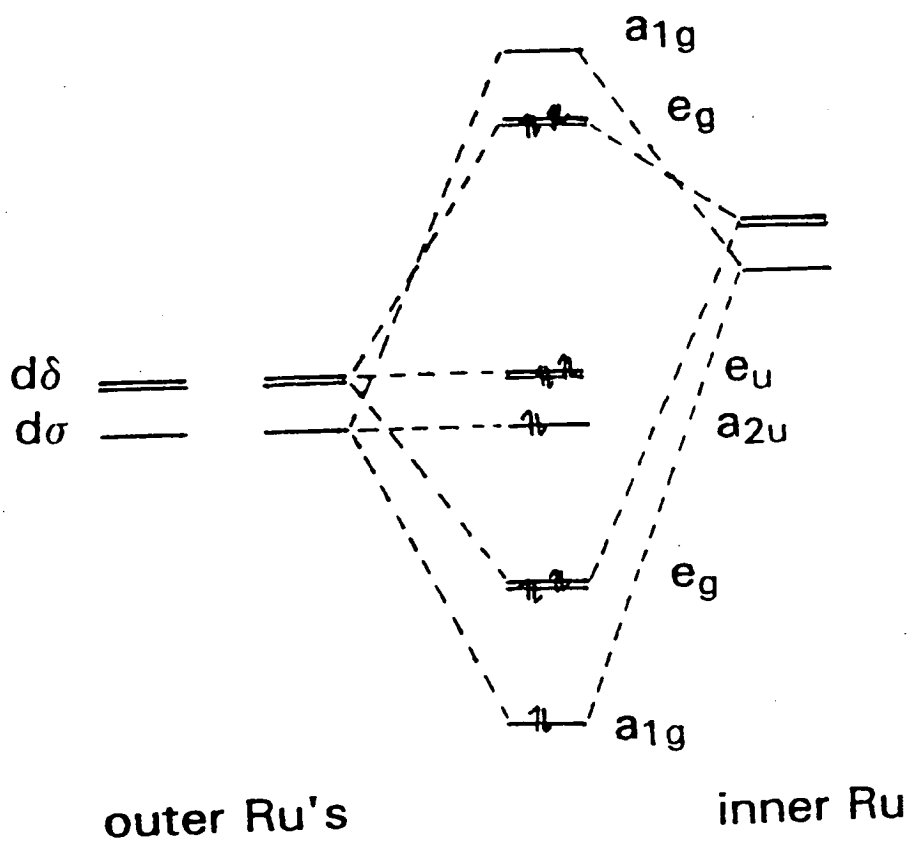
Electronically allowed transitions

$$e_u \longrightarrow a_{1g}$$
$$a_{2u} \longrightarrow a_{1g}$$
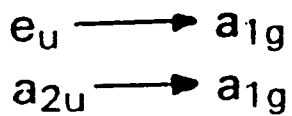
In face sharing trioctahedral complexes metal-metal bonding does not necessarily confer equivalent electron densities to the metal centres. Specifically, if the orbitals contributed by the central metal are of higher energy than those associated with the terminal metal centres then the central metal will make a greater contribution to the antibonding orbitals than the bonding orbitals. If this is the case then electron density will be greater at the terminal metal centres (ie. the central metal will have a higher formal oxidation state). It should be noted, however, that if the difference in energies of the contributed orbitals is too large then the mixing of orbitals will be so reduced that electrostatic repulsion forces dominate and metal-metal bonding will not occur.

In the above MO diagram there are a number of obvious assumptions which will have to be tested and possibly discarded when considering real systems such as $[Ru_3Cl_8(PR_3)_4]$. The most obvious assumption is that the influence of the ligands on any metal-metal bonding is negligible. We can test this assumption by varying the ligands and comparing the structural, electrochemical and spectroscopic data. Another factor to consider when dealing with real systems is that the symmetry will generally be lower than that assumed for the qualitative study. The complexes under study in this research have overall symmetry C_i. However the immediate environment of the metal centres, if we ignore the alkyl/aryl groups of the phosphine and arsine ligands, is essentially C_{2h}. The principal difference resulting from perturbation of the MO diagram to accommodate this lower symmetry is the loss of degeneracy of the e_g, e_u and e_g^* pairs. The *gerade* and *ungerade* character of the orbitals is retained, as C_{2h} and C_i are centrosymmetric point groups.

The literature contains three quantitative MO studies of face sharing trioctahedral complexes. The earliest study is of $[Ru_3Cl_{12}]^{4-}$[35], while the remaining studies concentrate on $[Ru_3Cl_8(PH_3)_4]$, a species which has not been successfully synthesised but represents the simplest example of $[Ru_3Cl_8(PR_3)_4]$. The MO calculations were based on the structural data of $[Ru_3Cl_8(PBu_3)_4]$ and idealised to C_{2h} symmetry. SCF-Xα-SW calculations (also used in the study of $[Ru_3Cl_{12}]^{4-}$) and Fenske-Hall calculations have been employed[39]. Qualitatively the results of these calculations are similar to those we have described above. To facilitate comparisons, the calculated energies, and the contributions from the central and terminal Ru atoms, of the 9 MOs corresponding to those given in Figure 4.10 are given in Table 4.1 (the data is taken from reference 39).

The major differences between quantitative and qualitative studies arise from mixing of orbitals of similar symmetry. The $d_{xy}/d_{x^2-y^2}$ pair on each Ru atom mix extensively with the d_{xz}/d_{yz} pair giving a hybrid degenerate pair involved in M-M interactions and another degenerate pair primarily involved in σ-bonding with the ligands. The intermetallic overlaps intermediate between those observed in "classical" π- and δ-bonding, much as has been reported in various studies of face sharing bioctahedral complexes (see the introduction to this chapter for more details). Additionally, significant mixing of the metal based orbitals with ligand based orbitals is reported. As a result of these factors some reordering of the

Table 4.1   Relative energies and %contributions of Mos in $[Ru_3Cl_8(PH_3)_4]$ (data from reference 39).

Orbital		Energy/eV		% Contributions (from SCF)	
$\underline{D_{3d}}$	$\underline{C_{2h}}$	$\underline{F\text{-}H}$	$\underline{SCF}$	$\underline{Ru_c}$	$\underline{Ru_t}$
$a_{1g}{}^*$	$18a_g$	-4.44	-7.788	28	58
a_{2u}	$16b_u$	-6.76	-8.295	0	78
e_u	$11a_u$	-6.97	-8.341	0	79
	$15b_u$	-7.82	-8.530	0	82
$e_g{}^*$	$12b_g$	-6.77	-8.344	1	78
	$17a_g{}^1$	-7.77	-8.499	6	76
e_g	$16a_g{}^1$	-6.92	-9.034	71	8
	$11b_g$	-7.49	-9.068	78	2
a_{1g}	$15a_g$	-8.80	-9.263	36	17^2

Notes:-

F-H = data from Fenske-Hall calculations; SCF = data from SCF-Xα-SW.

Ru_c, Ru_t = central and terminal Ru.

1 - In Fenske-Hall calculations $16a_g$ and $17a_g$ orbitals are reversed (based on relative contributions of Ru atoms).

2 - There is significant mixing between the d_z^2 orbitals, particularly of Ru_t based d_z^2 orbitals, with ligand based σ-bonding orbitals of a_{1g} character, hence the relatively low contribution from Ru_t.

weakly interacting and formally non-bonding orbitals is observed, such that the σ_u orbital appears to be the HOMO in "Ru$_3^{8+}$" complexes[35,39]. In [Ru$_3$Cl$_8$(PH$_3$)$_4$], the calculations suggest that energy gaps between orbitals that were degenerate in the D$_{3d}$ point group are very small (generally less than 0.1 eV). Quantitatively, the results suggest very similar electronic structures in [Ru$_3$Cl$_{12}$]$^{4-}$ and [Ru$_3$Cl$_8$(PH$_3$)$_4$]. There are, however, several significant differences between the two studies of the electronic structure of [Ru$_3$Cl$_8$(PH$_3$)$_4$]. A simple example of this is obtained by comparing the σ_g-σ_g* separation, calculated to be 1.475 eV by the SCF-Xα-SW method, but 4.36 eV by the Fenske-Hall approach. Thus the Fenske-Hall method implies much stronger Ru-Ru bonding than that suggested by the SCF-Xα-SW calculations. Additionally, there are differences in the ordering of the seven orbitals which lie between σ_g and σ_g* in energy.

4.2.4 Crystallographic Studies

Single crystal X-ray diffraction studies were carried out for [Ru$_3$Cl$_8$(PEt$_2$Ph)$_4$], [Ru$_3$Cl$_8$(PPr$^n_3$)$_4$] and [Ru$_3$Cl$_8$(AsPr$^n_3$)$_4$]. Views of these species are shown in Figures 4.11. - 4.17. Selected structural data for these complexes and for [Ru$_3$Cl$_{12}$]$^{4-}$, published by Bino and Cotton[38], are given in Table 4.2.

A number of points of interest regarding these complexes arise from the crystallographic studies. All the complexes exhibit short Ru-Ru distances of 2.80-2.86 Å (when the complexes prepared by Cotton and coworkers[28,38,39] are included).

Table 4.2.   Selected structural data for $[RuCl_8L_4]^{a-}$, a = 4 when L = Cl$^-$, otherwise a = 0

L	Cl$^-$*	PEt$_2$Ph	PPr$^n_3$	AsPr$^n_3$
Interatomic Distances				
Ru1-Ru2	2.805(1)	2.8391(11)	2.8447(14)	2.8097(11)
Ru1-Cl1t	2.371(1)	2.344(4)	2.343(5)	2.344(4)
Ru1-L1	2.367(3)	2.334(4)	2.332(5)	2.418(2)
Ru1-L2	2.370(3)	2.323(4)	2.314(5)	2.431(2)
Ru1-Cl1b	2.390(1)	2.494(3)	2.481(5)	2.464(4)
Ru1-Cl2b	2.374(1)	2.455(3)	2.478(4)	2.445(4)
Ru1-Cl3b	2.376(2)	2.380(3)	2.376(5)	2.373(4)
Ru2-Cl1b	2.382(2)	2.358(3)	2.360(4)	2.371(4)
Ru2-Cl2b	2.380(2)	2.355(3)	2.382(4)	2.363(4)
Ru2-Cl3b	2.351(2)	2.359(3)	2.348(4)	2.362(4)
Bond Angles				
Ru1-Cl1b-Ru2	72.00(6)	71.58(10)	71.58(12)	71.03(10)
Ru1-Cl2b-Ru2	72.31(6)	72.25(9)	71.98(12)	71.50(11)
Ru1-Cl3b-Ru2	72.78(7)	73.63(10)	74.04(13)	72.79(11)
Cl1b-Ru1-Cl2b	88.35(8)	82.90(11)	83.63(15)	84.19(13)
Cl1b-Ru1-Cl3b	88.26(8)	86.71(11)	88.61(15)	87.52(13)
Cl2b-Ru1-Cl3b	88.82(8)	89.96(11)	87.62(15)	91.02(13)
Cl1b-Ru2-Cl2b	88.41(8)	88.10(11)	88.42(15)	88.11(13)
Cl1b-Ru2-Cl3b	89.05(8)	90.54(11)	91.68(15)	89.99(12)

Note: * - Data taken from reference 38.

This distance is significantly shorter than that encountered in face sharing bioctahedral complexes of Ru featuring chloride bridges (see introduction for specific examples) and implies stronger metal-metal interaction than is observed in the binuclear complexes. The Ru-Cl-Ru bond angles are close to those predicted for idealised face sharing polyoctahedral geometries (70.53°), showing that steric and electrostatic repulsive forces are not dominant in these cases, and are indicative of metal-metal interactions. The symmetry of the complexes is C_i but the geometry about each metal centre is close to octahedral, therefore the qualitative MO diagram in Figure 4.10 should represent a reasonable approximation of the effects of symmetry on metal-metal bonding in these complexes.

The space filling diagrams (Figures 4.13, 4.15 and 4.17) show that these complexes are not sterically crowded, unlike many face sharing bioctahedral complexes such as $[Os_2Cl_3(PEt_3)_6]^{+}$[10] (shown in Figure 4.18). Therefore we predict that structural and spectroscopic properties will be dominated by electronic factors.

It is interesting to note that the chloride bridges are not symmetrical. The $Ru(1)-Cl_b$ bond lengths are longer than the corresponding $Ru(2)-Cl_b$ bond length. This effect is particularly pronounced in complexes containing phosphine and arsine terminal ligands, and is also true of the structures determined by Cotton and coworkers[28,39]. For example, in $[Ru_3Cl_8(PEt_2Ph)_3]$, the $Ru(1)-Cl_b$ distances are 2.494(3), 2.455(3) and 2.380(3) Å, while the corresponding $Ru(2)-Cl_b$ distances are 2.358(3), 2.355(3) and 2.359(3) Å. One possible explanantion is that the metal-metal bonding is polarised towards the terminal Ru atoms, thus resulting in lower

electron density about the central Ru and hence a shorter bond between it and the anionic chloride ligands.

Structurally, the complexes are all remarkably similar. In particular, the variation of the Ru-Ru distance is extremely small. This also applies to the complexes $[Ru_3Cl_8(PEt_3)_4]$, $[Ru_3Cl_8(PMe_3)_4]$ and $[Ru_3Cl_8(PBu_3)_4]$, which have Ru-Ru bond lengths of 2.86, 2.83 and 2.85 Å respectively[28.39].

The Ru-Ru distance in $[Ru_3Cl_{12}]^{4-}$ is significantly shorter than that in the phosphine containing complexes. This may be a result of the greater similarity of the environment of each Ru atom, which should result in the d-orbitals of the terminal Ru atoms being closer in energy to the corresponding orbitals of the central metal. This will allow more efficient mixing of the orbitals, giving a stronger Ru-Ru interaction. The Ru-Ru bond length is also shorter in the arsine complex than those featuring phosphines.

In addition to the species discussed above, structural data was reported in reference 39 for the complex $[Ru_3Cl_8(PEt_3)_4][SbF_6]$. This showed that oxidation had resulted in an increase in the Ru-Ru bond length, to a mean of 2.91 Å (the crystals contained two crystallographically independent trinuclear cations). The qualitative MO diagram shows that oxidation involves removal of an electron from an orbital that is formally antibonding, therefore one might have expected a shortening of the Ru-Ru distance. It is believed that the increased bond legth arises from the increase in electrostatic repulsion between the positively charged metal centres upon removal of the electron. It should also be noted that although the electron is removed from

Figure 4.11   View of [Ru$_3$Cl$_8$(PEt$_2$Ph)$_4$].
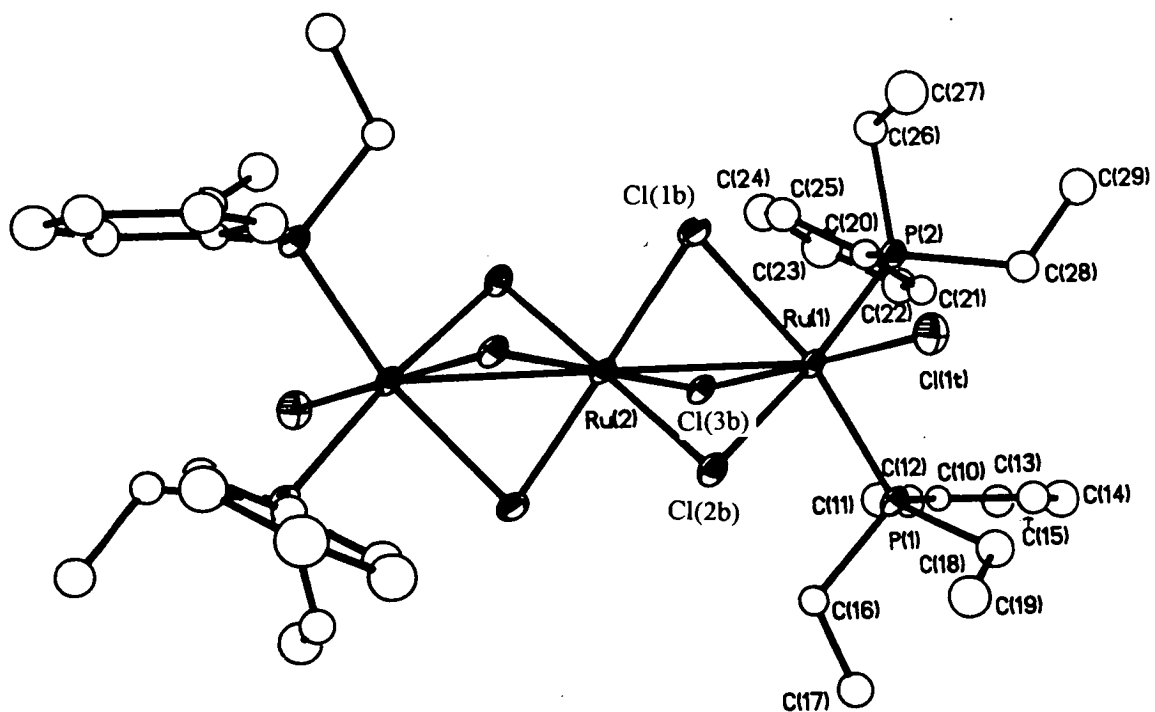
Figure 4.12.   View of [Ru$_3$Cl$_8$(PEt$_2$Ph)$_4$] with Et and Ph groups removed for clarity.
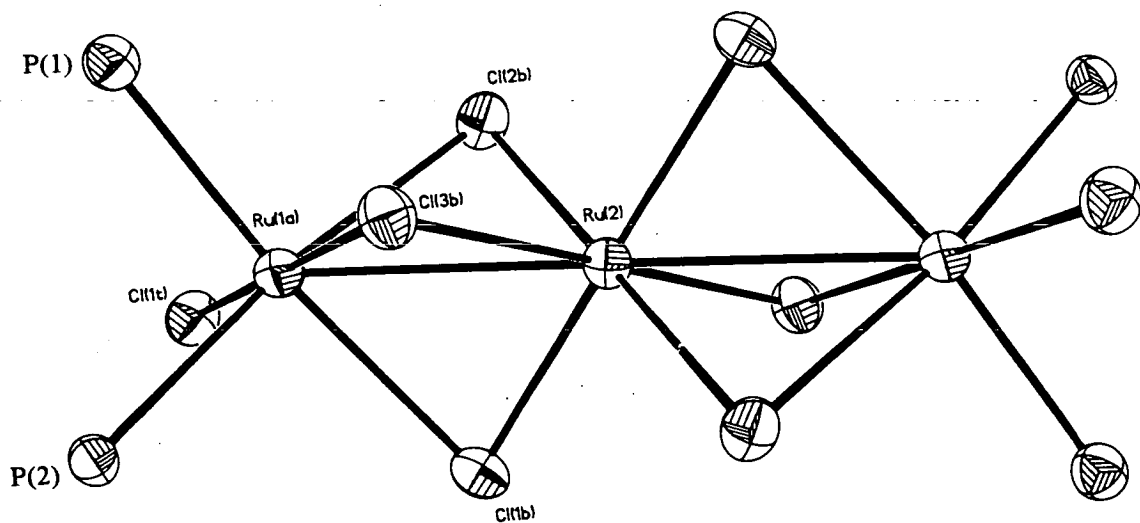
Figure 4.13   Space-filling diagram of [Ru$_3$Cl$_8$(PEt$_2$Ph)$_4$]
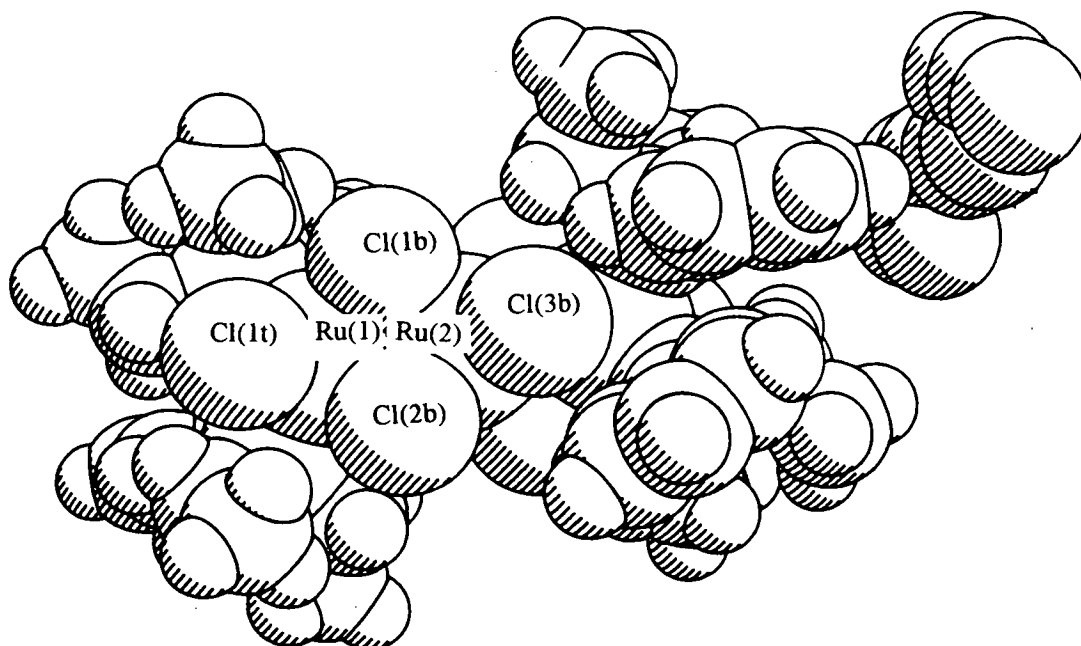
Figure 4.14   View of [Ru$_3$Cl$_8$(PPr$^n_3$)$_4$].
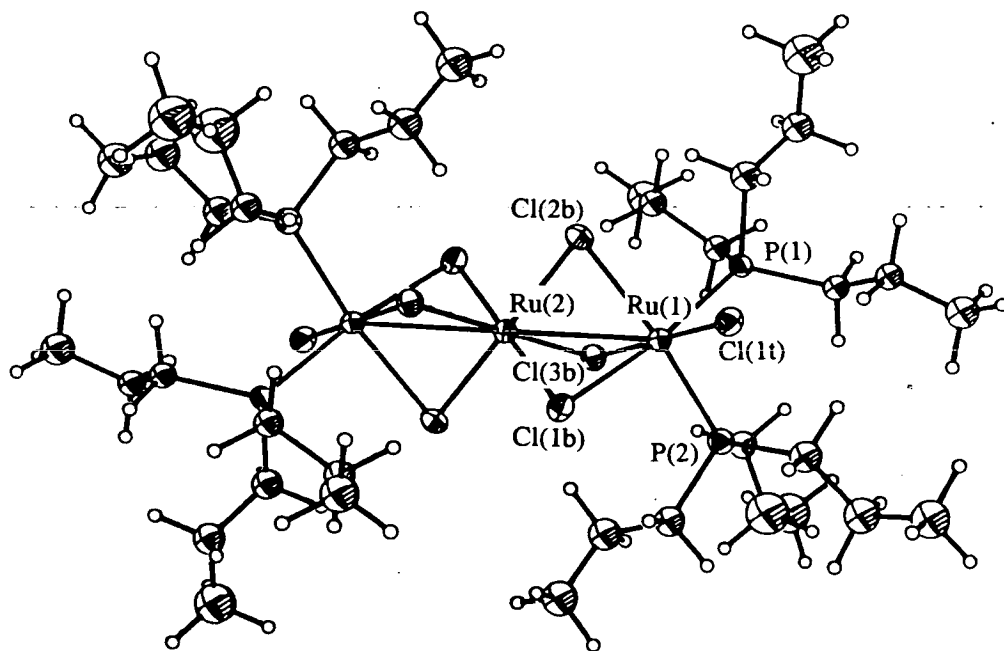
Figure 4.15   Space-filling diagram of $[Ru_3Cl_8(PPr^n_3)_4]$
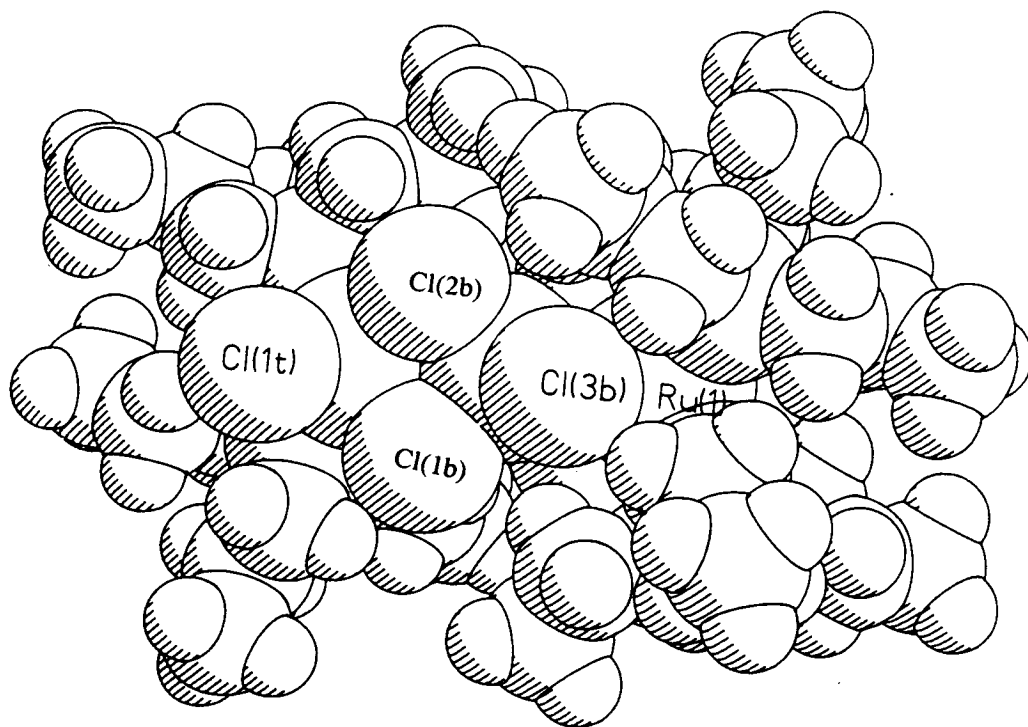
Figure 4.16   View of $[Ru_3Cl_8(AsPr^n_3)_4]$.
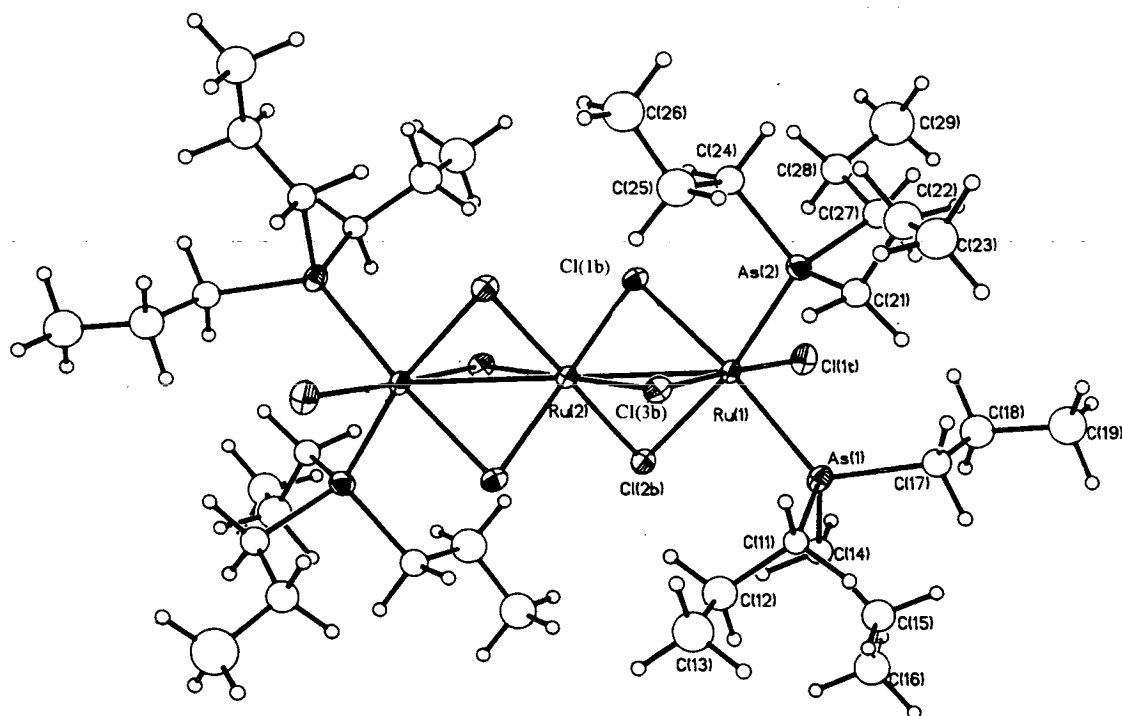
Figure 4.17   Space-filling diagram of [Ru$_3$Cl$_8$(AsPr$^n_3$)$_4$].
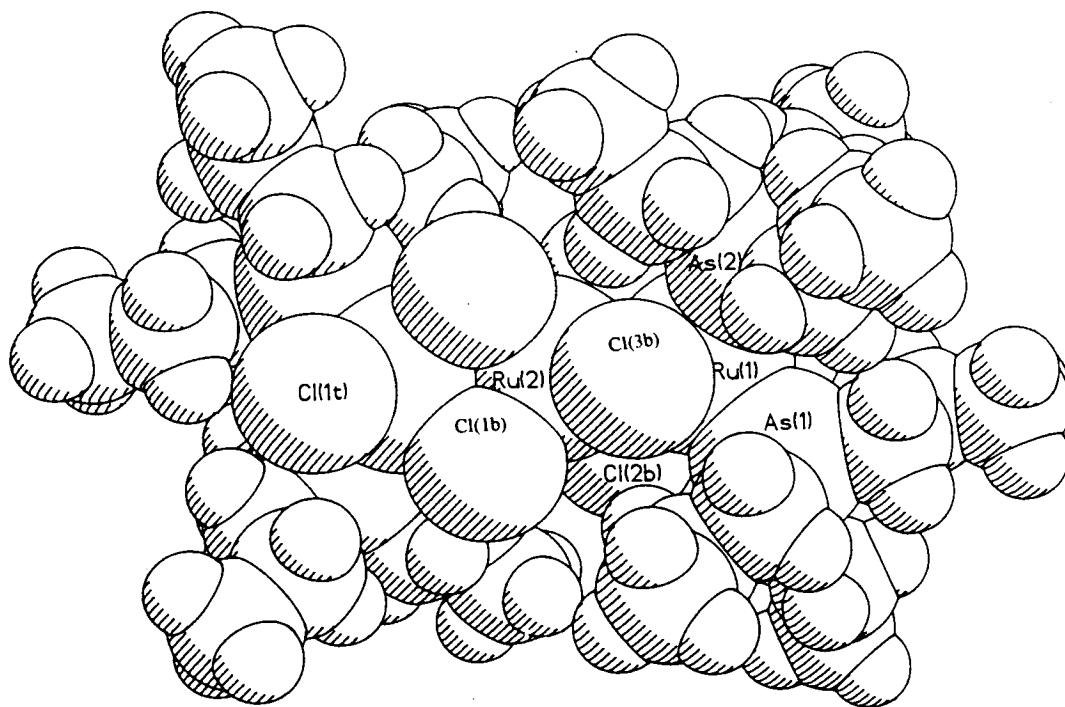
Figure 4.18   Space-filling diagram of [Os$_2$Cl$_3$(PEt$_3$)$_6$]$^+$ (taken from reference 10)
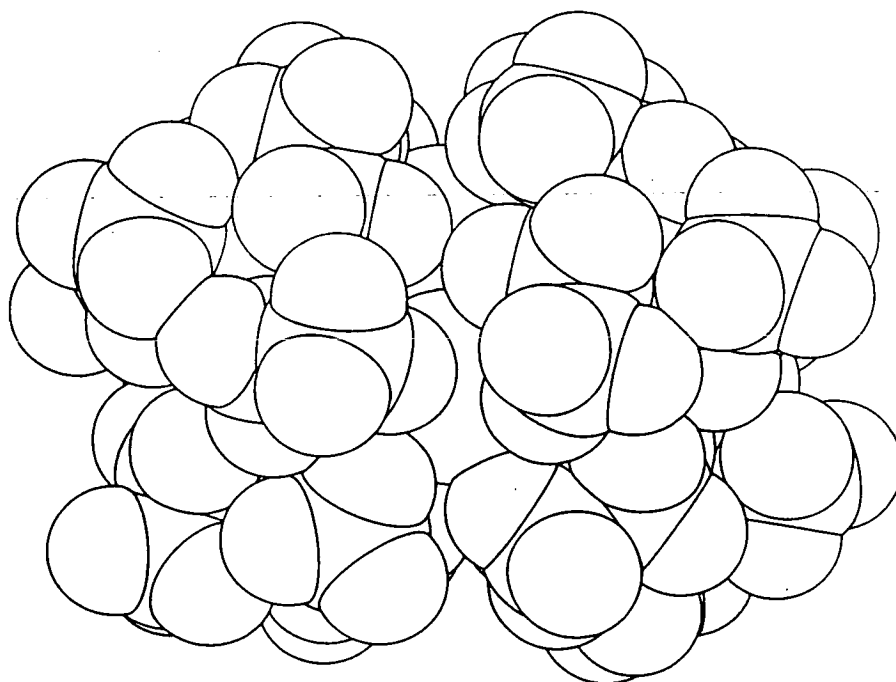
an antibonding orbital the overlap of the contributing orbitals on each metal centre to the e_g^* MOs is small, therefore any strengthening of the bonding associated with the oxidation process would be minimal. Alternatively, if the ordering of the orbitals given in the quantitative calculations[39] is accepted, the electron is formally being removed from the σ_u non-bonding orbital. Attempts were made to extend the known structural data of the cationic complexes by obtaining suitable crystals of $[Ru_3Cl_8(AsPr_3)_4]^+$ but these efforts have yet to bear fruit.

Various unsuccessful attempts were also made to obtain crystals of the reduction products of the trinuclear complexes discussed above. It is reasonable to expect, if the MO diagram is reliable, that reduction, corresponding to addition of an electron to the σ^*-orbital, would significantly weaken any metal-metal bond with a corresponding increase in the Ru-Ru bond length. Crystallographic data for the analogous "Ru_3^{7+}" complexes $[(PR_3)_3Ru(\mu\text{-}Cl)_3Ru(\mu\text{-}Cl)_3Ru(PR_3)_3]^+$ (R = Et, Bu^n) have been reported[45] which, as predicted above, have longer Ru-Ru distances than those observed for $[Ru_3Cl_8(PR_3)_4]$ (R = Et, Ru-Ru = 3.085(1) Å, R = Bu^n, Ru-Ru = 3.083(1) Å). However, direct comparisons between different oxidation states of the same complex would be more reliable, eliminating any possible steric or electronic (other than the change in oxidation state) differences imposed by the extra phosphine ligands in the "Ru_3^{7+}" complexes reported to date.

4.2.5 Magnetic Studies

The magnetic moments of $[Ru_3Cl_8L_4]$ (L = PEt_2Ph, PMe_3, PPr^n_3 or $AsPr^n_3$) were measured. The results of this study are given in Table 4.3. With the exception of $[Ru_3Cl_8(PEt_2Ph)_4]$, the species had very low magnetic moments, which were believed to arise from a small proportion of the complexes being in "high spin" configuration, where one electron is in the a_{1g}^* orbital thus giving a triplet species. In the case of $[Ru_3Cl_8(PEt_2Ph)_4]$, the reason for the higher magnetic moment is unclear but may arise from impurities in the sample studied.

These results are generally consistent with the findings of Cotton and Torralba[39], who reported μ_{eff} values for $[Ru_3Cl_8(PEt_3)_4]$ and $[Ru_3Cl_8(PBu_3)_4]$ of 0.93 and 0.74 BM respectively.

Table 4.3   Magnetic moments of $Ru_3Cl_8L_4$

L	PEt_2Ph	PMe_3	PPr_3	$AsPr_3$
μ_{eff}/BM	1.54	0.47	0.63	0.52

The ^{31}P nmr spectrum of $[Ru_3Cl_8(PEt_2Ph)_4]$ (recorded in $CDCl_3$) shows a singlet peak at 18.7 ppm, although the low solubility resulted in a poor signal to noise ratio and some decomposition was observed. In light of solubility and stability problems (the complexes were generally found to decompose in $CDCl_3$, presumably as a result of impurities in the solvent since the complexes were generally stable in $CHCl_3$) studies of the other complexes were not conducted. Singlets in the ^{31}P nmr spectrum

have also been reported in the literature for complexes of general formula $[Ru_3Cl_8(PR_3)_4]$. The chemical shift of the peak is 8.30 ppm when R = Me, 21.63 ppm when R = Et and 16.34 ppm when R = Bu[28,39].

4.2.6 Electrochemistry

The electrochemistry of the various trinuclear complexes prepared is very similar, all species exhibiting one reversible oxidation and two reversible reductions. We have conducted coulometric studies which show that these are all one electron processes. The potentials (versus Ag/AgCl) at which these processes occur (in CH_2Cl_2) are given in Table 4.4 below. A typical cyclic voltammogram is shown in Figure 4.19.

Table 4.4   Voltammetric data for $[Ru_3X_8L_4]$ in CH_2Cl_2.

X	L	$E_{1/2}$ vs Ag/AgCl
Cl	PEt₂Ph	+1.04, +0.34, -0.55
Cl	PPr₃	+1.02, +0.24, -0.68
Cl	PMe₃	+1.06, +0.34, -0.56
Cl	AsPr₃	+0.98, +0.08, -0.84
Br	PEt₂Ph	+0.90, +0.18, -0.72

Figure 4.19   Cyclic voltammogram of $[Ru_3Cl_x(PEt_2Ph)_4]$ in CH_2Cl_2 at 290 K.
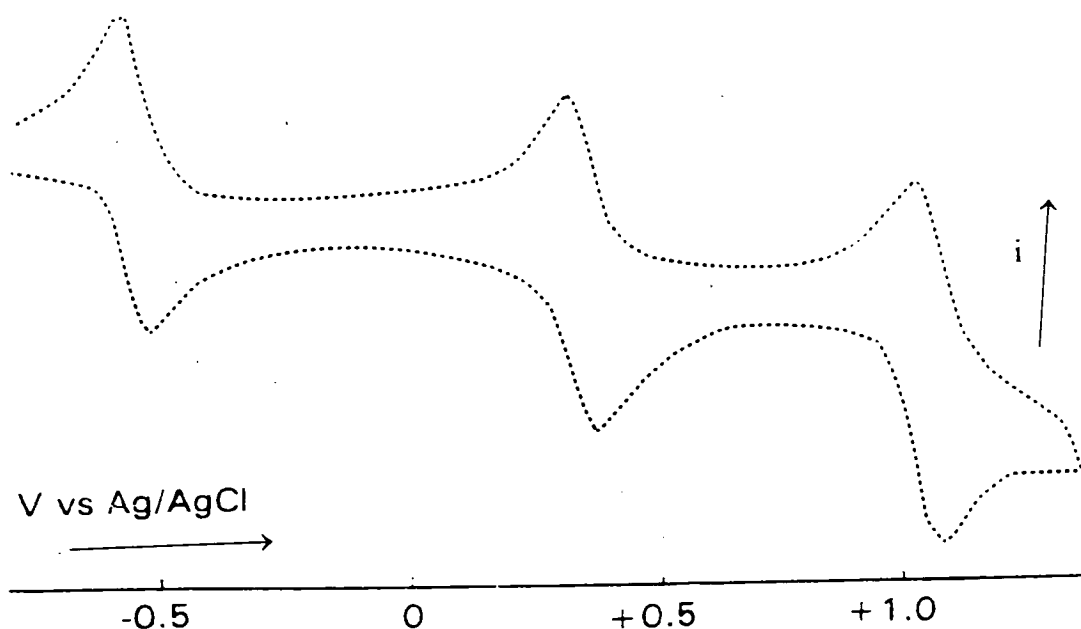
As can be seen from the above data, the effects of the ligands on the redox potentials are generally small, suggesting that both oxidations and reductions are predominantly metal-based. Additionally, the separation of the two reductions is remarkably consistent, ranging from 0.89 V to 0.92 V. This strongly suggests that the second reduction involves addition of an electron to the same orbital as the first reduction. These observations are consistent with delocalised electrons and metal-metal bonding as shown in Figure 4.10.

The separation of pairs of redox couples involving the same orbital is usually, at 0.5 to 0.6 V, close to the electron pairing energy (see, for example, the cyclic voltammogram of tcnq, in Chapter 2). A larger separation, such as that observed with $Ru_3Cl_8L_4$, arises when there is significant perturbation of the species (and the

relevant orbital) upon oxidation or reduction. We suggest that, in this case, the larger separation is related to the weakening, then breaking, of the Ru-Ru bond which arises from the reductions.

On the evidence of the above data it should be possible to prepare the oxidation and reduction products by electrochemical means or by using mild chemical oxidising or reducing agents. The redox potentials show, for example, that it should be possible to prepare the dianions, with the exception of $[Ru_3Cl_8(AsPr_3)_4]^{2-}$, by reduction with cobaltocene ($E_{1/2} = -0.79$ V).

It is noticeable that the replacement of P by As, or Cl by Br, results in a shift to less positive potentials of all the redox processes. This is consistent with increased electron density at the metal centres arising from a less electronegative ligand set. The data also show that the terminal ligands have a larger influence on the reduction potentials than the oxidation, ie. the terminal ligands make a larger contribution to the LUMO than the HOMO.

Electrochemical data reported by Cotton and Torralba[39] are generally similar to the results described above.

4.2.7 Electronic Absorption Spectroscopy

This was an area in which we were particularly keen to compare our results with those previously reported[28,39]. Cotton and coworkers reported that the UV/visible/NIR spectra of $[Ru_3Cl_8(PR_3)_4]$ contained, in addition to several bands in the visible and UV regions of the spectrum, a broad, intense bands with a maximum

between 800 and 850 nm (extinction coefficients were not quoted), depending on the phosphine used. This band was assigned, by comparison with the orbital energies determined by SCF-Xα-SW calculations, to the symmetry forbidden σ_g to σ_g^* transition[39], and the high intensity was attributed to ligand to metal charge transfer arising from the significant metal-ligand interaction within the σ_g orbital[39].

Initial studies of $[Ru_3Cl_8(PEt_2Ph)_4]$ in CH_2Cl_2 had shown a similar NIR band to that described above at 11720 cm^{-1} (850 nm) but had also shown a previously unreported band at 8500 cm^{-1} (see Figure 4.20). The respective extinction coefficients of these bands were 10000 and 6000 mol^{-1}cm^{-1}dm^3, an intensity which made it extremely unlikely that the bands arose from symmetry forbidden transitions.

We have studied the spectra of a range of face sharing trioctahedral compounds, including $[Ru_3Cl_8(PMe_3)_4]$, to determine if the lower energy NIR band was only present in the PEt$_2$Ph complex or was a general feature of these species. The results of this study are given in Table 4.5 and show that two NIR bands are observed in all the complexes prepared thus far. The extinction coefficients of the bands were largely unaffected by changes of ligand. The exception to this rule was the lower energy band in $[Ru_3Cl_8(AsPr_3)_4]$ which had an extinction coefficient of 4000 mol^{-1}cm^{-1}dm^3. Spectra of trinuclear complexes are shown in Figures 4.20 - 4.23.

The qualitative MO diagram in Figure 4.10 predicts two allowed transitions between metal-based orbitals, from e_u to a_{1g}^* and from a_{2u} to a_{1g}^*. It appears to be

more reasonable to assign the NIR bands to these transitions than a symmetry forbidden transition.

Table 4.5   Positions of NIR bands of $[Ru_3X_8L_4]$ in CH_2Cl_2.

$\underline{X}$	$\underline{L}$	$\underline{v_1/cm^{-1}(10^{-3}\varepsilon M^{-1}cm^{-1})}$	$\underline{v_2(10^{-3}\varepsilon)}$
Cl^-	PEt_2Ph	8500(6.0)	11720(10)
Cl^-	PPr_3	8900(6.0)	11860(10)
Cl^-	PMe_3	9100(6.0)	12500(10)
Cl^-	PPh_3*	9400	12500
Cl^-	$P(OMe)_3*$	10000	12500
Cl^-	$AsPr_3$	9400(4.0)	12200(10)
Br^-	PEt_2Ph	8400(6.0)	11200(10)

Note:-

* - Data reported for crude samples, hence ε not quoted.

Prediction of the relative intensities of the two allowed transitions is a non-trivial exercise in this case. Although statistically one might expect transition from the doubly degenerate e_u set to be twice as likely, it is also reasonable to predict that transition between a_{2u} and $a_{1g}*$, which both contain substantial d_z^2 components would occur more readily than e_u to $a_{1g}*$ transitions, as the probability of a transition is related to the square of the overlaps of the relevant orbitals[44]. The relative

intensities of the NIR bands is, therefore, not inconsistent with the ordering of the non-bonding orbitals shown in Figure 4.10, which predicts that the lower energy band will arise from promotion of δ_u based electrons, while the higher energy band arises from the σ_u to σ_g^* transition.

It is interesting to note that the relative intensities of the near infra-red bands *are* inconsistent with the relative energies of the *ungerade* orbitals predicted by the quantitative MO diagrams[39]. Both sets of calculations predict that the σ_u orbital is highest in energy, but is very close to one of the δ_u orbitals, while the other δ_u orbital is at significantly lower energy. On the basis of the calculations, one would predict two NIR bands in the electronic absorption spectrum, with the lower energy band would be considerably more intense than the higher energy band. This is not in accord with the experimental data.

Although the above spectra are generally very similar to each other, there are significant differences. Attempts to explain some of the observed differences are given below.

Let us first consider the effects of the bridging ligands. In bioctahedral complexes, as mentioned in the introduction to this chapter, the metal-metal distance is affected by the steric requirements of the bridging ligand. It is reasonable to expect a similar dependence in face sharing trioctahedral complexes, therefore one would predict a longer Ru-Ru distance in $[Ru_3Br_8(PEt_2Ph)_4]$ than in the corresponding octachloro complex. Consequently, mixing of the Ru orbitals to give metal-metal bonding would be less efficient and transitions to the σ^*-LUMO (from the a_{2u} and e_u non-bonding orbitals, for example) would require less energy. This is

consistent with the differences in the observed spectra of $[Ru_3Cl_8(PEt_2Ph)_4]$ and $[Ru_3Br_8(PEt_2Ph)_4]$, although those differences are fairly small (500 cm^{-1} in the case of the higher energy NIR band).

Conversely, a shorter Ru-Ru bond was observed in structural studies of $[Ru_3Cl_8(AsPr_3)_4]$ than in $[Ru_3Cl_8(PPr_3)_4]$. As a result more efficient mixing of orbitals would be expected in the arsine complex, and one would predict that the bands associated with transitions to the σ^*-LUMO would occur at higher energy in comparison with the corresponding phosphine complex, as was observed in the relevant electronic absorption spectra.

Figure 4.20 Electronic absorption spectrum of $[Ru_3Cl_8(PEt_2Ph)_4]$ in CH_2Cl_2 at 285 K.

216
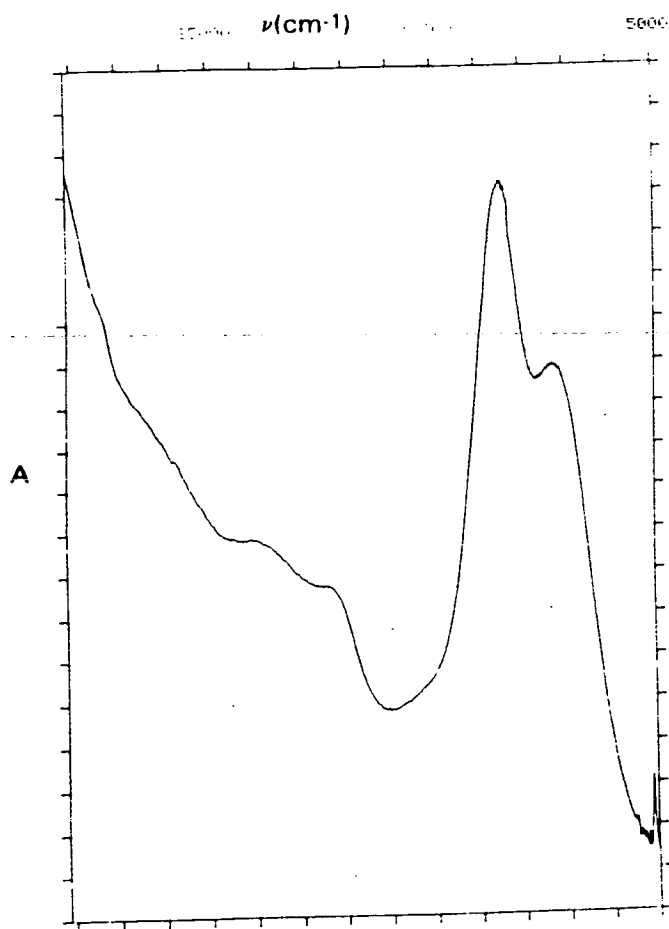
Figure 4.21 Electronic absorption spectrum of $[Ru_3Br_8(PEt_2Ph)_4]$ in CH_2Cl_2 at 290 K.
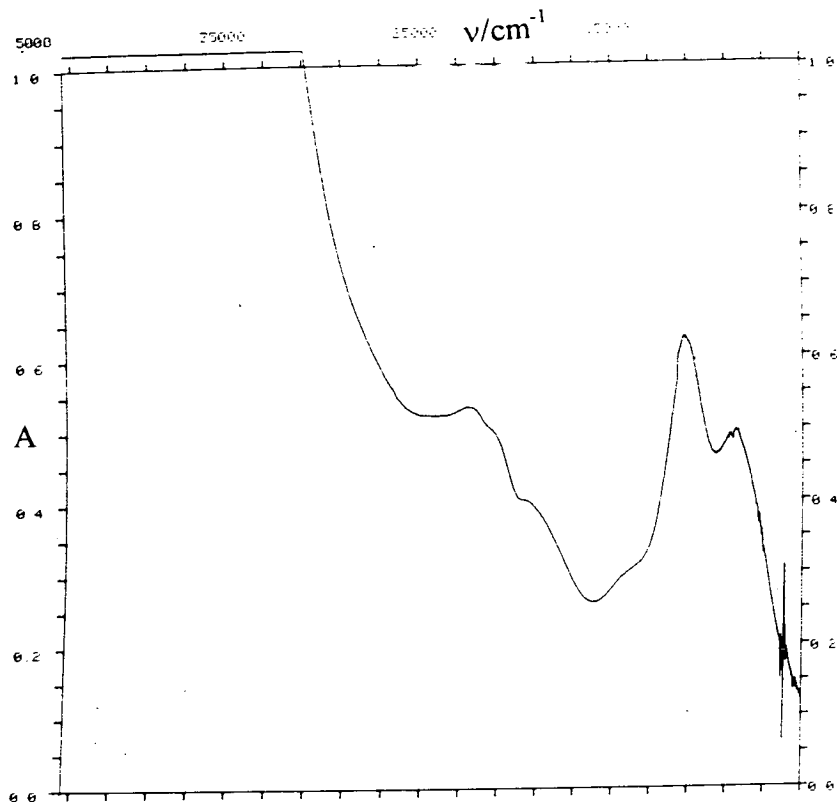
Figure 4.22 Electronic absorption spectrum of $[Ru_3Cl_8(PPr_3)_4]$ in CH_2Cl_2 at 285 K.
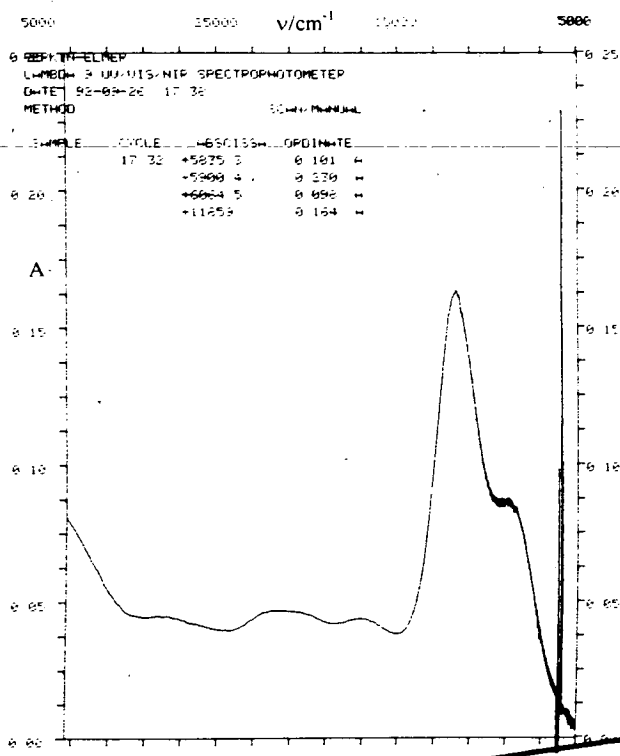
Figure 4.23 Electronic absorption spectrum of [Ru₃Cl₈(AsPr₃)₄] in CH₂Cl₂ at 290 K
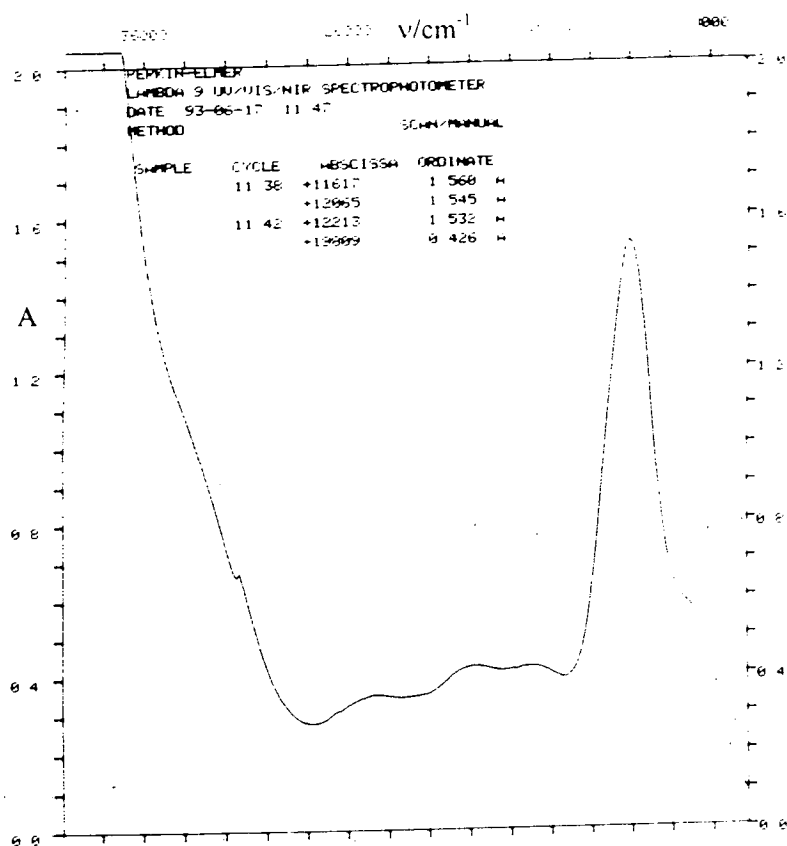
A number of other studies of the electronic absorption spectra of the trinuclear complexes were carried out. These included studies of the temperature dependence of the NIR bands (incorporated into the spectroelectrochemical studies), which showed that the intensities of the bands increased significantly upon cooling, showing that they arise from allowed transitions (Figure 4.24). There was no corresponding decrease in the width of the bands, thus suggesting that they are not classical IVCT bands but instead arise from metal-metal bonding.

Figure 4.24   Effect of cooling from 290 to 250 K on absorption spectrum of
$[Ru_3Br_8(PEt_2Ph)_4]$ in CH_2Cl_2.
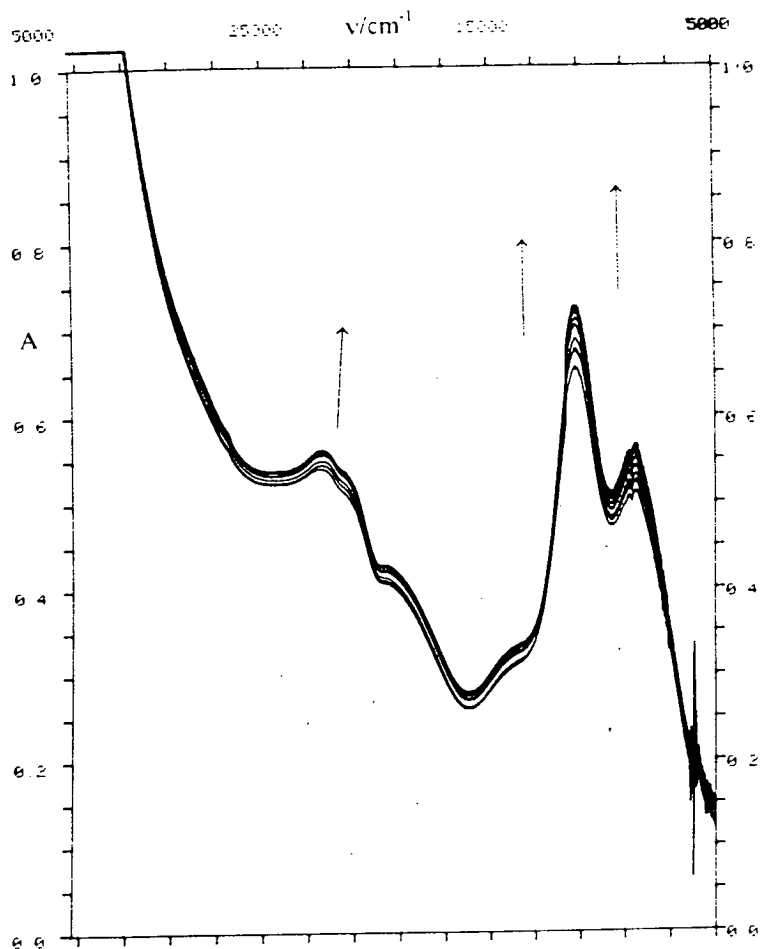
A study was also made of the solvent dependence of the NIR bands.   The

results of this study for $[Ru_3Cl_8(PEt_2Ph)_4]$ are presented in Table 4.6 (the other

complexes gave similar results).   It should be noted that the values of v_1 are

generally less accurate than those of v_2 due to partial superposition of the more

intense higher energy NIR band.   The results of the study show that there is some

variation in the band position with solvent.

Table 4.6   Maxima of the NIR bands of $[Ru_3Cl_8(PEt_2Ph)_4]$ and $[Ru_3Cl_8(PEt_2Ph)_4]^-$

(ν_{an}) in various solvents

Solvent	$1/D_s - 1/D_{op}$ [#]	ν_1/cm^{-1}	ν_2/cm^{-1}	ν_{an}/cm^{-1}
CH_2Cl_2	0.381	8500	11720	9300
$CHCl_3$	0.267	8900	11820	9470
THF	0.372	9000	11850	9560
Me_2CO^*	0.495	ca. 9000	11850	
$MeCN^*$	0.526	ca. 9000	11900	
DMF	0.462	9400	11950	
$DMSO^*$	0.438	9500	12050	

Notes

\# - Data obtained from reference 44.

* - The accuracy of the maxima quoted is reduced by the low solubility of the complex in these solvents.

If the bands arise from e_u to $a_{1g}*$ and a_{2u} to $a_{1g}*$ transitions as predicted above then a certain amount of solvent dependence is to be expected. This is because the formally non-bonding orbitals have, by definition, no contribution from the central Ru therefore electronic transitions from these orbitals to the $a_{1g}*$ LUMO will result in a small amount of charge transfer to the central metal from the terminal ones. As a result the transition would also induce rearrangement of the outer sphere solvent

220

molecules and the energy required for this reorganisation process would vary from solvent to solvent.

In the case of a transition from a_{1g} to $a_{1g}*$, as proposed by Cotton and Torralba[39] both orbitals would be expected to have significant contributions from all three Ru d_{z^2} atomic orbitals therefore there is unlikely to be significant charge transfer upon excitation and the position of the resultant band in the electronic absorption spectrum should be independent of the solvent. Clearly, this was not the case, therefore it is reasonable to conclude that the NIR bands arise from the symmetry allowed transitions (e_u and a_{2u} to $a_{1g}*$). It is interesting to note that, contrary to the predictions of Equation 4.3,[16] there is not a linear relationship between v and ($1/D_s$ - $1/D_{op}$).

Studies of the UV/visible/NIR spectroelectrochemistry were also carried out at 240 or 250 K. Once again behaviour of the various species followed a general pattern. Oxidation resulted in collapse of both NIR bands. Disappearance of both NIR bands was also observed upon reduction to the dianion. Formation of the monoanion, however, resulted in collapse of the higher energy NIR band leaving a single NIR bands with intensity close to that of the lower energy band in the neutral complex. Usually the position of this band is slightly greater than that of the lower energy band, the exception to this rule being [$Ru_3Br_8(PEt_2Ph)_4$] in which the energy of the band in the reduction product is very close in energy to the higher energy band in the neutral complex. Spectra illustrating these phenomena are shown in Figures 4.25 - 4.35. below.

The observed behaviour upon reduction is consistent with metal-metal bonding, as shown in the qualitative MO diagram shown in Figure 4.10. The first reduction involves addition of an electron to the a_{1g}^* LUMO, and would thus be expected to weaken the Ru-Ru bond, resulting in an increased Ru-Ru distance and less efficient mixing of Ru based orbitals with the corresponding orbitals on the other Ru atoms. It is therefore reasonable to expect that the energy of the a_{1g}^* LUMO would be lowered by reduction of the complex, thus reducing the energy required to promote electrons to this orbital. After the second reduction has taken place, the σ_g^* orbital is fully occupied, hence the absence of NIR bands in the electronic absorption spectrum.

The disappearance of the NIR bands upon oxidation was rather more surprising. The observed changes upon oxidation suggest that a localised system in which the Ru atoms are not bound to each other is being formed, possibly as a result of the increased electrostatic repulsion between the metal centres. As mentioned earlier, a structural study of the oxidised complex $[Ru_3Cl_8(PEt_3)_4]^+$ has been reported by Cotton and Torralba[39]. While this study did show an increase in the Ru-Ru bond length upon oxidation, the new distance was perhaps less (at 2.91 Å) than that which might be expected in a localised system where there was no metal-metal bonding.

Figure 4.25   Absorption spectral monitoring of reduction of $[Ru_3Cl_8(PMe_3)_4]$ in CH$_2$Cl$_2$ at 240 K, E$_{app}$ = +0.1 V.
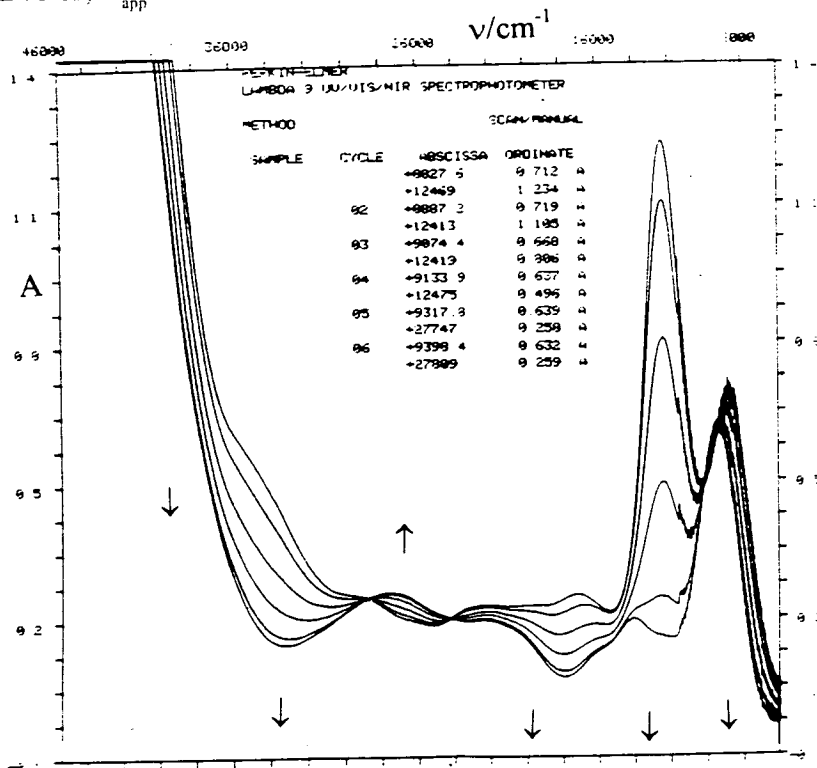
Figure 4.26   Absorption spectrum of $[Ru_3Cl_8(PMe_3)_4]^-$ in CH$_2$Cl$_2$ at 240 K.
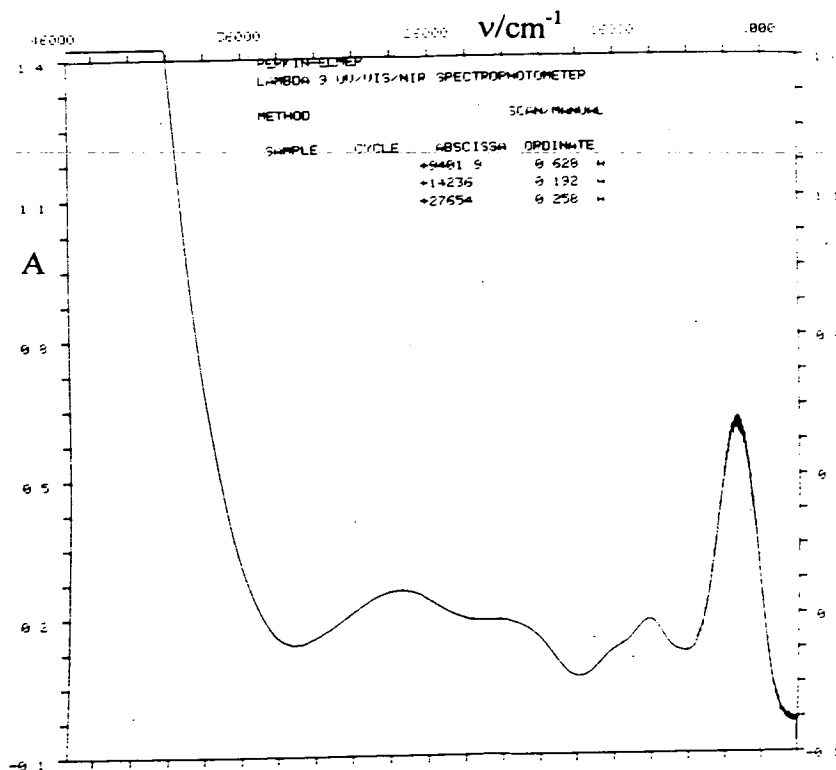
Figure 4.27   Absorption spectra showing reduction of $[Ru_3Cl_8(PMe_3)_4]^-$, CH_2Cl_2, 240 K, E_{app} = -0.8 V.
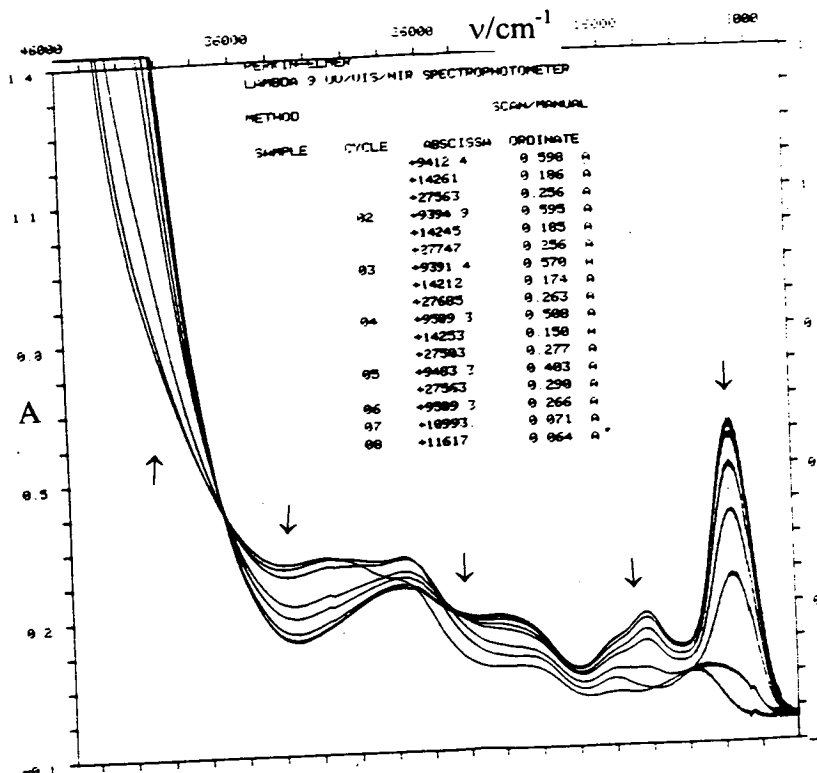
Figure 4.28   Absorption spectrum of $[Ru_3Cl_8(PMe_3)_4]^{2-}$ in CH_2Cl_2 at 240 K.
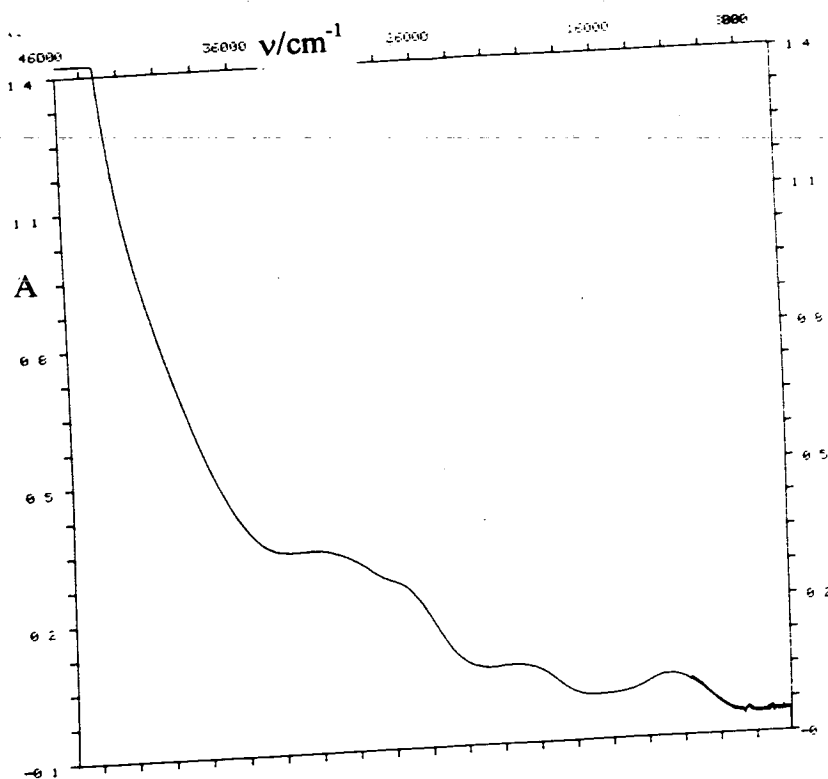
Figure 4.29   Absorption spectra showing reduction of $[Ru_3Cl_8(PMe_3)_4]^+$ in CH_2Cl_2

at 240 K, $E_{app} = +0.8$ V.
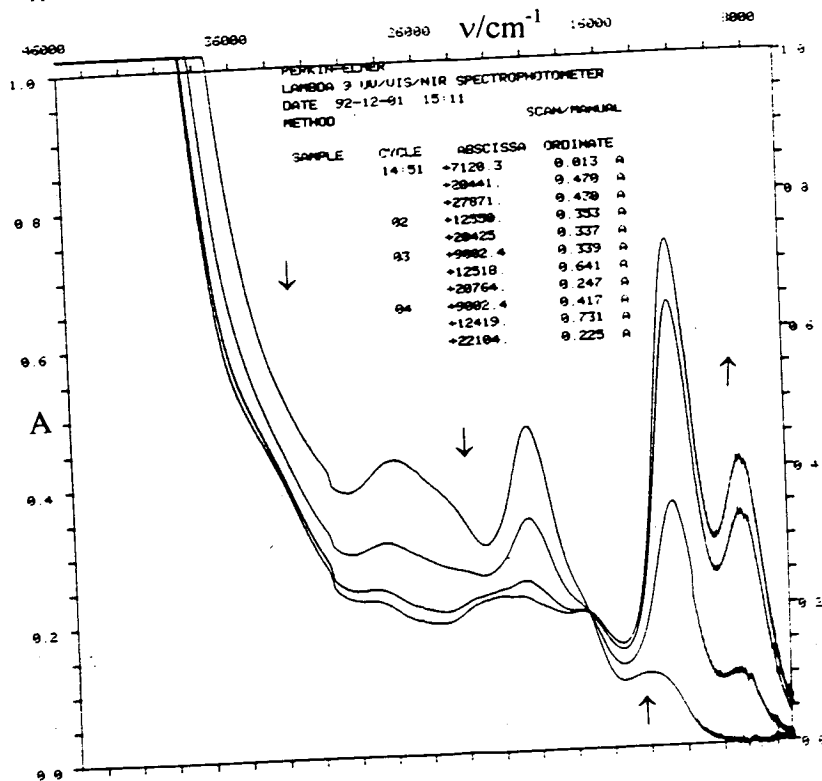
Figure 4.30   Absorption spectrum of $[Ru_3Cl_8(PMe_3)_4]^+$ in CH_2Cl_2 at 240 K.
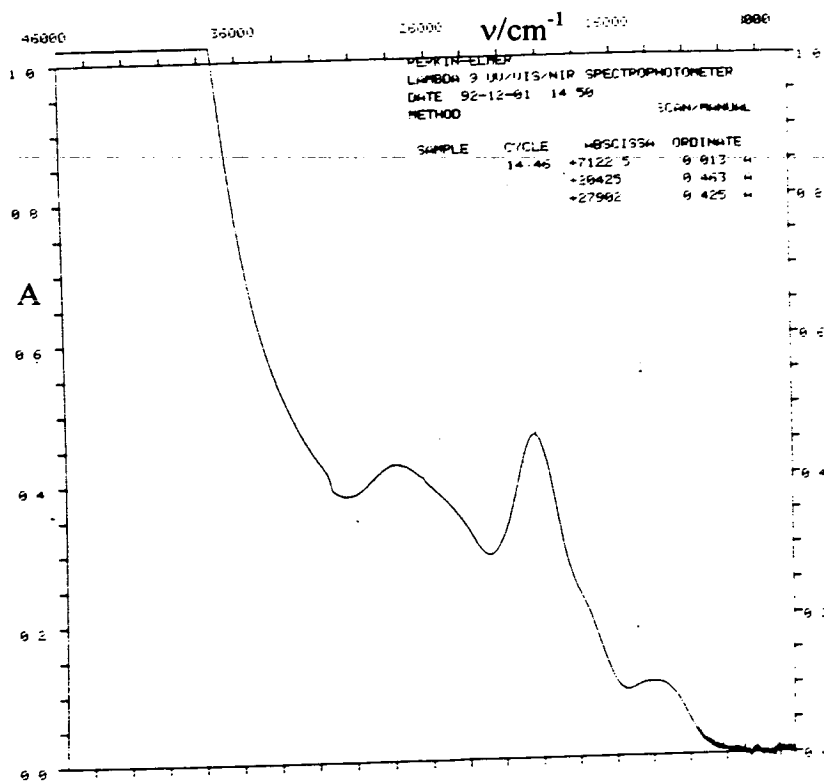
Figure 4.31   Absorption spectral monitoring of reduction of $[Ru_3Cl_8(AsPr_3)_4]$ in

CH_2Cl_2 at 240 K, E_{app} = -0.2 V.
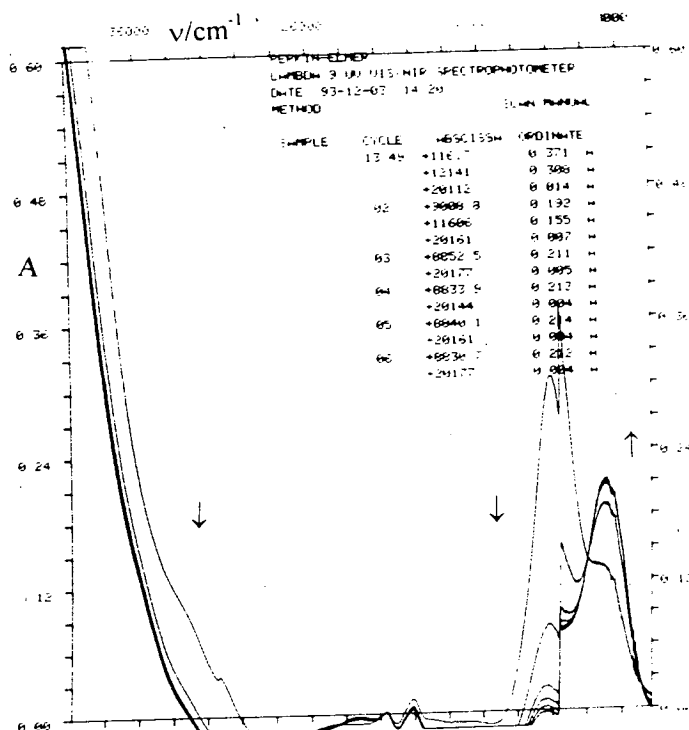
Figure 4.32   Absorption spectra showing reduction of $[Ru_3Cl_8(AsPr_3)_4]^-$ in CH_2Cl_2

at 240 K, E_{app} = -1.1 V.
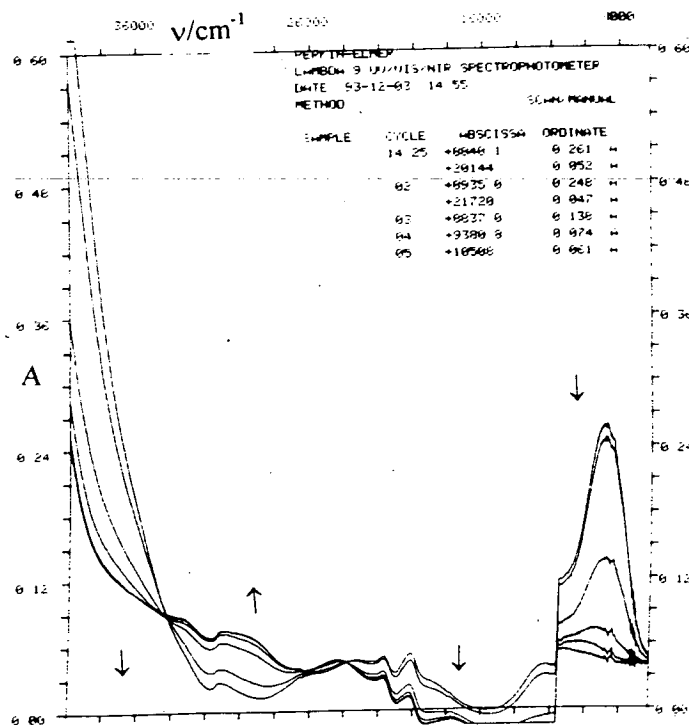
Figure 4.33   Absorption spectra showing oxidation of $[Ru_3Cl_8(AsPr_3)_4]$ in CH_2Cl_2

at 240 K, $E_{app} = +1.2$ V.
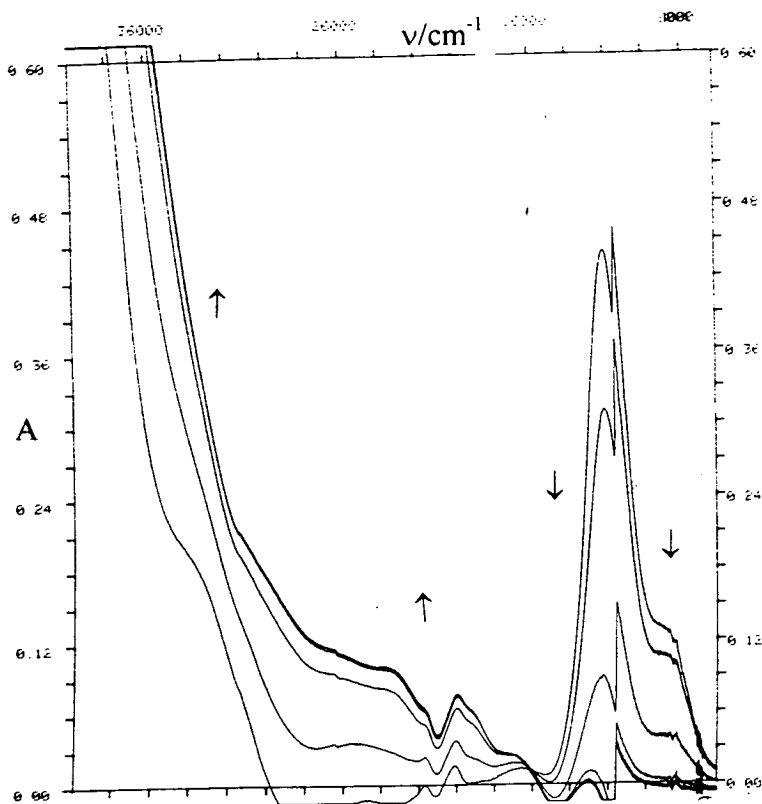
Figure 4.34   Absorption spectra showing reduction of $[Ru_3Br_8(PEt_2Ph)_4]$ in CH_2Cl_2

at 250 K, $E_{app} = -0.1$ V.
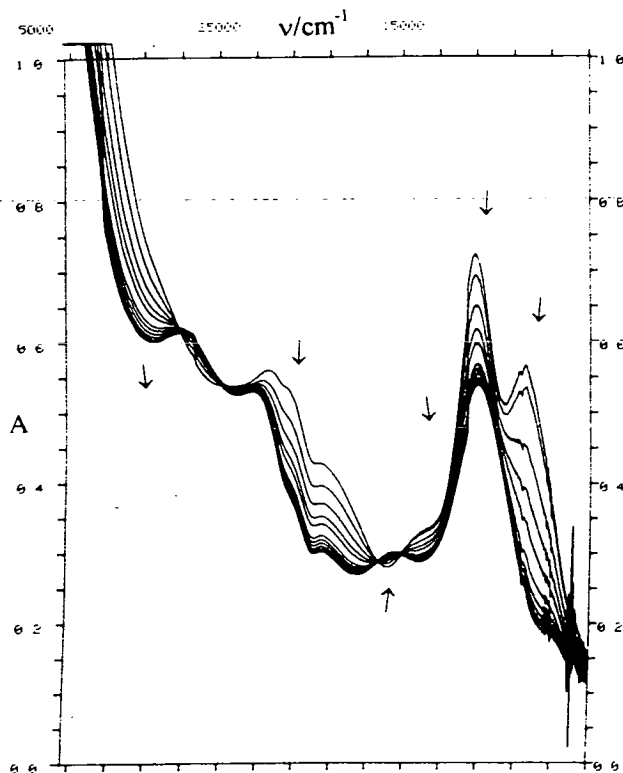
Figure 4.35 Absorption spectrum of [Ru$_3$Br$_8$(PEt$_2$Ph)$_4$]$^-$ in CH$_2$Cl$_2$ at 250 K.

5000   25000   v/cm^{-1} 15000

PERKIN-ELMER
LAMBDA 9 UU/UIS/NIR SPECTROPHOTOMETER
DATE 92-09-29 15:52
METHOD   SCAN/MANUAL

SAMPLE   CYCLE   ABSCISSA   ORDINATE
            15:47   +5776.3   0.155 A
                       +5863.9   0.189 A
                       +5928.4   0.270 A
                       +6003.6   0.156 A
                       +6095.3   0.161 A
                       +11037   0.538 A

A
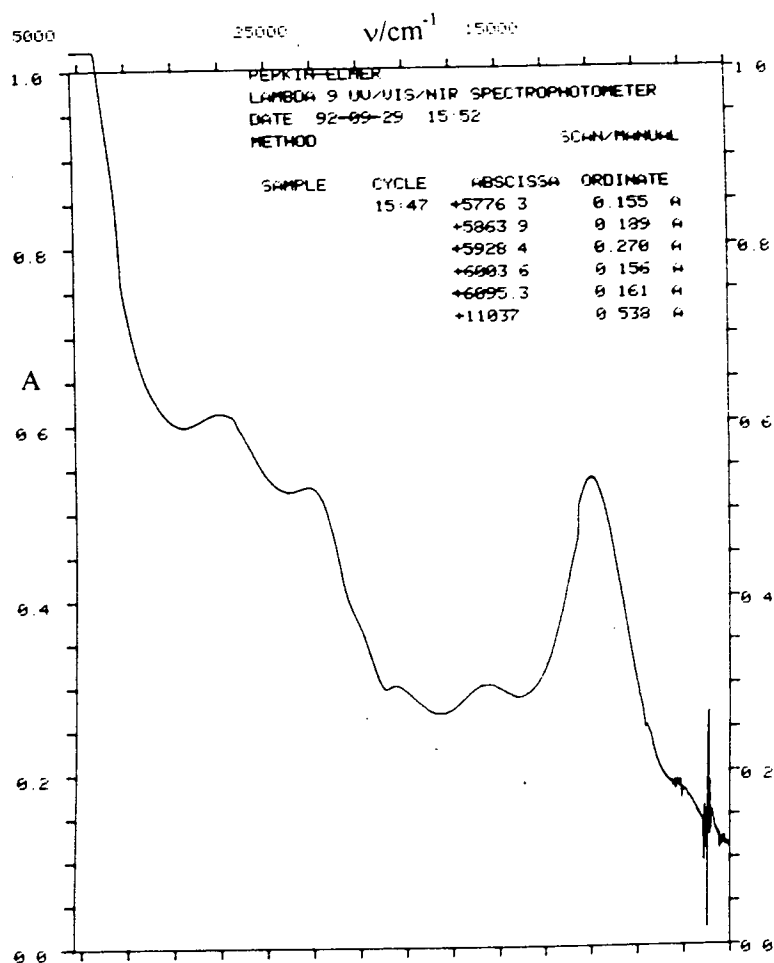
According to Hush theory[16], for a class II mixed-valence system, the width of any IVCT bands should agree to within 10% with the calculated value obtained from the equation

$$\Delta_{1/2}(\text{calc}) = (2310\nu_{CT})^{1/2} \text{ cm}^{-1}$$

as described in the introduction to this chapter. For [Ru$_3$Cl$_8$(PEt$_2$Ph)$_4$], in CH$_2$Cl$_2$, the calculated values of $\Delta_{1/2}$ for the bands at 8500 and 11720 cm^{-1} are 4430 and 5200 cm^{-1} respectively. Although accurate determination of the actual widths is hampered by the partial superposition of the two bands, $\Delta_{1/2}$ for the higher energy NIR band is

228

approximately 3000 cm^{-1}, considerably less than that predicted by Hush's equation. In the case of the anion, the maximum of the single NIR band is at 9300 cm^{-1} and has a band width of 2800 cm^{-1}, considerably less than the $\Delta_{1/2}$(calc) value of 4630 cm^{-1}. Similar results are obtained with the other trioctahedral complexes.

The degree of electron delocalisation may be obtained from the equation

$$\alpha^2 = 4.24 \times 10^{-4}(\varepsilon\Delta_{1/2}/\nu_{CT}d^2)$$

as described earlier. In class II mixed-valence species α lies between 0 and 0.25. Application of the above equation to [Ru$_3$Cl$_8$(PEt$_2$Ph)$_4$], using $\Delta_{1/2}$ values of 3000 cm^{-1} for both NIR bands, gives values of α of 0.33 for the lower energy band and 0.37 for the higher energy one. For the NIR band in [Ru$_3$Cl$_8$(PEt$_2$Ph)$_4$]$^-$, α was estimated (using d = 3.0 Å) to be 0.29.

In general, the above calculations show that, according to Hush theory, face sharing trioctahedral complexes show a greater degree of delocalisation than would be expected for a class II mixed-valence complex. The apparent degree of delocalisation, allied with the narrowness of the NIR bands, is consistent with Ru-Ru bonding.

4.2.8 EPR Spectroelectrochemistry

[Ru$_3$Cl$_8$(QR$_3$)$_4$] (Q = P, As) was EPR silent, as was its dianion, observations which were consistent with the MO diagram in Figure 4.10, which predicts that the

neutral complex and the dianion do not have any unpaired electrons. The oxidation product also failed to yield a signal at 77 K, consistent with the rapid relaxation that is observed when the species under study is in a multiply degenerate (or near degenerate) ground state. This suggests that there is at least one other orbital very close in energy to the SOMO. This could be confirmed by a study at lower (liquid He) temperatures, which may slow the relaxation process sufficiently to give an observable signal, but facilities for such a study were not available.

$[Ru_3Cl_8(QR_3)_4]^-$ was EPR active, and examples of the spectra obtained at 77 K are shown in Figures 4.36 and 4.37. Attempts to obtain isotropic spectra were invariably unsuccessful, although the reasons for this are not immediately apparent.

In the case of $[Ru_3Cl_8(AsPr_3)_4]^-$ (Figure 4.36), the anisotropic spectrum appears to be rather simpler than the spectra obtained with the phosphine complexes. At 77 K, in frozen CH_2Cl_2, the spectrum shows a rhombic signal with g_1 = 2.16, g_2 = 2.03 and g_3 = 1.86.

Assignment of the spectra of the anions in the cases of the phosphine ligands is no easy matter. Although a casual inspection of the spectrum of $[Ru_3Cl_8(PMe_3)_4]^-$ might suggest an axial signal with g values of 1.74 and 2.17, more careful study of the spectrum shows that the actual situation is more complicated (Figure 4.37). The two peaks at g values of 2.08 and 2.31 may appear to be satellites of the resonance at g = 2.17, but there is no element present which has a "moderately abundant" (20 - 60%, say) I = 1/2 isotope to induce such an effect (ruthenium possesses two I = 5/2 isotopes, ^{99}Ru, which has a natural abundance of 12.72% and ^{101}Ru, which has a

natural abundance of 17.07%). The spectrum of $[Ru_3Cl_8(PEt_2Ph)_4]^-$ is generally similar, with $g_3 = 1.73$, the crossover point at $g = 2.14$ and further peaks at $g = 2.01$ and 2.25 (with a shoulder at $g = 2.31$).

By way of comparison, spectra of the cobaltocenium salt of $[Ru_3Cl_8(PBu_3)_4]^-$ were reported as having a rhombic signal, with $g_1 = 2.23$, $g_2 = 2.11$ and $g_3 = 1.75$ but no spectra were actually shown in the paper[39], therefore a more detailed comparison is impossible.

Comparison is, however possible with epr spectra of the related face sharing bioctahedral complexes of general formula $[Ru_2Cl_5(PR_3)_4]$. The majority of the reported spectra[7] are for complexes of formula $[Cl(PR_3)_2Ru(\mu-Cl)_3Ru(PR_3)_2Cl]$, in which Ru-Ru bonding is observed. In these spectra the g-values (all the spectra have rhombic signals) obtained are not dissimilar to those obtained for the trinuclear anions, and the linewidths are very large, as was also observed with the trinuclear complexes. Conversely, the spectrum of $[Cl_2(PBu_3)Ru(\mu-Cl)_3Ru(PBu_3)_3]$, in which Ru-Ru bonding was not observed, shows an axial signal with $g_\perp = 2.44$ and $g_\parallel = 1.59$, but the peaks in the 1st derivative spectrum are much narrower.

At present a more detailed discussion of the epr spectra of complexes of formula $[Ru_3Cl_8(QR_3)_4]^-$ is impossible, but the linewidths and complexity of the spectra obtained are not inconsistent with Ru-Ru bonding. Further light might be shed by the recording of spectra at lower temperatures, or by the recording of "Q-band" spectra.

Figure 4.36 EPR spectrum of $[Ru_3Cl_8(AsPr_3)_4]^-$ in CH_2Cl_2 at 77 K.

$v = 9.35$ Ghz

2800 G

3800 G
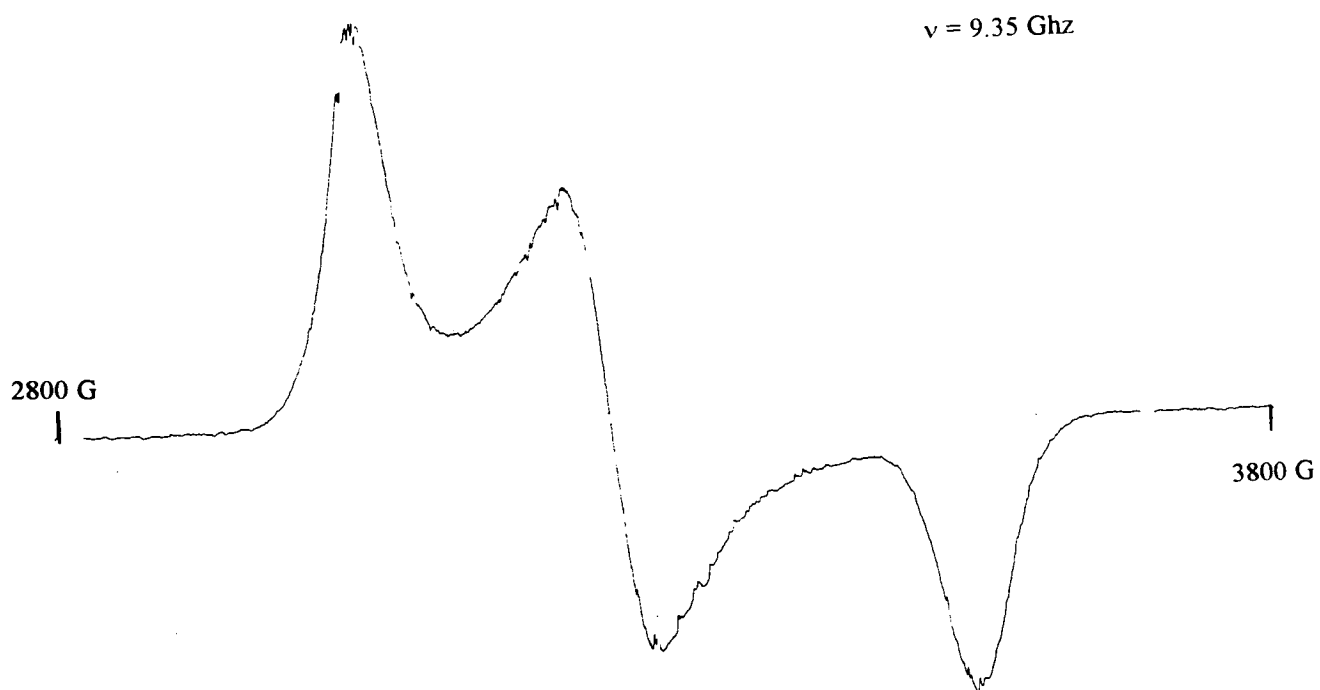
Figure 4.37 EPR spectrum of $[Ru_3Cl_8(PMe_3)_4]^-$ in CH_2Cl_2 at 77 K.

$v = 9.35$ Ghz

4300 G

2300 G
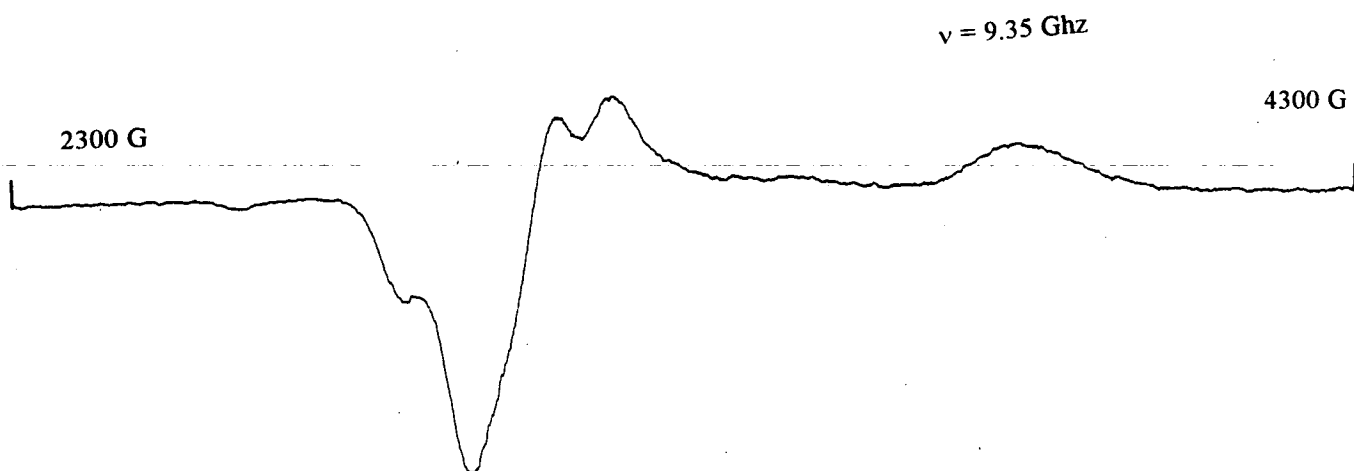
4.2.9 Conclusions

In general, the experimental data obtained for face sharing trioctahedral complexes of general formula $[Ru_3X_8(QR_3)_4]$ (X = Cl, Br, Q = P, As) are consistent with strong Ru-Ru interactions and delocalisation over the Ru centres of metal-based valence electrons. Specific evidence was found, for example, in the crystallographic studies, where the Ru-Ru distance was shorter than that in previously reported face sharing bioctahedral complexes which exhibited Ru-Ru bonding (2.81 - 2.86 Å[39] as compared with 2.97 - 3.20 Å for the Ru^{III}-Ru^{III} complexes[7] and 2.99[7] - 3.41[10] Å for Ru^{II}-Ru^{III} complexes, in the species with chloride bridging ligands) and the Ru-Cl(b)-Ru bond angles are relatively low - the mean angle for the new structures reported in this work is 72.3°.

Further evidence of Ru-Ru bonding was obtained, for example, in the NIR region of the electronic absorption spectrum which contained two intense bands, both of which were considerably narrower than predicted for a Class II mixed-valence complex by Hush Theory[16]. Metal-metal bonding was also supported by the low magnetic moments of the complexes, and the electrochemical studies, where three one-electron processes were observed.

In general the results obtained for the neutral complexes and the reduction products are consistent with the predictions of the qualitative MO diagram in Figure 4.10 (the first reduction appears to weaken the Ru-Ru interactions, while the second reduction breaks them). The case of the oxidation product is less clear cut, however. The absence of strong NIR bands in the electronic absorption spectrum suggests that

the Ru-Ru bonds have been broken by the increased electrostatic repulsion between the metals, and the structural study reported by Cotton and Torralba[39] shows an increase in the Ru-Ru distance, but not one so large as to suggest that the bonds have been broken. Also, the lack of an observable EPR signal at 77 K, which is suggestive of rapid relaxation arising from a multiplet ground state, is perhaps more consistent with a Ru-Ru bond rather than a localised system (an axial signal was reported for $[Ru_3Cl_8(PEt_3)_4][SbF_6]$ with $g\perp$ = 2.43 and $g_\parallel$ = 1.66[39]). Further light might be shed on the nature of $[Ru_3X_8L_4]^+$ by the recording of lower temperature EPR spectra (ie. using liquid He as coolant).

4.3 Experimental

CH_2Cl_2 was purified by neutralisation over KOH pellets, followed by distillation over P_2O_5, under N_2. THF was purified by distillation, under N_2, over Na wire and benzophenone. Et_2O was stored over Na wire. MeCN, Toluene, MeOH and EtOH were used as supplied.

$RuCl_3.xH_2O$ was stored in a dessicator and used as supplied (by Aldrich). PEt_2Ph, PPr^n_3 and $AsPr^n_3$ were stored in sealed ampules of known mass. PMe_3 was supplied as the 1.0 M solution in THF by Aldrich. $P(OMe)_3$ was supplied by Aldrich. Both PMe_3 and $P(OMe)_3$ were stored under N_2 and used as supplied. PPh_3 was also supplied by Aldrich and purified by recrystallisation from ethanol prior to use.

Silica gel G, used in all purifications, was supplied by Fluka.

234

All reactions, purifications and recrystallisations were carried out under N_2 or Ar.

The equipment used was the same as that used in Chapter 3, except as amneded below. EPR spectra were recorded using "conventional" EPR tubes. Electrosyntheses, when necessary for the recording of EPR spectra, were carried out at 233 K in a coulometric cell, using the Hi-Tek PPR1 waveform generator as the potential source. Magnetic moment measurements were carried out in the solid state, at room temperature (the temperature was measured in each case) using a Johnson Matthey magnetic susceptibility balance. All IR spectra were recorded on the Perkin-Elmer 598 IR spectrometer. Thioglycerol was again used as the matrix in the recording of FAB mass spectra.

Initial Preparation of $[Ru_3Cl_8(PEt_2Ph)_4]$

This preparation followed the method published by Chatt et al for synthesis of $[RuCl_3(PEt_2Ph)_3]$[40]. PEt_2Ph (1.0 g) was added to a deaerated solution of $RuCl_3.xH_2O$ (400 mg) and HCl (1 ml) in EtOH (10 ml). The reaction mixture was heated under reflux for 5 minutes then allowed to cool, the product mixture precipitating overnight. The product mixture was isolated by filtration (yield = 380 mg). Separation of the products was by column chromatography over silica gel G. Elution with CH_2Cl_2 gave $[Ru_3Cl_8(PEt_2Ph)_4]$, in pure form, as the first band (yield = 120 mg, 19%), while subsequent elutions with THF and MeCN yielded $[Ru_2Cl_5(PEt_2Ph)_4]$ and $[Ru_2Cl_3(PEt_2Ph)_6]^+$ respectively.

Crystals of the trinuclear complex suitable for single crystal X-ray diffraction were grown by diffusion of Et_2O into a CH_2Cl_2 solution of the complex.

Elemental analysis.　　　Found:-　　　　　%C = 42.0, %H = 5.76.

　　Calculated for $Ru_3Cl_8P_4C_{40}H_{60} \cdot 2C_4H_{10}O$:-　　%C = 41.2, %H = 5.76.

FAB Mass spectroscopy.

　　Found m/z = 1254 (expect, for $[Ru_3C_{40}H_{60}P_4Cl_8]^+$, m/z = 1250).

THF eluted fraction:-

　　Found m/z = 1044 (expect, for $[Ru_2C_{40}H_{60}P_4Cl_5]^+$, m/z = 1043)

MeCN eluted fraction:-

　　Found m/z = 1304 (expect, for $[Ru_2C_{60}H_{90}P_6Cl_3]^+$, m/z = 1305)

Crystal Data For $[Ru_3Cl_8(PEt_2Ph)_4]$

$Ru_3Cl_8C_{40}H_{60}P_4 \cdot C_4H_{10}O$, 　MW　=　1325.8,

Triclinic, Space group P$\overline{1}$, a = 9.744(9), b = 10.404(7), c = 13.417(12) Å, α = 88.70(7), β = 83.41(12), γ = 85.68(5)°, V = 1347 Å^3, (refined from 22 2θ reflections in the range 24 ≤ 2θ ≤ 26°, λ = 0.71073 Å), Z = 1, D_c = 1.64 gcm^{-3}, Data collected at 150.0(1) K, Dark red column of dimensions 0.08 x 0.12 x 0.27 mm, μ(Mo-Kα) = 1.304 mm^{-1}, F(000) = 628.

Data Collection and Processing

　　　　　　　The crystal was mounted within a mineral oil film on a Stadi-4 diffractometer and data were collected at 150 K in the ω - 2θ mode

using graphite-monochromated MoKα radiation, with a scan width of $(1.20 + 0.347 \tan\theta°)$, $5 \leq 2\theta \leq 45°$. 3857 data were collected $(-10 \leq h \leq 10, -11 \leq k \leq 11, 0 \leq l \leq 14)$. Of the 2702 unique reflections $(R_{int} = 0.050)$, 2101 with $F \geq 4\sigma(F)$ were used in all calculations. During data collection a 4.5% variation was observed in the selected standard reflections.

Structure Analysis and Refinement

Structure solution and refinement were carried out using SHELX76[41], one of the Ru atoms of the assymetric unit being located by Patterson Synthesis. All other non-hydrogen atoms were located by iterative cycles of least squares refinement and difference Fourier synthesis, all Ru, Cl and P atoms being allowed to refine anisotropically. All H atoms were refined in fixed, calculated positions (using the AFIX command). The C atoms of the phenyl rings were constrained to refine as regular hexagons, also using the AFIX command. An absorption correction was made using DIFABS[42] (maximum and minimum correction fators were 1.569 and 0.795 respectively). The weighting scheme $w^{-1} = \sigma^2(F) + 0.00158F^2$ gave satisfactory agreement analyses. At convergence, $(\Delta/\sigma)_{max}$ in the final cycle was 0.025 (for z/c in Cl$_s$; outwith the solvent atoms $(\Delta/\sigma)_{max}$ was 0.008) and the final values of R and R$_w$ were 0.060 and 0.076 respectively for 146 parameters, S = 1.060. The final Fourier synthesis showed no important features and the maximum and minimum residues were 1.29 (1.05 Å from Ru1) and -0.98 eÅ^{-3} respectively.

237

Table 4.7 Atomic coordinates for $[Ru_3Cl_8(PEt_2Ph)_4]$, with esds in parentheses.

	x	y	z	Ueq
Ru(1)	0.09068(11)	0.08793(9)	0.17850(9)	0.0134(7)
Ru(2)	0.00000(0)	0.00000(0)	0.00000(0)	0.0128(10)
Cl(1B)	-0.1089(3)	-0.0438(3)	0.1618(3)	0.0192(21)
Cl(2B)	0.2133(3)	-0.0678(3)	0.0586(3)	0.0172(21)
Cl(3B)	0.0162(3)	0.2164(3)	0.0430(3)	0.0152(20)
Cl(1T)	0.1610(3)	-0.0386(3)	0.3129(3)	0.0246(23)
P(1)	0.2895(3)	0.2000(3)	0.1633(3)	0.0162(22)
C(10)	0.2707(9)	0.3739(5)	0.1862(7)	0.013(3)
C(11)	0.2150(9)	0.4556(5)	0.1149(7)	0.026(4)
C(12)	0.2048(9)	0.5888(5)	0.1281(7)	0.025(3)
C(13)	0.2504(9)	0.6401(5)	0.2126(7)	0.024(3)
C(14)	0.3061(9)	0.5583(5)	0.2839(7)	0.031(4)
C(15)	0.3162(9)	0.4252(5)	0.2707(7)	0.022(3)
C(16)	0.3749(13)	0.1957(11)	0.0362(11)	0.018(3)
C(17)	0.4998(14)	0.2808(12)	0.0121(12)	0.025(4)
C(18)	0.4234(14)	0.1385(12)	0.2383(12)	0.026(4)
C(19)	0.4967(15)	0.0078(13)	0.2068(13)	0.030(4)
P(2)	-0.0458(3)	0.2169(3)	0.2972(3)	0.0157(22)
C(20)	-0.1162(9)	0.3728(6)	0.2548(7)	0.019(3)
C(21)	-0.0633(9)	0.4879(6)	0.2784(7)	0.019(3)
C(22)	-0.1230(9)	0.6054(6)	0.2462(7)	0.031(4)
C(23)	-0.2356(9)	0.6079(6)	0.1905(7)	0.039(4)
C(24)	-0.2885(9)	0.4929(6)	0.1670(7)	0.033(4)
C(25)	-0.2289(9)	0.3753(6)	0.1991(7)	0.025(4)
C(26)	-0.2042(14)	0.1457(12)	0.3526(11)	0.022(3)
C(27)	-0.1799(16)	0.0222(13)	0.4136(13)	0.035(4)
C(28)	0.0421(13)	0.2530(12)	0.4045(11)	0.019(3)
C(29)	-0.0503(15)	0.3154(13)	0.4952(12)	0.027(4)
C(1S)	0.505(4)	0.456(3)	0.498(3)	0.122(12)
C(2S)	0.371(4)	0.406(4)	0.546(3)	0.056(10)
C(3S)	0.509(4)	0.181(4)	0.546(3)	0.058(11)
C(4S)	0.425(5)	0.292(4)	0.547(4)	0.070(12)
C(5S)	0.514(5)	0.367(4)	0.505(4)	0.074(13)

Table 4.8 Atomic coordinates of H atoms for $[Ru_3Cl_8(PEt_2Ph)_4]$.

	x	y	z	Ueq
H(11)	0.1797	0.4159	0.0495	0.0400
H(12)	0.1617	0.6521	0.0729	0.0400
H(13)	0.2425	0.7432	0.2228	0.0400
H(14)	0.3413	0.5981	0.3493	0.0400
H(15)	0.3594	0.3619	0.3259	0.0400
H(16A)	0.2984	0.2269	-0.0132	0.0400
H(16B)	0.4117	0.0970	0.0203	0.0400
H(17A)	0.5411	0.2697	-0.0657	0.0400
H(17B)	0.5792	0.2508	0.0594	0.0400
H(17C)	0.4659	0.3807	0.0259	0.0400
H(18A)	0.3766	0.1284	0.3148	0.0400
H(18B)	0.5006	0.2082	0.2350	0.0400
H(19A)	0.5741	-0.0199	0.2563	0.0400
H(19B)	0.5459	0.0157	0.1308	0.0400
H(19C)	0.4219	-0.0641	0.2105	0.0400
H(21)	0.0239	0.4859	0.3215	0.0400
H(22)	-0.0820	0.6945	0.2645	0.0400
H(23)	-0.2818	0.6989	0.1657	0.0400
H(24)	-0.3757	0.4948	0.1239	0.0400
H(25)	-0.2698	0.2863	0.1809	0.0400
H(26A)	-0.2633	0.1242	0.2925	0.0400
H(26B)	-0.2633	0.2159	0.4014	0.0400
H(27A)	-0.2782	-0.0127	0.4432	0.0400
H(27B)	-0.1219	0.0418	0.4748	0.0400
H(27C)	-0.1220	-0.0499	0.3659	0.0400
H(28A)	0.1205	0.3182	0.3793	0.0400
H(28B)	0.0909	0.1638	0.4305	0.0400
H(29A)	0.0128	0.3323	0.5540	0.0400
H(29B)	-0.1289	0.2515	0.5229	0.0400
H(29C)	-0.0993	0.4059	0.4717	0.0400

Table 4.9 Anisotropic thermal parameters in Å^2 for $[Ru_3Cl_8(PEt_2Ph)_4]$.

	U11	U22	U33	U23	U13	U12
Ru(1)	0.010(1)	0.013(1)	0.018(1)	-0.003(0)	-0.005(1)	0.001(0)
Ru(2)	0.007(1)	0.013(1)	0.018(1)	-0.004(1)	-0.003(1)	0.001(1)
Cl(1B)	0.014(2)	0.021(2)	0.023(3)	-0.002(2)	-0.002(2)	-0.005(1)
Cl(2B)	0.014(2)	0.016(2)	0.021(3)	-0.003(1)	-0.007(2)	0.002(1)
Cl(3B)	0.012(2)	0.012(2)	0.022(3)	-0.001(1)	-0.006(1)	0.000(1)
Cl(1T)	0.026(2)	0.022(2)	0.026(3)	0.000(2)	-0.008(2)	0.002(1)
P(1)	0.011(2)	0.016(2)	0.021(3)	0.000(2)	-0.007(2)	0.001(1)
P(2)	0.014(2)	0.017(2)	0.016(3)	0.001(2)	-0.004(2)	-0.001(1)

Modified Preparation of [Ru$_3$Cl$_8$(PEt$_2$Ph)$_4$]

This was based on the methods of Cotton and Torralba[39]. PEt$_2$Ph (220 mg) was added to a stirred, purged solution of RuCl$_3$.xH$_2$O (250 mg) and HCl (0.1 ml) in MeOH (5 ml). The reaction mixture was stirred for 2 hours then left to stand for 1 week. The precipitated product was isolated and purified by column chromatography as above, in 40% yield.

[Ru$_3$Cl$_8$(PPr$^n_3$)$_4$]

PPr$^n_3$ (250 mg) was added to a solution of RuCl$_3$.xH$_2$O (300 mg) in N$_2$ purged MeOH (5 ml). The reaction mixture was stirred for two hours then left to stand for 4 days, by which time the product had precipitated, allowing it to be isolated by filtration. No purification of the product was required. The isolated yield was 235 mg (50%). Crystals suitable for single crystal X-ray diffraction were obtained by evaporation of a toluene solution.

Elemental Analysis:-   Found %C = 35.5, %H = 6.79.

Calculated, for Ru$_3$Cl$_8$P$_4$C$_{36}$H$_{84}$, %C = 35.2, %H = 6.90.

FAB-MS:-   Found m/z = 1227 (expected m/z, for [Ru$_3$Cl$_8$P$_4$C$_{36}$H$_{84}$]$^+$, = 1226)

Crystal Data for [Ru$_3$Cl$_8$(PPr$^n_3$)$_4$]

Ru$_3$C$_{36}$H$_{84}$Cl$_8$P$_4$, MW = 1227.8, Monoclinic, Space Group P2$_1$/c, a = 11.782(13), b = 15.661(5), c = 14.075(6) Å, $\alpha = \gamma = 90°$, $\beta = 95.51(6)°$, V = 2585 Å^3 (refined from 21 2θ rfeflections in the range $20 \leq 2\theta \leq 22°$,

$\lambda = 0.71073$ Å), Z = 2, D_c = 1.58 gcm^{-3}, Data collected at 150.0(1) K, Black plate of dimensions 0.31 x 0.23 x 0.08 mm, μ(Mo-Kα) = 1.360 mm^{-1}, F(000) = 1316.

Data Collection and Processing

The crystal was mounted in a Stadi-4 diffractometer and data were collected at 150 K in the ω - 2θ mode using graphite monochromated Mo-Kα radiation, with a scan width of (1.20 + 0.347tanθÛ). 3546 reflections were measured (5 $\leq$ 2θ $\leq$ 45°, -12 $\leq$ h $\leq$ 12, 0 $\leq$ k $\leq$ 16, 0 $\leq$ l $\leq$ 15), and 1881 of the 2829 unique data (R_{int} = 0.000) with F $\geq$ 4σ(F) were used in all calculations. An initial absorption correction was made[43] with maximum and minimum correction factors of 0.6876 and 0.3655 respectively. A drift in the intensities of the "standard" reflections of 1.1% was observed.

Structure Analysis and Refinement

Structure solution and refinement were carried out using SHELX76[41], the terminal Ru atom being located by use of a Patterson Synthesis (it was assumed that the central Ru atom would be located at a centre of inversion). All other non-hydrogen atoms were located by iterative cycles of least squares refinement and difference Fourier synthesis, all Ru, Cl and P atoms being allowed to refine anisotropically. All H atoms were refined in calculated positions (via the AFIX command). A final absorption correction was made using DIFABS[42]. The weighting scheme $w^{-1} = \sigma^2$(F) + 0.00230F^2 gave satisfactory agreement analyses.

At convergence, $(\Delta/\sigma)_{max}$ in the final cycle was 0.001 and the final values of R and R_w were 0.071 and 0.091 respectively for 142 parameters, S = 1.031. The final Fourier synthesis showed no important features and exhibited maximum and minimum residues of +2.00 (lying between the Ru atoms) and -1.12 eÅ^{-3} respectively.

Table 4.10 Atomic coordinates of $[Ru_3Cl_8(PPr^n_3)_4]$.

	x	y	z	Ueq
Ru(1)	-0.13699(14)	0.64465(8)	0.44523(10)	0.0190(8)
Ru(2)	0.00000(0)	0.50000(0)	0.50000(0)	0.0178(11)
Cl(1B)	-0.1766(4)	0.53194(25)	0.5614(3)	0.0252(25)
Cl(2B)	0.0564(4)	0.64259(25)	0.5317(3)	0.0239(24)
Cl(3B)	-0.0738(4)	0.53640(25)	0.3444(3)	0.0246(25)
P(1)	-0.0764(4)	0.75417(25)	0.3498(3)	0.021(3)
C(11)	-0.1792(17)	0.8283(9)	0.2895(12)	0.024(4)
C(12)	-0.2248(16)	0.8988(10)	0.3534(12)	0.026(4)
C(13)	-0.3271(18)	0.9419(12)	0.3015(14)	0.039(5)
C(14)	0.0282(18)	0.8260(11)	0.4172(13)	0.033(5)
C(15)	0.0702(18)	0.8993(11)	0.3614(13)	0.034(5)
C(16)	0.1474(22)	0.9584(14)	0.4247(17)	0.059(7)
C(17)	0.0013(17)	0.7189(10)	0.2493(12)	0.027(4)
C(18)	0.1248(17)	0.6824(10)	0.2761(13)	0.029(4)
C(19)	0.1761(20)	0.6566(12)	0.1862(14)	0.042(5)
P(2)	-0.3169(5)	0.6289(3)	0.3656(3)	0.025(3)
C(21)	-0.3909(17)	0.5350(10)	0.4005(13)	0.031(5)
C(22)	-0.3469(19)	0.4477(11)	0.3698(14)	0.038(5)
C(23)	-0.4054(19)	0.3729(11)	0.4119(14)	0.044(6)
C(24)	-0.4148(17)	0.7131(11)	0.3919(13)	0.034(5)
C(25)	-0.5314(19)	0.7229(12)	0.3352(15)	0.045(5)
C(26)	-0.5957(20)	0.7979(12)	0.3750(16)	0.049(6)
C(27)	-0.3159(18)	0.6195(11)	0.2348(12)	0.030(5)
C(28)	-0.4280(24)	0.5903(16)	0.1812(17)	0.070(8)
C(29)	-0.4314(23)	0.5909(14)	0.0791(17)	0.065(7)
Cl(1T)	-0.1988(4)	0.74965(25)	0.5471(3)	0.026(3)

Table 4.11 Atomic coordinates of H atoms in $[Ru_3Cl_8(PPr^n_3)_4]$.

	x	y	z	Ueq
H(11A)	- 0.2512	0.7915	0.2589	0.0400
H(11B)	- 0.1386	0.8593	0.2331	0.0400
H(12A)	- 0.1587	0.9456	0.3706	0.0400
H(12B)	- 0.2490	0.8703	0.4184	0.0400
H(13A)	- 0.3581	0.9908	0.3465	0.0400
H(13B)	- 0.3934	0.8952	0.2843	0.0400
H(13C)	- 0.3031	0.9705	0.2366	0.0400
H(14A)	0.1011	0.7880	0.4434	0.0400
H(14B)	- 0.0117	0.8520	0.4768	0.0400
H(15A)	0.1174	0.8744	0.3054	0.0400
H(15B)	- 0.0022	0.9353	0.3301	0.0400
H(16A)	0.1759	1.0103	0.3824	0.0400
H(16B)	0.2203	0.9230	0.4560	0.0400
H(16C)	0.1006	0.9839	0.4807	0.0400
H(17A)	0.0086	0.7730	0.2027	0.0400
H(17B)	- 0.0487	0.6696	0.2115	0.0400
H(18A)	0.1202	0.6274	0.3219	0.0400
H(18B)	0.1774	0.7308	0.3130	0.0400
H(19A)	0.2607	0.6315	0.2044	0.0400
H(19B)	0.1806	0.7117	0.1405	0.0400
H(19C)	0.1234	0.6082	0.1494	0.0400
H(21A)	- 0.4786	0.5405	0.3708	0.0400
H(21B)	- 0.3872	0.5350	0.4774	0.0400
H(22A)	- 0.2567	0.4439	0.3922	0.0400
H(22B)	- 0.3602	0.4433	0.2930	0.0400
H(23A)	- 0.3703	0.3141	0.3874	0.0400
H(23B)	- 0.4957	0.3753	0.3896	0.0400
H(23C)	- 0.3922	0.3758	0.4888	0.0400
H(24A)	- 0.3702	0.7726	0.3841	0.0400
H(24B)	- 0.4308	0.7048	0.4656	0.0400
H(25A)	- 0.5201	0.7347	0.2611	0.0400
H(25B)	- 0.5800	0.6650	0.3411	0.0400
H(26A)	- 0.6780	0.8046	0.3348	0.0400
H(26B)	- 0.5472	0.8559	0.3691	0.0400
H(26C)	- 0.6071	0.7862	0.4491	0.0400
H(27A)	- 0.2507	0.5740	0.2206	0.0400
H(27B)	- 0.2950	0.6813	0.2073	0.0400
H(28A)	- 0.4948	0.6319	0.2013	0.0400
H(28B)	- 0.4444	0.5258	0.2034	0.0400
H(29A)	- 0.5139	0.5693	0.0486	0.0400
H(29B)	- 0.3661	0.5490	0.0570	0.0400
H(29C)	- 0.4165	0.6550	0.0549	0.0400

Table 4.12 Anisotropic thermal parameters for $[Ru_3Cl_8(PPr^n_3)_4]$.

	U11	U22	U33	U23	U13	U12
Ru(1)	0.020(1)	0.019(1)	0.017(1)	0.001(1)	0.002(1)	0.000(1)
Ru(2)	0.019(1)	0.020(1)	0.015(1)	0.001(1)	0.005(1)	0.002(1)
Cl(1B)	0.022(3)	0.031(2)	0.022(2)	0.004(2)	0.005(2)	0.004(2)
Cl(2B)	0.028(3)	0.021(2)	0.022(2)	0.000(2)	0.006(2)	- 0.004(2)
Cl(3B)	0.029(3)	0.025(2)	0.019(2)	0.003(2)	0.002(2)	0.001(2)
P(1)	0.023(3)	0.019(2)	0.021(3)	0.002(2)	- 0.001(2)	- 0.002(2)
P(2)	0.025(3)	0.025(2)	0.025(3)	0.000(2)	0.003(2)	0.000(2)
Cl(1T)	0.026(3)	0.026(2)	0.026(2)	- 0.004(2)	0.001(2)	0.004(2)

[Ru$_3$Cl$_8$(AsPr$^n_3$)$_4$]

AsPr$_3$ (400 mg) was added to a solution of RuCl$_3$.xH$_2$O (380 mg) and HCl (0.1 ml) in N$_2$ purged MeOH (7 ml). The reaction mixture was stirred for 2 hours then left to stand for 4 days. The crude product was isolated by filtration and purified by elution with CH$_2$Cl$_2$ from a column of silica gel G. The yield of the purified product was 370 mg (55%). Crystals suitable for X-ray diffraction were obtained by diffusion of Et$_2$O into a CH$_2$Cl$_2$ solution of the product.

Elemental analysis:-   Found %C = 31.6, %H = 6.17.

Calculated, for Ru$_3$C$_{36}$H$_{84}$As$_4$Cl$_8$, %C = 30.8, %H = 6.03.

FAB-MS: Found m/z = 1403 (for [Ru$_3$C$_{36}$H$_{84}$As$_4$Cl$_8$]$^+$, expected m/z = 1402)

Crystal Data For Ru$_3$Cl$_8$(AsPr$^n_3$)$_4$

Ru$_3$C$_{36}$H$_{84}$Cl$_8$As$_4$,   MW   =   1403.6, Orthorhombic, Space Group P$_{cab}$ (Alternate orientation of P$_{bca}$), a = 14.034(4), b = 15.923(4), c = 24.152(5) Å, α=β=γ=90°, V = 5397 Å^3 (refined from 51 2θ reflections in the range 30 ≤ 2θ ≤ 32°, λ = 0.71073 Å), Z = 4, D$_c$ = 1.727 gcm^{-3}, Data collected at 150.0(1) K, Black plate of dimensions 0.29 x 0.22 x 0.07 mm, μ(Mo-Kα) = 3.668 mm^{-1}, F(000) = 2800.

Data Collection and Processing

The crystal was mounted in a Stadi-4(B) diffractometer, and data were collected at 150 K in the ω mode using graphite

monochromated MoKα radiation. 3972 reflections were measured, (scan width = $(1.20 + 0.347 \tan\theta°)$, $5 \leq 2\theta \leq 45°$, h = 0 to 15, k = 0 to 17, l = 0 to 26) of which 2641 (R_{int} = 0.000) were found to be unique and 1763 with $F \geq 4\sigma(F)$ were used in all calculations. An initial absorption correction was made[43] with maxima and minima of 0.989 and 0.872 respectively. A 4% random drift in the intensities of the standard reflections was observed.

Structure Analysis and Refinement

Structure solution and refinement were carried out using SHELX76[41], a Patterson Synthesis being employed to locate the terminal Ru atom of the asymmetric unit (it was assumed that the central Ru atom lay on a centre of inversion). All other non-H atoms were subsequently located by iterative cycles of least squares refinement and difference Fourier synthesis. All Ru, Cl and As atoms were allowed to refine anisotropically. The H atoms were refined in calculated positions (using the AFIX command). The weighting scheme $1.3596w^{-1} = \sigma^2(F) + 0.00163F^2$ gave satisfactory agreement analyses. At convergence $(\Delta/\sigma)_{max}$ in the final cycle was 0.002 and final values of R and R_w were 0.049 and 0.064 respectively for 142 parameters, S = 1.029. The final Fourier synthesis showed no important features and the maximum and minimum residues were +0.78 and -0.77 $e\text{Å}^{-3}$ respectively.

Table 4.13 Atomic coordinates for $Ru_3Cl_8(AsPr^n_3)_4$.

	x	y	z	Ueq
Ru(1)	-0.04277(8)	0.13881(7)	-0.06739(5)	0.0154(6)
Ru(2)	0.00000(0)	0.00000(0)	0.00000(0)	0.0146(9)
Cl(1T)	0.05665(25)	0.24473(24)	-0.10213(18)	0.0259(21)
Cl(1B)	-0.0746 (3)	-0.02874(22)	0.08562(17)	0.0229(21)
Cl(2B)	0.02948(24)	0.14136(23)	0.02560(16)	0.0203(20)
Cl(3B)	-0.15252(23)	0.03837(23)	-0.03273(16)	0.0190(20)
As(1)	-0.14554(11)	0.25345(10)	-0.03824(7)	0.0197(8)
C(11)	-0.2573 (10)	0.2203 (9)	0.0036 (7)	0.018 (3)
C(12)	-0.2349 (12)	0.1908 (10)	0.0633 (8)	0.034 (4)
C(13)	-0.3206 (12)	0.1518 (12)	0.0888 (9)	0.044 (5)
C(14)	-0.0789 (10)	0.3320 (9)	0.0103 (7)	0.023 (4)
C(15)	-0.1371 (12)	0.4088 (10)	0.0264 (8)	0.033 (4)
C(16)	-0.0821 (13)	0.4665 (11)	0.0657 (8)	0.041 (5)
C(17)	-0.2038 (10)	0.3302 (10)	-0.0928 (7)	0.024 (4)
C(18)	-0.1358 (12)	0.3830 (11)	-0.1263 (8)	0.035 (4)
C(19)	-0.1885 (13)	0.4446 (12)	-0.1648 (9)	0.045 (5)
As(2)	-0.11013(11)	0.10940(10)	-0.15747(7)	0.0205(9)
C(21)	-0.2482 (10)	0.1223 (9)	-0.1631 (7)	0.023 (4)
C(22)	-0.2884 (12)	0.1034 (12)	-0.2203 (8)	0.040 (5)
C(23)	-0.3988 (12)	0.0971 (12)	-0.2194 (9)	0.044 (5)
C(24)	-0.0934 (10)	-0.0055 (9)	-0.1824 (7)	0.025 (4)
C(25)	-0.1619 (12)	-0.0725 (11)	-0.1578 (9)	0.042 (5)
C(26)	-0.1404 (13)	-0.1589 (11)	-0.1814 (9)	0.045 (5)
C(27)	-0.0579 (10)	0.1709 (10)	-0.2205 (7)	0.026 (4)
C(28)	0.0443 (11)	0.1417 (10)	-0.2343 (7)	0.031 (4)
C(29)	0.0832 (15)	0.1818 (14)	-0.2863 (10)	0.064 (6)

246

Table 4.14 Atomic coordinates of H atoms in $Ru_3Cl_8(AsPr^n_3)_4$.

	x	y	z	Ueq
H(11A)	-0.29194	0.16945	-0.01804	0.0400
H(11B)	-0.30498	0.27341	0.00598	0.0400
H(12A)	-0.21317	0.24411	0.08782	0.0400
H(12B)	-0.17794	0.14522	0.06208	0.0400
H(13A)	-0.30382	0.13155	0.13032	0.0400
H(13B)	-0.34248	0.09831	0.06440	0.0400
H(13C)	-0.37770	0.19720	0.09015	0.0400
H(14A)	-0.01529	0.35306	-0.01061	0.0400
H(14B)	-0.05942	0.29906	0.04776	0.0400
H(15A)	-0.15490	0.44343	-0.01065	0.0400
H(15B)	-0.20174	0.38838	0.04658	0.0400
H(16A)	-0.12562	0.52016	0.07612	0.0400
H(16B)	-0.01745	0.48760	0.04580	0.0400
H(16C)	-0.06429	0.43255	0.10303	0.0400
H(17A)	-0.25059	0.37230	-0.07066	0.0400
H(17B)	-0.24504	0.29269	-0.12133	0.0400
H(18A)	-0.09113	0.41837	-0.09837	0.0400
H(18B)	-0.09197	0.34195	-0.15123	0.0400
H(19A)	-0.13717	0.48099	-0.18791	0.0400
H(19B)	-0.23220	0.48627	-0.14028	0.0400
H(19C)	-0.23304	0.40985	-0.19314	0.0400
H(21A)	-0.26611	0.18635	-0.15257	0.0400
H(21B)	-0.28117	0.08016	-0.13374	0.0400
H(22A)	-0.26772	0.15308	-0.24825	0.0400
H(22B)	-0.25936	0.04452	-0.23463	0.0400
H(23A)	-0.42446	0.08365	-0.26059	0.0400
H(23B)	-0.42851	0.15587	-0.20528	0.0400
H(23C)	-0.42016	0.04730	-0.19167	0.0400
H(24A)	-0.02151	-0.02413	-0.17230	0.0400
H(24B)	-0.10249	-0.00601	-0.22684	0.0400
H(25A)	-0.23445	-0.05576	-0.16774	0.0400
H(25B)	-0.15320	-0.07425	-0.11338	0.0400
H(26A)	-0.18868	-0.20415	-0.16373	0.0400
H(26B)	-0.06793	-0.17588	-0.17145	0.0400
H(26C)	-0.14918	-0.15739	-0.22580	0.0400
H(27A)	-0.05648	0.23709	-0.21071	0.0400
H(27B)	-0.10287	0.16061	-0.25614	0.0400
H(28A)	0.04371	0.07436	-0.23985	0.0400
H(28B)	0.09035	0.15767	-0.20008	0.0400
H(29A)	0.15455	0.15907	-0.29383	0.0400
H(29B)	0.08481	0.24918	-0.28123	0.0400
H(29C)	0.03817	0.16587	-0.32099	0.0400

Table 4.15 Anisotropic thermal parameters for $Ru_3Cl_8(PPr^n_3)_4$.

	U11	U22	U33	U23	U13	U12
Ru(1)	0.014(1)	0.014(1)	0.018(1)	0.002(1)	0.001(1)	0.002(1)
Ru(2)	0.015(1)	0.012(1)	0.017(1)	0.001(1)	-0.000(1)	0.002(1)
Cl(1T)	0.019(2)	0.024(2)	0.034(3)	0.006(2)	0.004(2)	0.001(2)
Cl(1B)	0.026(2)	0.020(2)	0.022(2)	-0.001(2)	0.006(2)	0.007(2)
Cl(2B)	0.019(2)	0.019(2)	0.023(2)	-0.002(2)	-0.003(2)	0.000(2)
Cl(3B)	0.013(2)	0.020(2)	0.024(2)	-0.002(2)	0.001(2)	0.000(2)
As(1)	0.016(1)	0.017(1)	0.026(1)	0.001(1)	0.002(1)	0.002(1)
As(2)	0.020(1)	0.024(1)	0.017(1)	-0.000(1)	-0.002(1)	0.003(1)

247

[Ru₃Cl₈(PMe₃)₄]

[Ru$_3$Cl$_8$(PMe$_3$)$_4$]

PMe$_3$ (1.60 ml of a 1.0 M solution in THF) was added to a solution of RuCl$_3$.xH$_2$O (300 mg) in N$_2$ purged MeOH (5 ml). After stirring for 2 hours the mixture was left to stand overnight. The solvent volume was reduced *in vacuo* to induce precipitation of the product, isolated two days later by filtration and purified by elution with CH$_2$Cl$_2$ from a column of silica gel G. The yield of purified product was 150 mg (45%).

Elemental analysis:- Found %C = 17.3, %H = 4.25.

Calculated, for Ru$_3$Cl$_8$P$_4$C$_{12}$H$_{36}$, %C = 16.2, %H = 4.07.

FAB-MS:-   Found m/z = 891 (for [Ru$_3$Cl$_8$P$_4$C$_{12}$H$_{36}$]$^+$, expected m/z = 890).

[Ru$_3$Cl$_8$(PPh$_3$)$_4$]

PPh$_3$ (300 mg) was added to a solution of RuCl$_3$.xH$_2$O (220 mg) in N$_2$ purged MeOH (4 ml). The reaction mixture was stirred for two hours, then left to stand for four days while precipitation occurred. The crude yield was 170 mg. The presence of the trinuclear complex in the crude product was confirmed by electronic absorption spectroscopy. Attempts to purify samples of the crude product by column chromatography resulted in decomposition of the trinuclear complex.

[Ru$_3$Cl$_8$(P{OMe}$_3$)$_4$]

P(OMe)$_3$ (0.12 ml, equivalent to 126 mg) was added to a solution of RuCl$_3$.xH$_2$O (200 mg) in deoxygenated MeOH (4 ml). After stirring for

two hours the reaction mixture was left overnight. As precipitation had not commenced the solvent volume was reduced *in vacuo* and the solution left to stand for three more days. The crude product was isolated by filtration with a yield of 80 mg.

[Ru₃Br₈(PEt₂Ph)₄]

"RuBr₃" was prepared by addition of LiBr (600 mg) to a deoxygenated solution of RuCl₃.xH₂O (300 mg) in MeOH (5 ml). The mixture was stirred for four days, by which time the solution had assumed a deep red/purple colour. To the "RuBr₃" solution was added PEt₂Ph (260 mg) and the reaction mixture was stirred for two hours before being left to stand for 5 further days. The crude product (yield = 210 mg) was isolated by filtration and purified by elution from a column of silica gel G with CH_2Cl_2. The yield of purified product was 24 mg (4%).

FAB-MS:-   Found m/z = 1607. For $[Ru_3Br_8P_4C_{40}H_{60}]^+$, expected m/z = 1610.

4.4   <u>References</u>

1.   M. B. Robin and P. Day, *Adv. Inorg. Chem. and Radiochem.*, **1967**, <u>10</u>, 247.

2.   I. M. Nowell and D. R. Russell, *J. Chem. Soc. (A)*, **1967**, 817.

3.   A. I. Nehhaev, G. G. Aleksandrov and E. I. Bagrii, *Metalloorg. Khim.*,

        1990, <u>3</u>, 926.

4.   S. I. Amer, T. S. Dasgupta and P. M. Henry, *Inorg. Chem.*, **1983**, <u>22</u>, 1970.

5.   R. W. Callaghan, G. M. Brown and T. J. Meyer, *Inorg. Chem.*,

        1975, <u>14</u>, 1443.

6.   K. A. Goldsby and T. J. Meyer, *Inorg. Chem.*, **1984**, <u>23</u>, 3002.

7.   F. A. Cotton and R. C. Torralba, *Inorg. Chem.*, **1991**, <u>30</u>, 2196.

8.   C. Creutz and H. Taube, *J. Am. Chem. Soc.*, **1969**, <u>91</u>, 3988.

9.   T. A. Stephenson and G. Wilkinson, *J. Inorg. Nucl. Chem.*, **1966**, <u>28</u>, 2285.

10.   R. J. Sorbie, PhD Thesis, University of Edinburgh, **1989**.

11.   C. Creutz, *Prog. Inorg. Chem.*, **1983**, <u>30</u>, 1.

12.   A. R. Chakravarty, F. A. Cotton, A. R. Cutler, S. M. Tetrick and

        R. A. Walton, *J. Am. Chem. Soc.*, **1985**, 1<u>07</u>, 4795.

13.   R. G. Abbot, F. A. Cotton and R. Falvello, *Inorg. Chem.*, **1990**, <u>29</u>, 514.

14.   F. A. Cotton, K. R. Dunbar and M. Matusz, *Inorg. Chem.*, **1986**, <u>25</u>, 1589.

15.   E. M. Kober, K. A. Goldsby, D. N. S. Narayana and T. J. Meyer,

        J. Am. Chem. Soc., **1983**, <u>105</u>, 4303.

16.   N. S. Hush, *Prog. Inorg. Chem.*, **1967**, <u>8</u>, 391.

17. F. A. Cotton and R. A. Walton, *Multiple Bonds between Metal Atoms*, *2nd Ed.*, Clarendon Press, **1993**.

18. R. W. Mitchell, A. Spencer and G. Wilkinson, *J. Chem. Soc. Dalton Trans.*, **1973**, 846.

19. J. Campbell, H. Ryan, M. Walsh, G. Ferguson and J. Gallagher, *Polyhedron*, **1991**, 10, 2273.

20. F. A. Cotton, *Polyhedron*, **1987**, 6, 667.

21. M. T. Flood, R. F. Ziolo, J. E. Earley and H. B. Gray, *Inorg. Chem.*, **1973**, 12, 2153.

22. A. R. Chakravarty, F. A. Cotton and D. A. Tocher, *Inorg. Chem.*, **1984**, 23, 4030.

23. M. M. Crozat and S. F. Watkins, *J. Chem. Soc. Dalton Trans.*, **1972**, 2512.

24. S. F. Watkins, *J. Chem. Soc. (A)*, **1969**, 1552.

25. B. M. Matson, J. R. Heiman and L. H. Pignolet, *Inorg. Chem.*, **1976**, 15, 564.

26. C. L. Raston and A. H. White, *J. Chem. Soc. Dalton Trans.*, **1975**, 2410. 27. A. R. Chakravarty, F. A. Cotton, M. P. Diebold, D. B. Lewis and W. J. Roth, *J. Am. Chem. Soc.*, **1986**, 108, 971.

28. F. A. Cotton, M. Matusz and R. C. Torralba, *Inorg. Chem.*, **1989**, 28, 1516.

29. F. A. Cotton and R. C. Torralba, *Inorg. Chem.*, **1991**, 30, 4392.

30. G. A. Heath and D. G. Humphrey, *J. Chem. Soc. Chem. Comm.*, **1990**, 672.

31. F. A. Cotton and D. A. Ucko, *Inorg. Chim. Acta*, **1972**, 6, 161.

32. R. H. Summerville and R. Hoffmann, *J. Am. Chem. Soc.*, **1979**, 101, 3821.

33. M.-H. Whangloo, M. J. Foshee and R. Hoffmann, *Inorg. Chem.*,

1980, 19, 1723.

34. A. P. Ginsberg, *J. Am. Chem. Soc.*, 1983, 102, 111.

35. B. E. Bursten, F. A. Cotton and A. Fang, *Inorg. Chem.*, 1983, 22, 2127.

36. D. Appleby, P. B. Hitchcock, K. R. Seddon, J. E. Turp, J. A. Zora,

C. L. Hussey, J. R Sanders and T. A. Ryan, *J. Chem. Soc. Dalton Trans.*,

1990, 1879.

37. M. B. Hursthouse, R. A. Jones, K. M. Abdul Malik and G. Wilkinson,

J. Am. Chem. Soc., 1979, 101, 4128.

38. A. Bino and F. A. Cotton, *J. Am. Chem. Soc.*, 1980, 102, 2196.

39. F. A. Cotton and R. C. Torralba, *Inorg. Chem.*, 1991, 30, 3293.

40. J. Chatt, G. J. Leigh, D. M. P. Mingos and R. J. Paske, *J. Chem. Soc. (A)*,

1968, 2636.

41. SHELX76 "A program for crystal structure determination and refinement",

G. M. Sheldrick, University of Cambridge, 1976.

42. DIFABS, N. Walker and D. Stuart, *Acta Cryst.*, 1983, A39, 158.

43. A. C. T. North, D. C. Phillips and F. S. Matthews, *Acta Cryst.*,

1968, A24, 351.

44. A. B. P. Lever, *Inorganic Electronic Spectroscopy*, Elsevier, 1984.

45. F. A. Cotton and R.C. Torralba, *Inorg. Chem.*, 1991, 30, 4386.

46. F. A. Cotton, P. E. Fanwick, L. D. Gage, B. Kalbacher, and D. S. Martin,

J. Am. Chem. Soc., 1977, 99, 5642.

Courses and Conferences Attended

ESR Spectroscopy, by Dr. R. E. P. Winpenny, 1991.

NMR spectroscopy, by Dr. I. Sadler and Dr. D. Reed, 1992.

An introduction to X-ray crystallography, by Drs A. J. Blake and R. O. Gould, 1992

ESR Spectroscopy, by Prof. P. Rieger, 1993.

Departmental research seminars and colloquia.

University of Strathclyde Inorganic Club conferences, 1991, '92 and '93.

Butler postgraduate electrochemistry meetings 1991, '92 and '93.

RSC Scottish Dalton meetings, 1992 and '93.

Irvine memorial lectures, University of St. Andrews, 1993.

RSC (Dalton Division) / Gesellschaft Deutscher Chemiker international conference on inorganic chemistry, University of Sussex, 1991.

RSC (Dalton Division) international conference on the chemistry of the platinum group metals, University of St. Andrews, 1993.